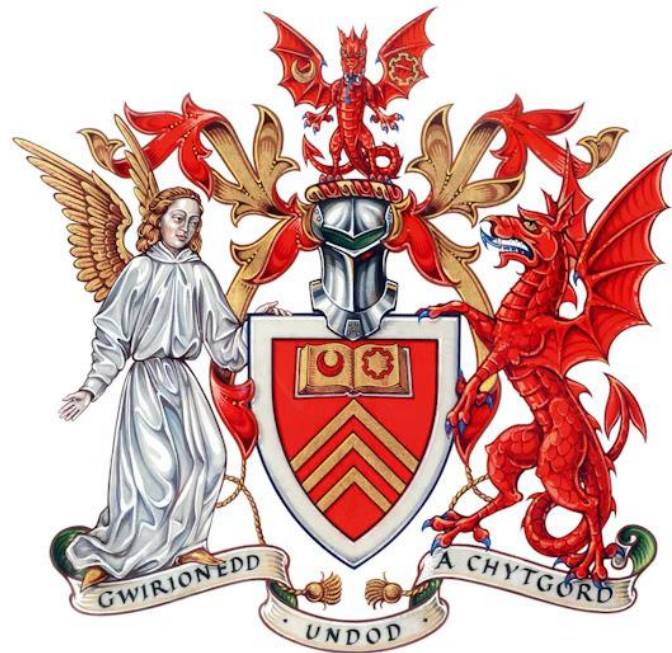


Developing novel screening assays and therapeutics for  
Niemann-Pick disease



Gareth Derek Fenn

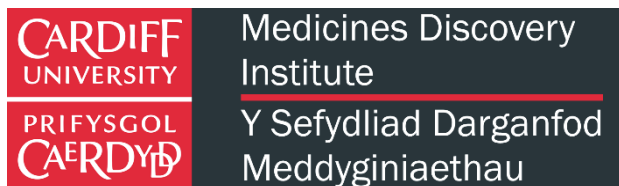
Medicines Discovery Institute

Cardiff University

A thesis submitted to Cardiff University for the degree of

Doctor of Philosophy

May 2024



## **Abstract**

In this thesis, screening assays, and compounds with potential therapeutic effects were developed and analysed for use in Niemann-Pick disease.

Niemann-Pick disease is a rare lysosomal storage disorder characterised by lysosomal sphingolipid accumulation. In Niemann-Pick Types A&B loss of acid sphingomyelinase is the primary cause of the disease, whereas in Niemann-Pick type C, loss of NPC1 protein activity results in lysosomal lipid accumulation.

We first evaluated a novel fluorescent molecule, AQ7, that we hypothesised to be NPC1 specific substrate. However, AQ7 was observed to have lysosomal entrapment, and thus led to the development of AQ7 as a novel lysosomal probe, possessing a range of improvements over other commercially available lysosomal probes.

We investigated a biomarker present in Niemann-Pick disease, free zinc and its ability to be used as a marker to identify novel therapeutics. An imaging-based zinc assay was developed using TSQ as a probe, which was used to screen a 1500-compound library for modulators of intracellular free zinc in patient derived NPC1 fibroblasts. A total of 20 hit compounds that reduced lysosomal volume by up to 45% in 24 hours in NPC1 mutant fibroblasts were identified.

Cannabidiol and copaiba, have been suggested as potential therapeutics in Niemann-Pick, and were investigated *in vitro*. Both cannabidiol and copaiba oil reduced lysosomal volume, sphingomyelin and cholesterol staining in patient fibroblasts. Increases in acid sphingomyelinase activity and protein expression was found upon cannabidiol and copaiba treatment, The increased acid sphingomyelinase expression, was postulated to be driven by an increase in TFE3 nuclear localisation, upon cannabidiol and copaiba treatment.

We have shown that AQ7 is not a suitable substrate for NPC1, but is a novel lysosome probe, with the ability to be used for time course assays without inducing lysosomal de-acidification. We have demonstrated that screening for zinc modulators is a viable screening strategy in Niemann-Pick and has allowed us to identify 20 potential starting points for therapeutics through their ability to both modulate zinc and reducing lysosomal volume. Furthermore, we've identified that cannabidiol and copaiba reduce lysosomal storage in Niemann-Pick disease through activating TFE3.

## ***Acknowledgments***

Thank you to the Academy of Medical Sciences and the Niemann-Pick Research Foundation (NPRF) for funding this project, and to NPRF for proposing the work into cannabidiol and copaiba oil. I would also like to thank Niemann-Pick UK (NPUK), for providing the funding for a summer project six years ago, through a very indirect route eventually led to this project.

Thanks to Mum and Dad for the support throughout the PhD, as well as all the times before that. Thanks to the rest of my family for the support throughout, and not asking how much I had left in the lab to do or how long I had left before I submitted, too often.

Special thanks to Helen Waller-Evans for being my manager and then supervisor over the last 6 years and helping guide me throughout the project, particularly when things didn't go to plan. Also, thanks to Emyr Lloyd-Evans for being my second supervisor and coming up with some useful feedback and support with the project.

Thanks to Siân, Mari, and Beth, all who have helped with various things both in and outside of the lab. Thanks to both Heulyn and Loren for all the post work runs and gym sessions over the last year. Particular thanks to Gaby for taking on the painful job of transferring the 1500 compounds of the Discovery probe library from individual tubes into plates.

Finally, thanks to all the other past and current MDI members and Lloyd-Evans lab members who helped make coming into the lab every day an enjoyable experience.

## Abbreviations

Abbreviation	Full name
3MA	3-Methyl adenine
A2AR	Adenosine A2A receptor
ACase	Acid ceramidase
ALS	Amyotrophic lateral sclerosis
ASAH1	N-Acylsphingosine amidohydrolase 1
aSMase	Acid sphingomyelinase
ASMD	Acid sphingomyelinase deficiency
ATP	Adenosine triphosphate
BCP	$\beta$ -Caryophyllene
CB	Cannabinoid receptor
CBD	Cannabidiol
CDF	Cation diffusion facilitator
CLEAR	Coordinated lysosomal expression and regulation
CNS	Central nervous system
CTD	C-terminal domain
DMEM	Dulbecco's modified Eagle medium
EGFR	Epidermal growth factor receptor
EMA	European Medicines Agency
ER	Endoplasmic Reticulum
ERT	Enzyme replacement therapy
ESH	Eukaryotic sterol homeostasis
FDA	Food and Drug Administration
FGFR	Fibroblast growth factor receptors
FITC	Fluorescein isothiocyanate

FRET	Förster resonance energy transfer
GABA	$\gamma$ -Aminobutyric acid
GAG	Glycosaminoglycans
GFP	Green fluorescent protein
HDAC	Histone de-acetylase
HME	heavy metal efflux
HMG-CoA	$\beta$ -Hydroxy $\beta$ - methylglutaryl-CoA
HMU	Hexadecanoylamino-4- methylumbelliferone
HSC	Haematopoietic stem cell
HSF	Heat shock factor
HSP	Heat shock proteins
HTS	High throughput screen
IPTG	Isopropyl $\beta$ -D-1- thiogalactopyranoside
IV	Intravenous
LAMP	Lysosomal associated membrane protein
LBPA	Lysobisphosphatidic acid
LC50	Lethal concentration (50%)
LDL	low-density lipoprotein
LE	Late endosome
LIMP	Lysosomal integral membrane protein
LSD	Lysosomal storage disease
MDI	Medicines Discovery Institute
MEM	Minimal essential media
MLD	Middle lumen domain
MLIV	Mucopolidosis Type 4
MPP	Matrix metalloproteinases
MPS	Mucopolysaccharidosis

mTOR	Mammalian target of rapamycin
NAM	Negative allosteric modulator
NCL	Neuronal ceroid lipofuscinoses
NICE	National Institute for Health and Care Excellence
NMDA	N-methyl-D-aspartate
NPA	Niemann-Pick type A
NPB	Niemann-Pick type B
NPC	Niemann-Pick type C
NPD	Niemann-Pick disease
NTD	N-Terminal domain
PBS	Phosphate buffered saline
PDE	Phosphodiesterase
PDGFR	Platelet-derived growth factor receptor
PFA	Paraformaldehyde
PI3K	phosphatidylinositol 3-kinase
PKC	Protein kinase C
RFP	Red fluorescent protein
RFU	Relative fluorescence units
RND	Resistance-nodulation-division

ROS	Reactive oxygen species
SAP	Sapoin-like
SLC	Solute carrier protein
SM	Sphingomyelin
SMPD	Sphingomyelin phosphodiesterase
SMS	Sphingomyelin synthase
SSD	Sterol sensing domain
TFE3	Transcription factor E3
TFEB	Transcription factor EB
TGN	Trans Golgi network
THC	Tetrahydrocannabinol
TRP	Transient receptor Potential
TSQ	6-Methoxy-(8-p-toluenesulfonamido) quinoline
VEGFR	Vascular endothelial growth factor
ZEB1	Zinc finger E-box-binding homeobox 1
ZIP	Zrt-/Irt-like proteins
ZRT	Zinc transporter proteins

## List of Figures

Figure 1.1. Overview of the eukaryotic endocytic system.....	2
Figure 1.2. Sphingolipid degradation pathway and associated diseases .....	9
Figure 1.3. Schematic of cholesterol trafficking through the lysosome mediated by NPC1 and NPC2 .....	20
Figure 1.4. <i>De novo</i> cholesterol synthesis pathways .....	21
Figure 1.5. Sphingomyelin and ceramide synthesis pathways .....	23
Figure 1.6. Schematic illustrating the overview of the synthesis of aSMase .....	26
Figure 1.7. Topology of human NPC1 protein .....	31
Figure 3.1. Structure of a range of earlier lysosomal probes.....	53
Figure 3.2. Structures of several recently developed lysosomal probes.....	54
Figure 3.3. NPC1 transports AQ2 out of lysosomes .....	56
Figure 3.4. Structures of anthraquinone derivates evaluated.....	57
Figure 3.5. Simplified diagram of AQ2 or analogue trafficking assay .....	58
Figure 3.6. Calibration of Real Time Glo assay with mouse glial cells.....	60
Figure 3.7. Toxicity analysis for AQ2 and analogues in mouse glial cells .....	61
Figure 3.8. Lysosomal localisation of AQ3 and AQ6.....	62
Figure 3.9. AQ3 trafficking in wild type mouse glial cells .....	63
Figure 3.10. Hoechst 33342 fluorescence bleed through into green AQ3 channel.....	64
Figure 3.11. Draq 5 prevents AQ3 nuclei localisation after 18 hours post AQ3 treatment .....	65
Figure 3.12. Nuclear localisation of CellLight BacMam 2.0.....	66
Figure 3.13. Emission filter comparison for cells treated with AQ3 .....	67
Figure 3.14. Emission spectra of AQ3 & AQ7 .....	69
Figure 3.15. Operetta excitation and emission filter determination for AQ2, AQ3 and AQ7 .....	71
Figure 3.16. <i>in vitro</i> fluorescence comparison of AQ2, AQ3 and AQ7.....	72
Figure 3.17. AQ7 concentration dependant effects upon puncta number and fluorescence <i>in vitro</i> .....	74
Figure 3.18. AQ7 co-localisation with LysoTracker Green .....	75
Figure 3.19. AQ7 can detect an induced NPC1 phenotype using U18666A .....	77
Figure 3.20. Co-localisation of AQ7 and LysoTracker Red with Cyto-ID.....	79
Figure 3.21. AQ7 can detect difference in lysosomes with trehalose and 3MA treatment .....	81
Figure 3.22. AQ7 puncta per cell and fluorescence intensity are not affected by chase time .....	83
Figure 3.23. AQ7 trafficking to lysosomes is temperature dependant .....	85
Figure 3.24. Bafilomycin treatment decreases the number of puncta of AQ7 and LysoTracker Red.....	87
Figure 3.25. Bafilomycin treatment after AQ7 decreases number of puncta detected without decreasing fluorescence intensity .....	89
Figure 3.26. AQ7 does not affect lysosomal pH .....	91
Figure 3.27. AQ7 and LysoTracker Green co-localisation in Niemann-Pick disease fibroblasts.....	93
Figure 3.28. AQ7 treatment leads to increased LysoTracker Green staining in fibroblasts .....	96
Figure 3.29. AQ7 leads to increased filipin staining in some Niemann-Pick disease cell lines.....	99
Figure 3.30. AQ7 staining in Niemann-Pick disease fibroblasts .....	101
Figure 3.31. AQ7 can detect improvement in disease phenotype when NPC cells are treated with cyclodextrin .....	104
Figure 3.32. Structures of AQ7 and compound 10 .....	106
Figure 4.1. Comparison of commonly used zinc probes fluorescence staining .....	117
Figure 4.2. Zinc puncta identification is TSQ concentration dependant .....	119
Figure 4.3. Removal of TSQ leads to quick dissipation of fluorescence .....	121

Figure 4.4. Pluronic F-127 reduces cells with TSQ puncta fluorescence .....	123
Figure 4.5. Elevated zinc storage is observed in Niemann-Pick disease cell lines .....	125
Figure 4.6. No plate patterning effects are observed with TSQ.....	127
Figure 4.7. High DMSO concentrations reduce zinc puncta and induce cellular toxicity .....	128
Figure 4.8. U18666A increases free zinc puncta in healthy control cells .....	130
Figure 4.9. Effect of zinc concentrations upon TSQ puncta .....	132
Figure 4.10. TPEN treatment does not affect intracellular free zinc storage .....	133
Figure 4.11. Imidazole increases free zinc puncta in healthy control cells .....	134
Figure 4.12. Clioquinol reduces zinc puncta .....	136
Figure 4.13. Phytic acid increases intracellular zinc puncta.....	138
Figure 4.14. Phytic acid reduces LBPA staining in Niemann-Pick disease .....	140
Figure 4.15. Zinc puncta are reduced upon HDAC inhibitor treatment in classical NPC fibroblasts .....	142
Figure 4.16. Compound library effects upon zinc in NPC1 P237S/1061T fibroblasts.....	145
Figure 4.17. Effect of zinc raising compounds upon LysoTracker Deep Red fluorescence in NPC1 cells .....	147
Figure 4.18. Effects of zinc lowering compounds upon LysoTracker Deep Red fluorescence in NPC1 cells. ....	149
Figure 5.1. Chemical structures of three significant members of the cannabinoid family.....	162
Figure 5.2. Comparison of acid sphingomyelinase activity in Niemann-Pick disease patient derived fibroblasts and healthy control fibroblasts .....	165
Figure 5.3. Cell viability assay for Niemann-Pick disease patient derived fibroblasts treated with cannabidiol .....	167
Figure 5.4. Cell viability assay for Niemann-Pick disease patient derived fibroblasts treated with copaiba .....	169
Figure 5.5. Comparison of LysoTracker Green fluorescence before and after cannabidiol treatment .....	171
Figure 5.6. Change in LysoTracker Green fluorescence when healthy control and Niemann-Pick fibroblasts are treated with copaiba .....	172
Figure 5.7. Cannabidiol and copaiba treatment reduces number of puncta and total puncta area in most Niemann-Pick disease fibroblasts when probed with LysoTracker Red .....	174
Figure 5.8. Cannabidiol and copaiba treatment recues lysosomal volume in most Niemann-Pick disease fibroblasts when probed with AQ7 .....	177
Figure 5.9. Sphingomyelin storage is reduced in Niemann-Pick cells with cannabidiol or copaiba treatment.....	180
Figure 5.10. Cannabidiol and copaiba reduces cholesterol storage in Niemann-Pick disease cells	183
Figure 5.11. Changes in GM1 staining with cannabidiol and copaiba are Niemann-Pick disease mutation dependant .....	186
Figure 5.12. Cannabidiol and copaiba treatment decreases LBPA staining In Niemann-Pick disease Type A & B fibroblasts.....	189
Figure 5.13. Comparison of acid sphingomyelinase activity in Niemann-Pick disease patient derived fibroblasts and healthy control fibroblasts cell lines treated with cannabidiol .....	191
Figure 5.14. Comparison of the fold change in acid sphingomyelinase activity between untreated and cells treated with 15µM cannabidiol.....	192
Figure 5.15. Comparison of acid sphingomyelinase activity in Niemann-Pick disease patient derived fibroblasts and healthy control fibroblasts treated with copaiba oil for 48-hours .....	194
Figure 5.16. Treatment of cells with copaiba oil leads to increased acid sphingomyelinase activity when compared to an untreated control.....	195

<b>Figure 5.17. Treatment of cell pellets with cannabidiol does not cause an increase in acid sphingomyelinase activity.....</b>	<b>197</b>
<b>Figure 5.18. Treating cell homogenate with copaiba does not produce the same increase in acid sphingomyelinase activity as treating cells with copaiba.....</b>	<b>199</b>
<b>Figure 5.19. Cannabidiol significantly increases acid sphingomyelinase expression in Niemann-Pick disease cells .....</b>	<b>200</b>
<b>Figure 5.20. Heat shock protein 70 expression is increased by cannabidiol or copaiba treatment</b>	<b>201</b>
<b>Figure 5.21. Cannabidiol increases acid ceramidase expression in acid sphingomyelinase deficient cell lines .....</b>	<b>202</b>
<b>Figure 5.22. Cannabidiol and copaiba promotes TFE3 nuclei localisation .....</b>	<b>205</b>

## List of Tables

<b>Table 2.1. Patient derived cell lines</b> .....	37
<b>Table 2.2. Primary antibodies</b> .....	45
<b>Table 2.3. Secondary antibodies</b> .....	46
<b>Table 2.4. Nuclei stains</b> .....	49
<b>Table 2.5. LysoTracker dyes used.</b> .....	50
<b>Table 4.1. Compounds that increased zinc storage and reduced lysosomal volume</b> .....	150
<b>Table 4.2. Compounds that reduced zinc storage and reduced lysosomal volume</b> .....	151
<b>Table 5.1. Major terpene constituents of copaiba oil based on data from Urasaki et al. 2020</b> .....	162

## Contents

1	Introduction .....	1
1.1	The endocytic system .....	1
1.1.1	Clathrin mediated endocytosis .....	2
1.1.2	Clathrin independent endocytosis .....	3
1.1.3	Endosomes .....	3
1.2	Lysosomes.....	4
1.2.1	Structure of a lysosome .....	4
1.2.2	Biogenesis.....	5
1.2.3	Lysosomal enzymes.....	6
1.2.4	Autophagy .....	7
1.3	Lysosomal storage disorders .....	7
1.3.1	Classification.....	7
1.3.2	Prevalence .....	12
1.4	Drug discovery in lysosomal storage disorders .....	13
1.4.1	Small molecule therapies .....	13
1.4.2	Enzyme replacement therapies .....	16
1.4.3	Gene replacement therapies.....	17
1.5	Niemann-Pick disease.....	18
1.6	Cholesterol metabolism .....	19
1.6.1	Cholesterol uptake by endocytosis .....	19
1.6.2	Intracellular cholesterol synthesis .....	20
1.7	Sphingomyelin metabolism .....	22
1.7.1	Sphingomyelin uptake by endocytosis.....	22
1.7.2	De novo sphingomyelin synthesis .....	23
1.8	Niemann-Pick types A & B .....	24
1.8.2	aSMase .....	25
1.8.3	aSMase and acid ceramidase/sphingosine .....	27
1.8.4	aSMase regulation in LSD's/NPD.....	27
1.8.5	Therapies in NPA/NPB.....	28
1.9	Niemann-Pick type C .....	29
1.9.1	Human NPC1 protein .....	29
1.9.2	NPC1 mutations .....	32
1.9.3	Clinical treatments for Niemann-Pick disease .....	33
1.10	Aims .....	35

2	Methods and materials .....	37
2.1	Cell culture.....	37
2.1.1	General cell culture .....	37
2.2	Drug treatments .....	37
2.2.1	Cannabidiol treatment .....	37
2.2.2	Copaiba treatment .....	38
2.2.3	Bafilomycin.....	38
2.2.4	Trehalose.....	38
2.2.5	3-Methyladenine (3MA).....	38
2.2.6	Zinc chloride .....	38
2.2.7	Phytic acid .....	38
2.2.8	TPEN .....	38
2.2.9	Imidazole .....	39
2.2.10	Clioquinol .....	39
2.2.11	Panobinostat.....	39
2.2.12	Vorinostat .....	39
2.3	Toxicity assays .....	39
2.3.1	Cell seeding density calibration for RealTime-Glo™ MT cell viability assay.....	39
2.3.2	AQ2 Analogues cellular toxicity assay using RealTime-Glo™ MT cell viability assay .....	40
2.3.3	Cellular toxicity assay using RealTime-Glo™ MT cell viability assay for cannabidiol and copaiba 40	
2.4	Biochemical assays .....	41
2.4.1	Enzyme assays.....	41
2.4.2	Protein quantification .....	42
2.5	Microscopy .....	42
2.5.1	Cell fixation.....	42
2.5.2	Blocking buffer .....	43
2.6	Western blotting.....	43
2.6.1	Homogenate preparation.....	43
2.6.2	Sample preparation.....	43
2.6.3	SDS-PAGE.....	44
2.6.4	Semi dry transfer .....	44
2.6.5	Membrane staining .....	44
2.6.6	Imaging.....	44
2.6.7	Quantification of western blots .....	44
2.7	Immunocytochemistry staining.....	45

2.7.1	Cholera toxin (Subunit B) staining.....	46
2.7.2	Filipin staining .....	46
2.7.3	AQ7 Imaging.....	47
2.7.4	Lysenin staining.....	47
2.7.5	Cyto-ID.....	48
2.7.6	Dextran lysosomal pH assay.....	48
2.7.7	Zinc probe comparisons .....	48
2.7.8	Pluronic F-127 .....	48
2.7.9	Nuclei stains .....	49
2.8	Lysotracker assays .....	49
2.8.1	Lysotracker quantification by multiwell plate assay.....	49
2.8.2	Lysotracker quantification by fluorescence microscopy.....	49
2.9	AQ2 Analogue excitation and emission filter determination.....	50
2.10	Zinc imaging assays.....	50
2.10.1	TSQ staining .....	50
2.10.2	TSQ assay buffer .....	51
2.10.3	Image analysis.....	51
2.10.4	Compound library .....	51
2.10.5	Zinc modulating compound screening plate preparation .....	51
2.11	Bac-Mam transfection .....	51
3	Identification of AQ7 as a novel lysosomal probe .....	52
3.1	Introduction.....	52
3.1.1	History of lysosomal probes.....	52
3.1.2	Limitations of current lysosomal probes.....	53
3.1.3	Characteristics for identification of novel lysosomal probes.....	54
3.1.4	RND permease probes .....	55
3.1.5	Anthraquinones as lysosomal probes .....	55
3.1.6	NPC1 activity assay.....	57
3.1.7	Aims of the chapter.....	59
3.2	Results .....	59
3.2.1	AQ2 and Analogues toxicity analysis.....	59
3.2.2	Lysosome localisation of AQ2 analogues .....	62
3.2.3	AQ2 analogue nuclei trafficking assay set up.....	62
3.2.4	Issues with development of an AQ2 analogue trafficking assay.....	68
3.2.5	Basic characterisation of AQ3 and AQ7 .....	68
3.2.6	AQ7 Characterisation .....	73

3.2.7	AQ7 effects upon lysosomal function .....	94
3.2.8	Evaluation of the sensitivity of AQ7 as a lysosomal probe .....	100
3.3	Discussion .....	105
3.3.1	Issues with development of an NPC1 trafficking assay.....	105
3.3.2	Selection of anthraquinone derivatives .....	105
3.3.3	AQ3 and AQ7 .....	106
3.3.4	AQ7 as a lysosomal probe .....	107
3.4	Conclusions.....	107
4	Development of a zinc based phenotypic screening assay suitable for HTS .....	108
4.1	Introduction.....	108
4.1.1	Cellular zinc homeostasis .....	108
4.1.2	Cellular zinc transporters .....	109
4.1.3	Zinc in disease .....	111
4.1.4	Zinc probes .....	114
4.1.5	Zinc screening.....	115
4.1.6	Aims.....	116
4.2	Results .....	116
4.2.1	Zinc probe selection .....	116
4.2.2	Assay optimisation .....	118
4.2.3	Zinc storage in Niemann-Pick disease cell lines .....	124
4.2.4	Plate uniformity testing.....	126
4.2.5	DMSO concentration effects on TSQ assay.....	127
4.2.6	Tool compound identification .....	128
4.2.7	Imidazole .....	134
4.2.8	Testing a potential Niemann-Pick therapeutic with zinc modulatory effects.....	137
4.2.9	Testing HDAC inhibitors with known benefit in Niemann-Pick cells <i>in vitro</i> .....	141
4.2.10	Zinc modulator screening .....	143
4.2.11	Hit screening .....	146
4.2.12	Hit analysis .....	150
4.3	Discussion .....	152
4.3.1	Aims of chapter .....	152
4.3.2	Analysis of hit compounds .....	154
4.3.3	Technical limitations .....	156
4.3.4	Future work.....	157
4.4	Conclusion .....	158
5	Investigation into cannabidiol and copaiba oil as potential therapeutics in Niemann-Pick.....	159

5.1	Introduction.....	159
5.1.1	aSMase regulation in LSD's/NPD.....	159
5.1.2	Cannabidiol.....	160
5.1.3	Cannabidiol in Niemann-Pick .....	161
5.1.4	Copaiba.....	162
5.1.5	Chapter aims .....	164
5.2	Results .....	164
5.2.1	aSMase activity in Niemann-Pick disease fibroblasts .....	164
5.2.2	Toxicity of cannabidiol and copaiba oil.....	166
5.2.3	Effect of cannabidiol and copaiba upon lysosomal storage in Niemann-Pick disease .	170
5.2.4	Effects of cannabidiol and copaiba on specific lysosomal lipid storage .....	178
5.2.5	Effects of cannabidiol and copaiba upon aSMase activity .....	190
5.2.6	Treatment of cell homogenate with cannabidiol and copaiba .....	196
5.2.7	Analysis of protein expression upon cannabidiol and copaiba treatment .....	200
5.2.8	Cannabidiol and copaiba effects upon transcription in Niemann-Pick.....	203
5.3	Discussion .....	206
5.3.1	Cellular tolerance to cannabidiol and copaiba treatments.....	206
5.3.2	Reduced lysosomal volume in cells treated with cannabidiol and copaiba.....	206
5.3.3	Reduction in lysosomal lipid storage .....	207
5.3.4	Activation of aSMase in vitro by cannabidiol and copaiba .....	207
5.3.5	Changes in protein expression and localisation.....	209
5.3.6	Cannabidiol and copaiba lead to nuclei localisation and thus activation of TFE3 .....	209
5.4	Conclusion .....	210
6	General Discussion.....	211
6.1	Summary.....	211
6.2	AQ7 is a novel lysosome specific probe. ....	211
6.3	Disease phenotype reducing compounds can be identified through zinc screening.....	212
6.4	Cannabidiol and copaiba increase aSMase activity in vitro and reduce NPA disease phenotype.....	214
7	Conclusion.....	216
8	Bibliography .....	217
9	Appendix .....	254
9.1	Appendix i.....	254
9.1.1	Table of therapeutic treatments in Niemann-Pick.....	254
9.2	Appendix ii.....	263
9.2.1	Hits from zinc phenotypic screening.....	263

9.3	Appendix iii .....	269
9.3.1	AQ7.....	269
9.3.2	Cannabidiol and copaiba .....	277
9.3.3	Western blot raw images .....	285
9.3.4	TSQ and zinc assay .....	287

# 1 Introduction

Niemann-Pick disease is a rare autosomal recessive lysosomal storage disease (LSD), characterised by the lysosomal accumulation of several lipids, primarily: glycosphingolipids, sphingomyelin, and cholesterol. Niemann-Pick, in common with other LSDs, is characterised by endocytic, and cellular recycling defects, which lead to diseases causing progressive physical and mental decline. Currently, enzyme replacement therapy is available for non-neuronal forms of Niemann Pick Type B (NPB), with only miglustat being approved for Niemann-Pick Type C (NPC), which helps to manage disease symptoms and slows the disease progression.

## *1.1 The endocytic system*

In Niemann-Pick and other lysosomal storage disorders, dysfunction occurs primarily in late endosomes and lysosomes, which form part of much larger intracellular trafficking pathway, the endocytic system. The endocytic system is a dual-purpose system, where in addition to the uptake of cellular metabolites, the pathway is also used to regulate cell surface receptors, as well as their downstream signalling pathways (Sorkin and von Zastrow 2009). The entry point into the endocytic system is through endocytosis, which can be broadly split into two mechanistically different pathways: clathrin mediated endocytosis or clathrin independent endocytosis (Kumari et al. 2010).

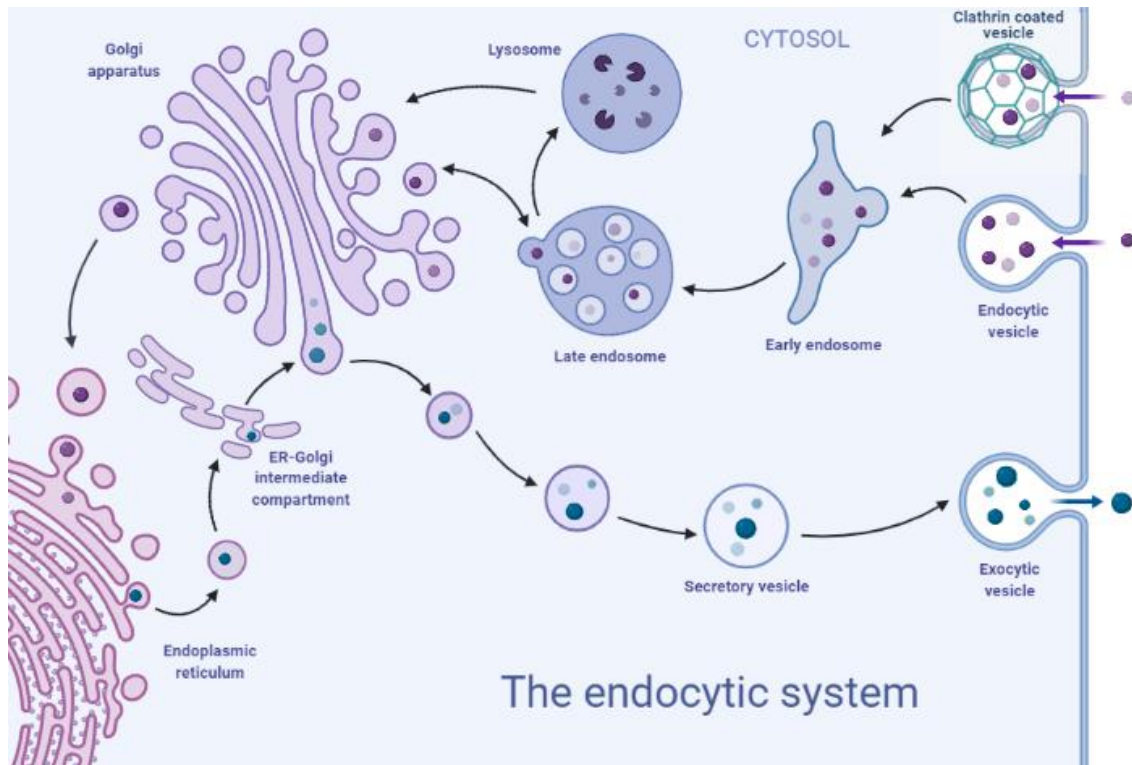


**Figure 1.1. Overview of the eukaryotic endocytic system**

The primary method of entry into the endocytic system is through endocytic vesicle formation, this can be clathrin mediated or clathrin independent. Endocytic vesicles undergo maturation from early to late endosomes which can become lysosomes (through fusion) or be transported to the Golgi. Vesicles from the Golgi are sorted with some vesicles destined for the Endoplasmic Reticulum (ER) and return to the Golgi for post translational modification. Some vesicles do not go to the ER and are instead directly exocytosed from the cells as secretory vesicles. Figure created using Biorender.

### 1.1.1 Clathrin mediated endocytosis

The primary method of endocytosis by mammalian cells, is through clathrin mediated endocytosis. Clathrin mediated endocytosis allows for targeted uptake of nutrients, as well as surface receptors (McMahon and Schmid 2007). Clathrin mediated endocytosis, occurs at specific sites on the cell membrane, which are enriched in clathrin, known as clathrin coated pits (Lampe et al. 2016). The process of clathrin mediated endocytosis can be dissected into four stages: initiation, stabilisation, maturation, and membrane fission (Mettlen et al. 2018). The four stages are controlled and proceed by a range of adaptor proteins, endocytic accessory proteins and dynamin to ensure vesicular fission (Schmid 2017).

### *1.1.2 Clathrin independent endocytosis*

Clathrin independent endocytosis, encompasses a range of different methods by which the cell can take up nutrients. A range of proteins are associated with clathrin independent endocytosis, including: flotillin, caveolae, and RhoA/Rac1 (Sandvig et al. 2011). Several of the proteins involved in clathrin independent endocytosis are involved in a number of endocytic pathways, therefore identifying a specific protein's role in one type of endocytosis remains an issue (Feng et al. 2010b). Clathrin independent endocytosis is responsible for the majority of fluid uptake by cells, possibly due to the nonspecific uptake of molecules through this process leading to increased endocytic requirements (Howes et al. 2010).

Both clathrin dependent and clathrin independent endocytosis, lead to the formation of endosomes, which require further intracellular sorting.

### *1.1.3 Endosomes*

Upon internalisation, endosomes can enter several different intracellular pathways depending on endosomal contents. Upon internalisation, the contents of endosomes are sorted, e.g. proteins being ubiquitinated can be sorted, and accumulate in vacuolar regions of the endosome (Geuze et al. 1987). The unselected residual constituents of the endosomes, such as cell surface receptors, are sorted and associated with the tubular microdomain (Mayor et al. 1993). These tubular microdomains can then be recycled to the cell membrane, in a process regulated by Rab4 or Rab11 (Mayor et al. 1993). The vacuolar regions of the endosomes are sorted and trafficked through early endosomes, to the point whereby endosomes undergo maturation into late endosomes; facilitated by recruitment and activation of a range of GTPases, including Rab5 and Rab7 (Somsel Rodman and Wandinger-Ness 2000). Late endosomes, unlike early endosomes, frequently contain multilamellar regions, which are believed to be required for late endosomal function; particularly for lipid and protein transport (Bissig and Gruenberg 2013). Late endosomes are known to undergo fission with lysosomes, allowing transfer of lumen contents, through a mechanism termed kiss-and-run (Luzio et al. 2007). Late endosomes are primarily characterised by an increasingly acid internal environment, driven by vATPase proton pumps (Lafourcade et al. 2008). Additionally, membrane proteins, including LAMP1 and

LAMP2 are present on late endosomes, which form part of the glycocalyx to prevent autolysis; due to the presence of luminal acid hydrolases and increased luminal acidification.

The final step in the degradatory endocytic pathways is the formation of lysosomes, which are extremely similar to late endosomes. Late endosomes and lysosomes are difficult to differentiate using conventional light microscopy, the two types of vesicles have differing physical properties, with lysosomes being denser than late endosomes, when separated by subcellular fractionation (Scott et al. 2014).

## *1.2 Lysosomes*

Lysosomes are membrane bound organelles, that are primarily involved in cellular macromolecule catabolism. Whilst originally believed to only be responsible for macromolecule catabolism, the lysosome has subsequently been identified to be involved in several other cellular processes, including several signalling pathways and autophagy (Yim and Mizushima 2020; Settembre and Perera 2024). Lysosomes function as crossroads for several different pathways, with lysosomes being the terminal state of endocytosis, after endosomes. Lysosomes can also interact and transfer materials to other organelles, including Golgi, Endoplasmic Reticulum (ER) and mitochondria (Lee and Blackstone 2020; Wang et al. 2023; Zhou et al. 2023).

The products from the lysosomal degradation can either be transported to either the ER or to the Golgi for recycling into new cellular components, or to be exported from the cell through exocytosis (Wu et al. 2014).

### *1.2.1 Structure of a lysosome*

The key defining feature of a lysosome is the acidified environment within the lumen of the organelle, with lysosomal pH of 4 – 4.5, compared to the cytosol with a pH of 7 – 7.5. To prevent autolysis, a thick glycocalyx is present on the luminal side of the lysosomal membrane.

The glycocalyx is primarily comprised of LAMP1 and LAMP2 proteins, along with a layer of polysaccharides, which form a physical barrier from the lysosomal lumen to the phospholipid bi-layer and prevents access of degradative factors to the bi-layer (Wilke et al. 2012).

Also present within the lysosomal membrane, are a range of transporters and receptors, including: TRMPL1, ZnT4, NPC1, and vATPase, which are involved in a range of signalling pathways, as well as maintaining lysosomal ion homeostasis and pH regulation (Winchester 2001). To ensure acidic lysosomal pH, vATPase functions as a proton pump to maintain the required proton concentration within the lysosomal lumen. Acidification of the intracellular environment is one of the key defining features of lysosomes, with early endosomes having pH of 6.5, close to the cytosol, with late endosomes having a pH of approximately 5.5, compared to that of lysosomes, which are broadly pH 4.5 (Hu et al. 2015). Additionally, lysosomes can be differentiated from late endosomes by the absence of Mannose-6-phosphate receptors (Pohlmann et al. 1989). LAMP family proteins, specifically LAMP1 & LAMP2 are frequently used as lysosomal markers, however they can also be present; albeit at lower concentrations in endosomes (Cook et al. 2004).

### *1.2.2 Biogenesis*

As well as being the major site of macromolecule catabolism, the roles lysosomes play in several signalling pathways, requires tight regulation to ensure correct signal control. In mammals, many of the genes that encode proteins involved with lysosomes or autophagy contain the 'coordinated lysosomal expression and regulation' (CLEAR) sequence. Contained within the CLEAR sequence is an E-box sequence, which is recognised by the MiT/TFE family of transcription factors (Yang and Wang 2021). Members of the MiT/TFE family of transcription factors includes both TFEB and TFE3 (La Spina et al. 2021). TFEB and TFE3 have been shown to bind to CLEAR elements, in turn leading to the upregulation of synthesis of lysosome associated proteins, promoting lysosome biogenesis (Palmieri et al. 2011).

TFEB and TFE3, under normal conditions are phosphorylated, and localised to lysosomal membranes (Puertollano et al. 2018). However, upon cellular stress, such starvation or other requirements for increased lysosomal activity, TFEB or TFE3 can be dephosphorylated, by a range of kinases, including mTOR, Akt and PKC (Chen et al. 2017). Dephosphorylation of TFEB/TFE3 leads to the transcription factors dissociating from lysosomal membranes, and moving to the nucleus where they bind CLEAR elements and upregulation of CLEAR genes occurring (Raben and Puertollano 2016).

### *1.2.3 Lysosomal enzymes*

The primary role of lysosomes, over endosomes, is the catabolism of macromolecules including; various lipids, polysaccharides, and proteins. Over 50 different acid hydrolases that are present within lysosomes have been identified; broadly characterised by their acidic pH optimum. This acidic pH optimum is required to ensure that enzymatic activity does not occur outside of lysosomes, where degradation is not required. Several lysosomal acid optimum enzymes also have neutral pH preference homologs, such as acid sphingomyelinase (aSMase) and neutral sphingomyelinase (nSMase) that are structurally very similar (Marchesini and Hannun 2004). Loss of expression or activity of any the acid hydrolases present within the lysosome leads to specific lysosomal storage disorders; due to the accumulation of undegraded enzyme specific substrate.

#### *1.2.3.1 Lysosomal enzyme biogenesis*

The majority of lysosomal enzymes synthesis is regulated by the CLEAR pathway. Transcription of mRNA for lysosomal enzymes occurs in the nucleus, with protein synthesis occurring within the rough ER. In the ER, pre cursor proteins are produced; usually with an additional 20-25 amino acids at the N terminal for ER trafficking as well as being glycosylated (Helenius and Aebi 2001). Precursor proteins are then trafficked from the ER to the Golgi, with enzymes destined for lysosomes having mannose rich oligosaccharides tagged with the mannose-6-phosphate motif (Lazarino and Gabel 1989). Within the Golgi are mannose-6-phosphate receptors, which sort the mannose-6-phosphate tagged lysosomal enzymes, allowing for their concentration (Kornfeld et al. 2003). These regions enriched with lysosomal enzymes are trafficked to lysosomes by clathrin coated vesicles (Brault and Bonifacino 2009). Several lysosomal enzymes require proteolytic activation for enzymatic activity, with several enzymes having a domain on the N terminal that requires cleavage for activation, usually by one of the cathepsin family of protease proteins (Roberts 2005). Thus, the requirement of proteolytic activation, only possible at lysosomal pH prevents prior activation of lysosomal enzymes and prevents autolysis at earlier stages of the enzyme synthesis and trafficking pathway.

### *1.2.4 Autophagy*

The major role of the lysosome in a cell at resting state, is the degradation of macromolecules delivered by endocytosis. However, lysosomes are also the endpoint of autophagy, where they degrade material delivered to them via autophagosome-lysosome fusion (Klionsky et al. 2014). Autophagy can be used to remove and recycle damaged, or superfluous organelles, or provide essential nutrients under times of starvation. One of the more well documented drivers of autophagy is mTORC1, whereby upon starvation conditions, mTORC1 is inactivated, leading to nuclear localisation of TFEB/TFE3 (Settembre et al. 2013).

Crucial to the ability of the cell to carry out autophagy are the SNARE proteins, which facilitate the membrane fusion of autophagosomes with lysosomes. To prevent premature or non-specific fusion, specific SNARE proteins are required, such as STX17, which is only found on mature autophagosomes, and thus only these can bind to lysosomes (Yim and Mizushima 2020). The resulting products from autolysosome degradation can be trafficked out from the lysosome, to be reused by other organelles (Xu and Ren 2015).

### *1.3 Lysosomal storage disorders*

Lysosomal storage disorders (LSDs) are a group of over 70 individually rare genetic metabolic disorders (Platt et al. 2018). Despite a range of underlying mutations, all disorders lead to defects in lysosomal function. Most lysosomal disorders are caused by mutations in a lysosomal enzyme involved in a degrading pathway. Lipid-degrading enzyme mutations are particularly common in LSDs including: Tay-Sachs, Krabbe, and Farber disease, however other proteins can lead to LSDs, such as membrane transport proteins, as present in NPC and Mucopolysaccharidosis type 4 (ML IV).

#### *1.3.1 Classification*

As well as being grouped by the type of protein deficiency, due to the highly heterogeneous nature of lysosomal diseases, they can be grouped based on the class of molecule that accumulates.

### 1.3.1.1 *Sphingolipidoses*

Sphingolipids are a group of lipids composed of sphingoid base or 'tail' joined to a variable 'head' domain, such as a fatty acid domain in ceramide, or a phosphocholine head group in sphingomyelin. Sphingolipids are a major constituent of mammalian cell membranes, forming chemically inert lipid bilayer. Additionally, some sphingolipids, such as ceramide and sphingosine, are important signalling molecules, involved in pathways including apoptosis and inflammation.

Sphingolipidoses share commonality in defects in the sphingolipid degradation pathway, driven by mutations in genes coding for these enzymes, in turn leading to either translational defects, or proteins that lack enzymatic activity. More common examples of sphingolipidosis include: Gaucher disease (most common single LSD), Fabry disease, and Krabbe disease with deficiencies in: glucocerebrosidase,  $\alpha$ -galactosidase, and galactosylceramidase leading to primary accumulation of glucosylceramide globotriaosylceramide and galactosylsphingosine (psychosine) respectively (Abed Rabbo et al. 2021).

Several sphingolipidosis share common symptoms, such as organomegaly, and thus diagnosis can be difficult to determine, due to the need to carry out biochemical characterisation to identify the protein defect driving the disease. Both Niemann Pick A/B and NPC are members of the sphingolipidosis family of lysosomal storage disorders, with the accumulation of sphingomyelin in NPA/B and sphingosine/cholesterol in NPC.

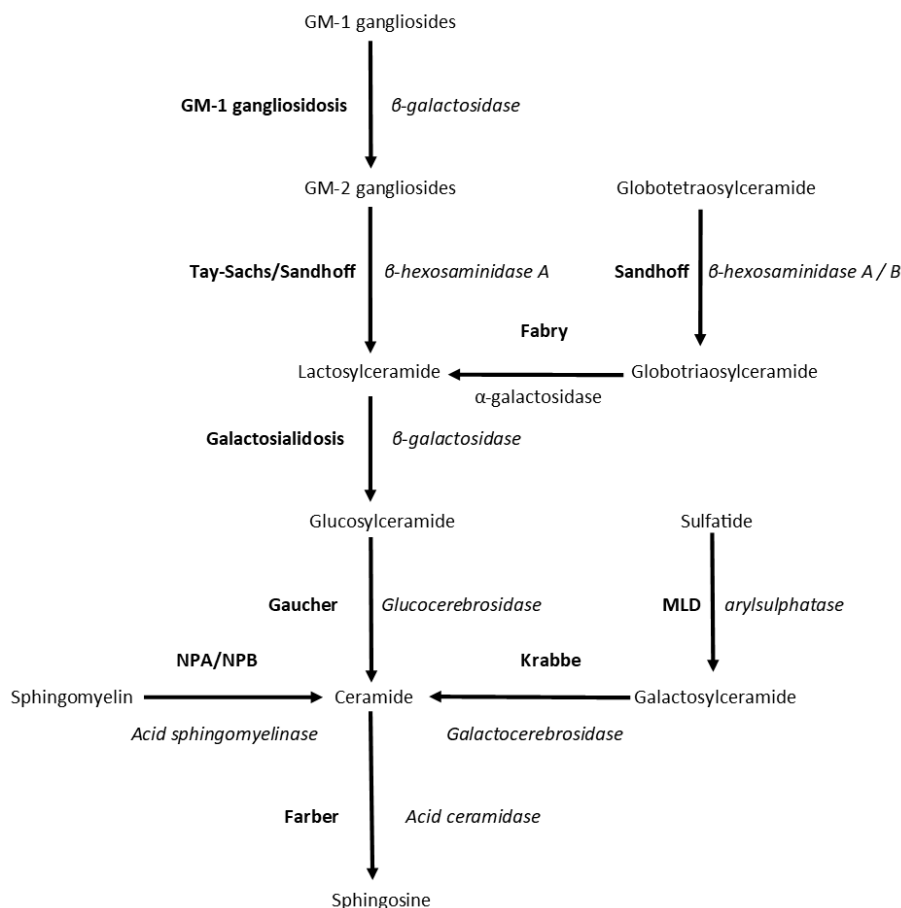


**Figure 1.2. Sphingolipid degradation pathway and associated diseases**

*Lysosomal sphingolipid catabolism pathways and associated diseases and enzymes involved. Sphingolipidosis, share defects in lipid degrading enzymes, which eventually leads to the production of ceramide or sphingosine. Diseases associated with enzymatic activity loss are highlighted in bold, with the enzyme regulating each step italicised. NPA- Niemann-Pick type A, NPB- Niemann-Pick type B, MLD- Metachromatic leukodystrophy.*

### 1.3.1.2 Mucopolysaccharidoses

Another broad group of lysosomal storage disorders are the mucopolysaccharidoses, whereby glycosaminoglycans (GAGs) accumulate within lysosomes. Glycosaminoglycans are comprised of repeating units of uronic and amino sugars, and can be split into four groups, heparin, chondroitin, keratan, and hyaluronic acid (Sasisekharan et al. 2006). The primary role of GAGs is as structural support of tissues, such as keratin sulfate and chondroitin sulfate, which acts as a scaffold matrix, often closely associated with collagen, and are found in high concentrations within tendons and cartilage. Due to the highly polar nature of GAGs, they are often utilised for the maintenance of cellular hydration, and are frequently found in cosmetic products, such as hyaluronic acid.

Examples of mucopolysaccharidoses include: Hurler Syndrome (MPS I), Morquio syndrome (MPS IV), and Sanfilippo syndrome (MPS III). Patients are frequently characterised by skeletal abnormalities, caused by accumulation of partially degraded GAGs, within bones leading to distinct skeletal deformities, termed dysostosis multiplex and gingival hyperplasia (White 2011). The accumulation of GAGs also leads to developmental delays and impaired organ function, with an associated, but variable prognosis, ranging from infant mortality as frequently observed in Hurler syndrome, to death within early adulthood, as seen with Scheie syndrome.

### *1.3.1.3 Mucopolipidoses*

Mucopolipidoses are characterised by defects in lysosomal enzyme processing or trafficking defects. I-cell disease (ML II) is characterised by mis-trafficking of lysosomal enzymes, due to defects in mannose-6-phosphate tagging, caused by loss of function of N-acetylglucosamine-1-phosphate transferase. Whilst N-acetylglucosamine-1-phosphate transferase is a Golgi localised enzyme, it is responsible for tagging of enzymes destined for the lysosome, and thus this loss of activity causes mis-trafficking and extracellular export of lysosomal enzymes (Kollmann et al. 2012). ML III or Pseudo-Hurler polydystrophy is also caused by the loss of N-acetylglucosamine-1-phosphate transferase activity, but more residual activity remains than in I-cell, and thus leads to a less severe disease phenotype (Raas-Rothschild et al. 2000). The loss of mannose-6-phosphate tagging leads to mis-trafficking and cellular secretion of lysosomal enzymes, in turn leading to the accumulation of partially degraded lipids, glycosaminoglycans (GAGs), and other macromolecules within lysosomes.

Unlike most other lysosomal disorders, MLIV is caused by deficiencies in a transmembrane transporter, TRPML1. As TRPML1 is a lysosomal ion channel, mutations within TRPML1 lead to lysosomal signalling and consequently trafficking defects within endosomes and lysosomes (Soyombo et al. 2006).

Mucopolipidosis can present similarly to mucopolysaccharidoses, often sharing the same skeletal deformities as observed in mucopolysaccharidoses diseases (dysostosis multiplex and gingival hyperplasia). Additionally, organomegaly commonly occurs along with developmental delays and mucosal thickening and subsequent airway narrowing, with corresponding repeat upper airway infections (Raas-Rothschild et al. 2000). Life expectancy is varied in mucopolipidosis, based on the disease and the severity of the mutation, with most

patients with mucopolysaccharidosis not surviving beyond a second decade of life, with more severe forms leading to death within the first decade of life.

#### *1.3.1.4 Oligosaccharidoses*

Diseases that are in the oligosaccharidosis family, are characterised by the storage of glycoproteins, and incomplete degradation of oligosaccharides (Bonesso et al. 2014). Glycoproteins, through their post-translational modification are involved in numerous intracellular and extracellular processes, including promotion of correct folding and improvement in protein stability, intracellular localisation (Mannose 6-phosphate), and cell to cell recognition. When glycoproteins are degraded, oligosaccharides are normally first present as glycans, joined to specific amino acid residues, such as: asparagine, threonine, or serine. During lysosomal catabolism, glycans are further broken down in a sequential process into constituents, such as mannose.

Examples of oligosaccharidosis include  $\alpha$ -mannosidase,  $\alpha$ -fucosidosis and Aspartylglucosaminuria, caused by loss of activity in:  $\alpha$ -D-mannosidase,  $\alpha$ -L-fucosidase and aspartylglucosylamine deaspartylase (Casado et al. 2017). Loss of any enzymes in the oligosaccharides degradation pathway leads to lysosomal accumulation of partially degraded oligosaccharides, such as N-acetylglucosamines in Aspartylglucosaminuria (Arvio and Mononen 2016). As is common with most LSDs, patients frequently have neurological issues and frequently possess skeletal defects, which are similar those observed in mucopolysaccharidoses.

#### *1.3.1.5 Neuronal Ceroid Lipofuscinoses*

Neuronal Ceroid Lipofuscinoses (NCLs) are characterised by the lysosomal localisation of auto-fluorescent lipopigments that contain mitochondrial ATP synthase subunit C and/or saposin D. At present, at least 14 NCLs have been identified, with the diseases in this group being commonly known as Batten's disease. NCLs have an extremely broad range of underlying protein defects, including both transporters and enzymes. Examples of NCLs include CLN3 and CLN8, which affects Cathepsin D, a proteolytic enzyme, and CLN1, which affects palmitoyl protein thioesterase 1, disturbing Mannose-6-phosphate signalling (Nittari et al. 2023).

NCLs can also be classified by age of symptom onset, with CLN1 being an early infantile form of the disease, CLN2 a late infantile onset, and CLN3, which is a juvenile onset form of

Batten's disease. NCL patients commonly suffer with symptoms such as: progressive epilepsy, blindness, and ataxia

#### *1.3.1.6 Glycogen storage disorders*

Glycogen storage disorder type 2, or Pompe disease, is an outlier amongst lysosomal storage disorders, being the only disease characterised by defects in glycogen metabolism. Glycogen is one of the primary sources of glucose for use in aerobic respiration, and thus the ability to convert glycogen into glucose is critical for maintenance of homeostasis, as well as meeting the glucose synthesis requirements at times of high aerobic metabolic load. Thus, the loss of activity in acid  $\alpha$ -glucosidase, which metabolises glycogen into glucose leads to accumulation of lysosomal glycogen, causing Pompe disease.

Pompe disease is broadly classified by age on onset, into early onset (infantile) and late onset, or juvenile/adult form, with the difference being driven by the severity of the mutation in acid  $\alpha$ -glucosidase. Patients with Pompe disease report skeletal muscle weakness and have hypertrophic cardiomyopathy. Patients with juvenile onset Pompe disease also frequently have impaired motor function.

One other disease associated with glycogen storage disorders is Danon disease, which historically was grouped with Pompe disease (Endo et al. 2015). However, Danon disease is caused by deficiencies in the membrane protein LAMP2, which leads to impairments in autophagy (Rowland et al. 2016). This impairment in autophagy leads to rapid and progressive cardiomyopathy, similar to that observed with Pompe disease (D'Souza et al. 2014). Additionally, patients with Danon disease also frequently have muscle weakness, and retinopathy has also been observed in some patients (Thiadens et al. 2012). Danon disease is more common in males, and often show symptoms at younger ages, with death, due to cardiac disease occurring in the second or third decade of life. Females diagnosed with the disease often have later onset of disease symptoms, often during the third decade of life, with patients being reported as living into their fifth decade.

#### *1.3.2 Prevalence*

Each lysosomal storage disease is individually rare, with incidence rates ranging from 1:50,000 to fewer than 1:2,000,000. When grouped together, lysosomal storage disorders occur in approximately 1:5,000 live births (Pinto et al. 2004). The most common LSD is

Gaucher disease, caused by a mutation in the GBA gene, leading to deficiencies in glucocerebrosidase activity, resulting in glucocerebroside accumulation (Sun 2018). One of the rarer LSDs is  $\alpha$ -fucosidosis, which has an incidence rate of 1:2,000,000, with fewer than 100 documented cases in the last 60 years. (Stepien et al. 2020).

The prevalence of Niemann-Pick is extremely low, with acid sphingomyelinase deficiency (ASMD)/NPA&NPB occurring in approximately every 1:250,000 births (Meikle et al. 1999). Niemann-Pick type C is more common than NPA/NPB, with the disease occurring in roughly 1:120,000 births based on current estimates in European populations (Vanier and Millat 2003). However, geographical regions have different incidence rates, with higher prevalence observed in eastern Canada, with an incidence rate of 1:80,000 (Labrecque et al. 2021).

#### ***1.4 Drug discovery in lysosomal storage disorders***

Despite the underlying genetic and protein differences between lysosomal storage disorders, the therapies that have been developed can be broadly grouped into three categories: small molecule, enzyme replacement, and gene replacement. A table showing all molecules to have gone through clinical trial for Niemann-Pick disease as of May 2024, is included in *Appendix i*.

##### ***1.4.1 Small molecule therapies***

Small molecule therapies are molecules able to bring about therapeutic benefit *in vitro* and *in vivo*. In lysosomal storage disorders, they can be split into three groups depending on the molecule's mechanism of action, either: substrate reduction therapies, pharmacological chaperones, or autophagy modulators.

Small molecule therapies have the advantage of normally having the least invasive administration process, with most being taken orally. Additionally, a variety of pathways can be targeted with small molecule therapies, and molecules have the potential to be used in combination. Compared to enzyme replacement therapy and gene replacement therapies, small molecule therapies usually have the lowest cost for treatment.

However, small molecule therapies in lysosomal storage disorders, are rarely able to target the underlying cause of the disease and instead target pathways linked to the mutant protein. Therefore, small molecules are not directly treating the underlying cause of the

disease, such as substrate reduction therapies, and instead reducing disease burden or managing the disease symptoms.

#### *1.4.1.1 Substrate reduction therapies*

Substrate reduction therapies are the most common of the approved treatments for lysosomal storage disorders. The first molecule to gain FDA approval was miglustat, an inhibitor of ceramide glucosyltransferase (Pastores 2012). By inhibiting ceramide glucosyltransferase, this prevents the synthesis of glucosylceramide from ceramide. Glucosylceramide is a key starting point for the synthesis of several lipid synthesis pathways, and therefore reducing the concentration of glucosylceramide reduces cellular ability to carry out synthesis of more complex glycosphingolipids (Shayman 2018). Therefore, by reducing cell's ability to synthesise these lipids, this leads to reductions in lysosomal lipid storage. Miglustat was originally trailed, and approved for the treatment of Gaucher disease, where glucosylceramide is the primary storage molecule. However, it has subsequently been approved for use in Fabry and Niemann-Pick type C diseases, where it reduces levels of globoside (primary storage) and ganglioside (secondary storage) respectively. Since the approval of miglustat, a range of other substrate reduction therapies have undergone clinical trial, including: eliglustat, lucerastat, and venglustat (Fernández-Pereira et al. 2021).

Eliglustat, lucerastat and venglustat are all glucosylceramide synthase inhibitors, as is miglustat, however eliglustat and venglustat are structurally dissimilar, whilst lucerastat is an iminosugar similar to miglustat. One advantage of both eliglustat and lucerastat over miglustat, is the reduction in side effects, particularly GI issues, such as diarrhoea (Guérard et al. 2017; Mistry et al. 2023). Venglustat has been shown to be a more potent inhibitor of glucosylceramide synthase than miglustat and to show better brain penetrance (Schiffmann et al. 2023).

#### *1.4.1.2 Pharmacological chaperones*

Another group of small molecule therapeutics is pharmacological chaperones, which promote correct protein folding and prevent aggregation of misfolded protein, and therefore can be used in lysosomal storage disorders where folding defects occur. Pharmacological chaperones include migalastat, which binds directly to the active site of  $\alpha$ -Galactosidase A and promotes the correct folding of the mutant protein within the ER.

Increasing the percentage of  $\alpha$ -Galactosidase that folds correctly, will lead to more of the active enzyme reaching the lysosome. Additionally, some Histone deacetylase (HDAC) inhibitors have been shown to lead to increases in upregulation of heat shock proteins that promote correct protein folding. Examples of these include vorinostat and panobinostat, with vorinostat increasing the unfolded protein response, including upregulation of HSP90 (Kahali et al. 2010).

It is believed that vorinostat and panobinostat function as HDAC inhibitors, in turn leading to epigenetic changes and increased expression of mutant NPC1. It is postulated that with increase synthesis of NPC1, more lysosomal localisation of mutant NPC1 will localise to lysosomes, with enough residual activity to correct the cholesterol accumulation and restore trafficking out of lysosomes (Pipalia et al. 2017). Vorinostat underwent phase I/II clinical trials for NPC, however, at present has not progressed further, with panobinostat being shown to beneficial *in vitro*.

Some compounds are able to activate the heat shock response, whilst not being HDAC inhibitors, including molecules such as arimoclomol. Arimoclomol upregulates HSP 70 and is believed to promote correct folding of misfolded proteins within the ER, leading to more functional NPC1 reaching lysosomes (Kirkegaard et al. 2010).

#### **1.4.1.3 Autophagy modulators.**

Proteostasis is required to ensure correct regulation of synthesis, trafficking, and the degradation of intracellular proteins. Some autophagy activations, such as celastrol, which has been shown to inhibit Akt and mTOR kinases leads to promotion of autophagy (Liu et al. 2019). Additionally, celastrol has been shown to have a secondary effect in upregulating heat shock response (Westerheide et al. 2004). Molecules that are known to upregulate autophagy can be used in combination with molecules that activate the heat shock pathway, have been suggested as dual therapies in LSDs with folding defects, to promote both correct lysosomal folding and lysosomal protein localisation (Mu et al. 2008).

Genistein has been shown to have a mechanism of action through TFEB activation (Argüello et al. 2021). Because of this upregulation in TFEB, glycosaminoglycans levels were found to be reduced and thus the molecule has potential as a treatment option in mucopolysaccharidosis (Moskot et al. 2014). However, genistein also inhibits

glycosaminoglycan synthesis, so it is unclear whether all of the effects are through TFEB activation, or if some are also being driven by reduced glycosaminoglycan synthesis (Piotrowska et al. 2006).

Additionally, upregulating autophagy may help to lead to further substrate reduction, in pathways not directly associated with the disease specific mutation. Therefore, activating TFEB has the potential to be an effective treatment for most LSDs, independent of the underlying genetic, and protein defects.

### *1.4.2 Enzyme replacement therapies*

Until recently, enzyme replacement therapies (ERT) have, where available, been the preferred treatment option for LSDs. With ERT, patients have recombinant protein transfused intravenously to correct for the enzyme deficiency that is causing the disease.

With ERT, the main source of therapeutic benefit is through restoration of lysosomal enzyme activity, driven by the recombinant protein entering cells through endocytosis and reaching the lysosome. Upon reaching the lysosome the recombinant protein restores the defective degradation pathway, alleviating lysosomal storage. Additionally, some recombinant protein remains extracellular, and thus can reduce the extracellular concentrations of the molecules driving the disease. and restores activity upon entry to the cell and trafficking to the lysosome.

The first ERT to be approved was alglucerase for Gaucher disease in 1991, however this therapy used  $\beta$ -glucocerebrosidase enzyme extracted from human placenta (Deegan and Cox 2012). Alglucerase was quickly withdrawn from the market as it was replaced by imiglucerase, a recombinant form of  $\beta$ -glucocerebrosidase. A further 7 LSD have had enzyme replacement therapies approved:  $\alpha$ -Mannosidosis, NPB, Fabry, Hunter syndrome, Hurler-Scheie, Maroteaux-Lamy, and Pompe disease (Lachmann 2011). Enzyme replacement therapies are also currently undergoing clinical trials for San Filippo disease and metachromatic leukodystrophy. It is likely that other lysosomal disease will have recombinant enzyme therapies undergo clinical trials in the future.

Enzyme replacement therapies have the advantage of being able to directly replace the missing protein present in the lysosomal storage disease. Therefore, ERT can directly treat

the underlying disease cause, and reduce the lysosomal storage through compensating for the defective protein. ERT can therefore lead to significant improvement in patient health and quality of life; and with continued treatments, reversal in disease progression can be observed.

However, ERT due to the production methods and administration methods is expensive and complicated to produce, as well as requiring fortnightly or monthly transfusions for life. - Additionally, ERT is only suitable for a sub-population of patients with LSDs, usually those with no neuronal disease pathology. This is due to the enzyme not being able to cross the blood brain barrier, and thus no improvement is observed in neuronal manifestations. Additionally, it is possible for immune response to be triggered with ERT, due to the external source of the recombinant protein (Coutinho et al. 2016).

### *1.4.3 Gene replacement therapies*

Gene replacement therapies are based upon ex-vivo gene correction. Cells are extracted from a patient (usually HSCs), the underlying mutation in the gene is corrected, and the cells transfused back into the patient. Gene replacement therapies have been developed and are undergoing clinical trials for a range of lysosomal storage diseases, including Fabry, Pompe, Gaucher, and Krabbe. At present only lenmeldy has been approved for a lysosomal storage disorder, for the treatment of metachromatic leukodystrophy (Mullard 2024). The treatment sees patients' Hematopoietic stem cells (HSCs) removed and treated with the gene replacement, leading to lasting correction in the HSC pool. These HSCs are then transplanted back in the patient (Horgan et al. 2023).

Gene replacement therapies are the newest of the possible treatment options for LSDs. However, they have been used frequently in other diseases, particularly blood disorders. Gene replacement therapies have the distinct advantage of being curative, requiring only one round of treatment, if successful. However, gene replacement therapies, are particularly invasive, require HSC stem cell extraction, in addition to how the therapy is delivered, whether that be intra cranial or IV transplantation. Therefore, if patients are immunocompromised or struggling with other disease effects, then they may not be able to receive the therapy.

### 1.5 Niemann-Pick disease

Niemann-Pick disease can be broadly classified into two distinct forms based on the underlying pathological cause of the disease, Niemann-Pick Type A/B (NPA/B), now classified as ASMD and Niemann-Pick Type C (NPC). Both types of Niemann-Pick disease share several overlapping pathological hallmarks. However, the underlying genetic cause differs between the two forms, and distinct biochemical differences can be observed between the two forms of the disease. Despite their differing underlying driving factors causing NPA/B and NPC, they all classified as Niemann-Pick disease based on a similar presentation that includes: hepatomegaly and splenomegaly, anaemia, cherry red spot of the macula with progressive blindness, and progressive mental and physical deterioration (Heitz et al. 2017). On a molecular level, Niemann-Pick disease cells also have sphingomyelin storage, to varying levels (Newton et al. 2018).

Niemann-Pick Type A and B are both caused by mutations in the *SMPD1* gene, which encodes acid sphingomyelinase (aSMase), a lysosomal enzyme that breaks down sphingomyelin into ceramide and phosphorylcholine (Wasserstein et al. 2006).

Differentiation between NPA and NPB is normally based on the disease phenotype, with NPB usually presenting as adult onset as a less severe form of NPA (Schuchman and Desnick 2017). The underlying genetic mutations in *SMPD1*, and subsequent aSMase mutations causing NPA/B are extremely varied, with over 180 mutations currently identified (Zampieri et al. 2016). The mutations that have been identified in the *SMPD1* gene include: point mutations, splicing abnormalities, whilst small deletions have also been reported in patients with NPA (Hu et al. 2021a). Additionally, no single loci of the *SMPD1* gene has been identified as being responsible for the loss of activity of the subsequent mutated aSMase (Hu et al. 2021a).

Whilst Niemann Pick Type A/B is associated with the lysosomal accumulation of sphingomyelin, NPC is primarily characterised by lysosomal cholesterol trafficking defects. NPC is caused by mutations in the *NPC1* or *NPC2* gene and protein, with 95% of cases being caused by mutations in *NPC1* (Shammas et al. 2019). NPC Intracellular Cholesterol Transporter 1 (*NPC1*) is believed to act as cholesterol transporter; trafficking cholesterol and other metabolites out of the lysosome in collaboration with *NPC2* (Walkley and Suzuki 2004). To date over 400 mutations have been identified in the *NPC1* gene, however, unlike

NPA/B, a small set of point mutations lead to majority of cases of NPC (McKay Bounford and Gissen 2014). In the UK, the two most commonly identified mutations leading to NPC are the I1061T and P1007A mutations, which comprise approximately half of the 75 NPC cases in the UK (Millat et al. 1999; Millat et al. 2005; Imrie et al. 2015). The most common biomarker for Niemann-Pick disease is storage of cholesterol, which is routinely used to diagnose NPC disease, however cholesterol storage can vary depending on the NPC1 mutation (Ribeiro et al. 2001).

## ***1.6 Cholesterol metabolism***

In humans, sterols, primarily cholesterol, are required for the regulation of membrane fluidity in addition to being a constituent for steroid based hormone synthesis (Yeagle 1991). Cells have several ways of obtaining cholesterol, including through endocytosis, and depending on the cell type cholesterol can be synthesised *de novo* by one of two pathways.

### ***1.6.1 Cholesterol uptake by endocytosis***

The majority of cholesterol uptake in the cells is through clathrin dependant endocytosis, with cholesterol entering the cell as low-density lipoprotein (LDL) (Grant and Donaldson 2009). When LDL enters the lysosome, it is cleaved by acid lipase (*Figure 1.3*) to produce free cholesterol, thus providing the major route for intracellular cholesterol catabolism (Li and Zhang 2019). Several other lipids, including sphingomyelin are frequently taken up as part of lipid rafts by clathrin independent endocytosis. The cholesterol is then trafficked out of the lysosome to a range of organelles, including the nucleus, however most cholesterol is transported to the ER or Golgi (Arenas et al. 2017). Lysosomal cholesterol trafficking is carried out by membrane bound proteins, including LIMP2 and NPC1, found exclusively in late endosomes and lysosomes (Shammas et al. 2019; Sakane et al. 2020).

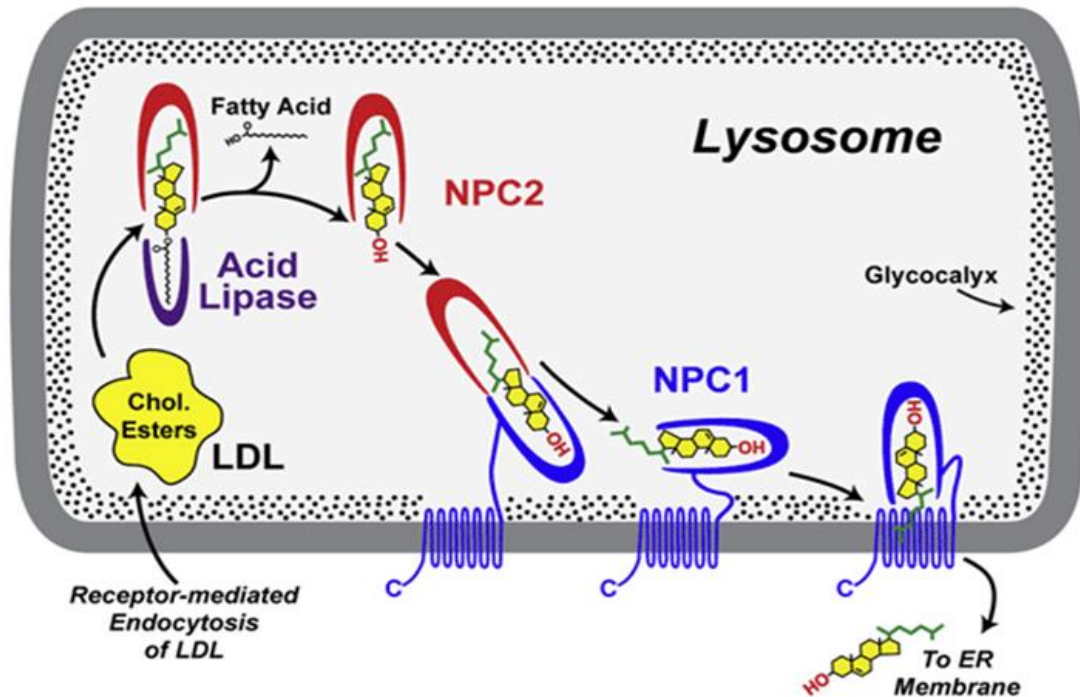


**Figure 1.3. Schematic of cholesterol trafficking through the lysosome mediated by NPC1 and NPC2**

Cholesterol enters the lysosome as cholesterol esters, which undergo cleavage by acid lipase to form cholesterol and free fatty acid. This free cholesterol is then chaperoned to the membrane by NPC2, whereby the cholesterol is transferred to NPC1 and actively exported from the lysosome. Figure adapted from Kwon et al 2009.

### 1.6.2 Intracellular cholesterol synthesis

Cholesterol can be synthesised intracellularly from HMG-CoA in a multi-step pathway known as Bloch and Kandutsch-Russell pathways (Figure 1.3) (Mazein et al. 2013), with preference for each pathway dependant on cell type. It is not known why two pathways for synthesising cholesterol have been conserved evolutionarily, nor is it known why cells show a preference for one pathway over the other. For example, testes and adrenal glands show a distinct preference for the Bloch cholesterol synthesis pathway, whilst: skin, preputial glands, and brain showed almost exclusive use of the Kandutsch-Russell pathway (Mitsche et al. 2015).

Recent work has suggested that cells may have a preference for one cholesterol synthesis pathway due to an intracellular requirement for one of the intermediates, which may be utilised by cells as a starting point for another synthesis pathway, such as bile acid synthesis (Wang et al. 2021).

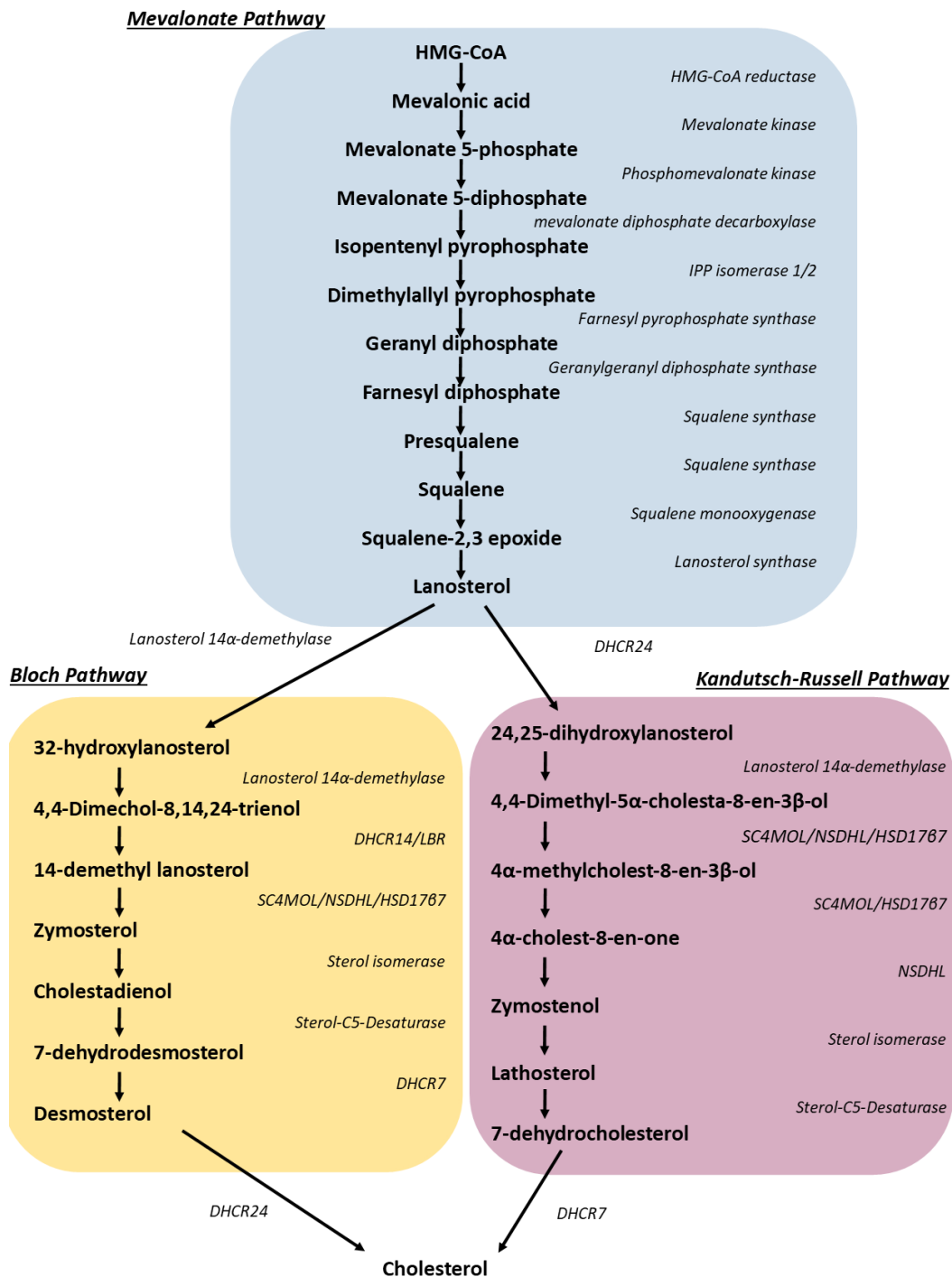


**Figure 1.4. De novo cholesterol synthesis pathways**

Intracellular cholesterol biosynthesis initially requires the reduction of HMG-CoA to form mevalonic acid, which is the rate limiting step in cholesterol synthesis de novo. The synthesis steps as far as lanosterol are shared between the Bloch and Kandutsch-Russell pathways, however the step following the synthesis of lanosterol is where the two pathways diverge. Whilst similar enzymes catalyse the steps of the two pathways, the order of the reactions differs between the two pathways, the Bloch pathways also utilises DHCR14/LBR, which is not used in the Kandutsch-Russell pathway. The two pathways show cell type specificity, with tissues preferring specific pathways. Reaction pathways steps was created using data from (Sharpe and Brown 2013).

## ***1.7 Sphingomyelin metabolism***

Sphingomyelin is an essential sphingolipid, and a major constituent of mammalian cell membranes. Unlike other mammalian lipids, sphingomyelin has been demonstrated to be crucial for cell growth *in vitro*, with loss of cells ability to produce sphingomyelin being lethal (Tafesse et al. 2007).

### ***1.7.1 Sphingomyelin uptake by endocytosis***

Sphingomyelin is made available to cells through two main routes, endocytosis or *de novo* synthesis. As cell membranes are rich in sphingomyelin, the majority of cellular sphingomyelin available to the cell is processed as a product of endocytosis. Uptake of sphingomyelin into cells through endocytosis forms part of the 'salvage pathway' that is used to produce sphingosine (*Figure 1.5*) (Kitatani et al. 2008). Disruption to clathrin mediated endocytosis has been reported in NPA and NPB, which is linked to disruption (and storage) of sphingomyelin in both diseases, leading to disruption in sphingolipid metabolism (Rappaport et al. 2014). Sphingomyelin taken up through endocytosis, can be metabolised by sphingomyelinase enzymes to produce ceramide and phosphocholine. Ceramide is a key signalling molecule, as well as being a starting point for the synthesis of several sphingolipids, and thus the pool of intracellular ceramide is tightly regulated (Kitatani et al. 2008).

The type of sphingomyelinase enzyme that metabolises the sphingomyelin is both tissue and intracellular localisation dependant, with acid, neutral and alkaline sphingomyelinases, with each group possessing several enzymes with tissue specificity (Gault et al. 2010).

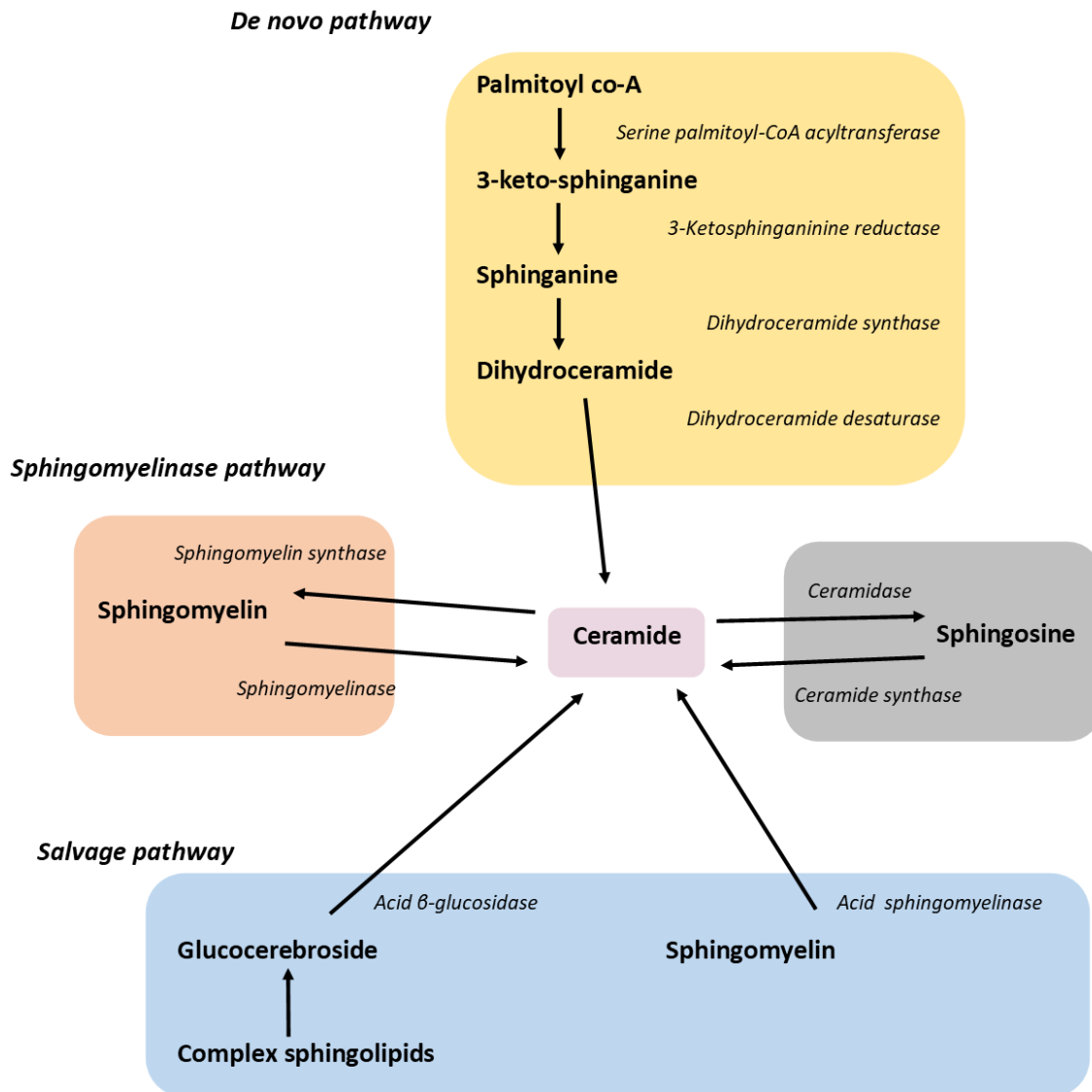


**Figure 1.5. Sphingomyelin and ceramide synthesis pathways**

Sphingomyelin is involved in multiple different intracellular pathways within the cell, as well as being closely linked with several ceramide metabolism and signalling pathways. Ceramide can be produced through a variety of pathways, including de novo synthesis from palmitoyl co-A, or produced within the lysosome through metabolism of other complex lipids, including sphingomyelin or glucocerebroside. Sphingomyelin can also be synthesised from ceramide when required by the cell. Pathway data obtained from (Kitatani et al. 2008).

**1.7.2 De novo sphingomyelin synthesis**

As well as taking in sphingomyelin from cell membranes via endocytosis, cells can synthesise sphingomyelin *de novo*. Sphingomyelin synthesis is catalysed by the sphingomyelin synthase (SMS) family of enzymes, whereby a phosphocholine head group is transferred to ceramide, producing sphingomyelin and diacylglycerol (Huitema et al. 2004).

The majority of sphingomyelin synthesis occurs in the trans-Golgi network where Sphingomyelin synthases 1 and 2 (SMS1&2) are both found. However, SMS2 is also localised to the plasma membrane, and can synthesise sphingomyelin to maintain cell membrane sphingomyelin levels (Chen and Cao 2017). As both sphingomyelin and ceramide are involved in processes, such as autophagy, there is a cellular requirement to ensure that homeostasis of both molecules is maintained to prevent off target cell signalling effects (Fanani and Maggio 2017). Through a combination of balancing endocytic uptake of sphingomyelin and SMS activity, cells can maintain the pool of bioavailable sphingomyelin to prevent depletion or accumulation of sphingomyelin (Bienias et al. 2016).

### ***1.8 Niemann-Pick types A & B***

Niemann-Pick disease types A & B are autosomal recessive diseases, resulting from allelic mutations in sphingomyelin phosphodiesterase 1 (SMPD1), which encodes the acid sphingomyelinase (aSMase) enzyme. NPA is characterised by almost complete loss of aSMase activity, with reported aSMase activity ranging from no activity to approximately 10% of healthy control enzyme activity (Poulos et al. 1983). NPB has a significant, but less severe loss of aSMase compared to NPA, with patients having a wide range of aSMase activity with 10-30% being reported (van Diggelen et al. 2005; Hu et al. 2021a).

#### ***1.8.1.1 Niemann-Pick Type A/B disease phenotypes***

Of NPA and NPB, NPA presents earliest with the most severe disease phenotype, usually presenting before 3 months of age, with retarded growth and hepatosplenomegaly. By one year of age, NPA patients have neurological symptoms, such as impaired motor skills and regression of developmental milestones (Qureshi et al. 2022). Patients with NPA do not usually survive beyond early childhood.

NPB usually presents in mid-childhood, with a less severe disease phenotype compared to that of NPA. Patients with NPB commonly have hepatosplenomegaly, thrombocytopenia, and stunted growth. Approximately one third of patients with NPB have CNS symptoms, such as ataxia, learning difficulties, and gross motor delays (Wasserstein et al. 2006). Additionally, a range of other rarer disease effects including liver dysfunction and osteoporosis (Wasserstein et al. 2012; Eskes et al. 2020). Patients with NPB generally do not live beyond teenage years, however it has been reported that patients can live beyond into their fourth and fifth decade of life (McGovern et al. 2013). It is believed that residual

lysosomal aSMase activity is enough to prevent ataxia or tremors, which is believed to partly explain the difference in disease phenotypes between NPA and NPB (Dhami et al. 2001).

### **1.8.2 aSMase**

Hydrolysis of sphingomyelin is carried out by sphingomyelinases (SMases), that catalyse the cleavage of the phosphodiester bond of sphingomyelin, producing ceramide and a phosphorylcholine group. SMases are classified by the pH optima for each enzyme's peak activity: with acid, neutral, and alkaline sphingomyelinases, and a further division possible based on the divalent cations required for enzymatic activity, such as  $Zn^{2+}$  or  $Mg^{2+}$  (Marchesini and Hannun 2004).

#### **1.8.2.1 Sphingomyelin Phosphodiesterase 1**

Mammals have a single gene, Sphingomyelin Phosphodiesterase 1 (SMPD1), that produces acid sphingomyelinase. In addition to SMPD1, mammals also possess a further three sphingomyelin phosphodiesterases (SMPD 2-4), which produce a range of neutral and alkaline sphingomyelinases (Goñi and Alonso 2002).

A single mRNA product of SMPD1 leads to three different splice variants, however only 1 of the transcripts produces a functional enzyme (Schuchman et al. 1991). Acid SMase is initially synthesised as a 75kDa prepro-enzyme form, including additional N-glycosylation sites (Jenkins et al. 2011). This prepro-aSMase first undergoes cleavage, by a currently unidentified protease within the ER/Golgi complex to form pro-aSMase with a molecular weight of either 72kDa or 70kDa, and upon maturation into the enzymatically active has a molecular size of 52kDa (Jenkins et al. 2011). In mammals, the aSMase protein is highly conserved, with 82% sequence homology between murine and human aSMase (Newrzella and Stoffel 1992).

Acid sphingomyelinase exists as two distinct enzymatic isoforms, the first is targeted to the endo-lysosomal compartment (Lysosomal aSMase), whereas the second form is secreted from the cell (secreted aSMase). The difference in trafficking of aSMase isoforms from the ER is due to the effect of phosphorylation, whereby mannose-6-phosphorylation leads to trafficking of pro-aSMase to the endo-lysosomal compartment.

The aSMase precursors that are not mannose 6-phosphorylated get trafficked to the Golgi, whereby N-terminal degradation occurs, which is believed to be linked to trafficking and subsequently required for the aSMase to be exocytosed (Jenkins et al. 2010).

### 1.8.2.2 aSMase Structural domains

It has been hypothesised that that amino acid residue (C-terminal) modification of aSMase serves as a mechanism to regulate enzyme activity. It has been demonstrated that removal of Cys629 from aSMase was required for enzymatic activity (Qiu et al. 2003). Based on these observations, it has been suggested that Cys629 functions as a “Cysteine Switch”, whereby the removal of a cysteine leads to Zn<sup>2+</sup> hydration leading to enzyme activation, as has been previously described for other enzymes, such as matrix metalloproteinases (MPP) (Van Wart and Birkedal-Hansen 1990). As the C-terminal processing is known for several other lysosomal enzymes that follow a similar synthesis pathway, such as cathepsin D, it is postulated that aSMase undergoes similar proteolytic processing to generate enzymatically active aSMase (Yonezawa et al. 1988).

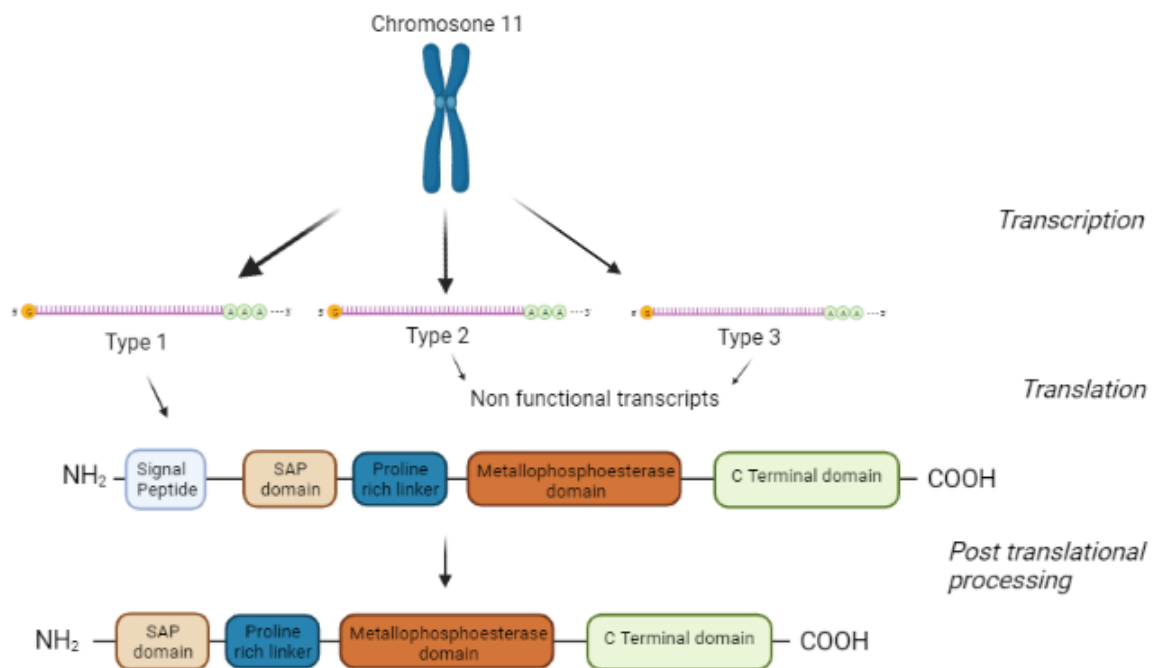


**Figure 1.6. Schematic illustrating the overview of the synthesis of aSMase**

Synthesis of aSMase is based on one functional SMPD1 mRNA transcribed from the 11p15.1-p15.4 chromosome loci. The SMPD1 mRNA is then translated into prepro-aSMase. The prepro-aSMase undergoes processing and N-terminal cleavage to become fully functional aSMase. Also illustrated on the finished aSMase are the functional domains with aSMase, from the N terminal saposin like domain (SAP), to the C-terminal domain.

In addition to trafficking motifs present in the N-terminal of aSMase, the N-terminus also contains a saposin-like (SAP) domain covering residues 89-165, adjacent to the signal peptide (Ponting 1994). The SAP domain allows mobilisation of lipids from the lysosomal membrane, bringing the lipid substrates into contact with the active site of lipid degrading enzymes; thus allowing enzymatic degradation, such as sphingomyelin into ceramide by aSMase (Kolter and Sandhoff 2005). As the SAP domain is distinct and separated from the catalytic MPP domain by a proline rich domain, it has been suggested that the SAP domain functions as an SM degradation activating region. In conjunction with the SAP domain functioning as an activating region, the proline rich domain is believed to function as a molecular hinge, between the SAP and MPP domains (Rommel et al. 2007). Site directed mutagenesis has demonstrated that mutations in the conserved residues of the SAP domain of aSMase led to impaired aSMase activity, which could be partially restored through the addition of exogenous SAP (Kölzer et al. 2004).

### *1.8.3 aSMase and acid ceramidase/sphingosine*

With aSMase producing ceramide, a key signalling molecule in several pathways, regulation of aSMase must be controlled by the cell (Wang et al. 2015). Loss of aSMase leads to significant effects in the ceramide salvage pathway, by preventing the production of the pathway's initial metabolite, ceramide (Mullen et al. 2012). This leads to reduced capabilities for acid ceramidase (ACase) to degrade ceramide into sphingosine. This decrease in lysosomal ceramide, reduces the bioavailability of sphingosine, in turn reducing the ability of other organelles to synthesise ceramide or sphingosine-1-phosphate, itself an important signalling molecule, from the exported lysosomal sphingosine (Breiden and Sandhoff 2021). This leads to several downstream effects, affecting several signalling pathways, including those responsible for controlling cell migration and differentiation (Blaho and Hla 2011).

### *1.8.4 aSMase regulation in LSD's/NPD*

Whilst loss of function of aSMase is most closely associated with NPA and NPB, significant loss of aSMase activity is observed in NPC disease, amongst others, including a-mannosidosis, I Cell, CLN5 and Gaucher disease. In NPC, aSMase activity is reduced by approximately 50%, coinciding with accumulation and mis-localisation of sphingomyelin

(Vanier et al. 1991). This significant decrease in aSMase activity in NPC, leads in part to the secondary sphingomyelin storage associated with the 'classical' presentation of NPC and may contribute to disease pathology.

The exact reason underpinning the decrease in aSMase activity in NPC is not fully understood, however two probable causes have been suggested. The first is due to cholesterol accumulation, which leads to downregulation of aSMase activity through post-translational modification, whereby it was suggested that cholesterol mediates disruption of a folding or sorting event leading to improper maturation of active aSMase (Reagan et al. 2000). The cholesterol post-translational modification was suggested as a mechanism of action as Reagan et al showed that, whilst increasing cholesterol concentration did not affect the quantity of aSMase within cells, it did reduce the activity significantly (Reagan et al. 2000).

The second cause for a reduction in aSMase activity is due to reduced protein kinase C (PKC) activity in NPC disease. Increased lysosomal sphingosine concentrations, as observed in NPC leads to decreased PKC activity; and may cause some of the associated endocytic defects through downregulation of Rab9 (Walter et al. 2009). PKC is known to be a positive regulator of aSMase activity, therefore if PKC activity is decreased in Niemann-Pick, aSMase activity will also be decreased. (Rodriguez-Lafrasse and Vanier 1999; Zeidan and Hannun 2007b).

### *1.8.5 Therapies in NPA/NPB*

At present, one therapy is approved for Niemann-Pick A/B (ASMD), being Xenpozyme (Olipudase alfa), however whilst the treatment is FDA approved, at present it is not currently approved for use throughout the UK. Olipudase alfa is an enzyme replacement therapy for acid sphingomyelinase deficiency, but only in cases without central nervous system (CNS) manifestations. Xenpozyme is given every two weeks, in the form of an infusion, with dose administered depending on patient weight (Keam 2022). Treatment is given in a dose escalation, to mitigate, and reduce the chance of side effects occurring. This dose escalation is termed 'debulking strategy', which is required to manage ceramide release from the increased aSMase activity. As ceramide is a pro-apoptotic molecule,

ceramide levels must be managed, to prevent excess production and the downstream apoptotic effects.

Patients given Xenpozyme, mainly those with a less severe disease phenotype, saw reversal in disease symptoms and greatly improved quality of life (Lachmann et al. 2023). However, the cost of the treatment has led to the decision by National Institute for Health and Care Excellence (NICE) to not approve the treatment, with the decision currently under appeal process.

A single phase 1 clinical trial took place for NPB sponsored by Pfizer, under the EMA in 2016 to investigate if giving anti-oxLDL IgM antibodies would reduce the presence of oxLDL in the blood, in turn reducing cellular cholesterol uptake, and thereafter reducing the amount of lysosomal lipid storage, particularly cholesterol. Despite the trial having an estimated completion date of 2017, at present no data has been published about the outcome of the study, so it is unclear whether this is a viable treatment option or is likely to be taken further.

## ***1.9 Niemann-Pick type C***

### ***1.9.1 Human NPC1 protein***

NPC1 is a member of the mammalian RND permease family of protein. RND permeases are found in both prokaryotes and eukaryotes, with the most well studied group of RND permeases being the multidrug drug resistance efflux pumps, found commonly in gram-negative bacteria (Nikaido 2018). Members of the gram-negative bacterial efflux pumps, have been identified as possessing an ability to actively transport a range of substances including: hydrophobic drugs, fatty acids, organic solvents, heavy metals, and lipooligosaccharides including endotoxin (Anes et al. 2015). In humans, the eukaryotic sterol homeostasis (ESH) branch of the RND permease family has been identified, with all members containing a highly conserved 5 transmembrane region, identified as a sterol sensing domain (SSD) (Winkler et al. 2019).

The human NPC1 protein is comprised of 1,278 amino acids and consists of 13 transmembrane helices and 4 distinct functional domains N-terminal domain (NTD), middle lumen domain (MLD), sterol sensing domain (SSD), and C-terminal domain (CTD) (*Figure 1.7*) (*Davies et al. 2000*). It is currently believed that the site of cholesterol transfer from

NPC2 is to a pocket in the 240 amino acid NTD of NPC1 through a mechanism termed “Hydrophobic handoff” (Kwon et al. 2009; Wang et al. 2010; Deffieu and Pfeffer 2011). This N terminal domain is connected to the first transmembrane domain with a proline rich linker sequence (Infante et al. 2008). This proline rich linker region has been hypothesised as a means of enabling transfer of cholesterol from the N terminal domain to another downstream pocket within NPC1 (Infante et al. 2008). The exact locus for the second cholesterol binding site has not been identified, however the existence of such a site is hypothesised from multiple publications (Nobutaka et al. 2004; Ohgane et al. 2013). Connected to the second TM domain is the middle luminal domain (MLD), which has been shown to be responsible for the binding of NPC1 to NPC2 *in vitro* (Deffieu and Pfeffer 2011). Spanning transmembrane domains 3-7 is the sterol sensing domain (SSD), this domain has been suggested as a potential regulator for NPC1 activity through sensing the free sterol concentration within lysosomes, which alter the transfer of cholesterol from the NTD or affect the binding capabilities of NPC2 with the MLD through allosteric hindrance (Li et al. 2016). Spanning TM domains 8 and 9 is the C terminal Domain (CTD), which is closely associated with the MLD and may be involved in NPC2 binding (Li et al. 2016). In addition to assisting NPC2 binding, the C terminal domain contains a dileucine motif that serves as a lysosomal targeting and internalization signal (Watari et al. 1999).

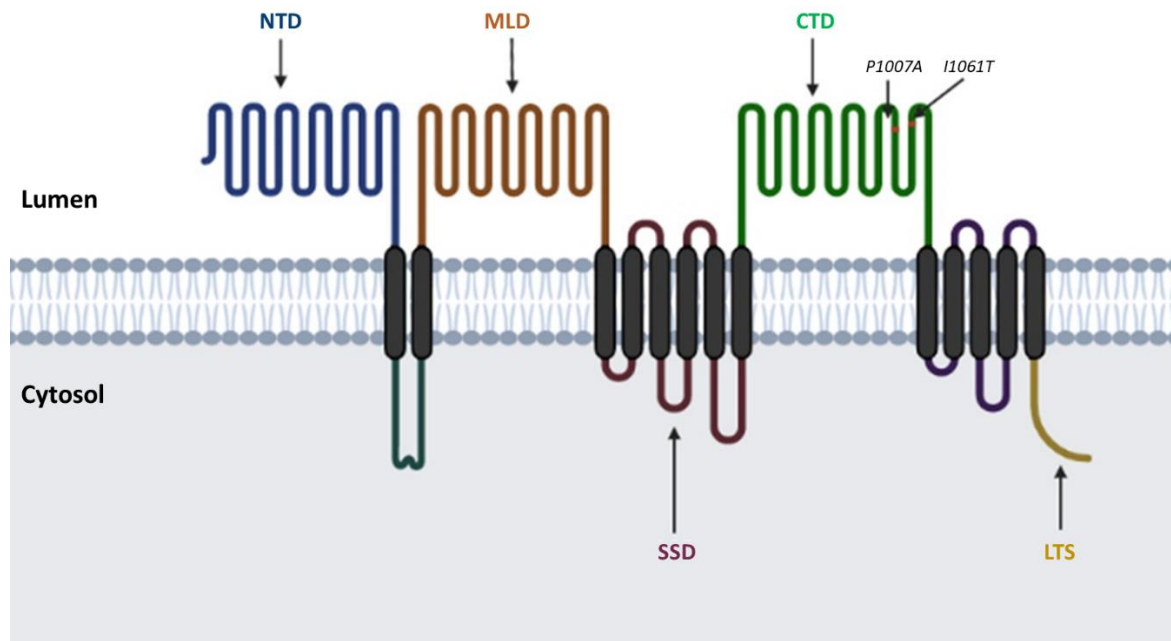


**Figure 1.7. Topology of human NPC1 protein**

Each domain of NPC1 is highlighted in a different colour. The two most common mutations in NPC disease, P1007A and I1061T, are both highlighted in their approximate positions in the CTD. The N terminal domain (NTD), Middle Luminal domain (MLD), sterol sensing domain (SSD), C terminal domain (CTD) and Lysosomal targeting sequence represent the main functional domains in NPC1.

NPC1 shares some structural similarities to NPC1 like 1 (NPC1L1), including the N-Terminal domain, however overall homology is approximately 40% (Altmann et al. 2004). The N-Terminal domain, which is structurally similar to that of NPC1, has been reported to directly bind to cholesterol (Zhang et al. 2011). Additionally, NPC1L1 also possesses an SSD, which is conserved in NPC1, and in NPC1L1 forms one domain of an internal tunnel within the protein (Hu et al. 2021b). However, unlike NPC1, NPC1L1 is not lysosomal, as it lacks the LTS, and is instead found on the cellular plasma membrane (Jia et al. 2011). The similarity in both NTD and SSD between NPC1 and NPC1L1 suggests that NPC1 can potentially traffic cholesterol.

In the context of disease biology, NPC1 has been suggested to be involved in several diseases and conditions including: tuberculosis infection, obesity, and Alzheimer's, however the only disease where NPC1 defects is the primary cause is NPC (Lamri et al. 2018). NPC causing mutations have been identified in all domains of NPC1, however two distinct disease phenotypes have been identified based on the mutations underpinning the disease. The first of these disease presentations, deemed "classical", is most closely associated with the more well characterised cellular phenotype, including impaired esterification of LDL

derived cholesterol and subsequent cytoplasmic punctate that can be stained with the cholesterol binding probe, filipin. The second disease presentation is named the “variant” phenotype. Unlike the classical phenotype where cholesterol levels patient derived cells are highly elevated and are the primary diagnostic indicator, in the variant phenotype cholesterol storage is only moderately elevated (Guatibonza Moreno et al. 2023). Therefore, diagnosing of the variant phenotype of NPC1 is particularly challenging. Why the variant phenotype has only limited cholesterol accumulation, compared to the classical phenotype is not fully understood, however it is believed to be linked to the specific mutation causing NPC (Feng et al. 2019).

### *1.9.2 NPC1 mutations*

The mutation most associated with the classical form of NPC is the I1061T mutation, which presents as juvenile onset (onset at 5-15 years of age) and occurs in approximately 25% of cases of NPC in the north western Europe (Millat et al. 1999). In addition to the classical presentation of NPC is the “variant” type of NPC, frequently presenting as late infantile (onset at 2-6 years of age). The variant can be biochemically differentiated from classical NPC through analysis of LDL derived cholesterol ester formation, as this rate is decreased in classical but not in the variant presentation. Staining with Filipin can be used in differentiation between forms of NPC, as the punctate formation is less ubiquitous in variant presentation due to the increased ratio of esterified cholesterol (Tängemo et al. 2011). The most common underlying cause of variant form is the P1007A mutation, which has been identified as the underlying cause in approximately 20% of northern European cases of NPC (Millat et al. 2005). Interestingly, there are differences in localisation between the P1007A and I1061T mutations that have been observed, whereby misfolded I1061T NPC1 is degraded in the endoplasmic reticulum, whereas P1007A NPC1 localizes to lysosomes, and through retaining residual activity, may partially reduce cholesterol storage.

Both P1007A and I1061T mutations are found in the cysteine rich CTD of NPC1. With the P1007A mutant, proline is known to be structurally important, and induces kinks in the protein, particularly in alpha helix's and therefore the substitution with an alanine, would not induce the same 3D structural change, and may cause other issues with correct protein folding. In the I1061T mutation, an isoleucine residue is substituted for a threonine residue,

which sees an aliphatic hydrophobic residue replaced with a polar hydrophilic residue. Changing from an isoleucine to threonine residue may potentially affect the ability of the CTD of NPC1 to bind cholesterol. Despite the differences in disease phenotypes, the currently approved therapies for NPC appear to improve disease symptoms in both classical and variant forms of NPC (Geberhiwot et al. 2018).

### *1.9.3 Clinical treatments for Niemann-Pick disease*

With NPC, there are currently no clinical methods of curing the disease. Treatment focuses on disease management, which remains mainly supportive, and symptomatic treatment to improve quality of life. The first medications used for Niemann-Pick disease were based on those for symptom management and included drugs such as: anti-epileptics, anticholinergic, or anti-depressants (Wraith and Imrie 2009). The first group of therapeutics to undergo clinical trial specifically for NPC disease were: cholestyramine, lovastatin, and nicotinic acid (Patterson et al. 1993). When used in combination, these cholesterol lowering drugs were found to lower total cholesterol, however no comment on neurological outcomes were made based on either each treatment individually or as a combination therapy. Whilst these treatments were able to reduce cholesterol, a range of frequent side effects were observed in up to 80% of patients, which included: showing redness, developing acanthosis nigricans, night-time agitation, or constipation.

The first, and only, treatment to be clinically approved for use in NPC is miglustat (Zavesca) a small iminosugar molecule, which can be used as substrate reduction therapy for glycosphingolipid LSDs (Platt 2014). Miglustat acts by inhibiting glucosylceramide synthase, which in turn prevents synthesis of glucosylceramide derivatives that become toxic upon lysosomal accumulation in LSDs (Platt et al. 1994). When given early in disease progression, miglustat delays the progression of neurological symptoms and deterioration of NPC patients, but it has no effect on the systemic manifestations. Whilst miglustat delays NPC disease neurological progression, it is not a cure for the disease as stopping treatment will cause ablation of the effects from treatment. Miglustat also has commonly reported side effects, including gastrointestinal upset and weight loss. However, this can be managed using anti-propulsive medication (Patterson et al. 2007).

In addition to miglustat, a range of treatments are currently going through clinical trial for NPC1, with the two most advanced candidates being 2-Hydroxypropyl- $\beta$ -cyclodextrin (HP- $\beta$ -CD) and arimoclomol. The mechanism that leads to the effects observed in NPC1 models treated with HP- $\beta$ -CD is not understood; however, it has been demonstrated *in vitro* to be efficacious in reversing the accumulation of unesterified cholesterol in addition to other associated lipids in neuronal cell lines (Ottinger et al. 2014). HP- $\beta$ -CD has been demonstrated to reduce stored cholesterol in neurons and glial cells in a dose dependant manner (Peake and Vance 2012). Murine NPC models have shown that treatment with HP- $\beta$ -CD delayed disease onset, reduced neuronal cholesterol and glycosphingolipid storage and reduced secondary markers of neurodegeneration as well as significantly increased lifespan (Davidson et al. 2009).

The effects of IV infusion of HP- $\beta$ -CD have led to a range of effects, with some patients not reporting any neurological improvements (Matsuo et al. 2013), some seeing a halt to disease progression (Matsuo et al. 2014), whilst others appear, anecdotally at least, to have had partial remission of NPC (Hastings et al. 2019). It is unclear to what extent this variation in response to HP- $\beta$ -CD is due to: the mutation driving the disease, the method by which the drug is administered, or the progression of NPC at the time of first treatment (Hastings et al. 2019). Transfusion of HP- $\beta$ -CD intracerebroventricularly has also been trialled, with the patient having halted disease progression, with only minor worsening in facial control (Matsuo et al. 2014). However, no improvement in seizure frequency, as well as only transient beneficial effects on neurological function were reported (Matsuo et al. 2014).

Arimoclomol causes up-regulation of the transcription factor heat shock factor 1 (HSF1), in turn upregulating several heat shock chaperone proteins, principally HSP70-chaperone along with other HSP-chaperones (Nakasone et al. 2014). It has been demonstrated that HSP70 is involved in promoting correct folding of NPC1, and it is this mechanism that is believed to bring about potential therapeutic effects (Ingemann and Kirkegaard 2014). As with miglustat and HP- $\beta$ -CD, arimoclomol functions by preventing the build-up of lipids or misfolded protein within the lysosome, rather than through direct modulation of NPC1 activity. However, in 2023 the FDA rejected approval for arimoclomol after a phase 3 clinical trial, likely due to only a limited improvement in disease phenotype.

Whilst therapies for NPC have been approved or going through clinical trial, no molecule has been shown to directly upregulate NPC1 function. This is due in part to a combination of factors including historically a poorly understood mechanism of action for NPC1; however, the main reason holding back the screening for NPC1 activators is that no probe or *in vitro* assay to directly monitor NPC1 activity has been published.

### 1.10 Aims

In this thesis, we wanted to identify novel compounds with therapeutic potential in Niemann-Pick disease. One aim was to develop new assays suitable for use in HTS using AQ2 (or analogues) to identify modulators of NPC1 activity. Resulting from the inability to complete the first aim, a new second aim was developed to create a zinc imaging-based assay with was suitable for a HTS work. A further sub-aim was to use the zinc assay to carry out a screen to identify molecules with novel zinc modulating effects in Niemann-Pick disease. The final aim was to evaluate the therapeutic potential of two therapeutics, (Cannabidiol and Copaiba oil) to improve the disease phenotype.

To meet the first aim of identifying novel molecules with therapeutic effect in Niemann-Pick, a time-course imaging-based assay was to be developed to detect NPC1 activity. The first sub aim was to develop an NPC1 trafficking assay suitable for HTS using a novel probe, identified from a series of analogues based off a known NPC1 substrate, AQ2. The second sub aim was to then use the NPC1 trafficking assay using the novel probe to screen an FDA approved compound library to look for disease improving molecules. However, as the novel AQ2 analogues were not a substrate for NPC1, AQ7 was to be evaluated for use as a lysosomal probe.

The second aim, resulting from the inability to develop an NPC1 trafficking assay was to develop a phenotypic imaging-based zinc screening assay suitable for Niemann-Pick. Zinc dyshomeostasis is reported in Niemann-Pick, and therefore we decided to determine if we could develop an imaging-based zinc phenotypic assay suitable for screening. Following this, we wanted to use the assay to screen a commercially available compound library to identify compounds that modulated zinc in Niemann-Pick. Finally, the hits identified were then to be validated through the use of LysoTracker, to determine the effect on lysosomal volume.

The final aim was to evaluate two treatments cannabidiol and copaiba oil, currently being used by some patients off label, with anecdotal benefits. As patients had reported improvements upon taking cannabidiol and copaiba oil, we wanted to determine whether distinct biochemical changes and mechanistic effects, and thus potential therapeutic effect in Niemann-Pick disease, could be observed. A combination of cell imaging and biochemical assays were to be used to determine what, if any, effects the therapeutics had upon lysosomal lipid storage, as well as enzyme activity and protein expression.

## 2 Methods and materials

### 2.1 Cell culture

#### 2.1.1 *General cell culture*

Unless otherwise stated, fibroblasts were obtained from Corriell cell repository. Glial cells were obtained from the Emyr Lloyd-Evans laboratory. Cells were grown in DMEM with NEAA, supplemented with 10% fetal bovine serum (FBS), 1% L-Glutamine and 1% Pen-Strep. Cells were grown in a humidified incubator at 37°C with 5% CO<sub>2</sub>, with twice weekly media changes and passaging once cells reached 90% confluency.

**Table 2.1. Patient derived cell lines**

<b>Disease</b>	<b>Corriel number</b>	<b>Sex and age</b>	<b>Mutation</b>
Healthy Control	GM01652	Female, 11 year old	N. A
Healthy Control	GM05399	Male, 1 year old	N. A
Niemann-Pick disease Type A	GM00370	Female, 1 year old	Unknown, 7% aSMase activity
Niemann-Pick disease Type B	GM11097	Male, 1 year old	p.L43_A44delA
Niemann-Pick disease C1	GM03123	Female, 9 year old	P237S/I1061T
Niemann-Pick disease C1	GM18420	Female, unknown	P1007A / g.IVS23+4delA
Niemann-Pick disease C1	GM18453	Male, unknown	I1061T/I1061T
Mucopolipidosis Type IV	GM02527	Male, 2 year old	IVS3AS,A>G,-2

### 2.2 Drug treatments

#### 2.2.1 *Cannabidiol treatment*

Cellular treatment was with cannabidiol from Carbosynth (FC19666), unless stated otherwise. Cells were treated with 15µM cannabidiol for 48 hours, diluted in DMEM as outlined in 2.1.1.

### *2.2.2 Copaiba treatment*

Cells treated with copaiba were treated with copaiba extract from Doterra (60203549) at a concentration of 10µg/ml. Cells were treated with copaiba for 48 hours in DMEM, as described in 2.1.1 unless otherwise stated.

### *2.2.3 Bafilomycin*

Stocks of Bafilomycin were made in DMSO to a concentration of 50mM, with an 8 point 1:3 dilution also produced and stored as single use aliquots. For cell treatment, stocks were diluted 1:1000 in either DMEM or Opti-MEM and cells incubated overnight at 37°C.

### *2.2.4 Trehalose*

Trehalose solutions were made fresh every time from powder stocks. For cell treatment a 100mM final concentration was used, with trehalose being dissolved in DMEM. Cells were incubated with trehalose overnight.

### *2.2.5 3-Methyladenine (3MA)*

3MA stock solutions were prepared fresh each time it was used. Final 3MA concentration applied to cells was 5mM, with 3MA being dissolved in DMEM. Cells were incubated with 3MA overnight.

### *2.2.6 Zinc chloride*

A 1M zinc chloride solution was made up in DMSO and stored at -20°C when not in use.

### *2.2.7 Phytic acid*

Phytic acid stock solution was made up as a 500mM solution in Milli-Q water. Stock solution was stored at -20°C until needed.

### *2.2.8 TPEN*

100mM TPEN stock solution was made up from powder in DMSO and stored at -20°C.

### 2.2.9 *Imidazole*

A 1M stock solution of imidazole was prepared from powdered solid, being dissolved in DMSO, and stored at -20°C.

### 2.2.10 *Clioquinol*

A stock solution of clioquinol was made to a concentration of 500mM in DMSO, and stored at -20°C.

### 2.2.11 *Panobinostat*

Panobinostat was made from powder stock to a concentration of 500mM in DMSO, and stored at -20°C.

### 2.2.12 *Vorinostat*

Vorinostat stored at concentration of 500mM in DMSO being made from powder, and stored at -20°C.

## 2.3 Toxicity assays

### 2.3.1 *Cell seeding density calibration for RealTime-Glo™ MT cell viability assay*

To set up the plate for the assay calibration, either mouse glial cells or patient derived fibroblast were trypsinised with TrypLE and returned to an incubator for 5 minutes, followed by transfer to a 15ml centrifuge tube and centrifuged for 5 minutes at 200xG and then resuspended in 1ml of PBS. Cells were counted using a Countess II automated cell counter. Cells were then seeded into clear bottomed, white walled 96 well plates at the following densities per well, all in triplicate: 1k, 2k, 5k, 10k, 25k, and 50k.

Cell viability was assayed using the RealTime-Glo™ MT Cell Viability Assay from Promega. The assay contained 1000x concentrations of a luciferase enzyme and MT cell viability substrate, which was added to the medium prior to placing on the cells.

To each well 200uL of medium containing substrate and detection reagent was added. For a negative control, 200uL of medium with the substrate and detection reagent were added to wells without any cells. Luminescence was recorded using a BMG Pherastar plate reader at

1-hour intervals over a 72-hour period, with the cells being returned to the incubator between recordings.

### *2.3.2 AQ2 Analogues cellular toxicity assay using RealTime-Glo™ MT cell viability assay*

Cells were: trypsinised with TrypLE and returned to an incubator for 5 minutes, followed by centrifugation for 5 minutes at 200xG, with the pellet being resuspended in 1ml of PBS. Cells were then seeded into clear bottomed, white walled 96 well plates, at a density of 25,000 NPC1 -/- cells per well. Added to this were AQ2 or an analogue at concentrations ranging from 1mM to 1nM.

To each well 200uL of medium containing substrate and detection reagent was added. For a negative control, 200uL of medium with the substrate and detection reagent were added to wells without any cells. For a positive control, 3 wells of cells were left untreated without either cannabidiol or copaiba respectively. Luminescence was recorded using a BMG Pherastar FSX plate reader at: 24-hour, 48-hour, and 72-hour time points; with the cells being returned to the incubator between recordings.

### *2.3.3 Cellular toxicity assay using RealTime-Glo™ MT cell viability assay for cannabidiol and copaiba*

Cells were; trypsinised with TrypLE and returned to an incubator for 5 minutes, followed by centrifugation for 5 minutes at 200xG, with the pellet being resuspended in 1ml of PBS. Cells were then seeded into clear bottomed, white walled 96 well plates. Disease patient cells were seeded at a density of 10,000 cells per well and 5,000 cells per well for the healthy control fibroblasts.

Cells were treated with either cannabidiol or copaiba in an 11-point serial dilution. For cells treated with cannabidiol, the highest concentration was 5mM down to 3.8µM. For cells treated with copaiba, the highest concentration was 100ug/ml down to 125ng/ml.

To each well, 200uL of medium containing substrate and detection reagent was added. For a negative control, 200uL of medium with the substrate and detection reagent were added to wells without any cells. For a positive control, 3 wells of cells were left untreated without

either cannabidiol or copaiba respectively. Luminescence was recorded using a BMG Pherastar FSX plate reader at: 24-hour, 48-hour, and 72-hour time points; with the cells being returned to the incubator between recordings.

## ***2.4 Biochemical assays***

### ***2.4.1 Enzyme assays***

#### ***2.4.1.1 Compound incubation***

Patient derived fibroblasts were grown to 75% confluency, whereby the media was refreshed with new cannabidiol or copaiba containing media. For cannabidiol enzyme assays, T75s were treated with either: 5 $\mu$ M, 15 $\mu$ M, or 30 $\mu$ M cannabidiol. Cells treated with copaiba had: 1 $\mu$ g/ml 5 $\mu$ g/ml, or 10 $\mu$ g/ml added to the media. All cannabidiol and copaiba treatments were left for 48 hours, unless stated otherwise.

#### ***2.4.1.2 Acid sphingomyelinase activity assay***

Fluorometric assays were carried out to assess lysosomal enzyme activities. The protocol is a modified version of that described (van Diggelen et al. 2005) utilising 6-Hexadecanoylamino-4-methylumbelliferone (6HMU) and HMU-sphingomyelin substrate. In black walled 96 well plates, 10 $\mu$ l of cell homogenate containing 2 $\mu$ g of protein was added to 10 $\mu$ l of 500 $\mu$ M HMU-sphingomyelin, in a buffer comprising 100mM sodium acetate with 0.2% sodium tauchlorate at pH 4.5.

A negative control sample was prepared by heat treating a sample to 95°C for 15 minutes to ensure protein denaturation. Also included was a sample treated with 1mM of zoledronic acid, a known acid sphingomyelinase inhibitor. After the addition of substrate, samples were incubated at 37°C, after 1 hour the reaction was stopped by the addition of 180 $\mu$ l stop buffer (100mM sodium carbonate, with 2.5% Triton at pH 10.9). Additionally, an 11-point 0.2-200uM HMU standard curve, diluted in stop buffer, was included in every plate.

Fluorescence was recorded using a BMG Pherastar FSX plate reader, with excitation at 350nm and emission at 450nm. In all cases, the enzyme activity was calculated using  $\mu$ mol/hour/ $\mu$ g protein.

## 2.4.2 *Protein quantification*

### 2.4.2.1 *DC Bio-Rad assay*

Bio-Rad DC Protein assay kit was used to determine protein concentration. This kit utilises a modified lowry assay, which has an increased tolerance to detergents and a reduced total assay time. Prior to the assay, cell pellets were resuspended in 75ul of Milli-Q water, and freeze-thawed twice, before being passaged 20 times through a 26-gauge needle. A 20µl of this homogenate was centrifuged at 13,000xG for 15 minutes to pellet the insoluble material. A 5ul of the clarified lysate was then transferred to clear 96 well plates in triplicate. A standard curve was run with each Bio-Rad DC Protein assay, with a 12-point serial dilution of BSA, ranging from 50mg/ml down to 0.024mg/ml made; each concentration being run in triplicate. To each well with 5µl of standard or sample, 25µl of Reagent A was added followed by 200µl of Reagent B. Absorbance was read immediately at 750nm using a BMG Pherastar FSX.

## 2.5 *Microscopy*

All microscopy, unless otherwise stated, was carried using an Operetta CLS spinning disc microscope (Perkin Elmer/Revvity). Two modes of operation were used, the first a basic single imaging set up involved imaging at a single magnification with user defined areas to image. The second mode of operation was 'PreciScan', which allows an initial imaging of the whole well of the plate at a low resolution (i.e. 10x) using a single channel termed a 'prescan', followed by a user defined preprogramed, automatic analysis pipeline to identify the regions of interest in the well.

Once the regions of interest had been identified in each well, a 'rescan' was carried out, such as at 40x magnification, with all the desired channels to be imaged utilised. Once imaging was complete, either using single imaging or Presci-Scan, an evaluation pipeline was carried out to identify regions of interest e.g.: cells, nuclei, lysosome, or puncta.

### 2.5.1 *Cell fixation*

#### 2.5.1.1 *Paraformaldehyde fixation*

For cells requiring preservation, or the use of antibody staining, cells were first washed three times in PBS, before being incubated in 4% paraformaldehyde for 10 minutes at room

temperature. Paraformaldehyde was then removed, and the cells washed three times in PBS. Following washing, cells were stored in PBS at 4°C.

#### *2.5.1.2 Methanol fixation*

As an alternative to paraformaldehyde fixation, methanol removes some membrane lipids and leads to cellular dehydration. For methanol fixation, cells were washed in PBS three times and then incubated with methanol for 10 minutes. After the elapsed time, the methanol was removed, and the cells washed three times in PBS. After washing, cells were stored in PBS and kept at 4°C. In certain instances, after paraformaldehyde fixation some cells were incubated with methanol for 10 minutes, prior to blocking to allow improved antibody binding, such as antibodies like LAMP1.

#### *2.5.2 Blocking buffer*

Blocking buffer was used after cellular fixation and before the addition of probes or antibodies to increase permeabilization and reduce nonspecific binding of antibodies. Blocking buffer used was comprised of PBS, supplemented with 1% BSA and 0.1% saponin.

### *2.6 Western blotting*

#### *2.6.1 Homogenate preparation*

Cell homogenate was resuspended in 75µL of lysis buffer. Lysis buffer was comprised of RIPA buffer (50mM Tris-HCL, 150mM NaCl, 1% NP-40, 0.5% sodium deoxycholate, 0.1% SDS pH8.0) supplemented with 1µM PMSF, Halt™ Protease Inhibitor Cocktail and Halt™ Phosphatase Inhibitor Cocktail. Homogenate was incubated with lysis buffer for 30 minutes on ice, with samples being vortexed every 10 minutes. After 30 minutes, homogenate was centrifuged at 17,000xG for 30 minutes at 4°C, and the supernatant collected.

#### *2.6.2 Sample preparation*

Samples had protein concentration quantified using DC assay, as outlined in 2.4.2, after which 2µg of sample was prepared, diluted in Milliq water. Laemmli buffer (125mM Tris HCl, 4% SDS, 20% glycerol, 10% 2-mercaptoethanol and 0.004% bromophenol blue) was added and samples heated to 95°C for 10 minutes.

### **2.6.3 SDS-PAGE**

Samples were run on a 4-20% Tris-glycine gradient gel (Thermo), at 140V, 200mA for 90 minutes, or until sufficient time for the dye front to reach the bottom of the gel. Gels were run in Tris-Glycine running buffer (25mM Tris Base, 192mM glycine, 0.1% SDS pH 8.3). PageRuler™ Prestained Protein Ladder, 10 to 180 kDa was used to identify protein bands.

### **2.6.4 Semi dry transfer**

Tri-glycine gels from SDS-Page were transferred onto PVDF membranes using semi dry transfer. Proteins were transferred onto PVDF membranes using Fisherbrand™ Owl™ Separation HEP-1 Semi Dry Electroblotting System. PVDF membranes were activated prior to transfer in methanol and rinsed in transfer buffer (25mM Tris base, 192mM glycine, 20% v/v methanol, 0.1% SDS pH7.8). Samples were transferred onto PVDF at 40mA for 2 hours per membrane.

### **2.6.5 Membrane staining**

Prior to staining membranes were blocked overnight with 2% BSA in PBS, at 4°C overnight. Membranes were then washed three times in PBS and stained with corresponding primary antibodies, as shown in Table 2.2. Membranes were incubated with primary antibodies, either overnight at 4°C or for 2 hours at room temperature. Membranes were washed three times with PBS and corresponding species specific IRDyes added (*Table 2.3*) for 1 hour at room temperature.

### **2.6.6 Imaging**

Membranes were imaged using a LI-COR Odyssey CLX, utilising both red and far-red detection wavelengths to negate the need to cut a membrane for staining to probe for different proteins.

### **2.6.7 Quantification of western blots**

Protein expression was quantified using Image J. For quantification, the total area of the bands was recorded for each sample, for both the protein of interest and the housekeeping gene (GAPDH). To standardise the protein expression, the area of the protein of interest was

divided by that of the housekeeping protein for the same sample. By dividing the band area by housekeeping protein produced a ratio of protein of interest to housekeeping gene, allowing for comparison between samples.

## 2.7 *Immunocytochemistry staining*

Fixed cells were either incubated either for 2 hours at room temperature or overnight at 4°C, all primary antibodies were incubated in blocking buffer (2.5.2). After incubation in primary antibody (Table 2.2), cells were washed three times in PBS, before the addition of the species-specific secondary antibody (Table 2.3) for 2 hours. Cells were then washed a further 3 times and imaged using an Operetta CLS as described in 2.5 unless stated otherwise.

**Table 2.2 Primary antibodies**

<b>Antibody</b>	<b>Host</b>	<b>Dilution</b>	<b>Supplier</b>
Acid ceramidase (612302)	Mouse	1:1000	BD Biosciences
Acid sphingomyelinase (Ab272729)	Rabbit	1:500	Abcam
Cannabinoid receptor 2 (Ab3561)	Rabbit	1:1000	Abcam
FAAH1 (L14B8)	Mouse	1:500	Cell Signalling
GAPDH (97166S)	Mouse	1:2000	Cell Signalling
GAPDH (2118S)	Rabbit	1:2000	Cell Signalling
6x His-tag (MA1-21315)	Mouse	1:1000	Thermo Fisher
HSP70 (4872S)	Rabbit	1:1000	Cell Signalling
LAMP1, Human (H4A3)	Mouse	1:200	Developmental Studies Hybridoma Bank
LAMP1, Mouse (1D4B)	Rat	1:200	Developmental Studies Hybridoma Bank
LBPA (Z-PLBPA)	Mouse	1:500	Echelon
Niemann-Pick C1 (ab134113)	Rabbit	1:500	Abcam
T7-Tag (D9E1X)	Rabbit	1:500	Cell Signalling
TFE3 (14779)	Rabbit	1:1000	Cell Signalling

**Table 2.3 Secondary antibodies**

<b>Antibody</b>	<b>Target</b>	<b>Dilution</b>	<b>Emission Wavelength (nm)</b>	<b>Supplier</b>
Alexa Fluor 488 (A11008)	Rabbit	1:500	525	Thermo Fisher
Alexa Fluor 488 (A11001)	Mouse	1:500	525	Thermo Fisher
Alexa Fluor 555 (A21434)	Rat	1:500	580	Thermo Fisher
Alexa Fluor 555 (A21245)	Mouse	1:500	580	Thermo Fisher
Alexa Fluor 647 (A21245)	Rabbit	1:500	670	Thermo Fisher
Alexa Fluor 647 (A21240)	Mouse	1:500	670	Thermo Fisher
IRDye 680	Mouse	1:1000	680	LI-COR
IRDye 800	Rabbit	1:1000	800	LI-COR

### **2.7.1 Cholera toxin (Subunit B) staining**

Gangliosides was stained in fixed cells using recombinant Alexafluor594-conjugate Cholera Toxin subunit B (CTxB). Cells were incubated in blocking buffer (2.5.2) containing 1µg/ml CTxB at 4°C overnight. Prior to imaging, cells were washed three times in PBS. Imaging was carried out using an Operetta CLS, with PreciScan mode as outlined in 2.5, with a 10x Hoechst filter pre-set pre-scan and a rescan at 40x (water objective) to utilising the Alexafluor594 channel pre-set (excitation 530-560nm emission 570-650nm) to image CTxB staining, followed by automated image evaluation.

### **2.7.2 Filipin staining**

Cellular cholesterol was stained using filipin, a naturally occurring blue fluorescent antibiotic, with high affinity for cholesterol originally isolated from *Streptomyces filipinensis*. Filipin was made to a concentration of 187.5µg/ml, by first dissolving 1mg of filipin in 40ul of DMSO, followed by diluting 7.5ul of the stock filipin solution in 1ml of DMEM.

Fixed cells were incubated in the filipin containing DMEM for 30 minutes in the dark at room temperature. After 30 minutes the cells were washed three times in PBS and imaged using an Operetta CLS, with PreciScan as outlined in 2.5. Pre-scan was done with a 10x To-Pro3 filter pre-set (excitation 615nm-645nm emission 655-760nm) and a rescan at 40x (water

objective) to utilising the Hoechst channel pre-set (excitation 355-385nm emission 430-500nm) to image filipin staining.

### **2.7.3 AQ7 Imaging**

#### **2.7.3.1 AQ2 analogue stock solution preparation**

All stocks of AQ2 were kindly provided by Professor Simon Pope, with AQ3-AQ7 all being synthesised by Deemah Alenazy, and also being a kind gift from both Deemah and Simon. All AQ molecules were made up as 50mM solutions in DMSO and stored at -20°C

#### **2.7.3.2 AQ7 Imaging**

Adherent cells were washed with PBS three times. AQ7 was added to either DMEM or Opti-Mem to a final concentration of 100µM. Cells were incubated with AQ7 for 4 hours, after which time the AQ7 containing medium was removed and the cells washed three times with PBS. Unless otherwise stated, cells were then incubated with a nuclei stain and then imaged.

#### **2.7.3.3 AQ2, AQ3 and AQ6 Imaging**

Unless otherwise stated, cells were treated with 100µM of AQ2 or analogue. Cells were incubated in Opti-MEM supplemented with AQ2 or analogue for 4 hours, after which the media was removed, and the cells washed three times with PBS, and then fresh Opti-MEM added to the cells with a corresponding nuclei stain.

### **2.7.4 Lysenin staining**

#### **2.7.4.1 Production of lysenin**

A lysenin containing construct was cloned into pET28b expression vector containing both a 6xHis tag and T7 tag. The Lysenin containing plasmid was then cloned into T7 Express BL21 *E.coli*. Transformed *E.coli* containing the lysenin expression plasmid were grown in Lb broth medium at 37°C with the addition of 100µg/ml of kanamycin. Once OD600 of 0.8 was reached, the temperature was lowered to 25°C, and 0.5mM IPTG was added to induce expression of the recombinant lysenin. After 16 hours, cells were: pelleted, re-suspended in lysis buffer (50mM Na<sub>2</sub>HPO<sub>4</sub>, 300mM NaCl, 10mM imidazole and EDTA free protease inhibitor cocktail; pH7.4) and stored at -80°C for later use. *E.coli* cultures were lysed by three freeze-thaw cycles followed by 5 cycles of 30 seconds of sonication, 30 seconds of rest. The resulting lysate was centrifuged, and the pellet discarded. The clarified lysate was

purified using a cobalt resin affinity column to purify the lysenin. An aliquot of the elutant was then taken and protein concentration determined as described in 2.4.2.1.

#### *2.7.4.2 Cell staining with lysenin*

Fixed cells were stained with 100ug/ml lysenin, diluted in blocking buffer. Cells were incubated with lysenin overnight at 4°C. Cells were then washed in PBS three times, before being incubated in T7-Tag primary antibody (Table 2.2) for 2 hours at room temperature or overnight at 4°C. After the elapsed times, the cells were again washed in PBS, and incubated with the species and fluorophore specific antibody as outlines in (Table 2.3) for 2 hours before a final three washes in PBS and subsequent imaging outlined in 2.5.

#### *2.7.5 Cyto-ID*

Cells for autophagosome labelling were incubated with a 1:500 dilution of Cyto-ID in Opti-MEM for 30 minutes at 37°C. Cells were washed in PBS three times and then incubated with a corresponding nuclei stain.

#### *2.7.6 Dextran lysosomal pH assay*

Cells were incubated with 500µg/ml FITC-Dextran and 250µg/ml Texas Red-Dextran (both 10,000MW) for 24 hours in DMEM. Cells were then incubated in Dextran free DMEM for a further 24 hours before imaging.

#### *2.7.7 Zinc probe comparisons*

Three zinc probes were tested for potential use as imaging-based probes, FluoZin-3, Zinquin, and TSQ. Both Flou-Zin3 and Zinquin were the cell permeant versions of the molecules. Flou-Zin3 was used at a concentration of 1µM, Zinquin 25µM and TSQ at 30µM, with cells being incubated with the probe diluted in PBS for 30 minutes in the dark. All probes were imaged with the corresponding excitation and emission filter combinations.

#### *2.7.8 Pluronic F-127*

Pluronic F-127 was trialled to determine whether it improved TSQ staining. Pluronic F-127 was bought as a 10% solution from Biotium, being diluted 1:1000 when mixed with TSQ prior to cell staining.

## 2.7.9 Nuclei stains

**Table 2.4 Nuclei stains**

<b>Name</b>	<b>Colour</b>	<b>Live/fixed Cell</b>	<b>Dilution</b>	<b>Emission wavelength (nm)</b>	<b>Supplier</b>
Hoechst 33342	Blue	Both	1:1000	361	Thermo Fisher
SYTOX™ Green	Green	Fixed	1:5000	524	Thermo Fisher
NucSpot® Live Cell	Green	Live	1:1000	518	Biotium
CellLight™ Nucleus-RFP	Red	Live		585	Thermo Fisher
DRAQ 5	Far Red	Live	1:1000	681	Thermo Fisher
TO-PRO3 Iodide	Far Red	Fixed	1:2500	661	Thero Fisher

## 2.8 Lysotracker assays

### 2.8.1 *Lysotracker quantification by multiwell plate assay*

Cells were seeded into black walled, clear bottom 96 well plates, at density of 5,000 cells per well. Cells were then treated with cannabidiol as described in 2.2.1. or copaiba as described in 2.2.2. for 48 hours. After this time, cells were washed 3 times in PBS, followed by the addition of 200nM Lysotracker-green DND-26 (Invitrogen) for 15 minutes at 37°C. Cells were washed a further three times with PBS, and kept in 200µl PBS. Plates were imaged using a BMG Pherastar FSX with excitation set at 485nm and emission at 520nm.

### 2.8.2 *Lysotracker quantification by fluorescence microscopy*

Cells were seeded into black clear Phenoplate, 96-well (Perkin Elmer/Revvity), at density of 2,000 cells per well. Cells were washed in PBS three times prior to staining. All LysoTracker dyes were diluted 1:5000 in PBS. Cells were incubated with LysoTracker dyes for 15 minutes in the dark. After this time, cells were washed three times and corresponding nuclei stain added.

Cells were imaged using an Operetta CLS utilising the PreciScan function. The prescan was done with the 10x air objective lens imaging in the Hoechst channel pre-set (excitation 355-

385nm emission 430-500nm) utilising the analysis pipeline to identify suitable loci within the well for re-imaging at a higher magnification. The rescan was carried out using the 40x water objective lens using the digital phase contrast channel, in addition to the LysoTracker red pre-set with an excitation 530nm-560nm emission 570nm-650nm and the Hoechst channel, (excitation 355-385nm emission 430-500nm). An evaluation pipeline was created utilising the digital phase contrast to find the area of the cells, the Hoechst channel to find nuclei and the LysoTracker channel to find fluorescent spots within the cell area identified in the digital phase contrast.

**Table 2.5 LysoTracker dyes used.**

<i>Name</i>	<i>Colour</i>	<i>Emission wavelength (nm)</i>	<i>Catalogue number</i>
LysoTracker™ DND-26	Green	510	L7526
LysoTracker™ DND-99	Red	590	L7528
LysoTracker™ Deep Red	Far red	688	L12492

## **2.9 AQ2 Analogue excitation and emission filter determination**

The excitation and emission filters installed within the MDI's Operetta, allow for 14 possible combinations of excitation/emission filters, as shown in *Figure 3.15(a)*. Healthy control human fibroblasts were used for spot identification. due to their enhanced imaging qualities when compared to glial cells. All excitation and emission filter settings were kept constant at 100% LED power and 100ms exposure time, in addition to imaging all three probes on the same plate to ensure consistency between probes and excitation and emission filter combinations.

## **2.10 Zinc imaging assays**

### **2.10.1 TSQ staining**

Cells were incubated with Sytox Green at a 1:5,000 dilution for 10 minutes, washed three times in PBS, and 100µM TSQ in TSQ assay buffer added. Plates were imaged immediately after adding TSQ.

### *2.10.2 TSQ assay buffer*

TSQ assay buffer comprised of PBS supplemented with 1mM CaCl<sub>2</sub>, 1mM MgCl<sub>2</sub> and 10mM HEPES, pH 7.4.

### *2.10.3 Image analysis*

Data obtained by imaging was analysed using Harmony software, with the analysis pipeline being kept consistent between plates. All readout data was mean per well of a minimum of 10 images per well. The Z' score was also generated for each plate using Harmony software.

### *2.10.4 Compound library*

The compound screening library was obtained from APEXBIO. The library used was the DiscoveryProbe™ FDA-approved Drug Library (L1021), consisting of 1499 FDA approved molecules. Compounds were aliquoted into plates at a concentration of 1mM. For screening all compounds were tested at 10µM. Plates were stored at -80°C when not in use.

### *2.10.5 Zinc modulating compound screening plate preparation*

2,000 cells were seeded per well into PhenoPlate 96 (Revvity) and grown overnight. The following day, compound was added to a final concentration of 10µM. Each plate contained untreated, positive (100µM ZnCl<sub>2</sub>) and negative (50µM clioquinol) controls. The next day the cells were washed with PBS and fixed for 10 minutes with cold 4% PFA. Cells were washed a further 3 times with PBS and stored at 4°C.

### *2.11 Bac-Mam transfection*

For Bac-Mam cellular transfection, 5,000 cells were seeded into Phenoplates overnight, and cells treated with Bac-Mam transfection reagent; ranging from 1µl up 8µl per well. The volume of media was decreased from initial assays at 150µl per well, to 100µl, followed by further decreases to 75µl and 50µl per well. Cells were incubated with Bac-Mam overnight before imaging or further cell treatment. Bac-Mam enhancer was also tested, with dilutions from 1:100 to 1:5000 when combined with Bac-Mam transfection reagent, however no improvement in the cellular uptake was observed.

# 3 Identification of AQ7 as a novel lysosomal probe

## 3.1 Introduction

In order to both identify and study the physiological effects of lysosomes; robust probes are required. Initial discovery and identification of lysosomes was achieved through centrifugation, as first carried out by De Duve, which required cell fractionation (Appelmans et al. 1955). Lysosomes were imaged for the first time soon after using electron microscopy, however it was several years before the first lysosome specific probes were identified allowing for the imaging of lysosomes *in vitro* in intact cells.

### 3.1.1 *History of lysosomal probes*

The first reports of lysosomal staining were published in 1960 and 1961, demonstrating that lysosomes in fibroblasts can be detected using neutral red stain (*Ogawa et al. 1961*). This was followed by confirmation that lysosomes could be stained with Azure A and methylene blue (Koenig 1963). The same group also identified that lysosomes responded to dyes that were sensitive to metal ions, such as copper and iron. The first fluorophore that was identified as a lysosome specific probe was acridine orange, which stained the lysosomes in a range of cultured cells and tissue samples (Allison and Mallucci 1964; Canonico and John 1969).

In the following decades, a range of other lysosomal specific probes were identified including: 1-anilinonaphthalene-8-sulfonate, Nile Blue, FITC-Dextran, TRITC-Dextran, DALCK, Sulforhodamine 101-Dextran (Texas Red), Cresyl Violet, Lucifer Yellow, MDC, SNAFL's and Rhodamine B (Ishikawa and Numakunai 1972; Hawiger and Timmons 1973; Ohkuma and Poole 1978; Berruti and Martegani 1984; Geisow 1984; Wang and Goren 1987; Gèze et al. 1993; Wisniewski et al. 1993; Biederbick et al. 1995; Brook et al. 1996; Vult von Steyern et al. 1996). Structures of some of these earliest lysosomal probes are included in *Figure 3.1*; of note is the structural similarity, including a tricyclic backbone in four of the molecules shown.

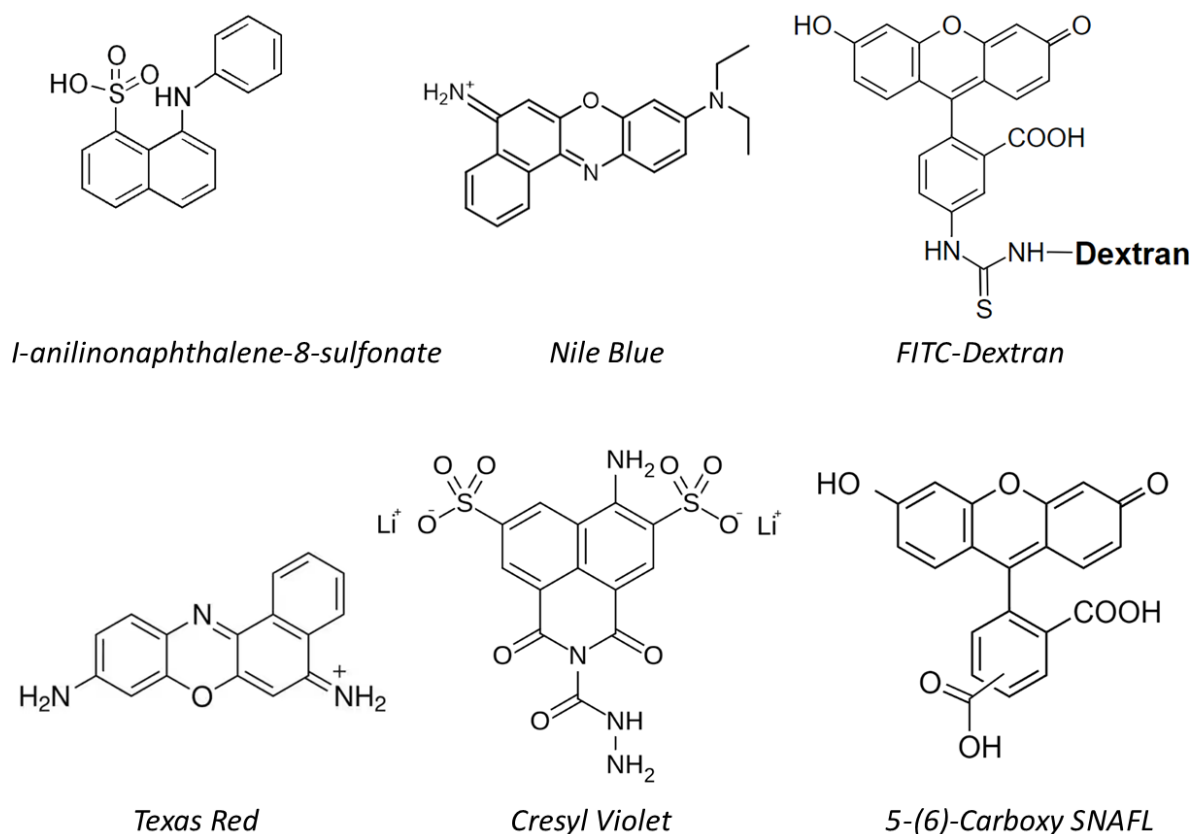


**Figure 3.1. Structure of a range of earlier lysosomal probes**

The structures of a range of early lysosomal probes are shown. The probes include a broad range of excitation and emission properties, including blue fluorescence (*I-anilinonaphthalene-8-sulfonate*), green fluorescence (*FITC-Dextran*), red fluorescence (*Cresyl Violet*), and far-red fluorescence (*Nile blue*).

However, the creation and availability of the LysoSensor and LysoTracker family of dyes in the early 1990's, led to LysoTracker Green DND-26 or LysoTracker Red DND-99 becoming the default fluorescent lysosomal probe (Thomas et al. 1997; White and Kaczmarek 1997).

### 3.1.2 Limitations of current lysosomal probes

Despite the widespread adoption of LysoTracker dyes as the standard, the nature of the molecules has known drawbacks to their use, including photoconversion and alkalinizing effects. All the LysoTracker family of dyes can induce an alkalinizing effect, whereby extended incubation, either through prolonged time or excess concentrations of LysoTracker leads to increased lysosomal pH. This alkalinizing effect is driven by the addition of amine containing side groups into the probes, which are used for lysosomal targeting (Folts et al. 2016).

Therefore, they cannot be used for time course assays, where prolonged lysosomal imaging is required. Additionally, some of the LysoTracker dyes are known to photoconvert,

particularly LysoTracker Red DND-99, which undergoes a shift to green fluorescence. Therefore, this limits the dyes use in situations where prolonged LED exposure times are likely or when repeat imaging would be required (Freundt et al. 2007).

With the known issues of LysoTracker dyes, several novel probes have been created that attempt to deal with some of their limitations. Some of these new probes include: BCECF, 6-O-dansyl-GlcNH<sub>2</sub>, NBD-PZ, Rlyso and DiEtNBODIPY(Holopainen et al. 2001; Glunde et al. 2003; Ishiguro et al. 2008; Urano et al. 2009). The structure of some of these newer probes are shown in *Figure 3.2*.

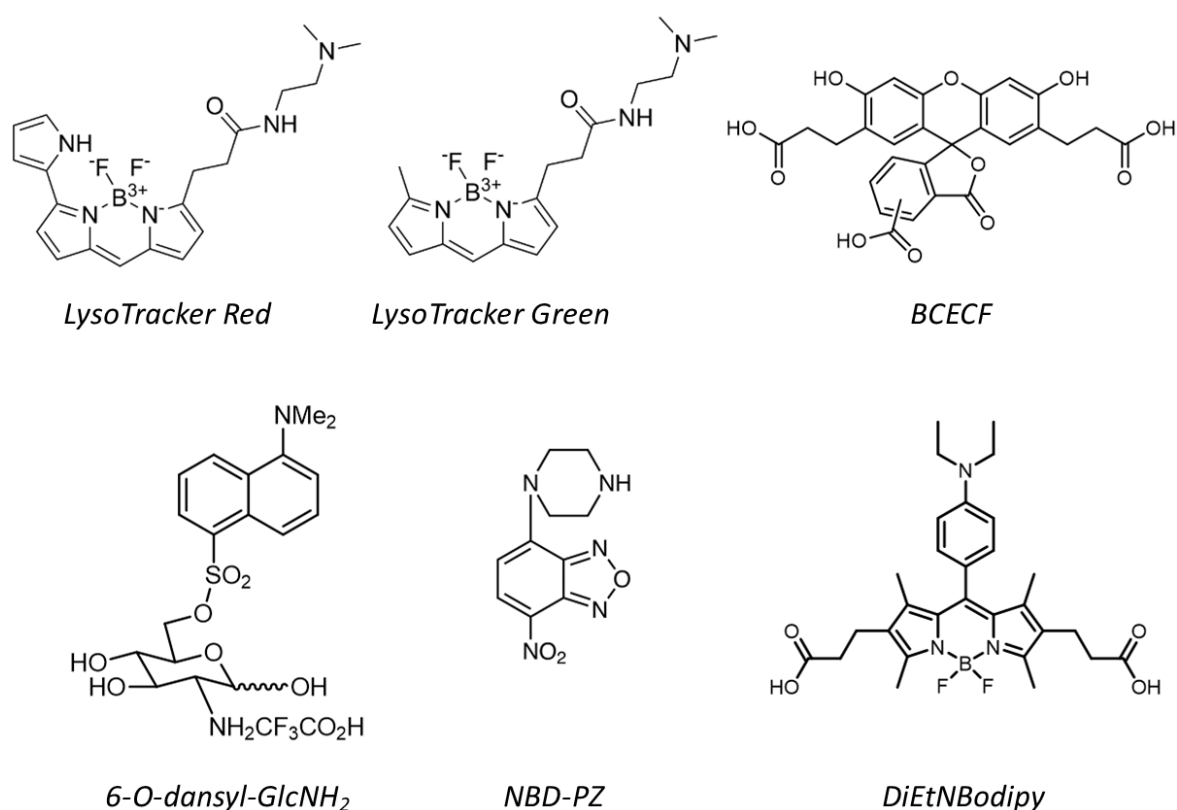


**Figure 3.2. Structures of several recently developed lysosomal probes**

Structures of LysoTracker and several newer lysosomal probes are shown. The newer lysosomal probes also show greater diversity in their structures compared to the earlier lysosomal probes. BCECF, 6-O-dansyl-GlcNH<sub>2</sub>, NBD-PZ and DiEtNBodipy emit fluorescence in the green spectrum, Rlyso has shown to be a red fluorescent probe.

### 3.1.3 Characteristics for identification of novel lysosomal probes

Considering the current range of lysosomal probes, there is a range of desirable characteristics when identifying potential lysosomal probes. The first consideration with identifying a new lysosomal probe is the specificity of the molecule, as the molecule must possess specificity for lysosomes over non-vesicular and vesicular organelles. Any suitable

probe must possess a fluorophore whose emission can be detected at low concentrations, preferably with fluorescence towards the red or far-red end of the emission spectra to limit background autofluorescence. Provided that the molecule contains a bright enough fluorophore, the molecule must also be non-toxic or induce severe lysosomal dysfunction at working concentrations. This should also include, where possible, the avoidance of the use of nitrogen containing side groups to prevent alkalinising of the lysosome and allow time course imaging with the probe. Whilst not directly related to the fluorescence properties of the molecule, any new probe's hydrophilicity, must also be considered, as molecules with poor solubility in water or DMSO are unlikely to be suitable probes.

#### *3.1.4 RND permease probes*

As NPC1 is a member of the RND permease family of proteins, it may be possible to identify chemical starting point for NPC1 specific substrates, through identification of substrates for other members of the RND permease family. In prokaryotes a group of the RND permease family are the acriflavine (Acr) efflux system. One member of the ACR efflux system is AcrABZ-TolC, which can export most commonly found antibiotics and various aromatic organic compounds (Anes et al. 2015). One such aromatic molecule actively effluxed by AcrABZ-TolC is the quinone derivative and topical antibiotic acriflavine, which has been identified to be a fluorescent compound with emission in the green part of the spectrum (Ex 416nm, Em 514nm). Acriflavine, and other structurally similar acridine derived molecules have, in addition to their fluorescent properties, been identified for being potent DNA intercalating agents (Alvi et al. 1985). Based on the identification of fluorescent substrates for prokaryote members of the RND permease family, the development of fluorescent probes for NPC1 is a potential area for further research and probe development.

#### *3.1.5 Anthraquinones as lysosomal probes*

Anthraquinone derivatives are a ubiquitous family of dyes of both natural and synthetic origins; with most naturally occurring red dyes being anthraquinone derivatives (Gordon and Gregory 1987). Anthraquinones can be considered annelated derivatives of p-benzoquinones, and can be described as two benzene rings linked by two carbonyl groups (Szymańska and Majerz 2021). The addition of electron donor groups into the molecule can be used to give anthraquinones anywhere from blue up to far red fluorescence (Ziarani et al.

2018). When certain functional groups are attached to the anthraquinone core, it is possible to cause highly specific organelle staining. An example of these organelle specific side groups, being that the addition of two pentane groups to anthraquinone leads to a lysosome specific probe (Patton et al. 2016). Therefore, with good photostability and the ability to localise to specific organelles, anthraquinone based molecules offer potential as lysosomal probes.

Through collaboration with Professor Simon Pope in Cardiff University School of Chemistry, a novel anthraquinone derivate, known as AQ2 has been developed. This molecule shares similarity in the anthraquinone derived antibiotics such as acriflavine, sharing an acridine backbone, however a pair of side groups have been added to the molecule to form AQ2. Work carried out by the Lloyd-Evans Laboratory has identified that AQ2 is trafficked through the endosomal system, and trafficking of AQ2 out of lysosomes is NPC1 dependant. This dependence on NPC1 for lysosomal export of NPC1 was determined through a series of experiments whereby control healthy cells and NPC1 overexpressing cells, were treated with either chemical NPC1 activator and inhibitor prior to treatment with AQ2.

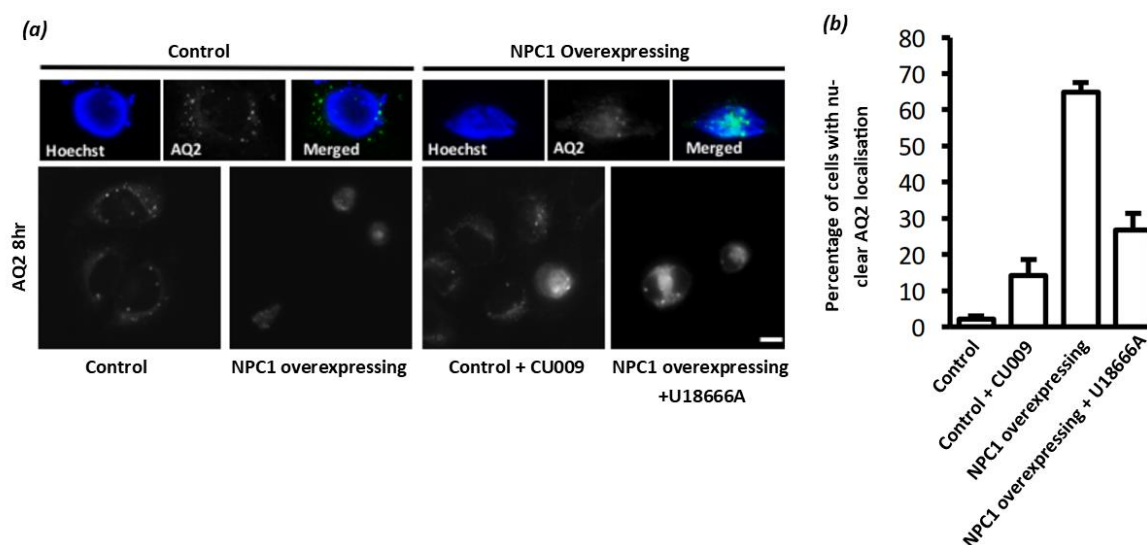


**Figure 3.3. NPC1 transports AQ2 out of lysosomes**

AQ2 is found in the nucleus of NPC1 overexpressing CHO 1-9 cells, but not control CHO H1 cells after 8h incubation. Nuclear localization is increased in CHO H1 by treatment with the NPC1 activator CU009, and reduced in CHO 1-9 by treatment with the NPC1 inhibitor U18666A. Representative pictures shown, n=2 (D) Quantification of cells with nuclear AQ2 following 8h incubation with AQ2. Graph shows mean +/- SD, n=2. Data generated by Prof. Emyr Lloyd-Evans and Dr. Helen Waller-Evans.

Whilst AQ2 was shown to be an NPC1 substrate, a difficult synthesis pathway, led to desire to create simpler anthraquinone derivates that are NPC1 substrates. A series of 4 molecules, sharing the same anthraquinone backbone as AQ2 were created by the Pope laboratory, with each molecule AQ3-6 having a different side group. From the first series, where AQ3 was selected, an improved molecule, AQ7 was created.

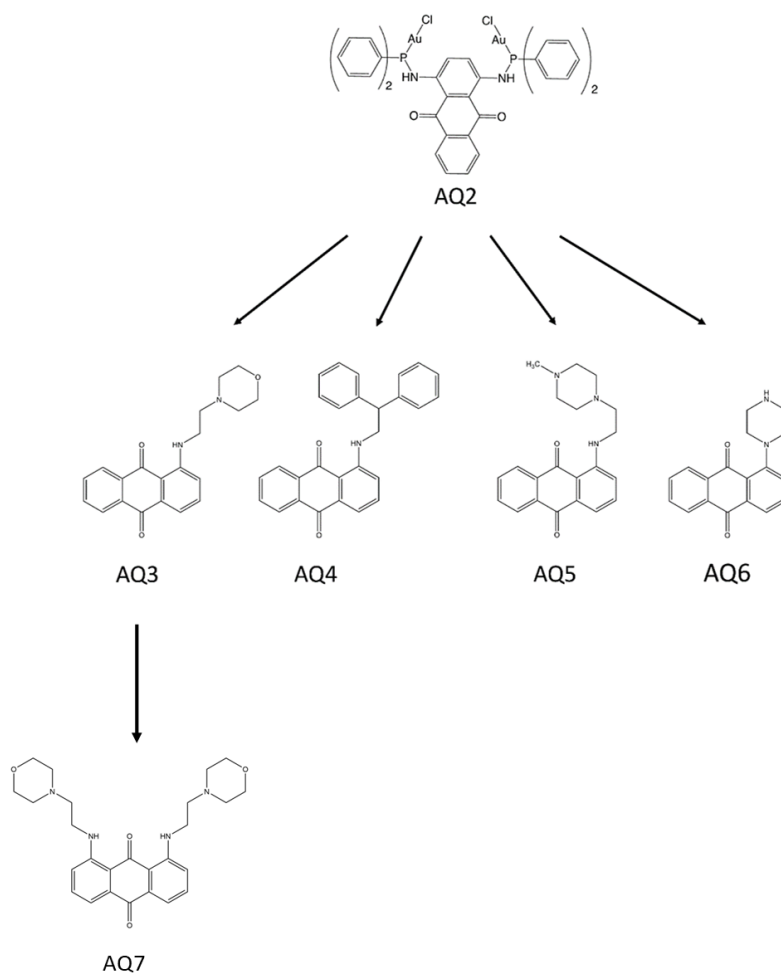


**Figure 3.4. Structures of anthraquinone derivates evaluated**

The initial anthraquinone derivate tested AQ2, contains complex side groups, including complex multi-step synthesis. Anthraquinone derivates with simpler lysosome targeting side groups were numbered AQ3-6. Based on screening of AQ3-6, a further improved version of AQ3 was synthesised with a second morpholine group both improved fluorescence intensity and further red shifted fluorescence emission named AQ7.

### 3.1.6 NPC1 activity assay

Despite the extensive research into Niemann-Pick disease, no definite role for NPC1 has been accepted. Whilst it has been suggested that NPC1 is primarily cholesterol transporters, other evidence contradicts this hypothesis (Lloyd-Evans et al. 2008). Therefore, with no clear substrate for NPC1, development of NPC1 specific activity assays has proved difficult.

One publication has shown that it is possible to identify NPC1 substrate, with acriflavine being transported by NPC1 (Davies et al. 2000). Data from the Lloyd-Evans laboratory showed that a molecule, AQ2, which contained a structurally similar core, was also transported by NPC1, with the additional benefit of possessing fluorescent properties. AQ2 was shown to initially be trafficked to the lysosome, however over time, the molecule would translocate to the nuclei. However, whilst the assay worked, AQ2 had several limitations as a probe, including low fluorescence emission, high cellular toxicity and poor solubility.

Therefore, initially we intended to identify an improved analogue of AQ2, with better molecular characteristics. We would then develop a trafficking assay, whereby the probe would first be entered to the lysosome, subsequently being exported by NPC1 and being trafficked to the nuclei. Comparison of the fluorescence in the nuclei to the lysosome could be used to determine NPC1 activity.

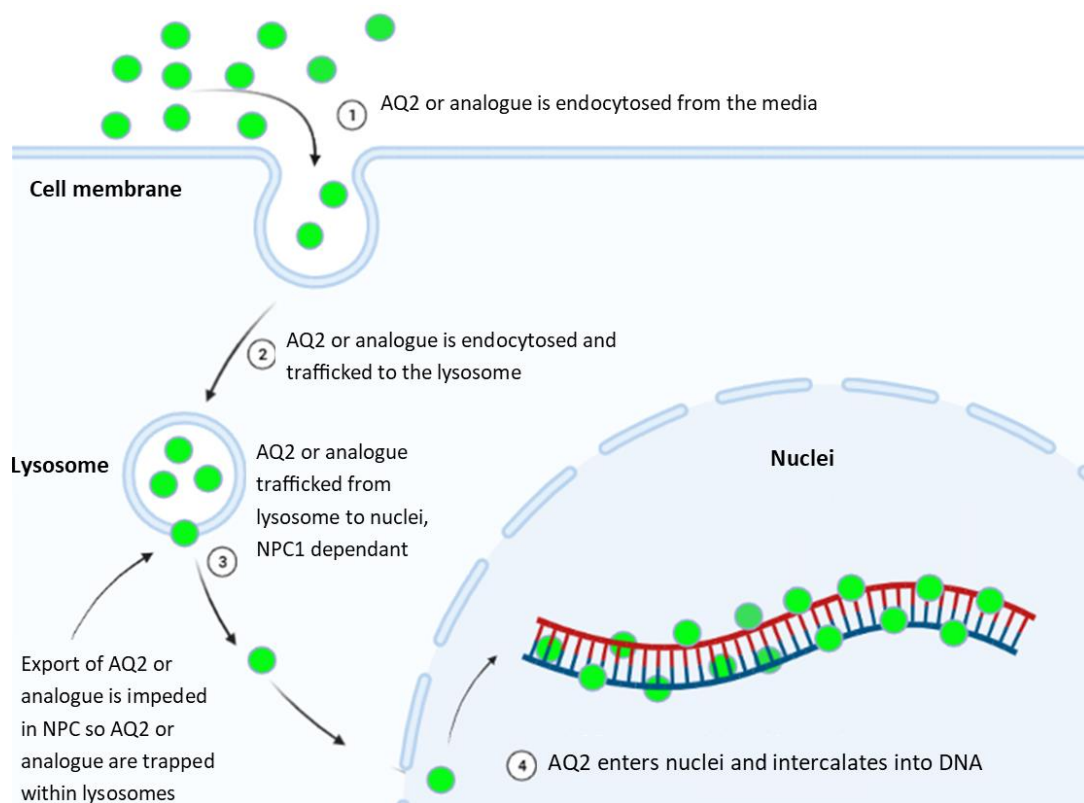


**Figure 3.5. Simplified diagram of AQ2 or analogue trafficking assay**

The diagram shows a very simplified version of the rationale of the AQ2 (or analogue) trafficking assay. The probe is first endocytosed into the cell, whereupon the probe ends up within the lysosome. Export of the probe from the lysosome leads to the probe migrating to the nuclei whereby it binds to DNA. The export of the probe from the lysosome, and thus the amount of the probe that reaches the nucleus is NPC1 dependant. Therefore, comparing the ratio of nuclei fluorescence to lysosomal fluorescence of the probe could be used to determine NPC1 activity.

### 3.1.7 Aims of the chapter

The aims covered in this chapter were to develop an NPC1 activity assay, this included:

1. Determine which of AQ2 analogues (AQ3-6) had the highest fluorescence emission, with the least cellular toxicity, which was to be taken forward for further evaluation; to be determined based on the probes cellular toxicity, as well as solubility when imaging.
2. Set up a cellular trafficking assay using AQ3 as selected in Aim 1.
3. Compare fluorescence characteristics of AQ3 and AQ7, to determine whether AQ7 is an improvement.
4. Compare AQ7 to LysoTracker dyes to assess whether AQ7 is a suitable lysosomal probe.

## 3.2 Results

### 3.2.1 AQ2 and Analogues toxicity analysis.

#### 3.2.1.1 Glial cell Realtime glo assay calibration

To determine the toxicity of AQ2 or analogues, toxicity assays were to be carried out, using the RealTime-Glo™ MT cell viability assay. Prior to testing AQ2 or analogues assay calibration was performed. The data in *Figure 3.6*. shows the calibration experiments required for use of the RealTime-Glo™ MT cell viability assay. Calibration of the cell seeding density was required to ensure that the cells did not enter exponential or nonlinear growth during the 72-hour period. Based on the data in *Figure 3.6(a)*, the 50,000 cells showed nonlinear increases in metabolic activity in the 50-70 hour window.

The cells seeded at 1,000 – 10,000 cells per well, were observed to have low luminescence over the elapsed time course of the assay, whilst remaining linear throughout. The 25,000 cells per wells consistently had higher luminescence, without reaching nonlinear growth phase over the 72-hour time period.

From the assay calibration data, 25,000 cells per well was decided as the future seeding density for 96 well plates for use in the toxicity assays with AQ2 analogues. Due to potential DNA intercalation from AQ2 or analogues, it was decided to use NPC1 -/- glia for the toxicity assays, as any toxicity observed would be likely from off target effects as no nuclei DNA

intercalation should be observed in the NPC1  $-/-$  glia. Of note, was that the proliferation of NPC1  $-/-$  was lower than that of the corresponding wild type glia.

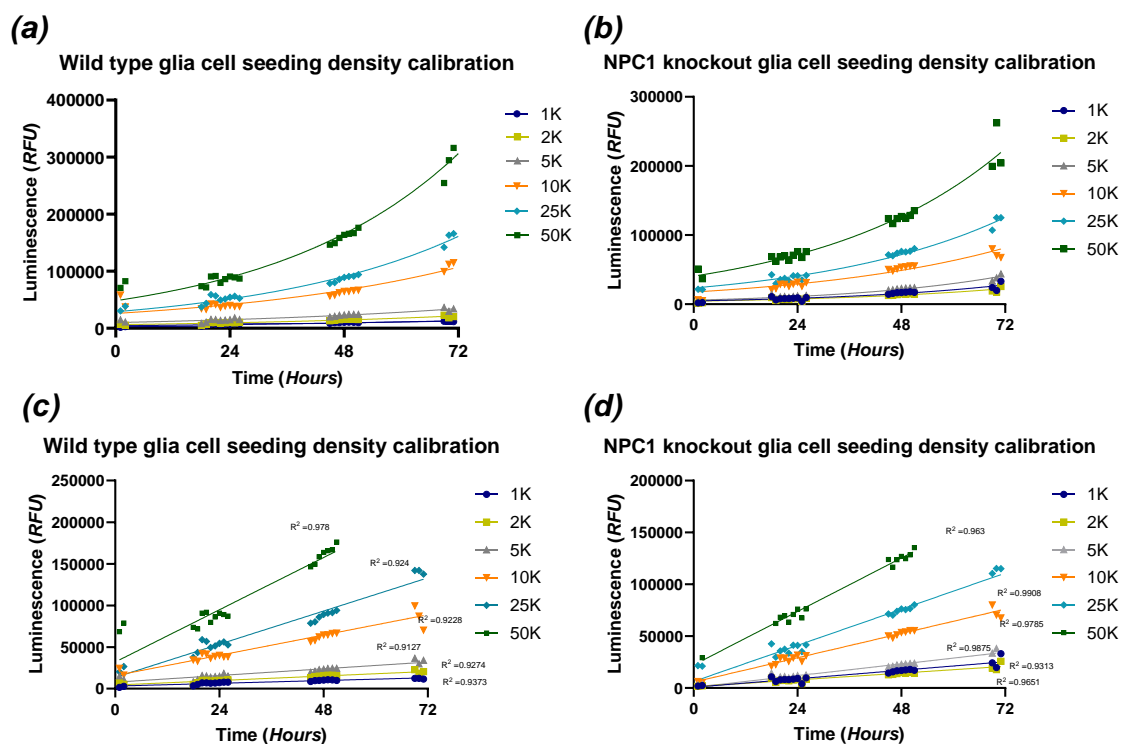


**Figure 3.6. Calibration of Real Time Glo assay with mouse glial cells**

Comparison of cell seeding densities detected using RealTime-Glo™ MT cell Viability assay. Both (a) and (c) correspond to data associated to wild type glia, with (b) and (d) being NPC1  $-/-$  glia. In (a) and (b) the data is fitted with nonlinear trendlines, with each data being plotted for each seeding density over a 72-hour period. In (c) and (d) a linear trendline has been fitted to each seeding density, with data being limited to only include the timepoints from when the proliferation was linear. Data is n=1.

### 3.2.1.2 AQ2 analogues LC50 comparisons

After the Realtime Glo calibration assays had been completed, toxicity analysis for AQ2 and analogues could be carried out. A range of concentration of each analogue was tested, with the effects upon viability across the concentration range for each analogue shown in Figure 3.7(a). Despite only having differences in the side group of each anthraquinone, this led to large differences in cellular viability, and therefore tolerance to the probes. AQ2 as a reference compound, had an LC50 value of 21 $\mu$ M.

Both AQ3 and AQ6 showed reduced toxicity over AQ2; with AQ3 having an LC50 of 154 $\mu$ M and AQ7 a value of 346 $\mu$ M. Subsequently, the addition of the second morpholine group to AQ7 led to an increased LC50 of approximately 200 $\mu$ M, an approximate two-fold increase in

LC-50. AQ6 exhibited the highest LC50, with an associated value of 494 $\mu$ M as shown in *Figure 3.7(b)*. Of the AQ2 analogues, AQ4 and AQ5 exhibited significant cellular toxicity across all concentrations, with AQ4 having an associated LC50 of 2 $\mu$ M, and AQ5 having an LC50 of 6 $\mu$ M. Both AQ4 and AQ5 had statistically significant decreased LC50 values compared to AQ2, AQ3 and AQ7. LC50 values for each analogue is shown in *Figure 3.7(b)*.

It was not clear why both AQ4 and AQ5 exhibited high cellular toxicity when compared to the other AQ2 analogues. However, as AQ4 and AQ5 have double ring side groups, which leads to the molecule being more lipophilic, particularly when compared to the more polar and subsequently hydrophilic side groups present in AQ3, AQ6 and AQ7, this may be responsible for the decreased cell viability observed with AQ4 and AQ5.

Due to toxicity mediated by AQ4 and AQ5 at working concentrations, assessment of these molecules was discontinued. Additionally, with the LC50 values for AQ4 and AQ5 being low, it is unlikely that treating cells with low micromolar or nanomolar concentrations of AQ4 or AQ5 would lead to observable fluorescence.

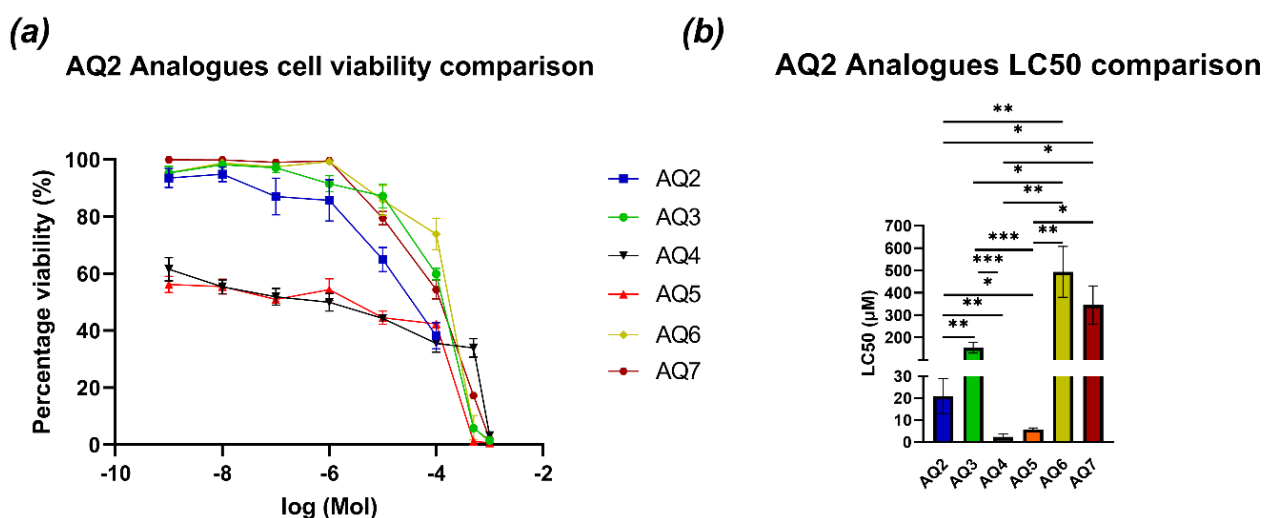


**Figure 3.7. Toxicity analysis for AQ2 and analogues in mouse glial cells**

Percentage cell viability is compared across a range of AQ2 and analogue concentrations (a). Cells were treated with one of AQ2 or an analogue for 4 hours, followed by 20 hours in media without the presence of AQ2 or analogues. Cell viability was determined using RealTime Glo, with treated cells being compared to that of untreated control. Panel (b) shows estimated LC50 values for each of the AQ2 analogues in NPC1  $-/-$  glial cells, which was determined using Boltzmann-Sigmoid curves. All data is  $n=3$ , with mean and standard deviation shown, statistical significance was determined through a one-way ANOVA, with post hoc Tukey test.

### 3.2.2 Lysosome localisation of AQ2 analogues

To determine whether the AQ2 analogues were localising to the lysosome, wild type glia cells were stained with AQ3 or AQ6. Both molecules showed lysosomal localisation after a 4-hour incubation period.

From this lysosomal imaging, AQ6 was discounted from future experiments, as throughout the assay, large aggregates of the molecule were observed that did not dissolve, even upon vortexing as shown in both *Figure 3.8* and *9.3.1.1*.

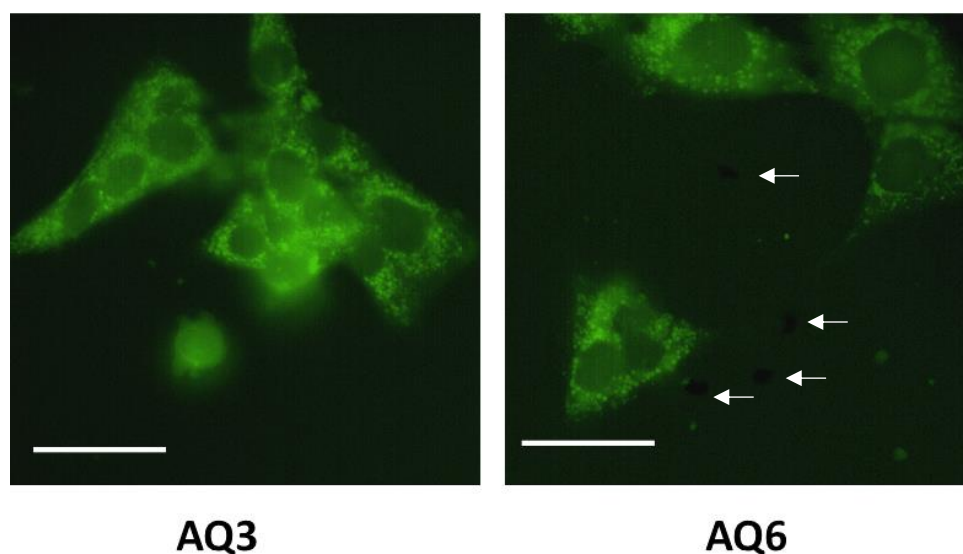


***Figure 3.8. Lysosomal localisation of AQ3 and AQ6***

*Wild type glia cells were incubated with 50 $\mu$ M of AQ3 or AQ6 for 4 hours. Cells were imaged in Opti-MEM, without the probe using an Operetta CLS using the x63 water objective lens. Of note in the AQ6 picture as marked by the arrows are dark regions, corresponding to insoluble aggregates of AQ6. Data is n=1. Scale bars represent 50 $\mu$ m.*

### 3.2.3 AQ2 analogue nuclei trafficking assay set up

As shown in 3.2.2, AQ3 localised to lysosomes after a 4-hour incubation period. To develop the NPC1 trafficking assay, required knowing how long the probe took to be trafficked to the lysosome, as well as, crucially, how long the probe would take to be trafficked out of the lysosome by NPC1 and to enter the nucleus. The next step in assay development was to carry out time course assays to determine how long AQ3 took to be trafficked out of the lysosome and to enter the nucleus. We subsequently confirmed that AQ2 analogues are localising to lysosomes, as shown in 3.2.6.2.

### 3.2.3.1 AQ3 trafficking assay chase time determination

Cells were treated with a range of concentrations from 1mM down to 1 $\mu$ M for a 4 hour 'Pulse'. Cells treated with upwards of 500 $\mu$ M AQ3 showed cellular toxicity within 4-5 hours, consistent with the LC50 data from the previous toxicity assay. Cells treated with 50 $\mu$ M or lower of AQ3, showed limited fluorescence, with the window between background and fluorescence signal from AQ3 being too small to be usable.

When following AQ3 trafficking, initial staining was consistent with lysosomal localisation (perinuclear puncta), with initial AQ3 export from the lysosomes occurring (diffuse cytoplasmic) after 8 hours since the probe was initially added. After a further 10 hours, and 18 hours in total, nuclei fluorescence from AQ3 was observed in some cells. Beyond 18 hours, no additional increase in nuclei fluorescence was observed in the glial cells, with nuclei fluorescence being observed in approximately 10-20% of cells. Cells treated with 200 $\mu$ M AQ3 showed the highest fluorescence window, without excessive toxicity, so 200 $\mu$ M AQ3 was used for subsequent assays.

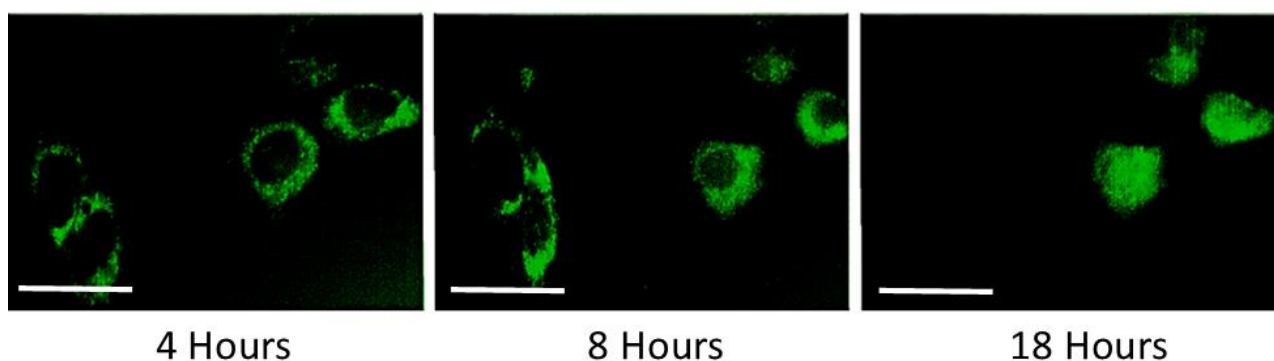


### **Figure 3.9. AQ3 trafficking in wild type mouse glial cells**

AQ3 can be seen being trafficked through the endocytosis pathway. At 4 hours, AQ3 can be visualised in the lysosomes, at 8 hours the AQ3 is localised to cytoplasm and at 18 hours AQ3 can be visualised in the nuclei. Wild type mouse glial cells were used, being treated with 100 $\mu$ M AQ3. Cells were imaged using x40 water objective on an Operetta CLS. Scale bars represent 50 $\mu$ m.

### 3.2.3.2 Nuclei probe identification

Once we had identified how long AQ3 took to both show lysosomal localisation 3.2.2, as well as subsequent nuclei localisation (3.2.3.1), the next step for developing the trafficking assay was to identify a suitable nuclei stain. Finding a suitable live-cell nuclei stain was critical for developing the assay for a HTS, as identifying the nuclei is the first step in the Harmony software analysis pipeline. Additionally, to compare the lysosomal AQ3 fluorescence to the nuclear AQ3 fluorescence, required the ability to accurately define the nuclear region.

Therefore, we needed to identify a suitable nuclei probe that did not have fluorescence bleed through into the AQ3 emission channel or induce cellular toxicity over the time course of the assay. Thus, we were looking for nuclei stains in the: blue, red, or far-red range that could be used in combination with AQ3.

#### 3.2.3.2.1 Hoechst 33342

One of the most commonly used nuclei stains, and the first to be tested was Hoechst 33342; a blue fluorescent nuclei stain. Hoechst 33342 is toxic to cells at higher concentrations, so Hoechst 33342 was added to the cells after the 4-hour pulse with AQ7 at a 1:10000 dilution; 50% lower than that used for normal cell imaging.

Despite lowering the concentration of Hoechst 33342 by 50%, an issue with the emission 'tail' of Hoechst and the emission filters on the Operetta led to bleed through of fluorescence from Hoechst into the AQ3 channel (500-550nm), as can be seen in *Figure 3.10*.

This was compounded by AQ3 having comparatively low fluorescence, requiring high LED power and long exposure times, which allows the tail of the Hoechst fluorescence saturate the channel. Therefore, it was apparent that the Hoechst signal would prevent detection of AQ3, or its subsequent trafficking when used in conjunction with the excitation/emission filter set initially used for imaging AQ3. In cells stained only with Hoechst 33342, fluorescence was detectable in the AQ3 excitation/emission imaging channel.

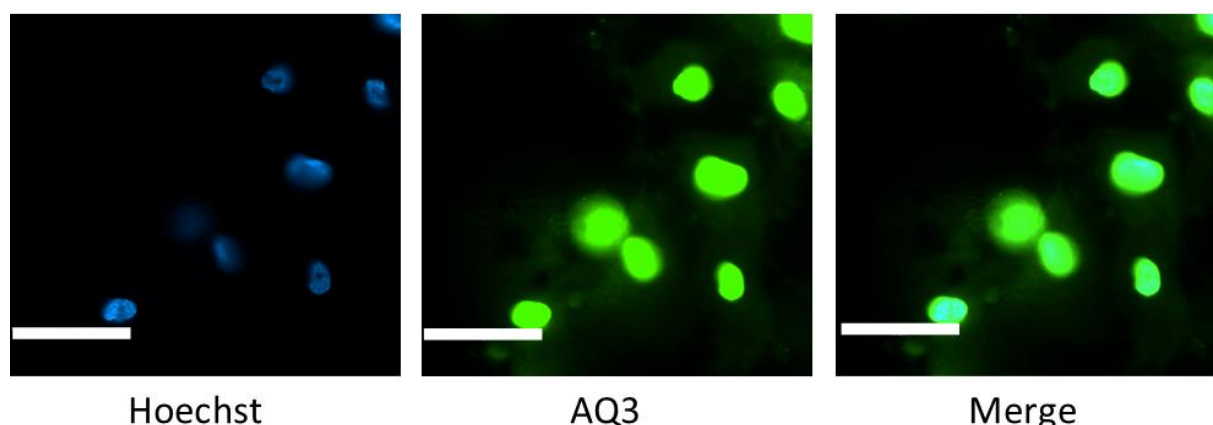


***Figure 3.10. Hoechst 33342 fluorescence bleed through into green AQ3 channel***

*Analysis of Hoechst emission peak, which can be seen bleeding over into the AQ3 green filter preset channel. Whilst the main emission peak of Hoechst 33342 is in the blue part of the spectrum, the emission tail overlaps with the green spectrum, albeit with lower fluorescence intensity. However, as AQ3 is weakly fluorescent, this required high LED power and long exposure time to image, which allows the Hoechst to saturate the image, before the AQ3 can be visualised. Scale bars represent 50µm.*

### 3.2.3.2.2 Draq 5

When cells were treated with 5 $\mu$ M Draq5, clear nuclei staining was observed in the far-red channel. Unlike the bleed through observed with Hoechst 33342, no cross-channel fluorescence bleed through was observed with Draq5 and AQ3 (Figure 3.11).

Another issue arose using Draq5 and AQ3, whereby it appeared that adding Draq5 after the 4-hour pulse, no AQ3 localisation was observed in the nuclei even after 24 hours. Cellular trafficking can be observed over a time course, so the cells remain viable, showing that cellular death is not responsible for stopping nuclear localisation. The lack of AQ3 nuclear fluorescence is likely to have occurred as both AQ3 and Draq5 are anthraquinone derivatives, with Draq5 being a known DNA minor groove intercalator. Considering the lack of AQ3 fluorescence in the nuclei of Draq5 stained cells, it is probable that AQ3 is also a minor groove intercalator, and thus is being blocked from binding to the DNA within the nuclei, due to the lack of fluorescence from within the nuclei. Therefore, this stops any of the Draq family of DNA/nuclei stains from being used to identify the nuclei, as they are all likely to interfere and stop AQ3 DNA binding. Decreasing Draq 5 concentrations would significantly reduce the fluorescence intensity and limit the imaging analysis software's ability to define the perimeter of the nuclei. Therefore, reducing Draq 5 concentration was not a viable alternative, and thus we needed to identify an alternative nuclei probe.

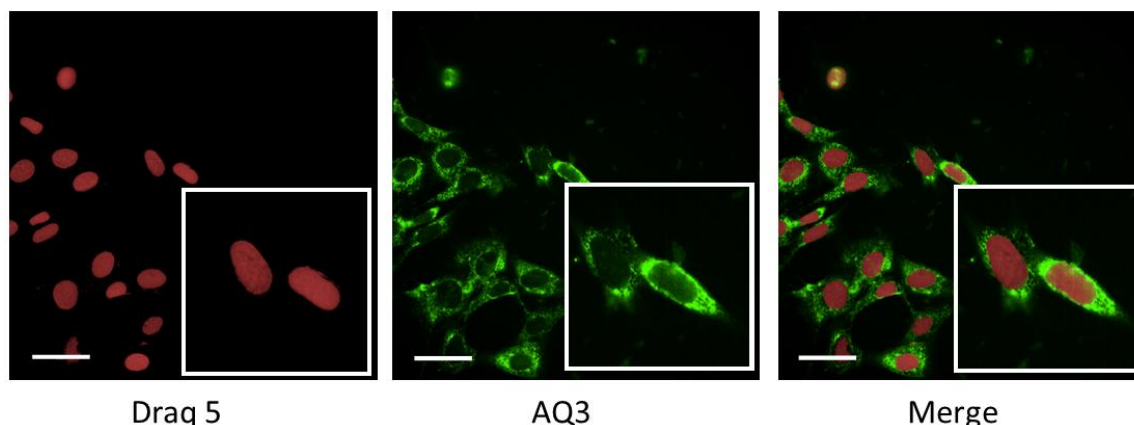


***Figure 3.11. Draq 5 prevents AQ3 nuclei localisation after 18 hours post AQ3 treatment***  
*Draq5 stops AQ3 from exhibiting nuclei localisation or fluorescence, and presumed DNA binding of AQ3. Cells were treated with AQ3 at 100 $\mu$ M for 4 hours, before being transferred into fresh media containing Draq 5 and incubated for 18 hours. Both AQ3 and Draq family of dyes are anthraquinone derivatives, so are likely competing for DNA minor groove binding sites. Scale bars represent 50 $\mu$ m.*

### 3.2.3.2.3 CellLight BacMam 2.0

After discounting both Hoechst 33342 and Draq5 from being potential nuclei stains, a search was made for a non-DNA binding red fluorescent nuclei stain.

An alternative fluorescent red probe was identified as the CellLight™ Nucleus-RFP, BacMam 2.0 from Thermo Fisher. Unlike traditional nuclei stains, BacMam CellLight uses baculovirus coupled to a mammalian promoter and transgene; in this case RFP fused to the SV40 nuclear localisation sequence. Therefore, when this probe is used, it doesn't bind directly to the DNA, nor does the probe induce any toxic effects.

It was decided that for future assays, 6µl of the probe would be added to the cells in 75µl of media, as this offered the highest transfection rates, whilst minimising the volume of nuclei probe being added to each well. Of note is that BacMam enhancer did not increase cellular transfection rates when trialled, so was not used. However, the percentage of transfected cells remained low at approximately 25% of cells being successfully transfected (9.3.1.2).

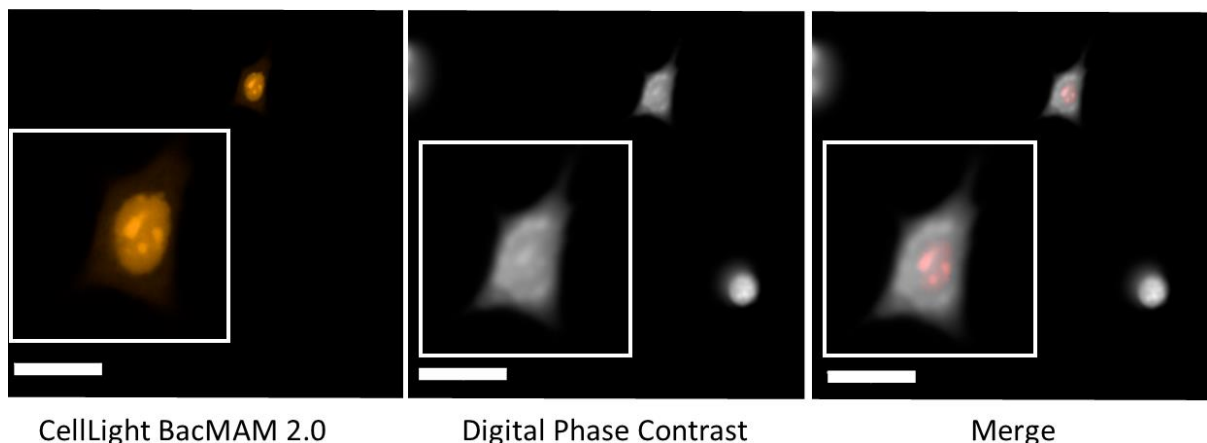


#### ***Figure 3.12. Nuclear localisation of CellLight BacMam 2.0***

*Nuclei staining of wild type glia cells treated with CellLight BacMam 2.0. Cells were treated with CellLight BacMam 2.0 overnight, and cells showed RFP fluorescence from the nuclei consistent with transfection undertaken. Co localisation images are shown with RFP fluorescence, digital phase contrast and a merged image. Images were obtained using 40x water objective on an Operetta CLS. Scale bars represent 50µm.*

### 3.2.3.3 AQ3 Trafficking assay with CellLight RFP

Initial AQ3 trafficking assays showed that both CellLight and AQ3 could be visualised in wild type mouse glial cells, with correct localisation after a 4-hour pulse with AQ3 as shown in *Figure 3.13. (a)*. Whilst some nuclei localisation of AQ3 was observed after an 18-hour chase, this was only occurring in a small proportion of the cells; no more than 10%. As we were not able improve the percentage of cells with nuclear AQ3 localisation development of the trafficking assay was stopped, as it was not viable to continue assay development.

However, whilst a small number of cells showed only lysosomal fluorescence in the green emission filter (em 500-550nm), a noticeable number of cells were shown to have fluorescence outside of the nuclei in the 570-650nm emission channel. When non-nuclei fluorescence observed in the RFP channel was compared to that of AQ3 localised to the late endosomes/lysosomes, it was clear that there was significant overlap in the fluorescence as shown in *Figure 3.13(b)*.

From this overlap in fluorescence, it was therefore postulated that AQ3 was emitting fluorescence in the red region of the spectrum as emission was detected in the em 570-650nm range. This was not expected, as we believed that AQ3 was going to have an emission peak around 525nm, without a significant 'tail' in the red region of the spectrum; this fluorescence was later confirmed in 3.2.5.2.

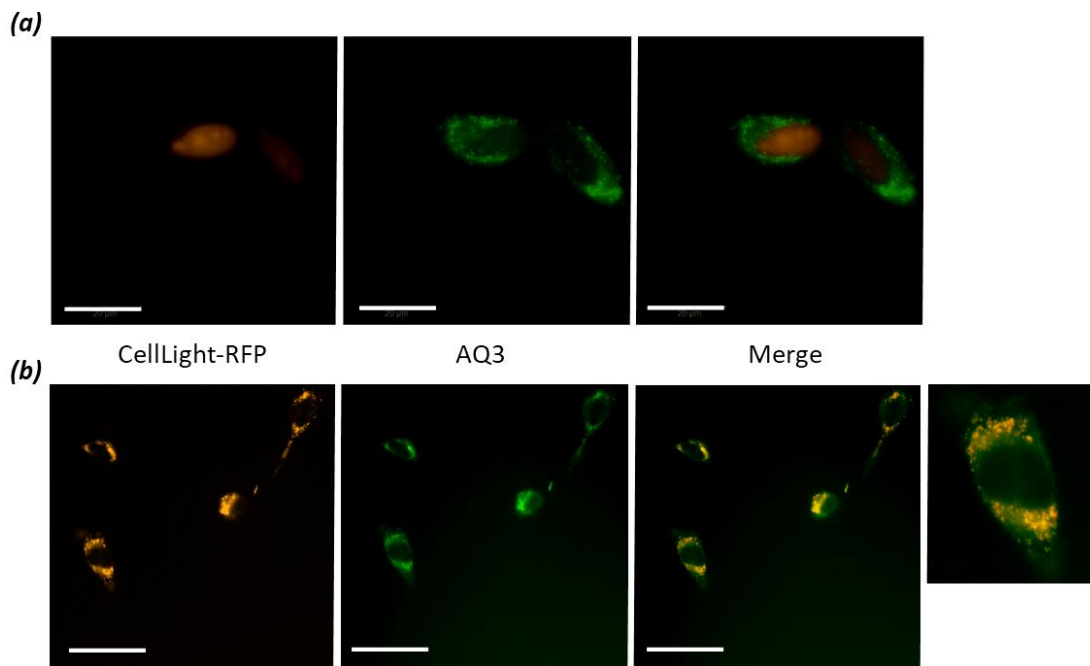


***Figure 3.13. Emission filter comparison for cells treated with AQ3***

*Imaging of mouse glial cells transfected with CellLight and treated with AQ3 showed fluorescence overlap. (a) Images showing CellLight nuclei fluorescence, and AQ3 lysosomal fluorescence after 4-hour treatment with AQ3. (b) Cross channel fluorescence emission of AQ3 in both 'green' emission filter wavelengths (500-550nm) and 'red' emission filter wavelengths previously used for with CellLight RFP (570-650nm). Scale bars in (a) represent 20µm and in (b) 50µm.*

### *3.2.4 Issues with development of an AQ2 analogue trafficking assay*

Despite several repeats of the trafficking assay combining AQ3 and CellLight, it was not possible to consistently observe AQ3 nuclei localisation. In most assays AQ3 was observed to be trapped within the lysosome in a large subset of the cells, even up to 24 hours after the probe was added.

Therefore, it was decided that AQ3 was not a suitable candidate to be taken forward for the development of a trafficking assay, as despite attempts to optimise the assay, it was not possible to get the assay to a point of desired robustness. As we observed unexpected red fluorescence, we decided to further investigate the molecules fluorescent properties. Furthermore, we went on to develop the potential use as of the analogues as a lysosomal probe lysosomal entrapment was observed.

### *3.2.5 Basic characterisation of AQ3 and AQ7*

#### *3.2.5.1 AQ7*

Following conversation with Professor Simon Pope about the limitations of AQ3, led to the creation of AQ7. The anthraquinone derivative AQ7 is structurally similar to AQ3, but possesses a second morpholine group. The addition of a second morpholine group, was believed to increase the fluorescence emission intensity, as well as being believed to lead to a far-red shift in fluorescence. Due to a limited supply of AQ2, it was decided to not use AQ2 for excitation and emission filter determination.

#### *3.2.5.2 Spectral analysis of AQ3 and AQ7*

Following the unsuccessful attempts to develop an NPC1 dependant activity assay, it was decided to assess the full excitation and emission spectra of AQ3 and AQ7, to determine the optimal excitation and emission filter combinations to use on the Operetta.

##### *3.2.5.2.1 Emission spectra of AQ3 & AQ7*

Comparison of fluorescence between AQ3 and AQ7 at 100mM. The emission spectra clearly shows a shift towards far-red for AQ7 when compared to AQ3 *Figure 3.14(a)*. Peak fluorescence emission for AQ3 was at approximately 510nm, whilst AQ7 had a peak fluorescence emission intensity at 620nm. Peak fluorescence intensity for AQ3, was approximately 120,000 RFU, whilst AQ7 had a peak fluorescence intensity of 250,000, double that of AQ3. From this data it was shown that outside of cells, AQ7 was a brighter fluorophore than AQ3, with a further shifted excitation and emission spectra.

(a)

### Flourescence emission of AQ3 and AQ7

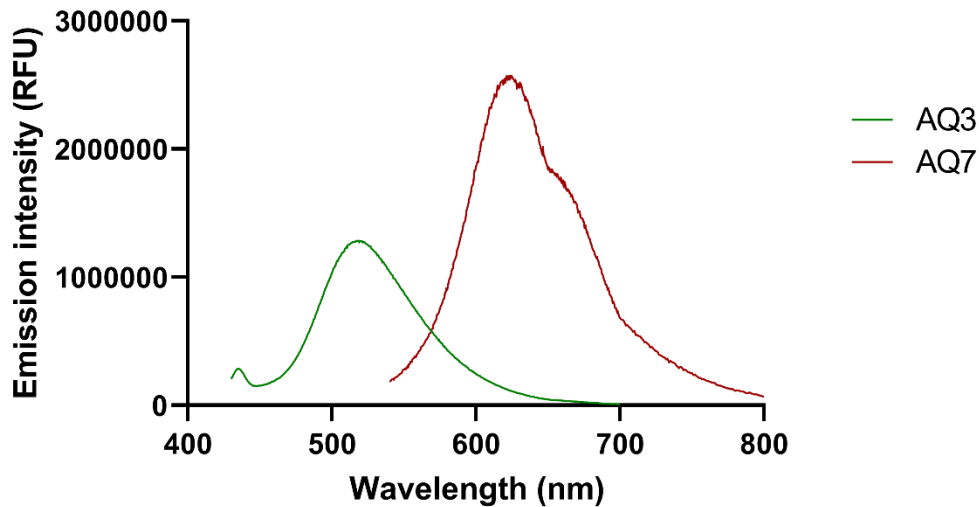


#### **Figure 3.14. Emission spectra of AQ3 & AQ7**

Emission spectra of both AQ3 and AQ7 showing the corresponding far-red shift of AQ7 compared to AQ3. Also illustrated is the corresponding increased peak fluorescence intensity for AQ7 over AQ3. AQ3 was excited at 400nm, with AQ7 being excited at 500nm. Data provided by Dr. Deemah Alenazy.

#### **3.2.5.3 Operetta excitation and emission filter determination for AQ2, AQ3 and AQ7**

As shown in *Figure 3.15(a)*, of these 14 possible Operetta filter combinations, 7 combinations led to identifiable: AQ2, AQ3, or AQ7 punctate, with excitation ranging from 390-420nm to 615-645nm, and emission in the 570-650nm or 655-760nm range.

For AQ2, as shown in *Figure 3.15(b)*, the peak puncta numbers were identified with a 530-560nm excitation filter and the 655-760nm emission filter. Statistically significant increases in the number of puncta of AQ2 was observed in the 530-560nm excitation 655-760nm emission compared to using lower excitation and emission filters.

AQ2 puncta intensity was broadly consistent across the excitation and emission filter as shown in *Figure 3.15(c)*, with the exceptions of the 615-645 excitation 655-760 emission filter settings. For the other excitation and emission channels where puncta were observed, there was no significant differences in intensity, with less than 20% variation in mean puncta intensity across the channels.

Analysis of the AQ3 treated cells showed the highest number of puncta were observed with the 490-515nm excitation and 570-615nm emission filter settings, with a mean puncta per

cell of 8. As seen with AQ2 and AQ7 further increasing the excitation wavelength only led to a reduction in puncta detected.

Comparison of puncta intensity for AQ3 (*Figure 3.15(e)*) shows that the highest puncta fluorescence intensity was in the 490-515nm excitation 570-650nm emission, which is a lower peak excitation wavelength than that for AQ2 and AQ7. This lower excitation wavelength of 490-515nm had a significant increase in puncta fluorescence intensity compared to the 530-560nm excitation 655-760nm emission channel combination, where the highest fluorescence intensity was observed with AQ2 and AQ7.

The number of puncta of AQ7 observed increased with a corresponding shift towards the red end of the spectra in both excitation and emission, to a peak of 12.5 puncta per cell observed in the 530-560nm excitation 655-760nm emission filter combination. As shown in *Figure 3.15(f)*, the 530-560nm excitation 655-760nm emission combination led to a significant increase in the number of puncta identified compared to all other combinations where puncta were observed.

With the puncta intensity of AQ7 (*Figure 3.15(g)*) increasing the wavelength of both the excitation and emission channels increased the fluorescence intensity. Maximum puncta fluorescence was observed in the 530-560nm excitation 655-760nm emission channel, consistent with the maximum number of puncta also being observed in the same channel. The fluorescence in the 530-560nm excitation 655-760nm emission channel was significantly higher than all but the 490-515nm and 530-560 excitation with a 570-650m emission.

From these data shown in *Figure 3.15*, the 530-560nm excitation 655-760nm emission filter combination provided the highest number of puncta identified for all three probes. Additionally, for AQ2 and AQ7 the 530-560nm excitation 655-760nm emission filter also had the highest mean puncta fluorescence when compared to background noise. Therefore, the 530-560nm excitation 655-760nm emission filter would be used for future assays with AQ2, AQ3 and AQ7.

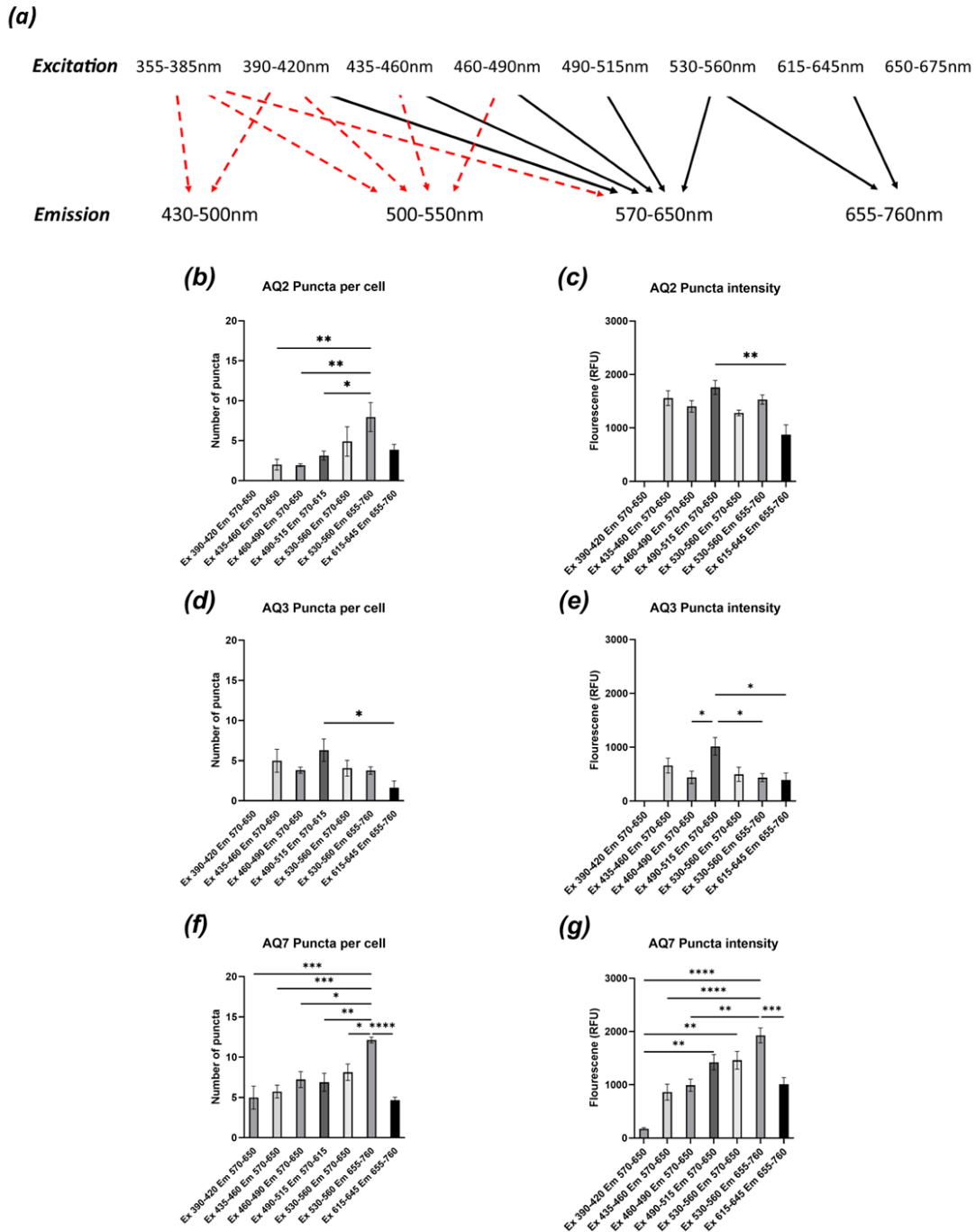


**Figure 3.15. Operetta excitation and emission filter determination for AQ2, AQ3 and AQ7**  
 Analysis of all possible combinations of excitation and emission filters with the Operetta CLS are shown in (a). In (b), (d) and (f), the number of puncta observed for AQ2, AQ3 and AQ7 respectively is shown with all filter combinations where puncta were observed. The mean puncta fluorescence for each excitation and emission filter combination for AQ2, AQ3, and AQ7 is shown in (c), (e) and (g). All probes were used at 200 $\mu$ M for 4 hours and imaged at 100% power for 100ms to ensure consistency. All data is n=3, with mean and standard deviation shown, statistical significance was determined through a one-way ANOVA, with post hoc Tukey test.

### 3.2.5.4 AQ2, AQ3 and AQ7 cell-based imaging fluorescence comparison

Comparison of the number of puncta per cell observed when treated with: AQ2, AQ3, or AQ7, shows that the highest number of puncta was observed with AQ7 (Figure 3.16(a)).

When using the 530-560nm excitation 655-760nm emission channel, a mean of 13 puncta per cell were observed for AQ7, compared to the 8 spots with AQ2 and 6 spots with AQ3.

The data in Figure 3.16(b) shows that AQ7 fluorescence is significantly increased over both AQ2 and AQ3, with mean puncta fluorescence values of: 1530, 210 and 1930 for AQ2, AQ3, and AQ7 respectively. The increase in fluorescence intensity from AQ7 over AQ3, is likely due to the addition of a second morpholine group to the molecule. AQ7 also has higher fluorescence emission than AQ2, improving the imaging characteristics *in vitro*. This increase in number of puncta detected and fluorescence intensity, suggests that AQ7 is a more sensitive probe, detecting smaller or less bright objects, that were previously not detectable using AQ2, or AQ3.

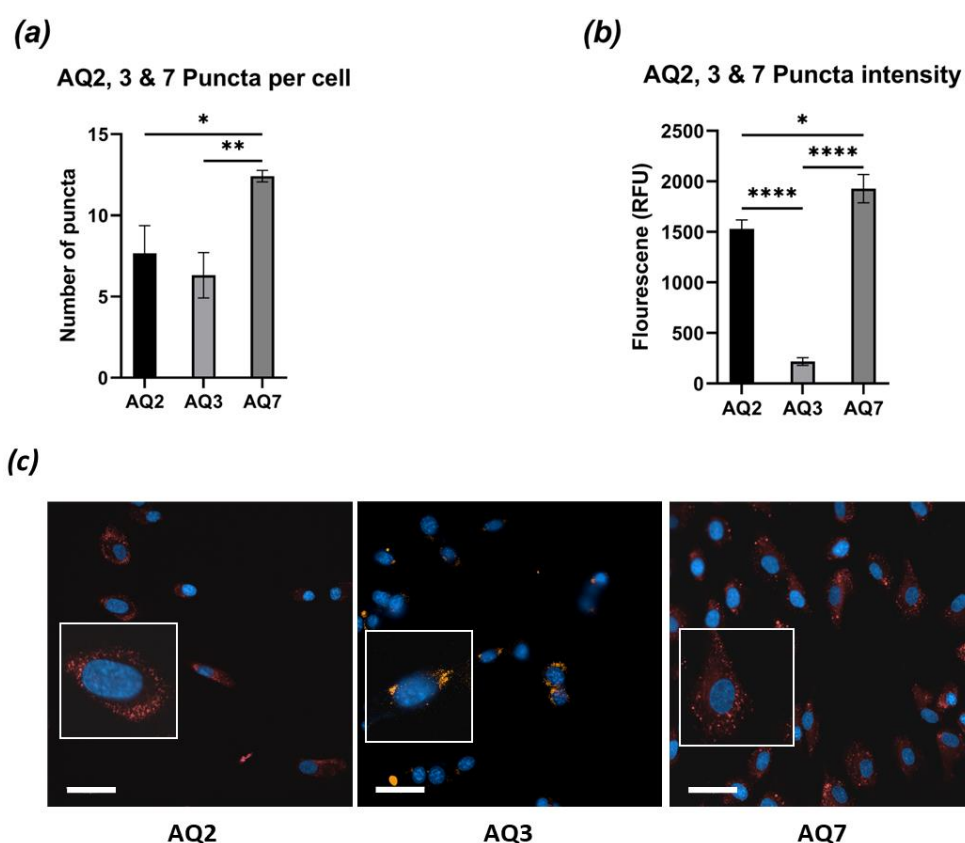


**Figure 3.16. *in vitro* fluorescence comparison of AQ2, AQ3 and AQ7**

Direct comparison of fluorescence from healthy control cells treated with AQ2, AQ3 or AQ7. In (a) comparison of the number of puncta identified when treated with AQ2, AQ3 or AQ7 is shown, with (b) showing the corresponding mean puncta fluorescence intensity. In (c) example images of cells treated with: AQ2, AQ3, or AQ7 is shown. All data is  $n=3$ , with mean and standard deviation shown, statistical significance was determined through a one-way ANOVA, with post hoc Tukey test. Scale bars represent  $50\mu\text{m}$ .

### 3.2.6 AQ7 Characterisation

As we had previously (3.2.3) unsuccessfully attempted to set up an AQ2 analogue trafficking assay, it was decided to evaluate other uses for AQ7. When attempting to set up the AQ2 analogue trafficking assay with AQ3, the localisation after 4 hours, appeared to be lysosomal. As we believed that AQ3 showed lysosomal specificity, we wanted to determine if an AQ2 derivative could be used as a lysosomal probe.

As we had shown that AQ7 had improved fluorescence characterises over AQ3 (3.2.5.4), we decided to test whether AQ7 could be used as a lysosomal probe. To do this, we needed to both find a suitable concentration of AQ7 for cellular use, and to confirm whether AQ7 also had lysosomal localisation, like AQ2 and AQ3.

#### 3.2.6.1 AQ7 concentration determination

The first step in evaluating AQ7 as a lysosomal probe was to determine the optimal concentration for use *in vitro*. A range of concentrations from 500 $\mu$ M to 100nM were selected to compare how the concentrations of AQ7 affected, both the number of puncta, and the corresponding puncta intensity. As can be seen from the data in *Figure 3.17(a)*, the number of puncta observed was consistent with a mean number of puncta per cell, with approximately 40 puncta being observed; from 500 $\mu$ M down to 100 $\mu$ M. However, lowering the AQ7 concentration from 100 $\mu$ M led to significantly less puncta being observed, with over 50% less puncta being identified at 10 $\mu$ M, and no puncta being observed at either 1 $\mu$ M or 100nM.

Of the puncta identified in *Figure 3.17(a)*, the brightest fluorescence intensities were observed at 500 $\mu$ M and 200 $\mu$ M of AQ7 with no significant differences between either concentration. However, decreasing the concentration of AQ7 to 100 $\mu$ M caused a significant decrease in puncta fluorescence as seen in *Figure 3.17(b)*. Further decreasing the concentration of AQ7 to 10 $\mu$ M and lower led to additional significant decreases in puncta fluorescence.

Based on the data in *Figure 3.17* it was decided that 200 $\mu$ M AQ7 would be used for future assay development with the probe.

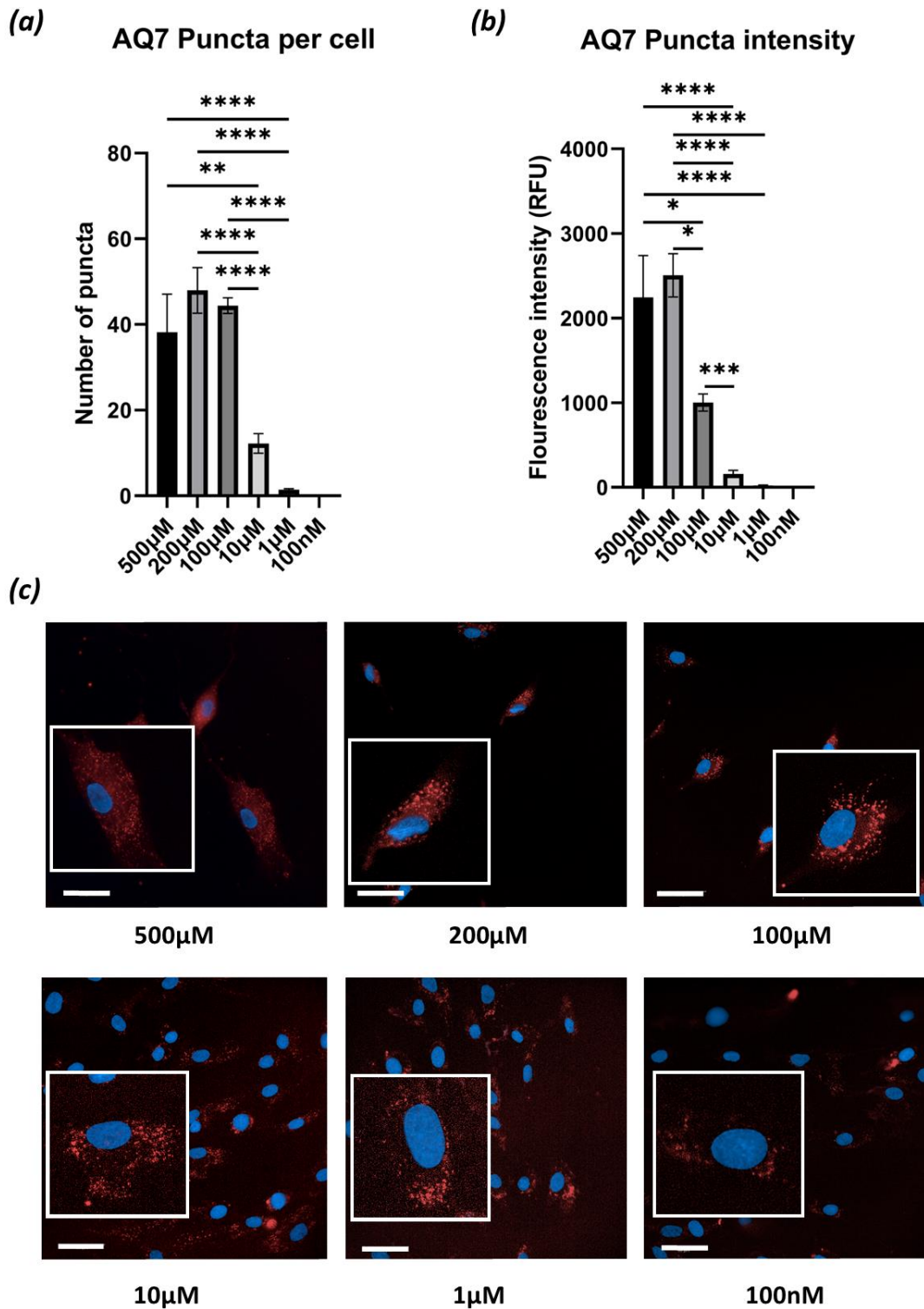


**Figure 3.17. AQ7 concentration dependant effects upon puncta number and fluorescence in vitro**

In (a) mean puncta per cell is shown, with (b) showing the corresponding flourescence intensity of the puncta for each AQ7 concentration. A reference image for each AQ7 concentration is shown in (c). Number of puncta and puncta flourescence was corrected by subtraction of values from that of untreated cells. All cells were pulsed with AQ7 for 4 hours, imaged and analysed using the same

evaluation pipeline. All data is  $n=3$ , with mean and standard deviation shown, statistical significance was determined through a one-way ANOVA, with post hoc Tukey test. Scale bars represent  $50\mu\text{m}$ .

### 3.2.6.2 AQ7 Late endosome/Lysosome localisation

To determine if AQ7 was co-localising with late endosomes/lysosomes, LysoTracker Green was used to compare the loci of fluorescence emission and the co-localisation of AQ7 to LysoTracker Green.

From the data in *Figure 3.18*, it is clear that AQ7 co-localises with LysoTracker Green as can be seen in *Figure 3.18(c)*. Comparison of the number of puncta of AQ7 and LysoTracker Green shows no significant difference between either, with AQ7 having a trend of a slightly higher number of puncta being identified (*Figure 3.18(a)*). Comparison of puncta localisation showed that approximately 95% of puncta of AQ7 were localised to puncta of LysoTracker Green (*Figure 3.18(b)*).

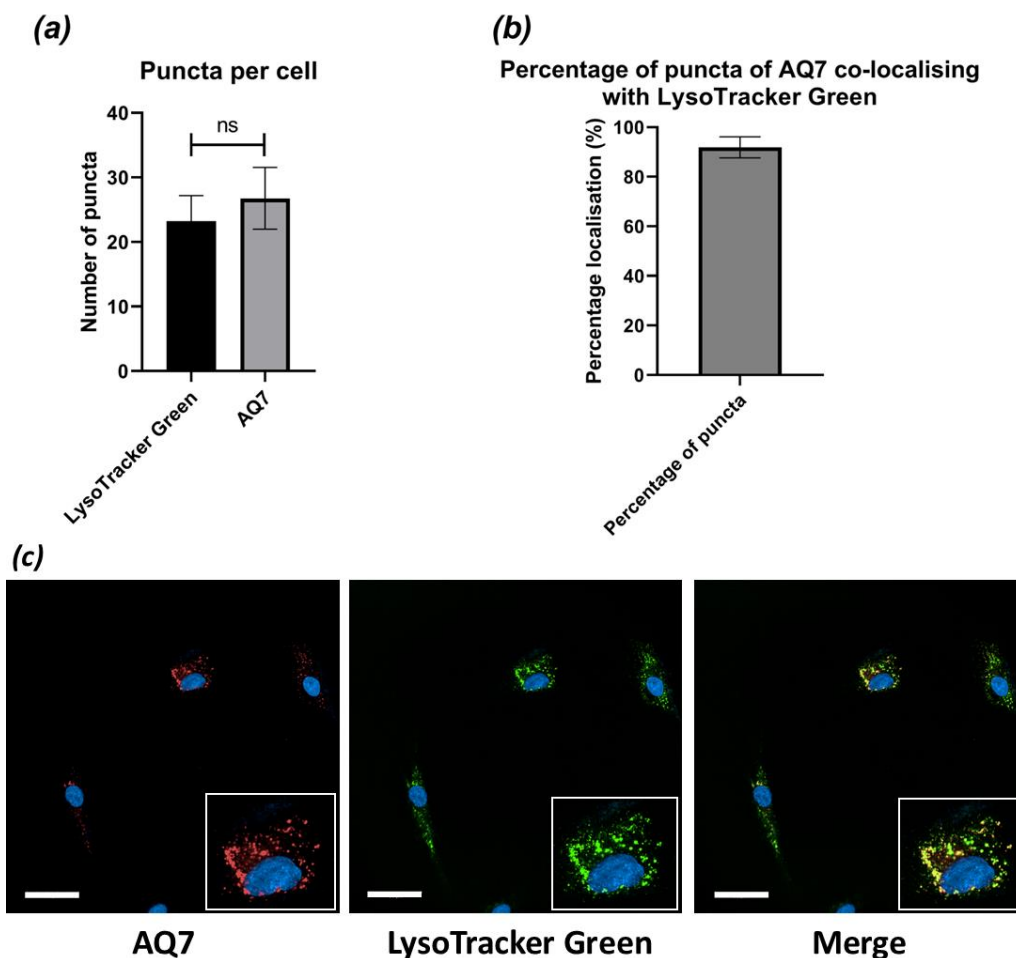


#### ***Figure 3.18. AQ7 co-localisation with LysoTracker Green***

*Comparison of number of puncta identified with AQ7 and LysoTracker Green and their corresponding co localisation is shown in Figure 3.18. In (a) a comparison of the mean number of puncta identified using both AQ7 and LysoTracker red is shown. In (b) and (c) the intracellular co localisation of AQ7*

and LysoTracker Green is shown, both as a percentage of puncta and in images of fibroblasts stained with both AQ7 and LysoTracker Green. All data is  $n=3$ , with mean and standard deviation shown, statistical significance was determined through two tailed student T-test. Scale bars represent  $50\mu\text{m}$ .

### 3.2.6.3 AQ7 can detect lysosomal storage induced by U18666A

As we had had shown that AQ7 localises to lysosomes, we decided to determine if AQ7 could detect lysosomal storage, when induced in healthy control cells. To induce an NPC like phenotype, cells were treated with U18666A, which binds to the sterol-sensing domain of NPC1, inducing inhibition of NPC1 activity.

To compare the sensitivity of AQ7 at detecting an induced NPC1 phenotype, cells were also stained with LysoTracker Red to allow direct comparison between probes to determine any differences in the staining characteristics between AQ7 and LysoTracker Red.

As shown in *Figure 3.19(a & b)*, treating healthy control cells with U18666A led to an approximate 50% increase in the number of puncta being detected with both AQ7 and LysoTracker Red. For both AQ7 and LysoTracker Red, U18666A led to a significant increase in the number of puncta observed. Of note, was that there was no significant difference in the percentage increase of number of puncta in the U18666A cells between AQ7 and LysoTracker Red.

When the healthy control cells were treated with U18666A, both AQ7 and LysoTracker Red showed increased puncta fluorescence intensity (*Figure 3.19 (c)*). Puncta fluorescence intensity was slightly higher in AQ7, in both untreated and U18666A, when compared to LysoTracker Red. For the percentage change in puncta intensity, there was a small insignificant increase in the percentage increase in the puncta intensity for LysoTracker Red, with an approximately 10% increase in fluorescence intensity over AQ7.

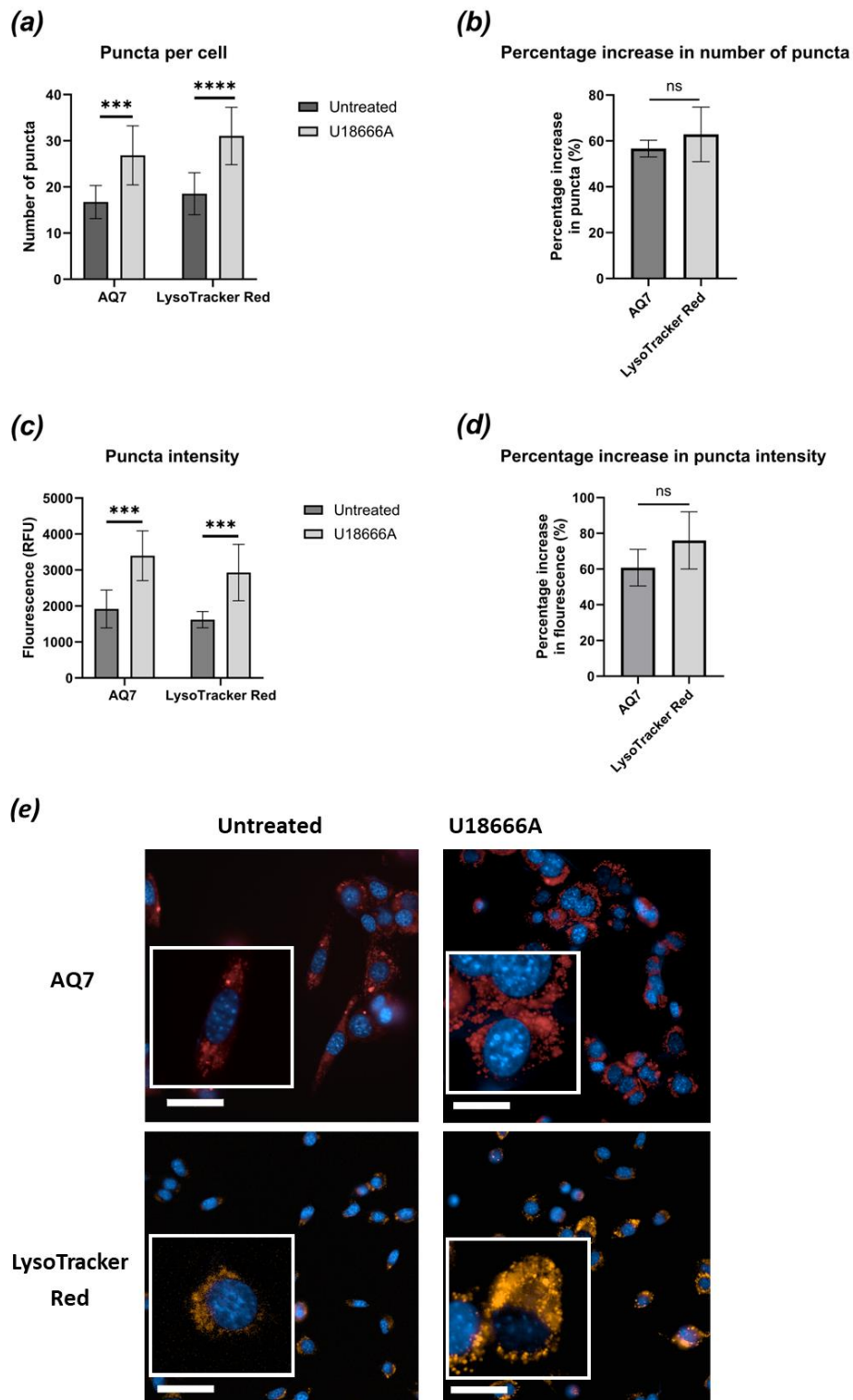


**Figure 3.19. AQ7 can detect an induced NPC1 phenotype using U18666A**

Cells treated with U18666A show increased puncta of AQ7, as well as increased puncta fluorescence comparable with LysoTracker Red. In (a), number of puncta is shown for both AQ7 and LysoTracker Red, with the percentage change in number of puncta shown in (b). In (c) the corresponding puncta fluorescence intensity is shown for AQ7 and LysoTracker Red, with the percentage change in fluorescence intensity shown in (d). Representative reference images are shown in (e). Data is n=3 with mean and standard deviation shown with statistical significance between groups was determined using multiple two tailed student T-tests. Scale bars represent 50µm.

#### 3.2.6.4 AQ7 only partially co-localises with Cyto-ID

As shown in 3.2.6.2, a significant percentage of the puncta of AQ7 co-localise to puncta of late endosomes and lysosomes. Following this comparison of localisation of AQ7 with Cyto-ID was undertaken to determine whether AQ7 was also co-localising with autophagolysosomes.

Comparison of the number of puncta of AQ7 and LysoTracker Red overall and localised to autolysosomes, showed no difference in either the number of puncta overall or in the number of puncta that was co-localised to autophagolysosomes per cell (*Figure 3.20(a)*). Both AQ7 and LysoTracker Red showed similar levels of co-localisation to autophagolysosomes, with both probes having approximately 50% localisation to Cyto-ID (*Figure 3.20(b)*).

Considering these data, it suggests that AQ7 partially co localises to autophagolysosomes, however primarily localises to late endosomes and lysosomes. Therefore, whilst AQ7 partially co-localises to autophagolysosomes, this percentage is consistent with LysoTracker Red, and therefore not suited for use as an autophagolysosome probe.

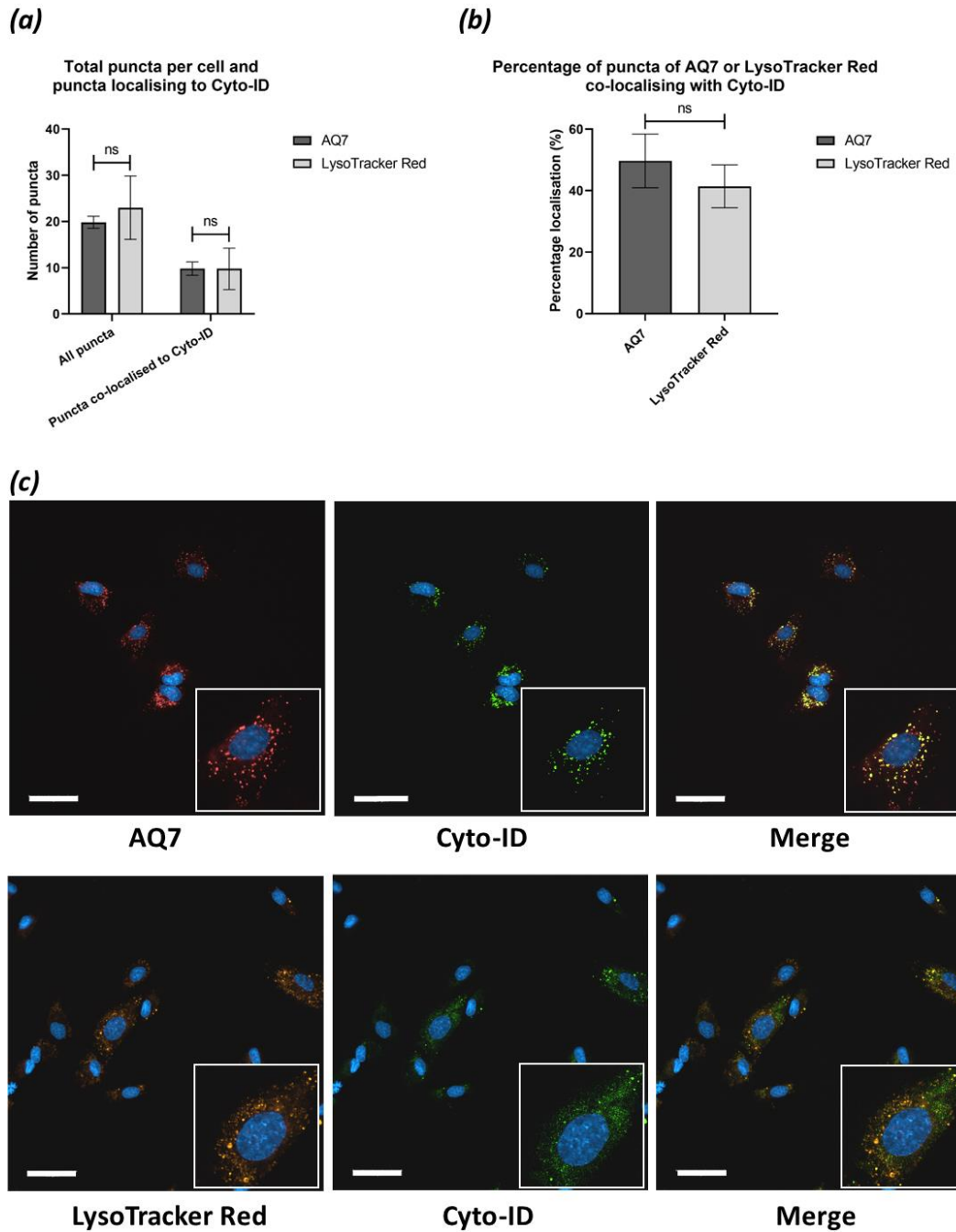


**Figure 3.20. Co-localisation of AQ7 and LysoTracker Red with Cyto-ID**

AQ7 and LysoTracker Red show only partial co-localisation with Cyto-ID. In (a) the mean total number of puncta per cell with AQ7 and LysoTracker Red are shown. Also included is the mean number of puncta per cell that are co-localised with a corresponding puncta of Cyto-ID. Panel (b) shows the percentage of puncta of AQ7 and LysoTracker Red that were co-localised to a corresponding puncta of Cyto-ID. In (c) representative images for cells treated with AQ7 or LysoTracker Red and co stained with Cyto-ID are shown, with single channel and merged images shown. All data is  $n=3$ , with mean and standard deviation shown, statistical significance was determined through multiple two-tailed student T-tests. Scale bars represent  $50\mu\text{m}$ .

### 3.2.6.5 AQ7 can detect difference in lysosomes with known autophagy modulators

As we had shown that AQ7 could detect changes within lysosomes when treated with storage inducing molecules, the next step was to determine if AQ7 could also detect changes with known autophagy modulators. Trehalose is a commonly used autophagy modulator that has been shown to lead to upregulation in autophagy through TFEB activation, however it is known to be mTOR independent. 3-MA is a known inhibitor of phosphatidylinositol 3-kinase (PI3K). PI3K is known to regulate autophagy, and inhibiting PI3K prevents the activation of mTOR.

It is clear that from the data in 3.2.6.4(a) that AQ7 and LysoTracker Red are detecting the same change in autophagy, when the known modulating compounds are used. As can be seen in *Figure 3.21(a)* when cells were treated with trehalose, an increase in the number of puncta detected by AQ7 and LysoTracker Red was shown. When cells were treated with 3MA, both probes had a significant difference compared to the trehalose treated cells, however only AQ7 showed a significant decrease in the number when compared to the untreated control. Neither AQ7 nor LysoTracker Red showed any significant changes in puncta intensity or mean puncta area when treated with either 3MA or trehalose (*Figure 3.21(b) &(d)*).

Consistent with the change in the number of puncta, the total puncta area per cell was significantly changed when treated with either 3MA or trehalose. However, whilst AQ7 was able to detect differences between untreated and trehalose and trehalose and 3MA, LysoTracker Red was only able to distinguish between trehalose and 3MA; therefore it appears that AQ7 is a more sensitive probe in this assay (*Figure 3.21(c)*). Both AQ7 and LysoTracker Red show similar patterns of change in the puncta per area cell, with both showing a significant increase between untreated and trehalose, and a significant difference between trehalose and 3MA.

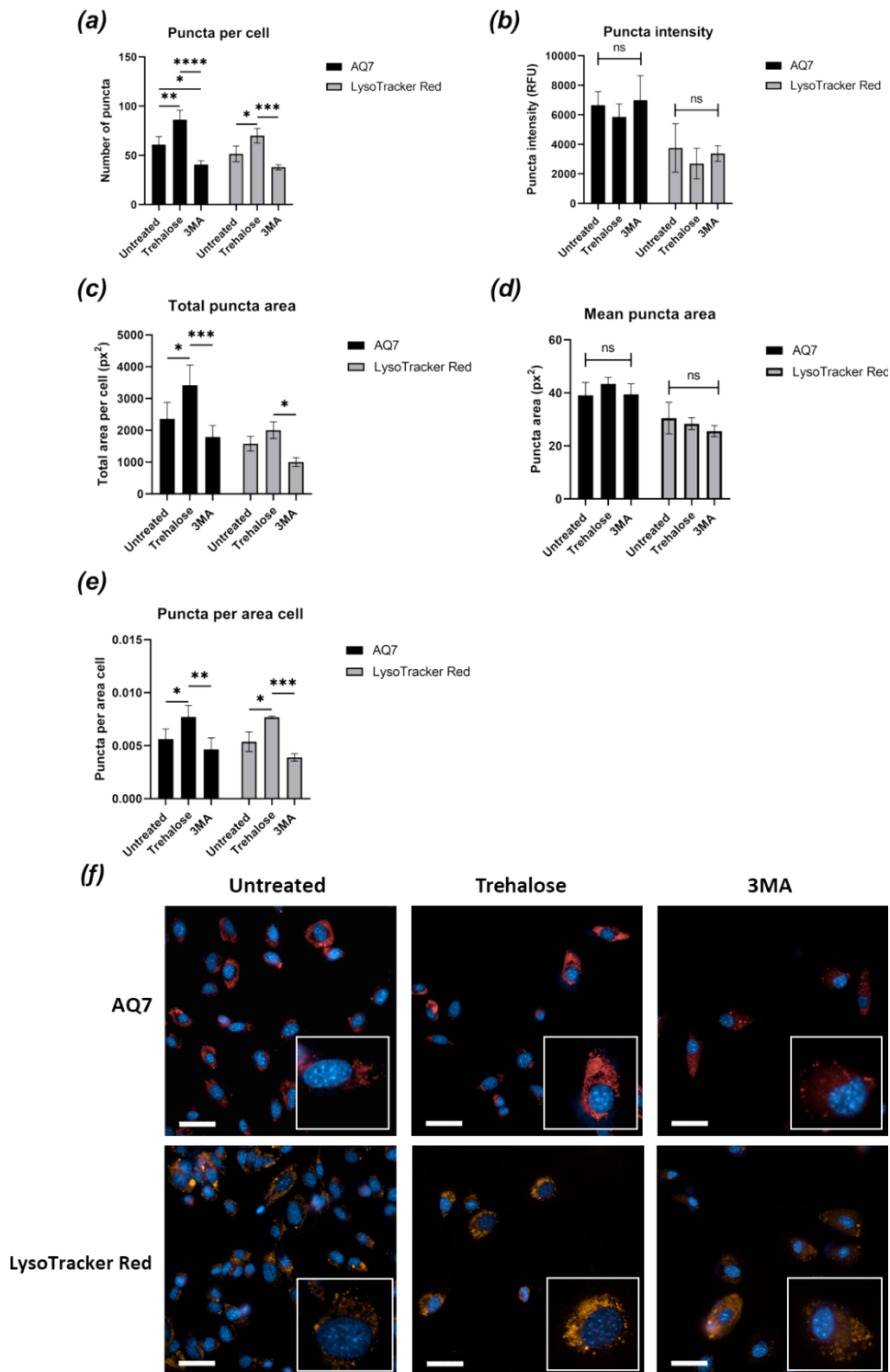


**Figure 3.21. AQ7 can detect difference in lysosomes with trehalose and 3MA treatment**

When cells are treated with 3MA or trehalose, both AQ7 and LysoTracker Red detect similar changes within cells. In (a) the number of puncta per cell is shown, with the corresponding puncta fluorescence in (b). The mean total combined puncta area per cell is shown in (c), with the mean AQ7 or LysoTracker Red puncta area in (d). In (e) the number of puncta per area shown. Representative images for each probe and treatment condition are shown in (f). All data is n=3, statistical significance was determined through a one-way ANOVA, with post-hoc Tukey tests. Scale bars represent 50 $\mu$ m.

### 3.2.6.6 AQ7 48hr time course assay

LysoTracker is not suitable for use in prolonged imaging experiments, due to a known lysosomal de-acidification effect, and inducing cellular toxicity when cells are treated with LysoTracker for prolonged periods, such as over an hour. Therefore, if AQ7 is photostable, and does not induce cellular toxicity, then the probe would have clear advantages over the LysoTracker dyes.

The data in *Figure 3.22(a)* shows that there is no significant decrease in the mean number of puncta per cell, however an overall slight trend of decreasing number of puncta was observed over the full time period. This data is consistent with what is to be expected if AQ7 is undergoing lysosomal entrapment, due to the apparent lack of lysosomal export of AQ7.

No significant decrease in fluorescence of the puncta of AQ7 was observed over the 48-hour time period, as shown in *Figure 3.22(b)*. There is a trend of decreasing fluorescence over the first 2 hours of the chase after AQ7 was removed from the media. This is likely due to the reduction in AQ7 entering the cell through endocytosis, with the amount of AQ7 within the cell remaining constant after a 4-hour chase at the 8-hour timepoint. After the 8-hour time point, there is a slight trend of increasing fluorescence, which may be caused by early endosomes containing AQ7 maturing into lysosomes. It is also possible that some merging of lysosomes is occurring, as there is a slight trend of decreasing number of puncta, corresponding to increasing puncta intensity.

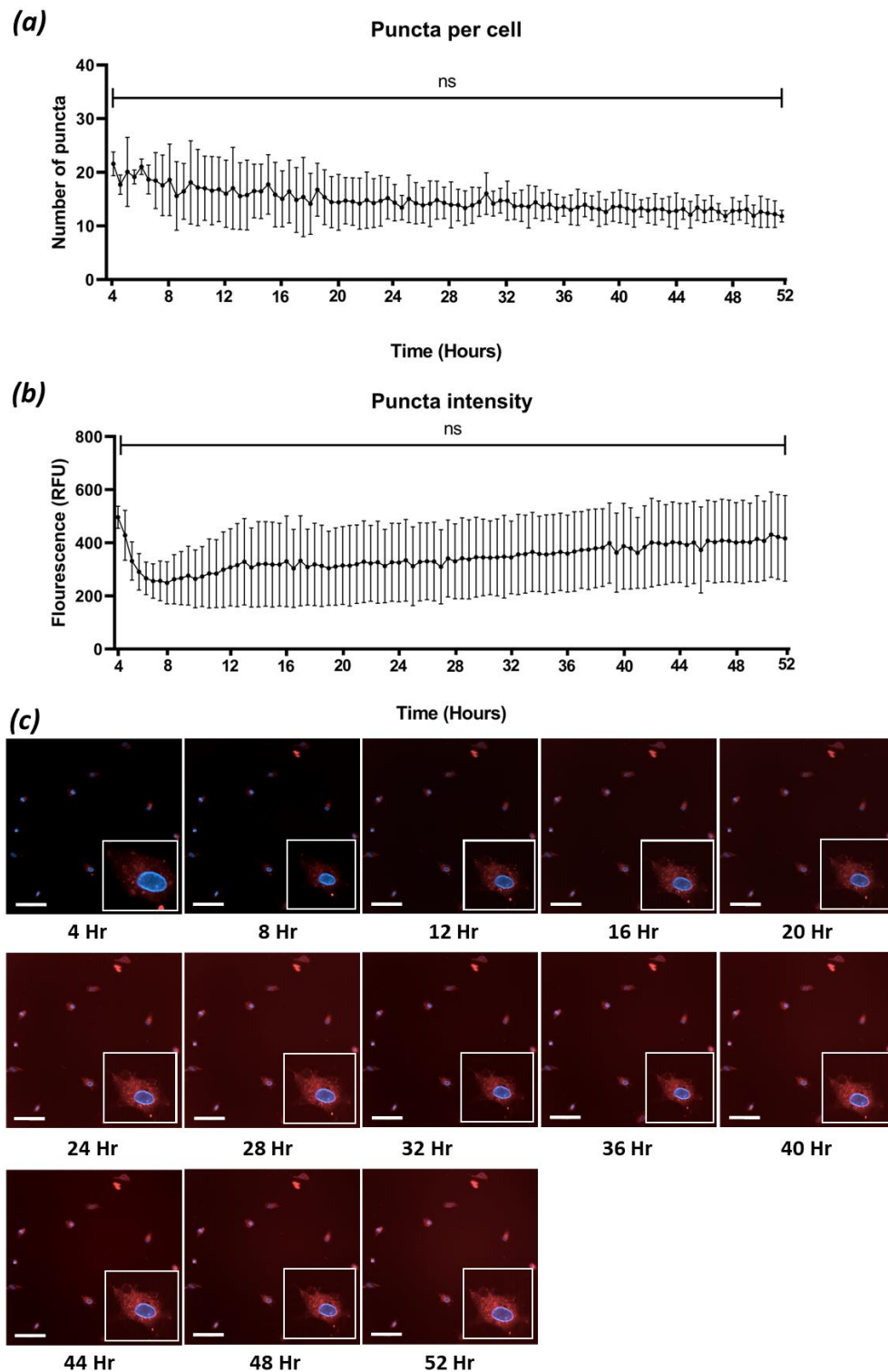


***Figure 3.22. AQ7 puncta per cell and fluorescence intensity are not affected by chase time***

*Time course assay comparing both the number of puncta and the puncta fluorescence intensity over a 4-hour pulse followed by a 48-hour chase is shown. Imaging was done using the x20 water objective on an Operetta CLS, with the cells being imaged every 30 minutes following the 4-hour pulse, with the cells being maintained at 37°C and 5% humidity between imaging. In (a) and (b) the mean number of puncta per cell, and the corresponding puncta fluorescence intensity is shown. In (c) reference images from every 4 hours of the imaging are shown. All data is n=3, with mean and standard deviation shown, statistical significance was determined through a one-way ANOVA. Scale bars represent 50µm.*

### 3.2.6.7 AQ7 cellular uptake is temperature dependant

As we had shown that AQ7 localised to lysosomes, the next step was to determine the effect of cell incubation temperature to understand better how AQ7 was reaching the lysosome.

The data in *Figure 3.23*, shows that for AQ7 increasing temperature up to 37°C led to increased number of puncta being observed of AQ7, in two different healthy patient fibroblasts. However, when the same cells lines were treated with LysoTracker Red, no significant differences in the number of puncta was observed. In both cells treated with AQ7 and LysoTracker Red, no significant differences in the puncta fluorescence intensity were observed at any of the temperatures.

No differences were observed between the male and female non age matched cell lines tested, as both cell lines had similar number of puncta across all the incubation temperatures for AQ7 and LysoTracker Red (*Figure 3.23a&b*). No difference in puncta fluorescence intensities was observed between the two healthy control cell lines, with both having corrected fluorescence intensities for AQ7 of approximately 1,000 and 1,200 for LysoTracker Red (*Figure 3.23c&d*).

Imaging of cells whilst differencing the pulse temperatures shows a differing mechanism of cellular uptake and lysosomal localisation for AQ7 and LysoTracker Red. LysoTracker Red is known to diffuse into the cell, which is supported by the data in *Figure 3.23*, as temperature did not affect the number of puncta observed. However, as the temperature at which cells are incubated with AQ7 does affect the number of puncta observed, the mechanism for cellular uptake for AQ7 is probably different to that of LysoTracker Red. Based on the data presented in *Figure 3.23*, it is likely that AQ7 is being actively transported into the cells, due to the significant decrease in the number of puncta observed when the temperature is decreased. Decreasing the temperature at which the cells are incubated with AQ7 will reduce the rate of active transport at the cell plasma membrane, corresponding to the stepwise decrease in the number of puncta of AQ7 from 37°C through 20°C, down to 4°C. Whilst some AQ7 was observed to leak from the lysosome into the cytoplasm, this is most pronounced in the 37°C cells, further suggesting that most AQ7 was taken up at this temperature.

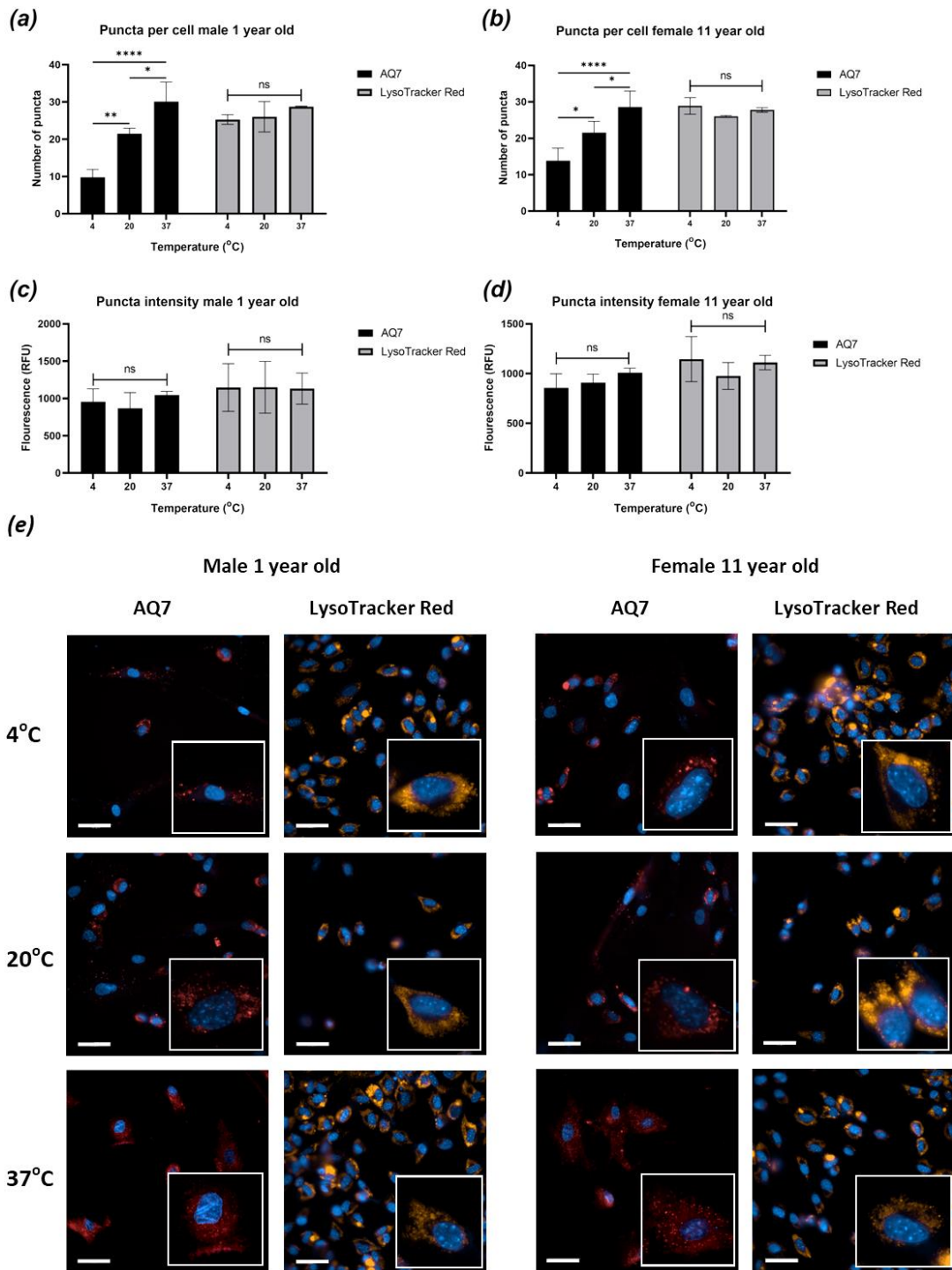


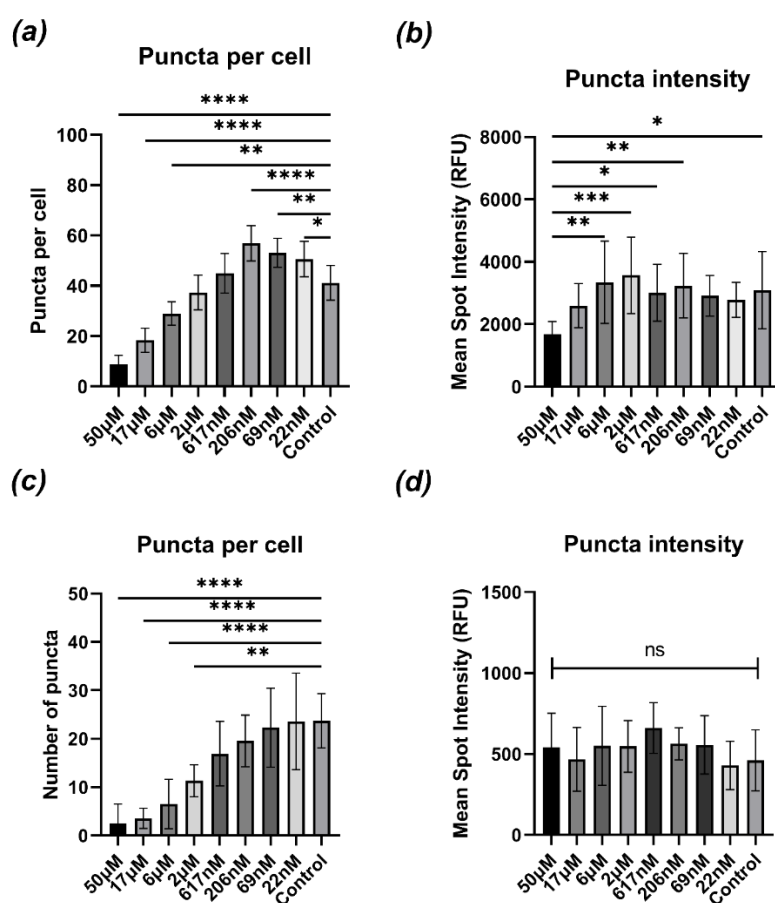
***Figure 3.23. AQ7 trafficking to lysosomes is temperature dependant***

*Comparison of number of puncta per cell, and the corresponding puncta fluorescence intensity for AQ7 and LysoTracker Red at 3 different temperatures in healthy control cells. In (a) and (b) the number of puncta per cell is compared for both AQ7 and LysoTracker Red across three temperatures points in two different healthy control cell lines. In figures (c) and (d) the puncta fluorescence intensity is shown for both AQ7 and LysoTracker Red across the three different temperatures (e). All data is n=3, with mean and standard deviation shown, statistical significance was determined through a one-way ANOVA, with post hoc Tukey test. Scale bars represent 50µm.*

### 3.2.6.8 Bafilomycin treatment prior to AQ7 staining decreases cellular uptake of AQ7

To determine if pH sensitivity of AQ7 could be detected *in vitro*, bafilomycin, a vATPase inhibitor was used to de-acidify lysosomes. We wanted to determine if a change in AQ7 fluorescence could be detected *in vitro*. To do to this, cells were treated with bafilomycin overnight and then AQ7 or LysoTracker Red added and imaged.

As can be seen from the data in *Figure 3.24(a) &(c)* increasing bafilomycin concentration reduced the number of puncta observed of both AQ7 and LysoTracker Red. For AQ7 treated cells, low concentrations of bafilomycin led to an increase in the number of puncta observed, which would be consistent with partial lysosomal de-acidification. With LysoTracker Red no increase in the number of puncta was observed with low concentrations of bafilomycin, however the trend of decreasing number of puncta being identified with increasing bafilomycin concentration was also observed. LysoTracker Red showed no change in the puncta fluorescence intensity when treated with bafilomycin *Figure 3.24 (d)*. AQ7 did show a change in the puncta fluorescence intensity, with lower fluorescence at the highest concentrations of bafilomycin (*Figure 3.24.(b)*).



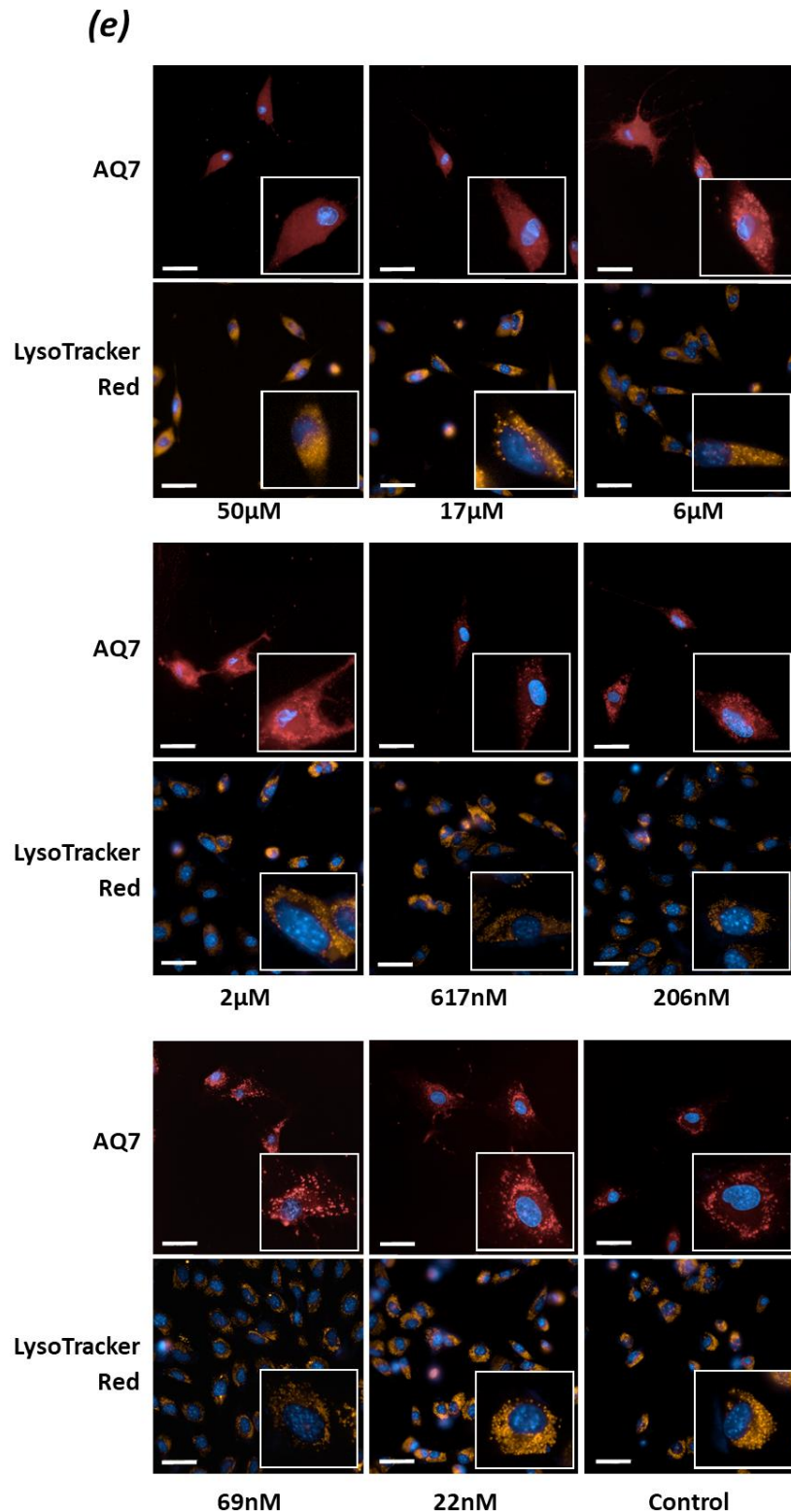


**Figure 3.24. Bafilomycin treatment decreases the number of puncta of AQ7 and LysoTracker Red**

Healthy control cells treated overnight with a range of bafilomycin concentrations were probed with either AQ7 or LysoTracker Red. In (a) the puncta per cell for AQ7 treated cells is shown, with the corresponding puncta fluorescence intensity in (b). Cells treated with the same concentrations of bafilomycin but probed with LysoTracker Red puncta per cell is shown in (c), with the mean puncta fluorescence intensity in (d). All data is  $n=3$ , statistical significance was determined through a one-way ANOVA, with post-hoc Tukey tests. Scale bars represent  $50\mu\text{m}$ .

### 3.2.6.9 *Bafilomycin treatment post AQ7 incubation decreases AQ7 puncta number*

As we had seen that de-acidifying lysosomes before treating with AQ7 led to changes in number of puncta and puncta fluorescence (*Figure 3.24*), we wanted to see determine if we could differentiate between changes in lysosomal pH and changes in AQ7 uptake caused by lysosomal de-acidification.

The data in *Figure 3.25 (a)* shows that treating cells with bafilomycin even after AQ7 is in the lysosomes, significantly reduces the number of puncta observed, when compared to the control at all bafilomycin concentrations. Whilst the number of puncta observed is reduced, there is no decrease in the fluorescence intensity of the puncta, other than at the highest bafilomycin concentration *Figure 3.25 (b)*. In all the cells treated with bafilomycin, there was a clear diffuse AQ7 staining (*Figure 3.25(c)*), which increased with bafilomycin concentration, suggesting that bafilomycin was causing either mis-localisation of AQ7, or that AQ7 was being released from the lysosomes due to the de-acidification.

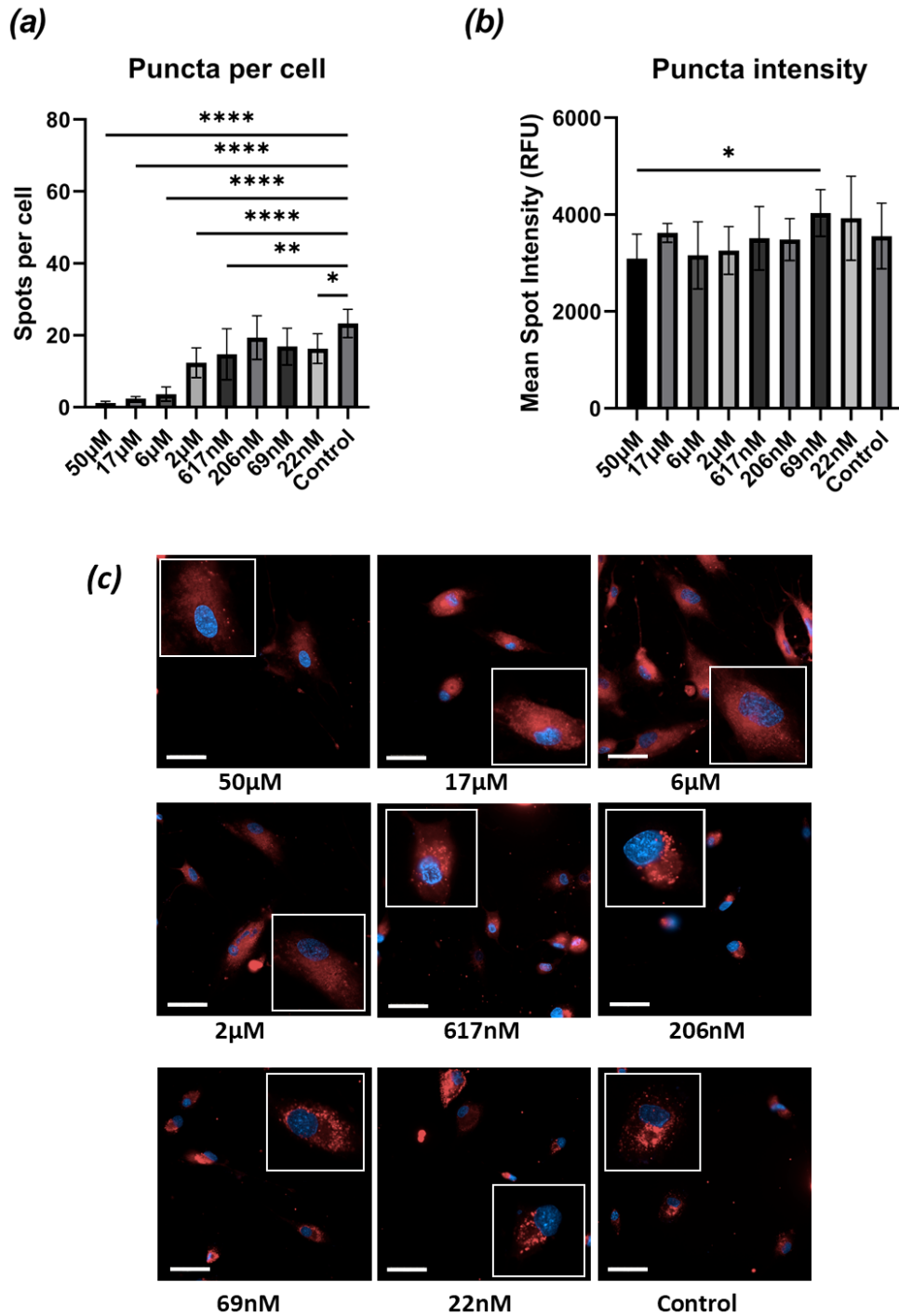


**Figure 3.25. Bafilomycin treatment after AQ7 decreases number of puncta detected without decreasing fluorescence intensity**

Healthy control cells were pulsed with AQ7 for 4 hours, followed by overnight bafilomycin treatment. In (a) the number of puncta of AQ7 after bafilomycin treatment is shown, with corresponding puncta fluorescence in (b). Reference images for each bafilomycin concentration are shown in (c). All data is  $n=3$ , statistical significance was determined through a one-way ANOVA, with post-hoc Tukey tests. Scale bars represent  $50\mu\text{m}$ .

#### 3.2.6.10 AQ7 does not affect lysosomal pH after 24 hours of treatment

LysoTracker dyes are known to affect lysosomal pH, therefore if AQ7 did not affect lysosomal pH, the molecule would have a clear advantage over LysoTracker dyes. To determine the effect on pH, a combination of two fluorescent conjugated dextrans, one of which is pH sensitive, were used in a ratiometric imaging assay.

The data in *Figure 3.26(a)* shows clearly that treating cells with AQ7 for 24 hours does not affect significantly the ratio of FITC/Texas Red when compared to non AQ7 treated cells. No significant change in the ratio of FITC/Texas Red was observed at the 4-hour time point when compared to either the untreated or 24-hour time point. Therefore, it is suggested that the presence of AQ7 within lysosomes does not lead to de-acidification of lysosomes over a 24-hour incubation period. Thus, lysosomal deacidification is not the cause of increased cholesterol storage as shown in 3.2.7.2, further suggesting that AQ7 has a possible NPC1 inhibitory effect.

The lack of effect of AQ7 upon lysosomal pH is in contrast to the known effects of de-acidification with prolonged use of the LysoTracker series of dyes. Therefore, AQ7 is significantly better than the LysoTracker series of dyes when there is a requirement for an incubation time over 30 minutes.

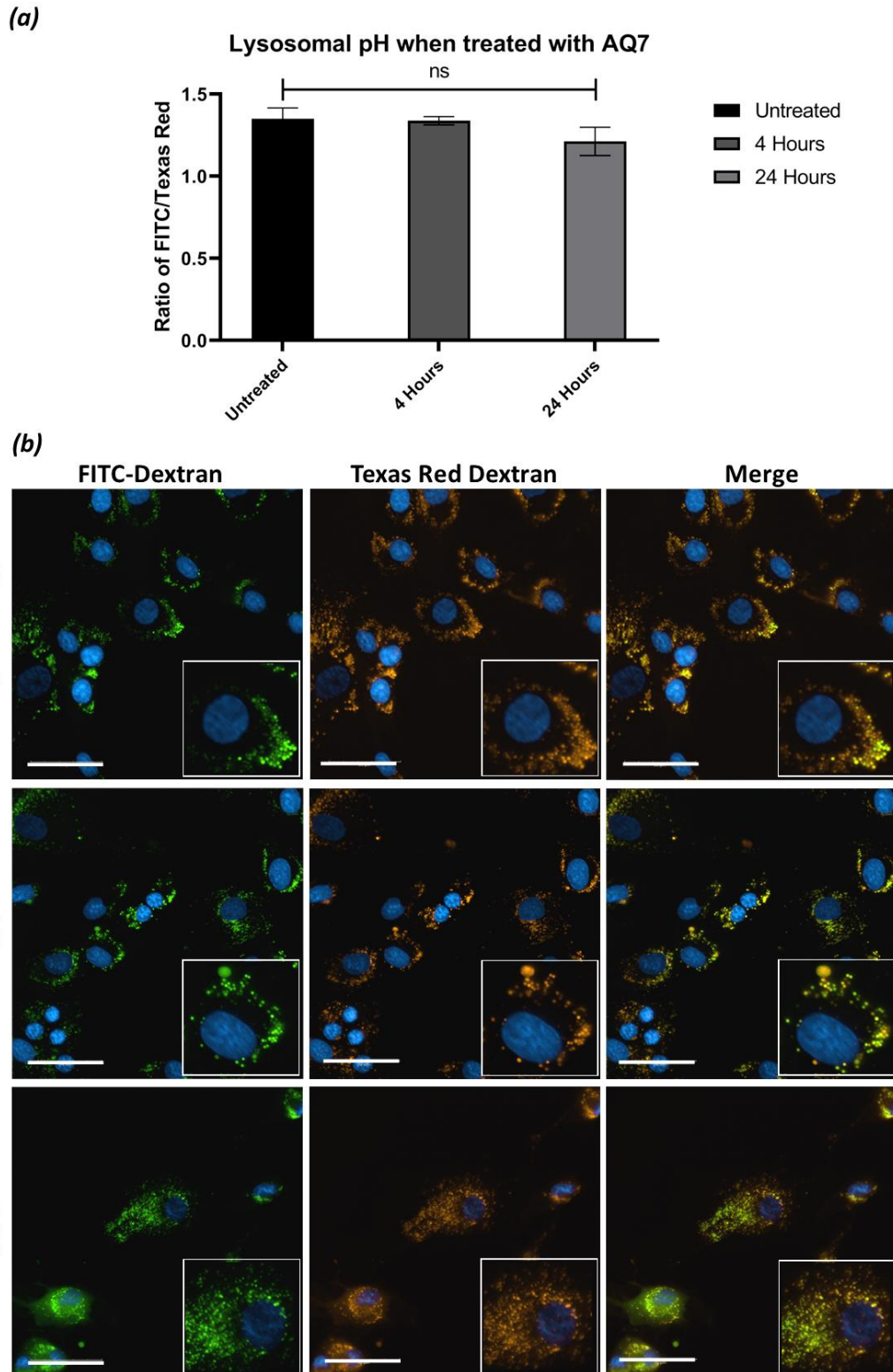


**Figure 3.26. AQ7 does not affect lysosomal pH**

AQ7 does not affect the ratio of fluorescence of pH sensitive FITC-dextran compared to pH-insensitive Texas Red-dextran. In (a), cells were pulsed with the dextrans and treated with AQ7 for 4 or 24 hours or left untreated as a control. Cells were imaged and the fluorescence of FITC compared to that of Texas red, to determine lysosomal pH. Reference images for all treatment times are shown in (c). All data is n=3, with mean and standard deviation shown, statistical significance was determined through a one-way ANOVA. Scale bars represent 50µm.

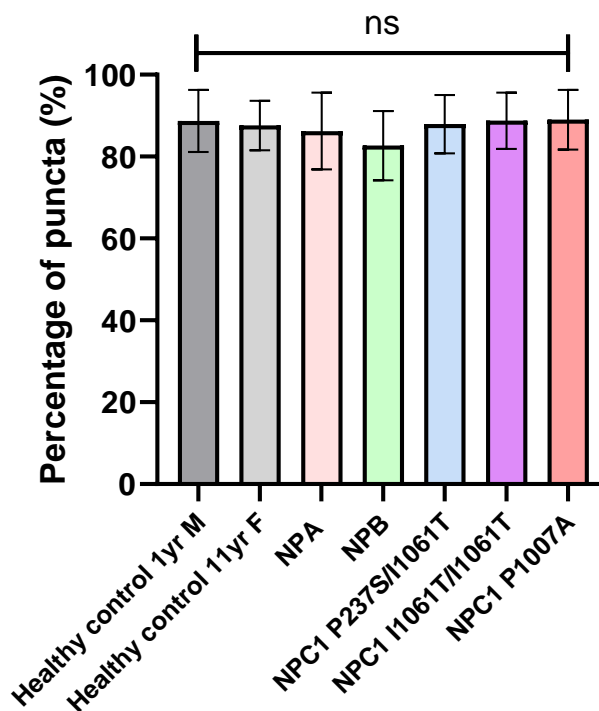
### 3.2.6.11 AQ7 and LysoTracker Red co-localisation is consistent across Niemann-Pick Disease cell lines

As we had shown that AQ7 is actively transported into cells 3.2.6.7, it was decided to determine if AQ7 was being correctly trafficked within cells with known trafficking defects. Comparison of localisation of AQ7 compared to LysoTracker Green in patient Niemann-Pick disease cells were used to determine whether trafficking defects were leading to AQ7 and LysoTracker Green not being co-localised.

Staining with AQ7 and LysoTracker Green, showed that similar numbers of puncta were observed with each probe, with AQ7 being slightly higher, possibly due to better fluorescence emission from AQ7 or better detection using the Operetta. As the data in *Figure 3.27* shows, there is no significant difference in the percentage of AQ7 puncta co localising with LysoTracker Green across the Niemann-Pick disease cell lines tested. Therefore, it is likely that AQ7 is being correctly localised to lysosomes, even in cell lines with known trafficking defects and lysosomal storage.

Based on the data in *Figure 3.27*, AQ7 lysosomal localisation is constant across all cell lines tested, and thus endocytic or intracellular trafficking defects should not affect the data when comparing AQ7 staining across differing cell lines.

**(a)** Percentage of puncta of AQ7 co localising with LysoTracker Green



(b)

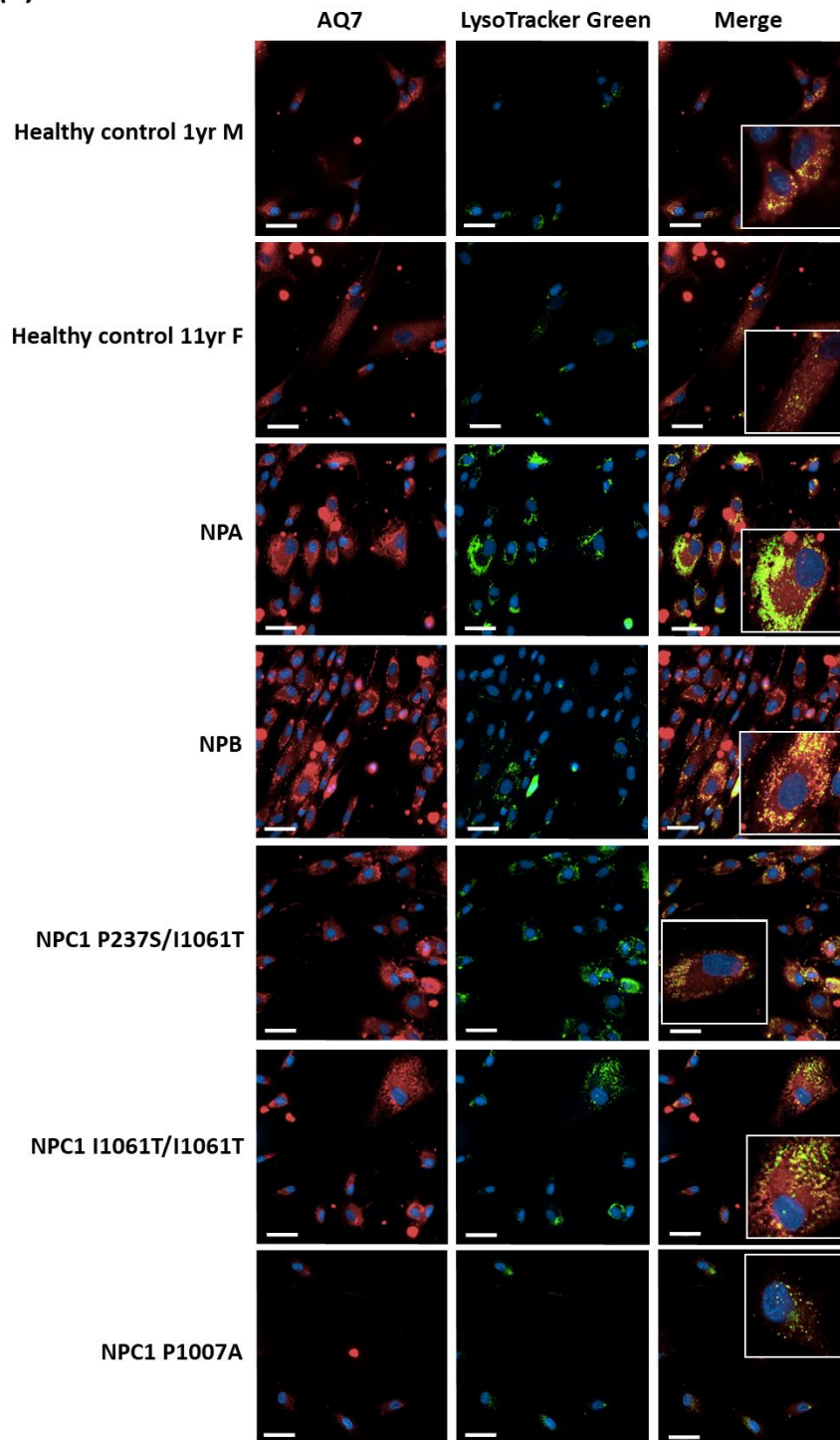


***Figure 3.27. AQ7 and LysoTracker Green co-localisation in Niemann-Pick disease fibroblasts***

*Comparison of AQ7 and LysoTracker Green staining in a range of Niemann-Pick disease variants patient derived fibroblasts. In (a) percentage of spots of AQ7 co-localising with LysoTracker Green was determined by determining the number of puncta of AQ7 also co-localised with a corresponding puncta of LysoTracker Green and dividing by the total number of puncta of AQ7 per cell. In (b) representative images for each of the cell lines and probes used as well as a merged image of AQ7 and LysoTracker Green are shown. All data is n=3, with mean and standard deviation shown, statistical significance was determined through a one-way ANOVA. Scale bars represent 50µm.*

### 3.2.7 AQ7 effects upon lysosomal function

In early assays, it was noticed that cells treated with AQ7 appeared to increase the number of lysosomes in healthy cells. Therefore, it was decided to determine if AQ7 affects endocytosis and leads to lysosomal storage.

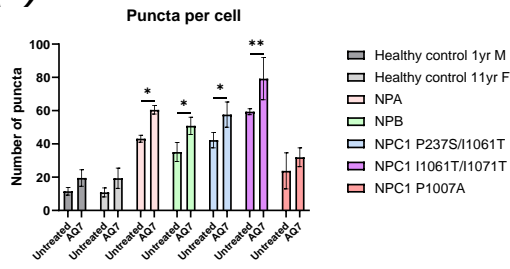
#### 3.2.7.1 AQ7 leads to increased lysosomal area in patient derived fibroblasts

As shown in *Figure 3.28(a)*, a statistically significant increase in the number of puncta per cell was observed in: NPA, NPB, and NPC1 cell lines with the I1061T mutation. Whilst not statistically significant, a trend of increasing puncta per cell was observed in the healthy control and the NPC P1007A cell lines. Significantly increased puncta fluorescence was also observed in: NPA, NPB, and NPC I1061T mutant cell lines (*Figure 3.28(b)*), consistent with the increase in the number of puncta identified.

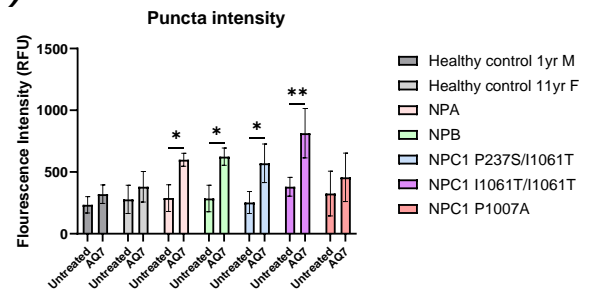
Whilst no significant changes were observed in the average puncta area (*Figure 3.28(d)*), there was a trend of AQ7 treatment leading to decreased puncta area across all cell lines. However, whilst there was a trend of decreasing puncta area, this did not affect the total lysosomal volume per cell, as this was significantly increased in: NPA, NPB, and NPC I1061T mutant cell lines, in line with the increase in number of puncta *Figure 3.28(c)*. Whilst the total puncta area per cell significantly increased, the puncta per area cell did not significantly increase (*Figure 3.28(d)*), suggesting that the cellular volume also expanded to compensate for the increased lysosomal volume.

From the data in *Figure 3.28*, it is clear that treatment with AQ7 leads to an increased lysosomal volume in most cell lines tested, including healthy control fibroblasts. This suggests that AQ7 is potentially leading to lysosomal lipid accumulation, which would account for the increased total lysosomal volume upon AQ7 treatment, with the most significant increases occurring in the Niemann-Pick disease cells, which already have lipid metabolism defects. With anthraquinones being putative NPC1 substrates, it is possible that the addition of the two morpholine groups in AQ7, potentially causes a loss of this substrate capacity, and in turn AQ7 may function as an NPC1 inhibitor.

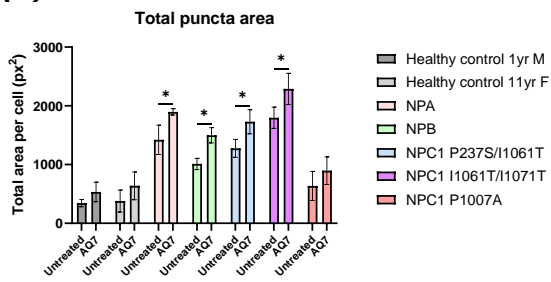
(a)



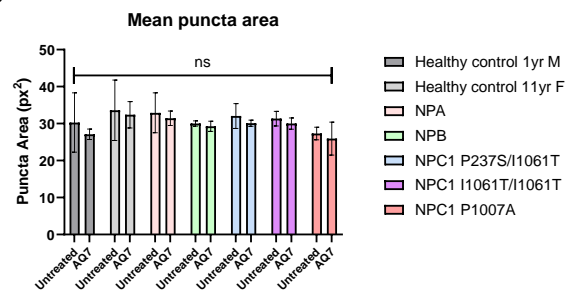
(b)



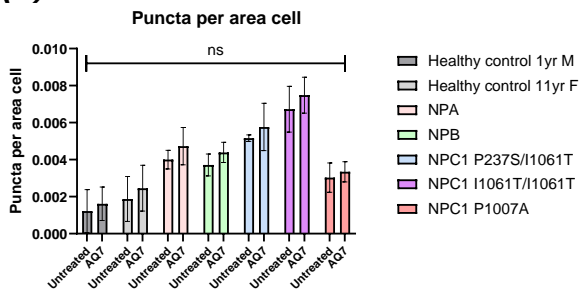
(c)



(d)



(e)



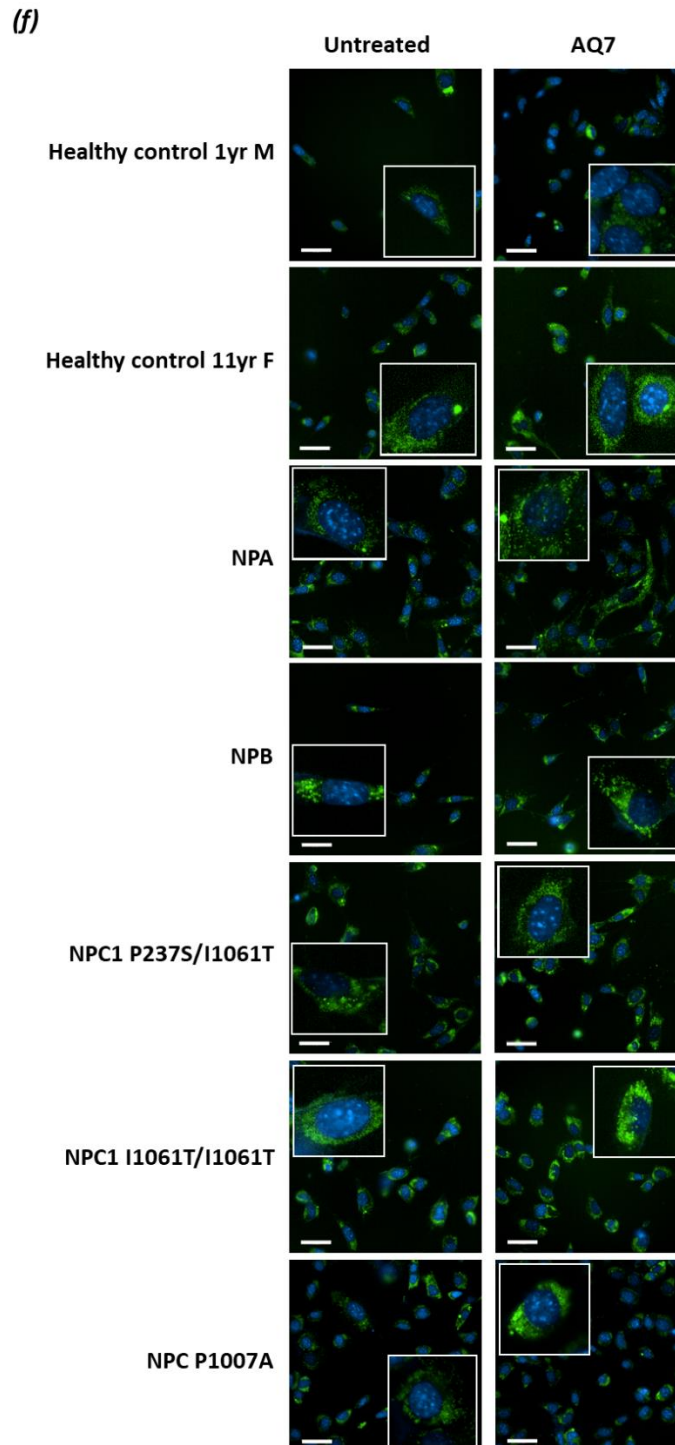


**Figure 3.28. AQ7 treatment leads to increased LysoTracker Green staining in fibroblasts**

LysoTracker Green staining is shown comparing untreated and cells treated with AQ7 lysosomal volume. In (a) the mean number of puncta per cell is shown, whilst (b) shows the corresponding fluorescence intensity for these puncta. In (c) the mean total puncta area per cell is included whereby the number of puncta is multiplied by the mean puncta area, with (d) showing the mean fluorescent puncta area. In (e) the mean puncta per area cell is shown, whereby the total puncta area is divided by the total cell volume. In (f) representative images for all cell lines both treated with AQ7 and untreated are shown. All data is  $n=3$ , with mean and standard deviation shown, statistical significance was determined through a one-way ANOVA with post hoc Tukey test. Scale bars represent  $50\mu\text{m}$ .

### 3.2.7.2 AQ7 leads to increased number of puncta of cholesterol being identified

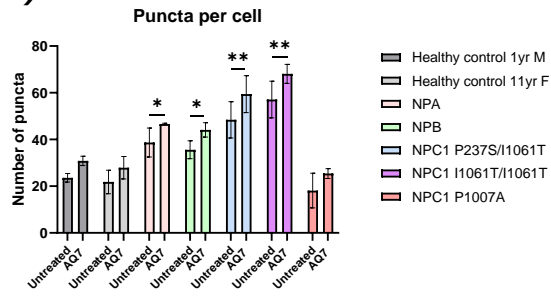
With AQ7 showing an effect of increasing lysosomal volume in cells, it was decided to determine if this increase in lysosomal volume was associated with increased lipid storage. As loss of NPC1 activity is usually associated with increased cholesterol accumulation, cells were treated with AQ7 before being imaged using filipin to visualise cellular cholesterol.

An increased number of puncta of filipin was observed in: NPA, NPB, and NPC I1061T mutant cell lines *Figure 3.29(a)*, consistent with the increase in the number of puncta as observed in *Figure 3.28*. Significantly increased puncta fluorescence was observed in NPA and NPB cells treated with AQ7, suggesting increased cholesterol accumulation within each lysosome (*Figure 3.29(b)*). Whilst not significant, in the other cell lines a similar trend of increased fluorescence in AQ7 treated cells was observed, suggesting that AQ7 is leading to lysosomal cholesterol accumulation.

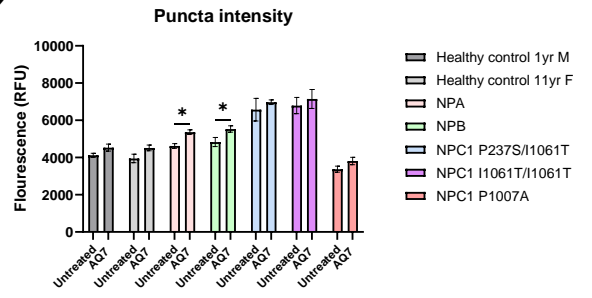
A significant increase in the total volume of filipin staining, was observed in: NPA, NPB, and NPC cell lines with the classical disease phenotype (*Figure 3.29(c)*). Thus, the total cholesterol within these cells is elevated, consistent with lysosomal cholesterol storage. This data shows that AQ7 is leading to significant increased area of cholesterol accumulation within Niemann-Pick disease cell lines, where cholesterol accumulation is already known to be a phenotypic marker. The mean puncta area of filipin staining was only significantly changed in the NPA cell line, where an increase in the mean puncta area was observed (*Figure 3.29(d)*). It is unclear for the reason for the increased puncta size observed in the treated NPA cells, however AQ7 leading to exacerbation of trafficking defects in NPA is a possible cause.

A trend was observed of increased density of cholesterol puncta being found in all cell lines; however, these trends were not statistically significant (*Figure 3.29(e)*). The trend of increased cholesterol puncta density is consistent with cholesterol accumulation, which is being driven by AQ7. The increase in cholesterol accumulation is possibly caused by a possible inhibitory effect of AQ7 upon NPC1, which would lead to associated cholesterol accumulation.

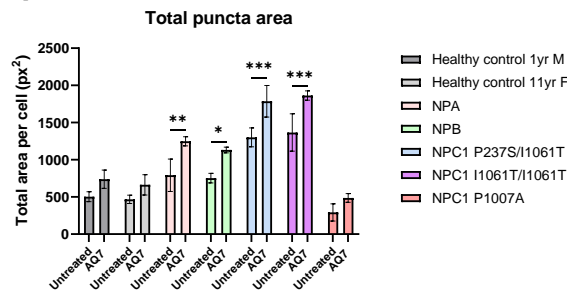
(a)



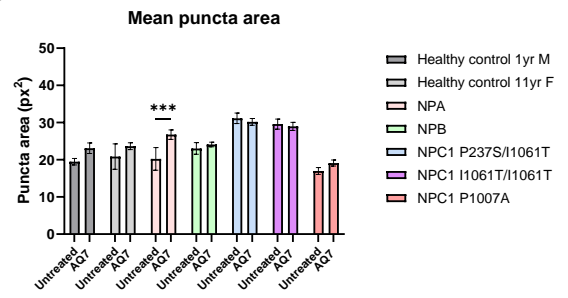
(b)



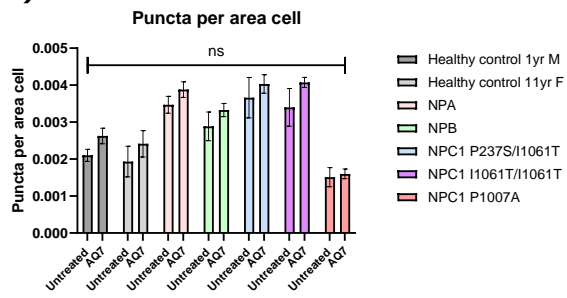
(c)



(d)



(e)



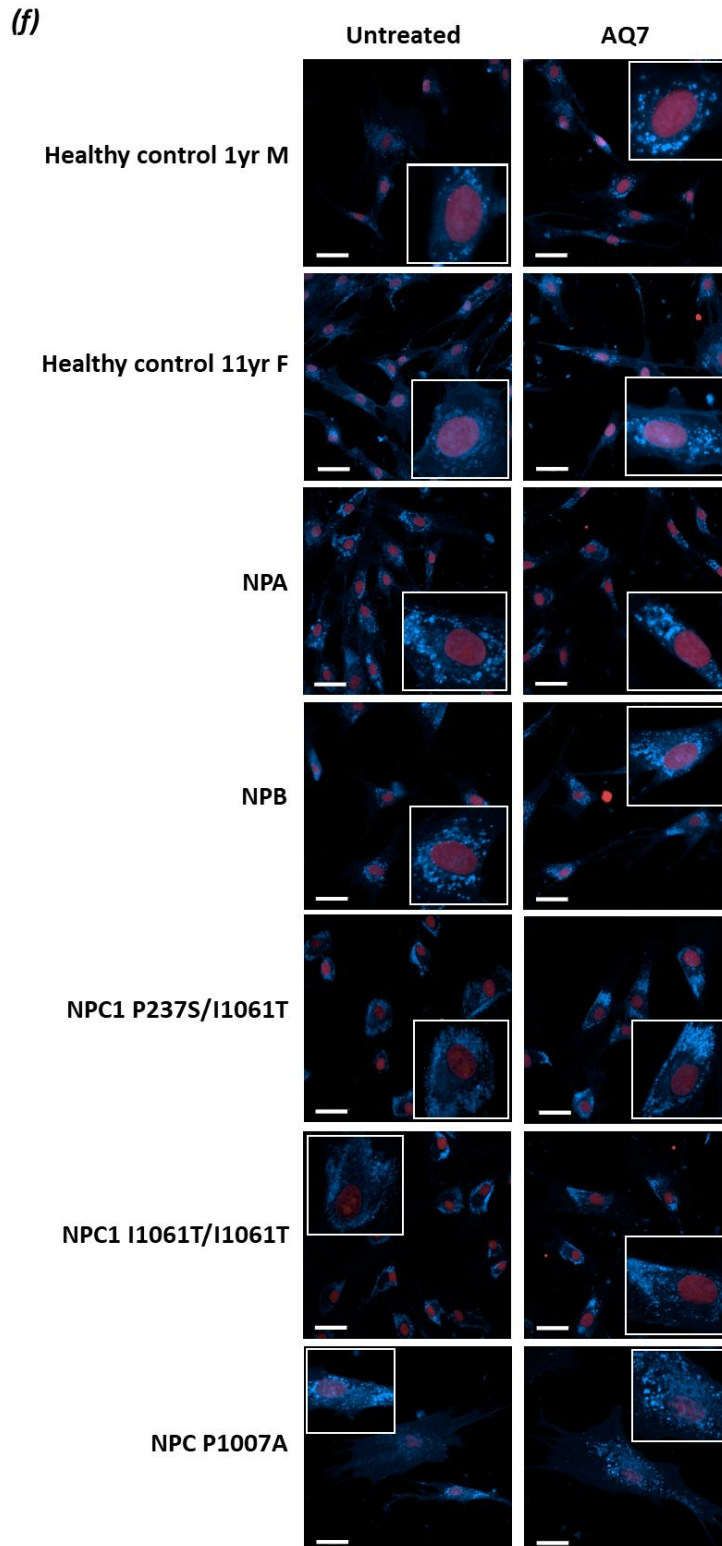


**Figure 3.29. AQ7 leads to increased filipin staining in some Niemann-Pick disease cell lines**  
 Cells treated with AQ7 have increased cholesterol accumulation. Cells were treated with 200 $\mu$ M AQ7 for 4 hours, before being fixed and stained with filipin and imaged. Fluorescent puncta of filipin were analysed using analysis parameters as shown (a-e), with reference images in (f). All data is n=3, with mean and standard deviation shown, statistical significance was determined through a two-way ANOVA with post-hoc Tukey test. Scale bars represent 50 $\mu$ m.

### 3.2.8 Evaluation of the sensitivity of AQ7 as a lysosomal probe

#### 3.2.8.1 AQ7 can be used to differentiate between Niemann-Pick disease phenotypes

Following the characterisation of AQ7 in 3.2.6, it was decided to evaluate the sensitivity of AQ7 as a probe, to determine the potential usefulness of AQ7 in imaging-based assays. It was decided to determine if AQ7 could detect phenotypic difference between Niemann-Pick disease cells, each with a distinct phenotype.

As shown in *Figure 3.30*, AQ7 shows sensitivity as a probe to be able to differentiate between Niemann-Pick disease cell lines, across a range of different analysis parameters. Across all the parameters analysed, AQ7 showed highly significant differences across the cell lines tested, with differences between: NPA, NPB, and NPC disease phenotypes. The data for number of puncta per cell. As well as average puncta area and total puncta area are consistent with previously reported data using LysoTracker dyes. Data for puncta per area cell for Niemann-Pick disease cell lines has not been reported, however all Niemann-Pick disease cell lines have more puncta per area cell than healthy controls, which is consistent with the nature of lysosomal storage disorders. AQ7 shows a decrease in fluorescence in the Niemann-Pick disease cell lines compared to healthy controls, which suggests that some lysosomal de-acidification is present in the Niemann-Pick disease cell lines.

Also of note is possible inhibitory effect of AQ7 on NPC1, as the NPC1 I1061T/I1061T cell line show the highest number of puncta of all cell lines, being approximately 50% higher than the NPC1 cell line with a P237S/I1061T mutation *Figure 3.30(a)*. A corresponding approximate 50% decrease in AQ7 puncta fluorescence intensity is also observed in the NPC1 I1061T/I1061T compared to the NPC1 I1061T heterozygous cell line *Figure 3.30(b)*, which may correspond to increased lysosomal storage.

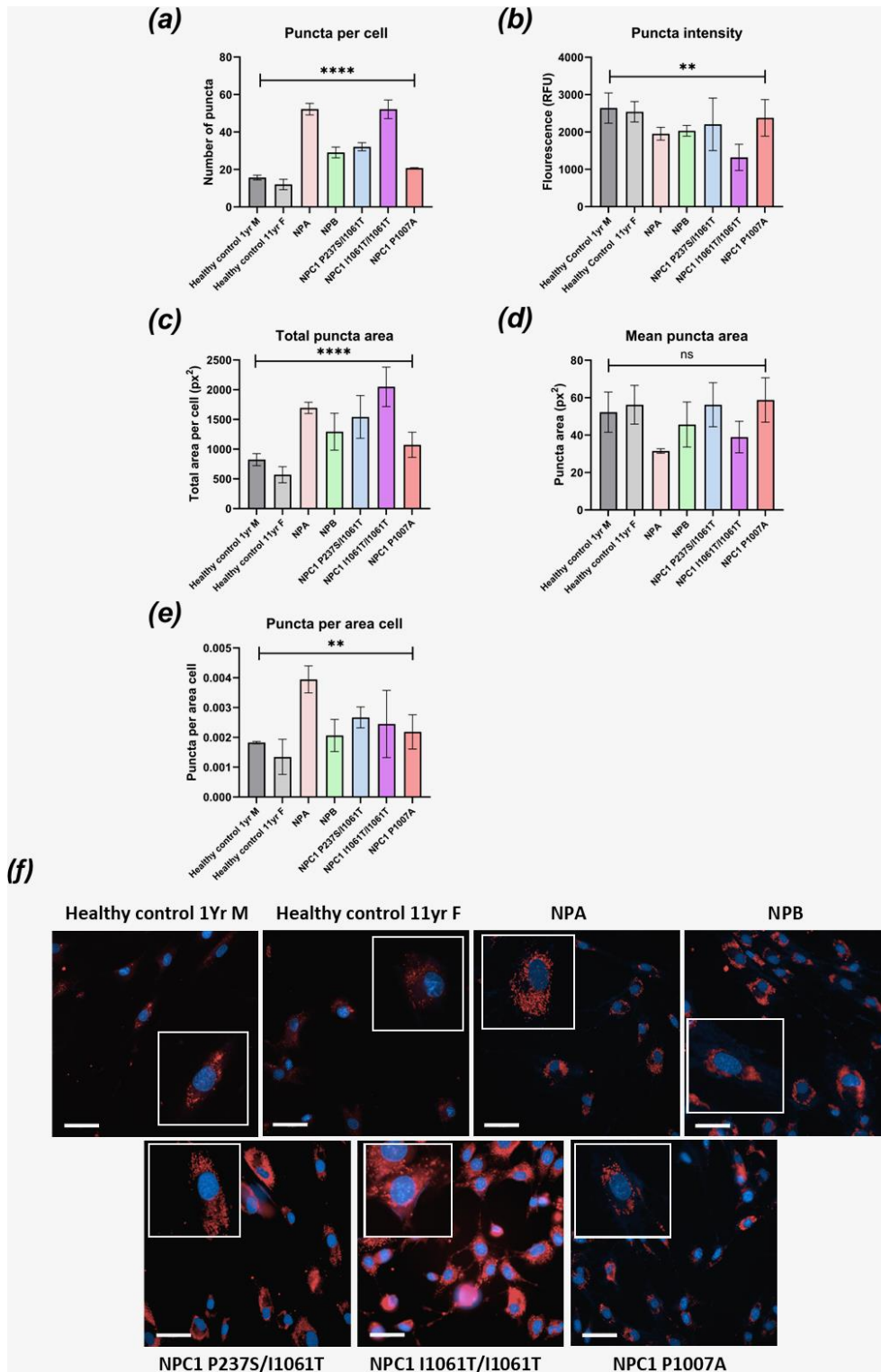


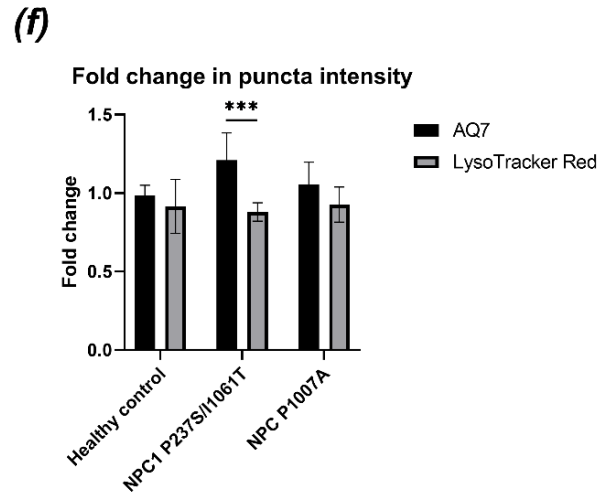
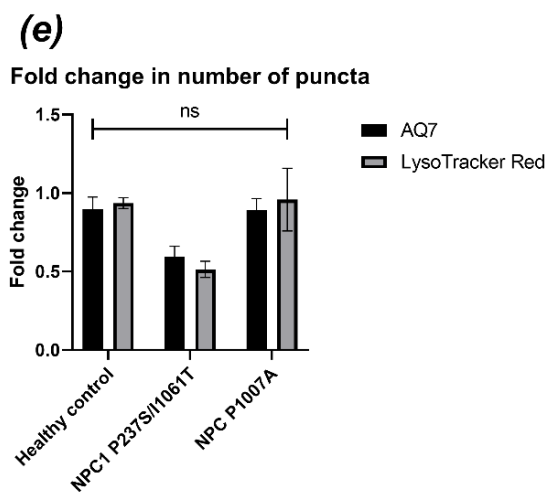
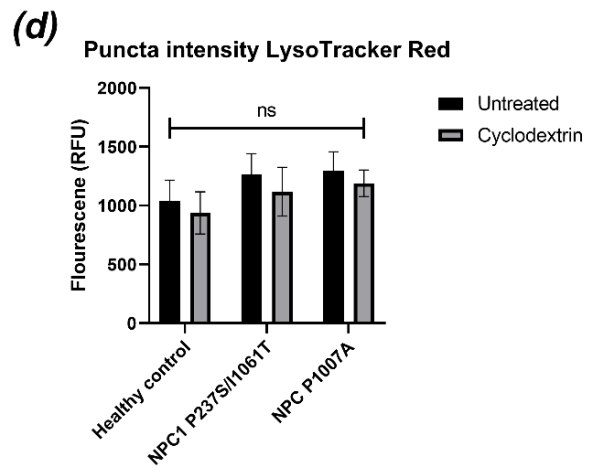
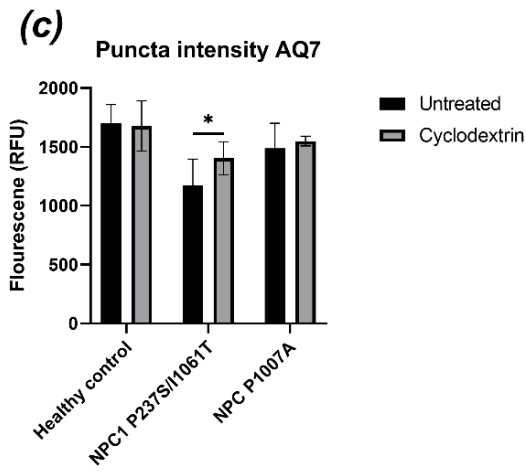
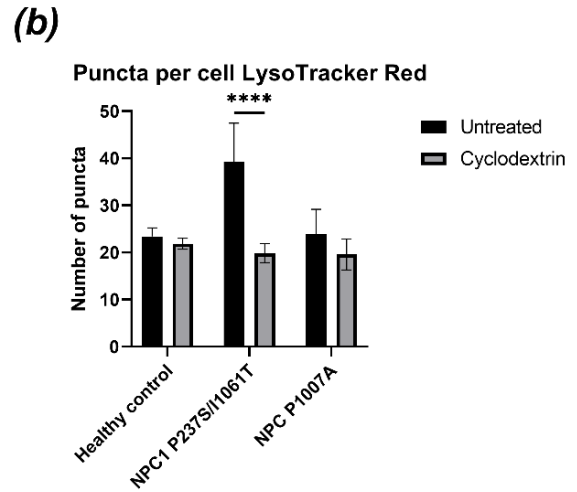
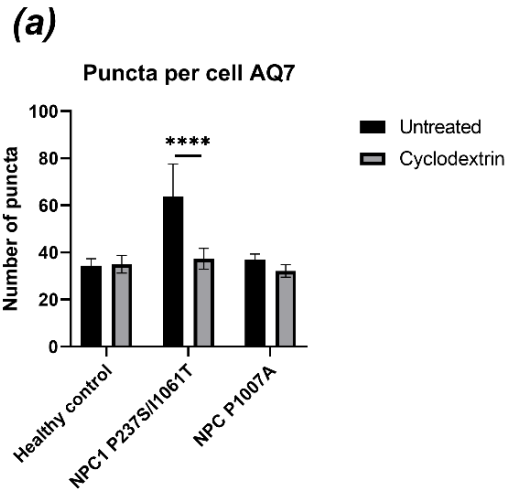
**Figure 3.30. AQ7 staining in Niemann-Pick disease fibroblasts**

Comparison of staining by AQ7 in various healthy and Niemann-Pick disease patient derived fibroblasts. Cells were treated with 200 $\mu$ M AQ7 for 4 hours, before being transferred into AQ7 free Opti-MEM and imaged. In (a-e), several different analysis parameters are shown, with comparisons between all cell lines tested. In (f) representative reference images for each cell stained with AQ7 are shown. All data is n=3, with mean and standard deviation shown with statistical significance between groups was determined using a one-way ANOVA. Scale bars represent 50 $\mu$ m.

### 3.2.8.2 AQ7 can detect improvements in NPC1 phenotype using Cyclodextrin

Once it had been determined that AQ7 was sensitive enough as a probe to detect lysosomal storage in Niemann-Pick disease fibroblasts, we wanted to determine if AQ7 could be used to identify phenotypic changes induced by potential NPC1 therapies. Cyclodextrin is known to reduce NPC1 phenotypes *in vitro*, with accompanying reduced lysosomal storage so was used to determine if AQ7 could detect differences in cells treated with cyclodextrin.

As can be seen in *Figure 3.31(a)*, AQ7 can detect improvements in NPC1 disease phenotype, with significantly decreased puncta numbers in NPC1 P237S/I1061T cells, but not in NPC1 P1007A or in healthy control cells. This pattern of decrease in puncta observed in NPC1 P237S/I1061T when treated with cyclodextrin is also observed with LysoTracker Red (*Figure 3.31(b)*), as is the lack of effect in the healthy control and NPC1 P1007A cells. Some differences in puncta fluorescence intensity are observed when comparing AQ7 and LysoTracker Red. A significant increase in puncta intensity with AQ7 is observed when NPC1 P237S/I1061T are treated with cyclodextrin (*Figure 3.31(c)*), whereas no effect is observed with LysoTracker Red (*Figure 3.31(d)*). The data in *Figure 3.31 (e)* shows that there is no significant difference in the fold change upon cyclodextrin treatment when comparing AQ7 to LysoTracker red. In *Figure 3.31 (f)* the change in AQ7 fluorescence is significantly different compared to LysoTracker Red for the cyclodextrin treated NPC1 P237/I1061T cells. This is likely due to the improved trafficking induced by the cyclodextrin, allowing more AQ7 to enter the lysosomes increasing the fluorescence.



(g)

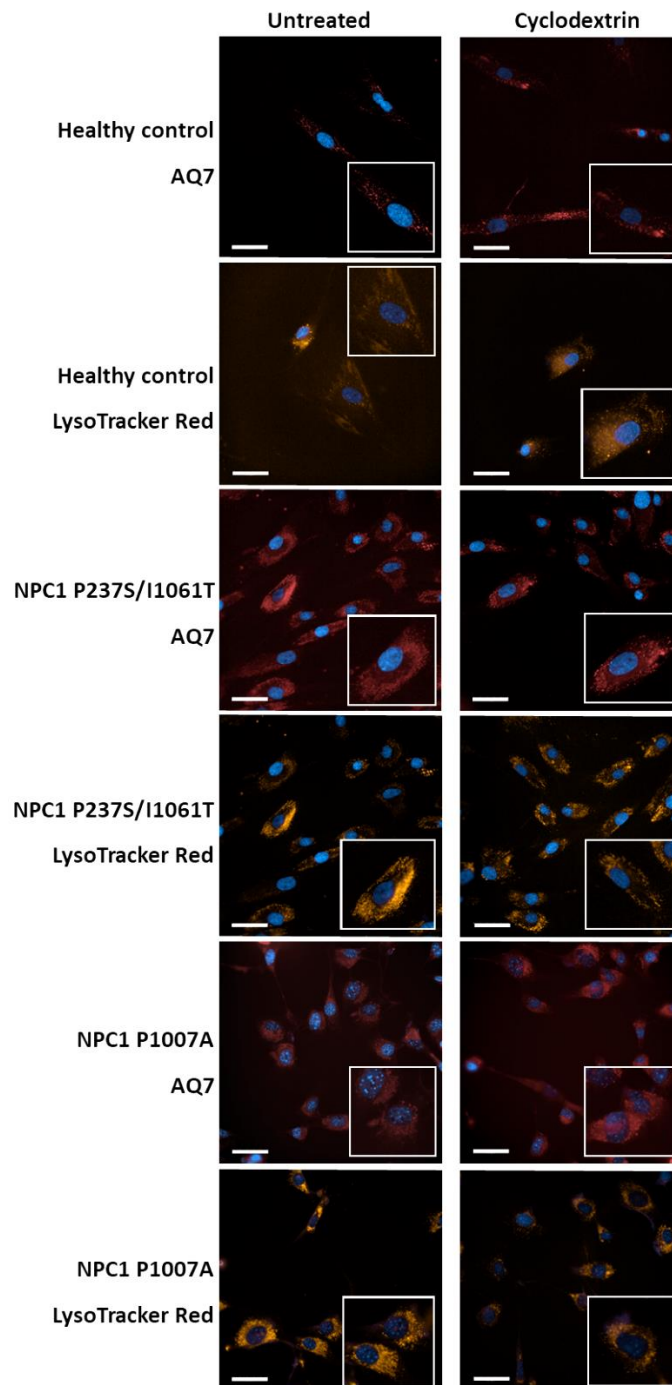


**Figure 3.31. AQ7 can detect improvement in disease phenotype when NPC cells are treated with cyclodextrin**

In (a) and (b) the number of puncta per cell in three cell lines before and after treatment with cyclodextrin. With (a) being stained with AQ7 and (b) being stained with LysoTracker Red. Graphs (c) and (d) show the puncta fluorescence intensities, both pre and post cyclodextrin treatment, with both AQ7 and LysoTracker Red. In (e) the fold change in number of puncta is shown, with comparisons between AQ7 and LysoTracker red in the three cell lines tested, whilst (f) shows the fold change in puncta intensity for each cell line, with the comparison between AQ7 and LysoTracker Red. Reference images for each cell line before and after treatment and with each probe are shown in (g). All data is  $n=3$ , statistical significance was determined through multiple two-tailed student T-tests. Scale bars represent  $50\mu\text{m}$ .

### 3.3 Discussion

#### *3.3.1 Issues with development of an NPC1 trafficking assay*

The aim of this chapter initially was to develop an NPC1 trafficking assay, utilising an AQ2 analogue. However, the issues encountered, including lysosomal entrapment of AQ3 and AQ7 prevented the development of the assay. Whilst some cells showed nuclear AQ3 fluorescence, this was never higher than 20% of all cells; despite changing assay parameters to attempt to improve the localisation. Therefore, it was not possible to take the assay further, as the assay lacked the robustness to be suitable for use as an assay or as part of a HTS screening programme. However, the decision to stop development of AQ3 as a primary NPC1 HTS screening assay, led to increased time available to carry out assay development of a zinc assay suitable for use in a HTS.

#### *3.3.2 Selection of anthraquinone derivatives*

The initial aim in setting up a AQ2 analogue trafficking assay was to identify the best analogue from a series of anthraquinone derivatives. The AQ2 analogues showed highly variable toxicity based on the side group attached, two of the initial series, AQ4 and AQ5 contained lipophilic side groups, and both exhibited high toxicity *in vitro* NPC1 null cells. This toxicity is unlikely to be due to the molecule being exocytosed from the lysosome and intercalating with the DNA, therefore it is possible that the molecule is affecting lysosomal function. Anthraquinones depending on the side group, are able to induce cytotoxicity, with some derivatives being known to induce apoptosis being suggested as potential anti-cancer therapeutics (Sendelbach 1989; Chen et al. 2007) Therefore, it is possible that AQ4 and AQ5 are inducing apoptosis, and thus makes them unsuitable for the use as long-lived lysosomal imaging probes. AQ6, despite showing minimal toxicity, had very poor solubility, thus preventing it from further consideration or development as a probe. This left AQ3 as the best candidate molecule from the initial series, with the brightest fluorescence and cell tolerance, however the molecule, whilst brighter than AQ2, still had limited fluorescence. From AQ3, a second morpholine group was added which produced AQ7, which possessed red shifted fluorescence.

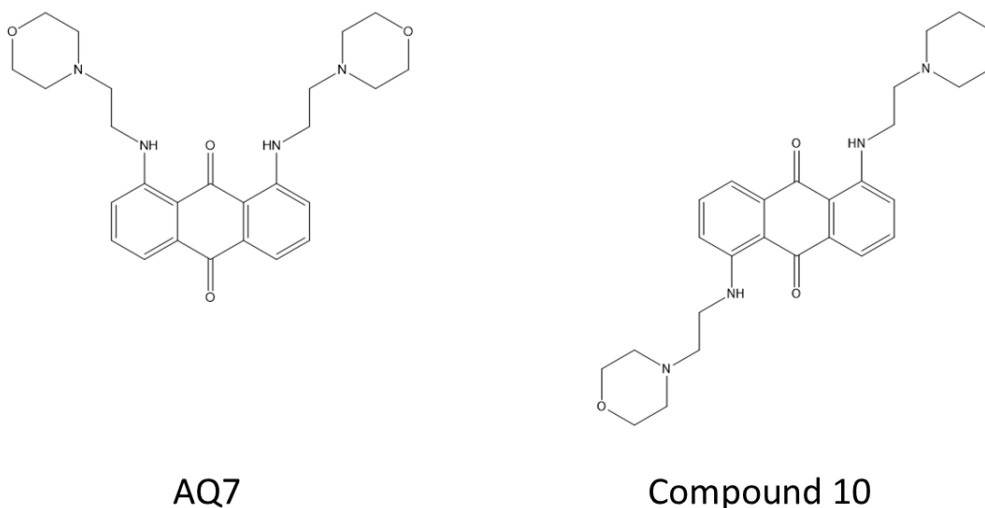


***Figure 3.32. Structures of AQ7 and compound 10***

*Comparison of the structures of the structurally similar AQ7 and compound 10. AQ7 possesses two morpholine groups in the 1,1 positions, whilst compound 10 has the morpholine groups opposed in the 1,5 position (Errington et al. 2018). Both molecules have can be excited with 500nm light, with fluorescence emission maxima at approximately 620nm providing fluorescence in the red/far-red range.*

### 3.3.3 AQ3 and AQ7

Following the unsuitable nature of AQ3 or AQ7 as a trafficking probe, the next aim was to determine the fluorescence characteristics of AQ3 and AQ7. The addition of the second morpholino group to AQ3 to create AQ7 both shifted the fluorescence towards far red fluorescence and improved the molecules fluorescence intensity at both neutral and acidic pHs. Based on all of these properties, AQ7 was determined the best probe for further evaluation.

Whilst it may be possible to further improve the fluorescence of AQ7 through the addition of a halogen, changing the position of the morpholine groups is highly likely to affect cellular localisation. Other research groups have shown that changing the morpholine groups from the 1,1 position in AQ7 to a 1,5 position as found Compound 10 (*Figure 3.32*), that the molecule localises to the nucleus and perinuclear regions, as opposed to the lysosome we observed with AQ7 (Errington et al. 2018). Thus, it is postulated that the current positioning of the morpholine side groups in AQ7 are required for the molecule to localise to the lysosome.

### *3.3.4 AQ7 as a lysosomal probe*

However, whilst the entrapment of AQ3 and AQ7 within lysosomes was an issue for a trafficking assay, it made both molecules potentially suitable lysosomal probes, due to their long retention time.

Therefore, the final aim of the chapter was to assess whether AQ7 could be utilised as a lysosomal probe. Comparison between AQ7 and LysoTracker showed that for most situations the probes are directly comparable and could be used interchangeably. The clearest advantage of AQ7 over LysoTracker dyes is the ability to carry out long time course imaging with AQ7, without inducing cellular toxicity or undergoing fluorescence quenching from repeated imaging. AQ7 is also comparable to LysoTracker dyes in both localisation and number of puncta of lysosomes identified. AQ7 can also detect difference in lysosome number when treated with 3MA or trehalose in a similar manner to LysoTracker Red.

However, a significant difference between AQ7 and LysoTracker Red is that the number of puncta identified with AQ7 was incubation temperature sensitive, unlike LysoTracker Red, thus suggesting that AQ7 is being actively endocytosed into the cell. Therefore, this must be considered as part of the assay design, as the bafilomycin data clearly showed that the data can be influenced when AQ7 is added during the experiment.

### *3.4 Conclusions*

The data in this chapter shows that of the anthraquinone derivatives tested, AQ7 possesses the best combination of cellular tolerance and fluorescence emission intensity. However, AQ7 is not suitable for the development of a trafficking assay, due to AQ7 being retained within lysosomes. This lysosomal retention means that AQ7 can be used as a lysosomal probe due to its prolonged lysosomal retention.

AQ7 possesses some distinct advantages over the LysoTracker series of dyes. The high photostability and limited cell toxicity of AQ7 make it a viable alternative to the LysoTracker family of dyes. AQ7 shows similar lysosome sensitivity to LysoTracker dyes and detects differences in cell phenotypes similar to those previously established using LysoTracker dyes. Therefore, we believe that AQ7 is a suitable novel lysosomal probe, with distinct advantages over LysoTracker dyes.

## 4 Development of a zinc based phenotypic screening assay suitable for HTS

### 4.1 Introduction

Zinc is a trace mineral, found ubiquitously within the body, with a variety of intracellular roles, including: catalytic, structural, and cell signalling. Whilst total zinc levels are usually comparable to that of other metal ions, such as iron, the majority of intracellular zinc is present in the form of co-factors associated with proteins.

One of the first intracellular roles to be identified for zinc, was within enzymes, whereby zinc co-ordination is commonly observed within the active site (Coleman 1998). The first enzyme identified to require zinc as a co-factor, was carbonic anhydrase, which regulates the ratio of carbon dioxide to carbonic acid (Keilin and Mann 1985). This was followed by the identification of a structural role for zinc ions within proteins, with one such example being the 'zinc finger' motifs present in multiple proteins, including several transcription factors (Miller et al. 1985; Zhang et al. 2015). However not all structural motifs containing zinc are used to bind nucleic acids, with both protein and lipid binding domains being identified (Gamsjaeger et al. 2007).

More recently zinc, in the form of  $Zn^{2+}$ , has been identified as a signalling ion, required for cellular regulation (Maret 2013). This is consistent with the identification of numerous zinc transporters required to tightly control cytosolic zinc release; with zinc transporters including the ZnT and Zip families (Kimura and Kambe 2016).

#### 4.1.1 *Cellular zinc homeostasis*

Intracellular zinc concentrations have been shown ranging from 10-100 $\mu$ M, however the free  $Zn^{2+}$  concentration is reported to be in the picomolar to nanomolar range, due the majority of zinc being protein bound (Yamasaki et al. 2007; Colvin et al. 2008; Qin et al. 2013). Cytosolic zinc concentrations have been shown to be in the low nanomolar range, with the free zinc concentration significantly lower again (Krezel and Maret 2006).

Intracellular zinc concentrations require tight regulation, as very high free Zn<sup>2+</sup> concentrations would lead to unspecific zinc binding, with displacement of other divalent metal ions from proteins (Maret 2013). Both Golgi and ER normally contain zinc at high nanomolar concentrations, however the free Zn<sup>2+</sup> concentration is at 1pM (Qin et al. 2011). If elevated cytosolic concentrations occur, both ER and Golgi can act as a reservoir to reduce cytosolic zinc concentrations, reducing downstream effects, such as modulation of signalling pathways (Qin et al. 2011).

Intracellular vesicles, such as lysosomes, contain micromolar to millimolar concentrations of total zinc, functioning as vesicular zinc stores, with lysosomes that contain high concentrations of zinc being termed 'zincosomes' (Haase and Beyersmann 1999; Minckley et al. 2019; Du et al. 2021). It is unclear what the free Zn<sup>2+</sup> concentration is within lysosomes; however, this is likely to be nanomolar range, broadly in line with the elevated total zinc content present within the organelles. Free Zn<sup>2+</sup> concentrations within zincosomes can fluctuate, postulated to be in the micromolar range (Palmiter et al. 1996a).

It is unclear whether zincosomes are a discrete organelle or a late endosome/lysosome with increased zinc storage. However, unlike lysosomes, de-acidification of these organelles does not disrupt cellular zinc storage (Palmiter et al. 1996a). It has been suggested that zincosomes are a primary method of storing excess intracellular zinc, acting as a buffer for cytosolic zinc, with stored zinc being able to be exported back to the cytosol when required (Duffy et al. 2001). In *C. elegans*, lysosome like organelles can sequester excess zinc to maintain homeostasis, and slowly release zinc back into the cytosol as required (Mendoza et al. 2024).

#### 4.1.2 Cellular zinc transporters

Trafficking and transport of zinc across intracellular membranes requires a range of zinc-specific transporters. Zinc transporters are ubiquitous across all living organisms, with a range of zinc transporter families identified in yeasts, plants and vertebrates (Kambe et al. 2015). The first zinc transporter identified was Zrc1, from *Saccharomyces cerevisiae*, which transports zinc across the vacuole membrane to protect against zinc induced toxicity (Kamizono et al. 1989).

In humans, two families of zinc transporters have been identified, the SLC30 (including the ZnT family) and the SLC39 family (ZIP family). Transporters in the ZnT family are membrane proteins with 6 transmembrane domains, which regulate the transport of zinc out of the cytosol (Huang and Tepasorndech 2013). The ZIP family of zinc transporters regulate the transport of zinc into the cytosol from organelles, with a characteristic of the family being the 8 transmembrane domains (Guerinot 2000; Kambe et al. 2006).

#### 4.1.2.1 Zinc efflux transporters

The first human zinc transporter successfully cloned was the ZNT1 transporter (Palmiter and Findley 1995). Additional members of the ZNT family were identified soon after, being identified as Znt2 and Znt3, also both members of the cation diffusion facilitators (CDF) superfamily (Palmiter et al. 1996a; Palmiter et al. 1996b). At present 10 members of the ZnT family of transporters have been identified, however it is possible that further members of the family remain unidentified (Bosomworth et al. 2012). Additional zinc transporters are in the CDF, family but are not ZnT's, which include some members of the TMEM family; with TMEM163 being abundant in lysosomes (Cuajungco et al. 2014; Escobar et al. 2022; Wu et al. 2023).

#### 4.1.2.2 Zinc influx transporters

Whilst the ZnT family of receptors are responsible for trafficking zinc from the cytosol into other organelles, zinc transporters in the SLC39 family are responsible for trafficking zinc into the cytosol (Liuzzi and Cousins 2004). The largest group of SLC39 transporters is the ZIP family, with 14 members of the family identified so far (Baltaci and Yuce 2018). However, the Zip family are not ubiquitous throughout the cell. In humans: ZIP8, ZIP9, and ZIP14 are lysosomal, being identified as co-localising with LAMP1 (Aydemir et al. 2009; Zhao et al. 2010; Qiu et al. 2020).

However, it is possible that additional members of the ZIP family can co-localise to lysosomes, as ZIPT2 and ZNPT3 are known to localise to lysosomes in *C. elegans* models (Mendoza et al. 2024). Unlike the Zinc efflux transporters, no evidence of dimerization, or localisation with other zinc channels has been reported.

### 4.1.3 Zinc in disease

Whilst in healthy cells, zinc homeostasis is tightly controlled, both the dysregulation of intracellular zinc levels has both been linked to several conditions and diseases.

#### 4.1.3.1 Hypozincaemia

Depletion of cellular zinc levels was known to cause several growth and developmental effects in rodents as early as the 1930's, however the effects of zinc deficiency on humans took several more decades to understand (Todd et al. 1980). Severe zinc deficiency can present with growth impairment, skin rashes, alopecia, hypogonadism and neurological impairment (Prasad 2012).

A moderate zinc deficiency has been reported to occur in a range of conditions, including alcoholic liver disease, sickle cell disease, and in chronic kidney disease. A range of differing manifestations of moderate zinc deficiency include: growth retardation, poor appetite, mental lethargy, and delayed wound healing (Prasad et al. 1978).

#### 4.1.3.2 Hyperzincemia

Excess accumulation of zinc is much less common than zinc deficiencies, however it does occur. Hyperzincemia, is often characterised by copper deficiency and anaemia, usually caused by the increased zinc concentration leading to upregulation of metallothionein, which have a preference for binding copper atoms over zinc (Merza et al. 2015). Prolonged hyperzincemia and subsequent hypocupraemia can lead to spinal and peripheral nerve injury, as well as ataxia (Kumar et al. 2004).

#### 4.1.3.3 Zinc dysregulation

Whilst both hypozincaemia and hyperzincemia are well characterised, zinc dyshomeostasis has also been observed in a range of other diseases.

##### 4.1.3.3.1 Diabetes

Pancreatic beta cells are known to possess some of the highest zinc concentrations within the human body, with zinc being involved in the process of insulin synthesis and secretion (Chausmer 1998). It has been hypothesised that ZnT8 is required to allow the formation of insulin containing vesicles, with insulin co-ordinating with zinc to form hexamers (Chimienti et al. 2005). Targeting of ZnT8 by autoantigens has been reported to occur in 60-80% of Type 1 diabetes cases (Wenzlau et al. 2007). Point mutations in ZnT8 are believed to increase susceptibility to type 2 diabetes, with associated reduced insulin release, caused by

zinc dyshomeostasis and less insulin storage vesicles being formed (Mocchegiani et al. 2008).

#### 4.1.3.3.2 Cancer

Zinc transporter defects, and subsequent zinc dyshomeostasis has been reported in a range of cancers including breast: lung, prostate, pancreatic, and liver cancers (Bendellaa et al. 2024). In these cancers, mutations, or changes in activity of specific ZIPs leads to tissue specific cancers effects, with a range of effects upon prognosis. Hypozincaemia in cancer has been reported to lead to chromosome instability, and a reduction in the presence of micronuclei (Blackburn et al. 2015; Bai et al. 2016). However, in some cancers, activity of ZIP6 and ZIP10, both involved in mitosis, been reported to be increased, which is associated with poor prognosis. Some zinc chelators have been evaluated for effectiveness in cancer, including clioquinol, which underwent a clinical trial, as a metal chelator in haematological cancers (Valli et al. 2020).

#### 4.1.3.3.3 Infectious disease

Zinc deficiency is linked to the severity of several infectious diseases including HIV, tuberculosis and malaria (Sigel et al. 2013). This is believed to be driven by zinc deficiency, leading to impaired immune function, particularly the innate immune system (Walker and Black 2004). Additionally, the adaptive immune system can be impaired by zinc dyshomeostasis, as disruption in zinc levels reduces monocyte adhesion. It is unclear whether zinc directly affects inflammation, as zinc has been reported to both be a modulator of pro-inflammatory and anti-inflammatory pathways (Maywald and Rink 2022).

#### 4.1.3.3.4 Neurodegeneration

Metals dyshomeostasis is known to be a contributing factor in neurodegeneration, including zinc (Chen et al. 2016). Zinc dyshomeostasis is linked to a variety of neurological disorders, including: Alzheimer's disease, amyotrophic lateral sclerosis (ALS), and Parkinsons disease (Szewczyk 2013). Free zinc is known to accumulate in synaptic vesicles, whereby the release of these vesicles can modulate both NMDA and GABA receptors (Prakash et al. 2015). Neurons also possess a zinc sensing receptor, GPR39, which can lead to downstream modulation of intracellular zinc (Besser et al. 2009; Frimurer et al. 2017). At normal concentrations, zinc exhibits neuroprotective activity, however hyperzincemia is known to be neurotoxic (Choi et al. 1988). Zinc accumulation is also believed to lead to development

of tauopathies and neurofibrillary tangles, and possibly be a driver of Alzheimer's disease (Craddock et al. 2012).

#### *4.1.3.4 Zinc in lysosomal storage disorders*

Whilst lipid storage is the primary accumulation molecule in lysosomal storage disorders, metal dyshomeostasis has also been reported. Altered metal levels has been reported in the Neuronal ceroid lipofuscinosis (NCL)(Johansson et al. 1990). In NCL cells: iron, manganese, and zinc levels have been reported to be altered (Bras 2013; Kanninen et al. 2013). Patients with Gaucher disease are known to have decreased zinc and copper levels, which remain uncorrected, even after enzyme replacement therapy (Zahran et al. 2015).

Mucopolipidosis IV (MLIV) is an LSD, characterised by loss of TRPML1 activity. MLIV patient cells are known to have increased LysoTracker staining, corresponding to lipid storage, however free zinc accumulation is also a biomarker of MLIV disease (Eichelsdoerfer et al. 2010). The increased zinc storage in MLIV is likely being driven by defects in the TRPML1 associated transporters, such as TMEM-163 or ZnT4 (Kukic et al. 2013).

In NPC, in both murine and human brains, dyshomeostasis of several metal ions occurs, including: manganese, iron, copper, and zinc (Hung et al. 2014). Upregulation of metalloproteins has been reported in NPC fibroblasts, likely to compensate for the increased: manganese, iron, and zinc levels (Reddy et al. 2006). In the brain, elevated levels of manganese, iron, and zinc were reported, with a decrease in copper. However, in the liver: manganese, iron, and zinc levels were significantly decreased, with copper being increased (Hung et al. 2014). There is also correlation between the levels of metal ion dyshomeostasis and the severity of the NPC disease phenotype (Hung et al. 2014).

In NPC1 null mice, increased plasma zinc was observed prior to symptoms of NPC disease, which is consistent with other published findings, whereby 3-week-old NPC1 null mice exhibit white matter loss (Guo et al. 2018).

However, in NPC1 patient samples, plasma zinc was decreased significantly, which was not corrected by miglustat treatment (Prasad et al. 1990). Therefore, it is postulated that the increased brain free zinc concentrations is likely a driver of the tauopathies and neurofibrillary tangles that have been reported in NPC disease (Auer et al. 1995; Treiber-Held et al. 2003).

NPC1 is a member of the RND permease superfamily of membrane proteins, with NPC1 having high homology with other members of the RND permease family (Davies et al. 2000). Several of the RND permease family of proteins are known as heavy metal efflux (HME) family, which are capable of both heavy metal transport as well as divalent efflux, including: copper, manganese, and zinc (Waldron et al. 2009). Some of this family includes pumps that have been shown to primarily transport zinc functioning as zinc efflux pumps, including ZneA and CzcCBA (Pak et al. 2013; Stahl et al. 2015). NPC1 shares similarity to the Zn<sup>2+</sup> efflux pump ZneA, including conservation of all the amino acids required for Zn<sup>2+</sup> transport (Maguire 2017).

Therefore, NPC1 may have the capability, like other RND permease members to be able to transport zinc and act as an efflux pump, which is supported by data from the Lloyd-Evans laboratory, which showed that loss of NPC1 led to early Zn<sup>2+</sup> accumulation (Maguire 2017).

#### 4.1.4 *Zinc probes*

Cellular imaging of zinc is a relatively recent development, in part due to the lack of understanding of the significance of zinc signalling within cells (Frederickson 2003). Early attempts to visualise metals was primarily carried out on brain sections and stained with compounds that bound to a range of metals. Initial probes used to label metals included, dithizone, quinoline, and silver amplification. Of these only quinoline is a fluorescent probe, however lacks the sensitivity of the other early probes, and is not zinc specific (Czaplinska et al. 2018).

One of the earliest zinc specific fluorescence probes to be identified was N-(6-Methoxy-8-quinolyl)-p-toluenesulfonamide (TSQ). TSQ is a blue fluorescence probe that binds to free zinc, with an emission peak of 470 nm (Frederickson et al. 1987). Attempts to improve the characteristics of TSQ has led to the creation of Zinquin and TflZn, amongst others (Pratt et al. 2021).

A range of non TSQ derived zinc binding probes exist, including Newport Green, which is a membrane impermeant dye that can bind to loosely bound zinc (Karim and Petering 2016). Another commonly used zinc binding probe is Flou-Zin 3, however this probe is known to have diffuse intracellular localisation and variable fluorescence intensity (Qin et al. 2013).

Additionally, neither Newport Green nor Flou-Zin 3 are suitable for use as a ratiometric probe.

A range of novel zinc probes have been synthesised within the last decade, including SpiroZin2 and Zinpyr-1, that appear to have improved characteristics; including improved fluorescence emission and better stability (Thompson 2005; Han et al. 2018).

A range of other zinc sensors have been developed, including sensors that comprise a metallothionein to a FRET group that allow for proportional zinc fluorescence (Maret 2009). Another published sensor includes conjugation of carbonic anhydrase to a fluorophore that can bind to FRET reported allowing for ratiometric zinc analysis (Fluorescence-based biosensing of zinc using carbonic anhydrase (Fierke and Thompson 2001).

#### *4.1.5 Zinc screening*

High-throughput screens are commonplace now, however only limited screens that have used zinc as a biomarker have taken place. One example was a screen carried out to identify modulators of fungal zinc homeostasis (Simm et al. 2011). However, instead of using a fluorescent probe to measure intracellular zinc, a GFP conjugate only expressed upon zinc depletion (Simm et al. 2011). The probe functioned through conjugation of GFP to the ZRT1 promotor, which upon zinc depletion leads to the uncoupling of Zap1 from ZRT1, leading to increased transcription of ZRT1 and GFP, in turn increasing GFP expression and subsequent fluorescence.

A screen for zinc modulators, focussing on ATP13A2, in which mutations cause Kufor-Rakeb syndrome, has been carried out in both yeast and zebrafish, using both an optical density and phenotypic based analysis (Heins-Marroquin et al. 2019). At present, no published zinc modulation phenotypic screens have been published for any lysosomal storage disease. Therefore, there is potential to screen for zinc modulators in Niemann-Pick and identify novel chemicals starting points for potential future development as a therapeutic.

#### 4.1.6 Aims

The aims covered in this chapter were to develop an imaging-based zinc assay and carry out a primary screen to identify compounds that modulated intracellular zinc. Zinc modulating compounds will be assessed for their ability to reduce lysosomal storage in NPC cells. To do this, the following aims were determined:

1. Identify a suitable zinc imaging probe for live or fixed cell imaging
2. Optimise zinc probe concentration, and determine if live or fixed cells are to be used
3. Identify tool compounds that increase and decrease zinc storage
4. Test assay to determine if the assay can identify known zinc modulators
5. Screen a compound library with NPC cells to identify hit compounds
6. Test hit compounds in a LysoTracker based assay to identify if molecules decrease lysosomal storage.

## 4.2 Results

### 4.2.1 Zinc probe selection

Three commonly used zinc probes were tested to determine which was the most suitable for use with the Operetta CLS. The three probes were: FluoZin-3, Zinquin ethyl ester, and TSQ, which are known to bind free  $Zn^{2+}$ .

Of the three probes tested, TSQ had both the highest puncta observed across untreated and both drug treatments, as well as highest puncta fluorescence. Both FluoZin-3 and Zinquin had similar number of puncta, with neither probe showing significant differences in puncta number or fluorescence when treated with U18666A or  $ZnCl_2$ .

Previous studies had shown that TSQ was specific for zinc, and did not bind to other metals at physiological conditions. Our data also shows that when known zinc modulators U18666A or  $ZnCl_2$  was tested, a corresponding increase in zinc puncta and fluorescence intensity was observed.

Therefore, based off the data in *Figure 4.1*, it was clear that TSQ was the most suitable probe for use for measuring free  $Zn^{2+}$ . For future zinc assay development TSQ, was to be used as the probe to identify free  $Zn^{2+}$ .

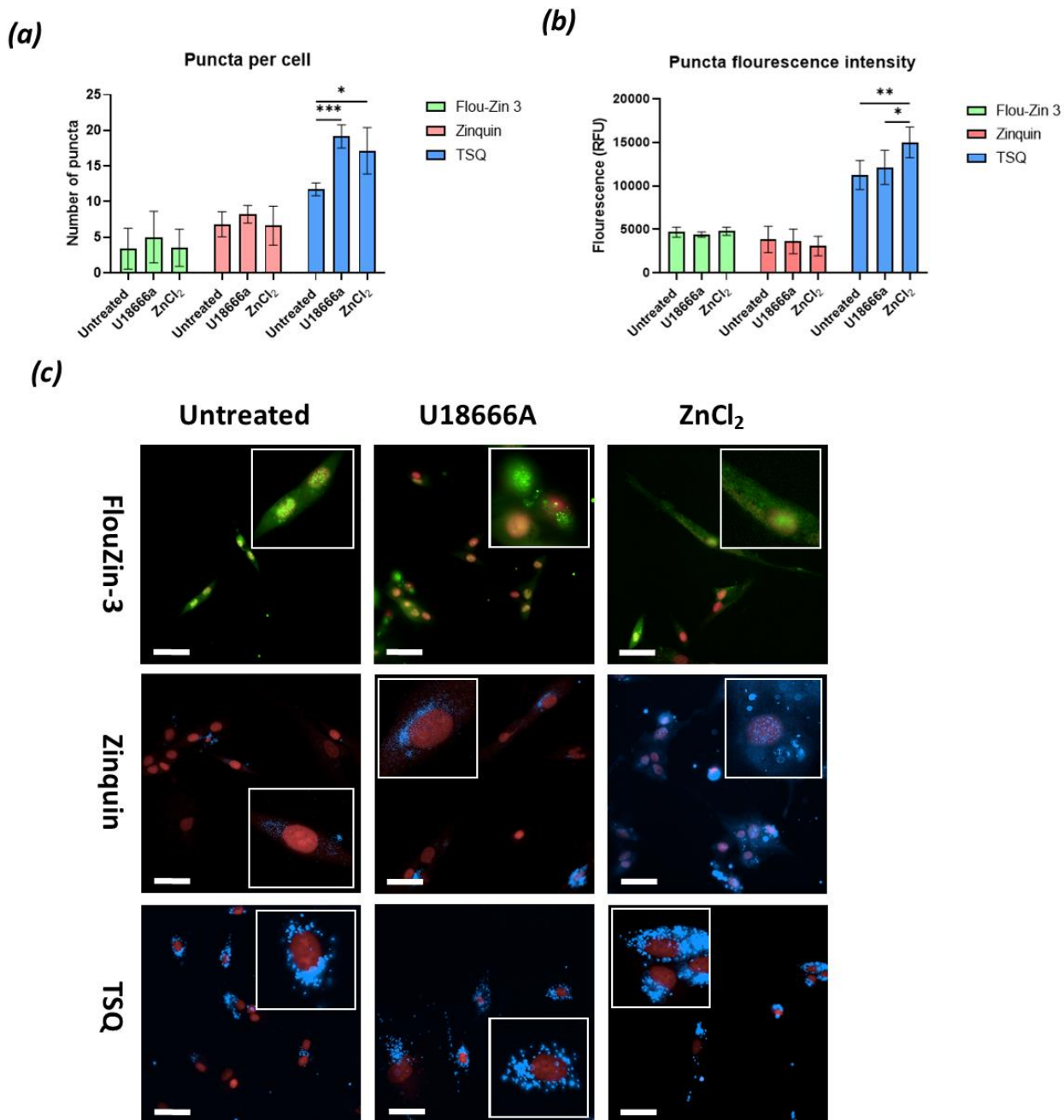


**Figure 4.1. Comparison of commonly used zinc probes fluorescence staining**

In (a) the mean number of puncta per cell, for all probes, with known zinc modulators. The corresponding puncta fluorescence intensity is shown in (b). Representative images for each probe and treatment conditions are shown in (c). Data is  $n=3$  and statistical significance was determined using a two-way ANOVA and post hoc Tukey tests.  $*=p<0.05$ ,  $**=p<0.01$ ,  $***=p<0.001$ ,  $****=p<0.0001$ , data shown is mean  $\pm$  SD. Scale bars represent  $50\mu\text{m}$ .

## 4.2.2 Assay optimisation

### 4.2.2.1 TSQ concentration determination

Once TSQ had been selected as the  $Zn^{2+}$  probe to be used, the next step was to determine the optimal concentration of TSQ. Most publications used TSQ in the mid micromolar range, so a range of concentrations of TSQ were selected around this. Both healthy control and Niemann-Pick fibroblasts were tested to determine if a difference between the cell lines would also be observed by changing TSQ concentrations.

In all concentrations above  $10\mu M$  the Niemann-Pick type C fibroblasts had more puncta of TSQ staining. The  $200\mu M$  concentration had the highest number of puncta, however a similar difference between healthy control and Niemann-Pick disease fibroblasts was observed in the  $100\mu M$ . Increasing the TSQ concentration beyond  $200\mu M$  did not lead to an increase in the number of puncta.

Based on this assay,  $100\mu M$  TSQ offered the best window between healthy control and Niemann-Pick disease cell line. Therefore,  $100\mu M$  was selected as the concentration to be used in further zinc assay set up and the HTS.

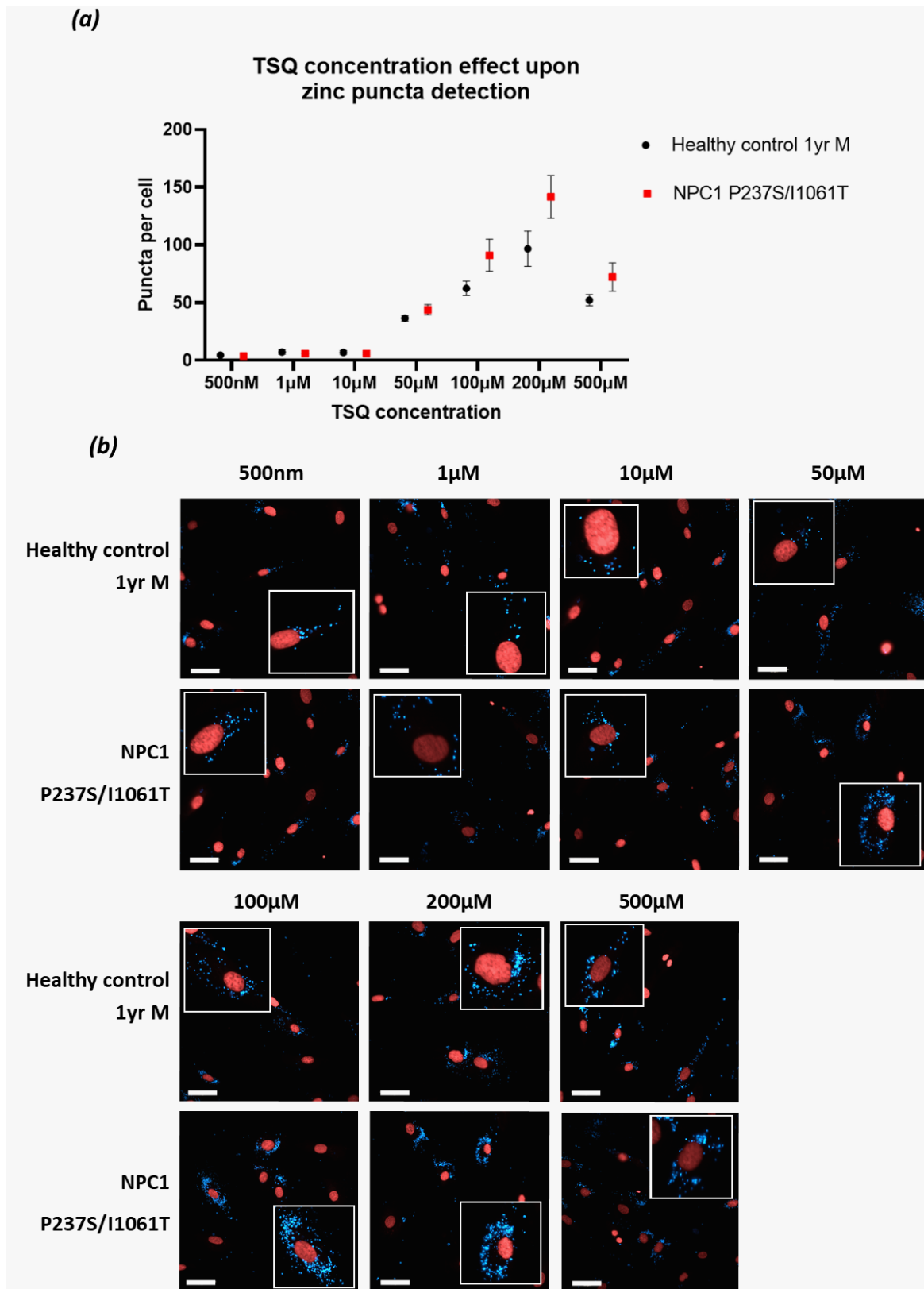


**Figure 4.2. Zinc puncta identification is TSQ concentration dependant**

In (a) the number of zinc puncta identified in both healthy control and Niemann-Pick type C disease fibroblasts are probed with varying concentrations of TSQ. In (b) reference images for both cell lines and with all concentrations of TSQ used are shown. Data is  $n=3$  with mean and Standard deviation shown. Scale bars represent  $50\mu\text{m}$ .

#### 4.2.2.2 *Removal of TSQ after staining leads to loss of fluorescence over time*

Once a suitable TSQ concentration had been identified, the next step was to determine if the probe was stable to be removed from the cells prior to imaging. For this, both live and fixed cells were tested, and healthy control and Niemann-Pick type C fibroblasts used.

From the data in *Figure 4.3*, it is clear that in both live and fixed cells, TSQ fluorescence is quick to dissipate upon removal of the probe. In the live cells, the number of puncta halved within 10 minutes of TSQ removal. With a similar trend also observed in the fixed cells. In the live cells, most fluorescence had been lost within 10 minutes, followed by only a small further decrease in the number of puncta. However, in the fixed cells, the number of puncta detected continued to decrease over the hour time period.

Therefore, based on this data, it appears that the probe readily dissociates from the free  $Zn^{2+}$  within the cell, rather than intracellular changes occurring. This is postulated, as quenching was observed in the fixed cells at equal rates for both healthy control and Niemann-Pick type C cells. Based on these findings, when imaging with TSQ, the cells must be maintained in buffer containing TSQ for the duration of imaging.

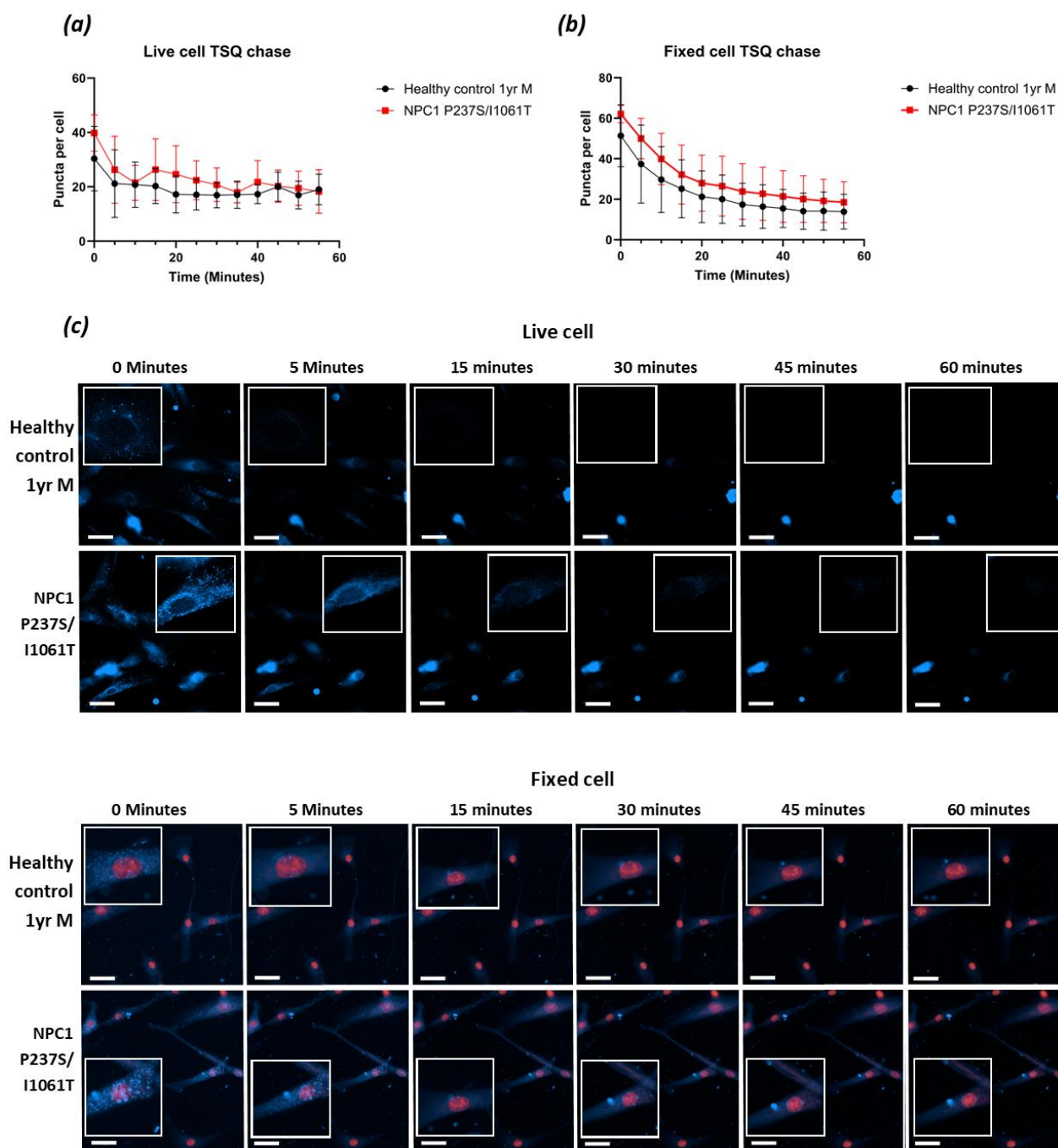


**Figure 4.3. Removal of TSQ leads to quick dissipation of fluorescence**

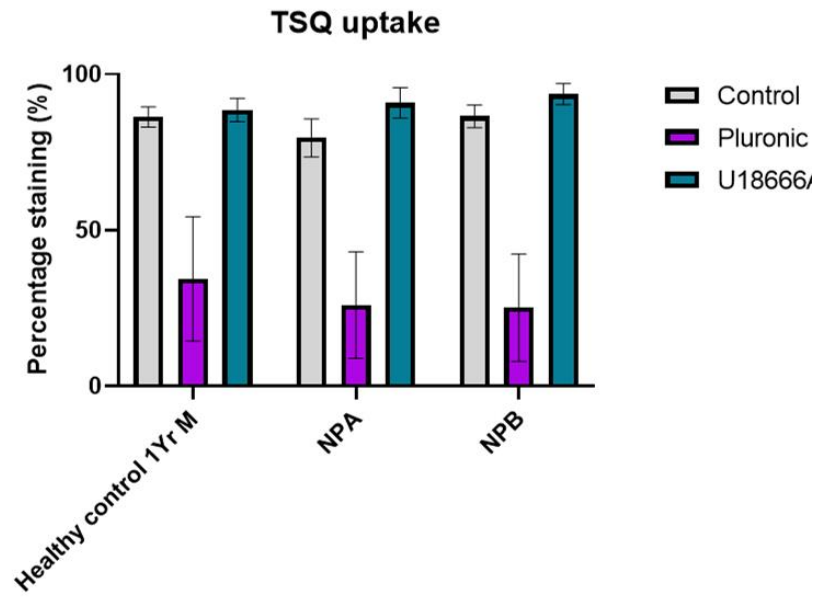
In (a) live cells were incubated with TSQ for 30 minutes prior to imaging, with fixed cells being used in (b). The TSQ was removed, and the cells imaged every 5 minutes for 1-hour total time. In both live and fixed cells, both healthy control and Niemann-Pick type C cells were tested. In (c) reference images for both live and fixed cells, in both cells lines over the time course are shown. Scale bars represent 50 $\mu$ m.

#### *4.2.2.3 Determining if Pluronic F-127 improves cellular probe uptake*

Early assays where staining with TSQ was used, showed that approximately 10 – 15% of cells did not have TSQ staining. To address this, Pluronic F-127 was tested to determine if the addition of Pluronic F-127 to TSQ when the cells were being stained would improve cellular uptake of the probe. U18666A was also tested to determine if the induction of an Niemann-Pick Type C like phenotype would affect the percentage of staining.

In all three cell lines tested, Pluronic-F127 decreased the percentage of cells with staining, down to approximately 30%. Unlike the Pluronic F-127, treating cells with U18666A does not affect the percentage of cells with staining. Based off the data it is clear that Pluronic F-127 does not improve TSQ staining, worsening the percentage of cells with staining. Therefore, Pluronic F-127 was not used for future TSQ assays.

(a)



(b)

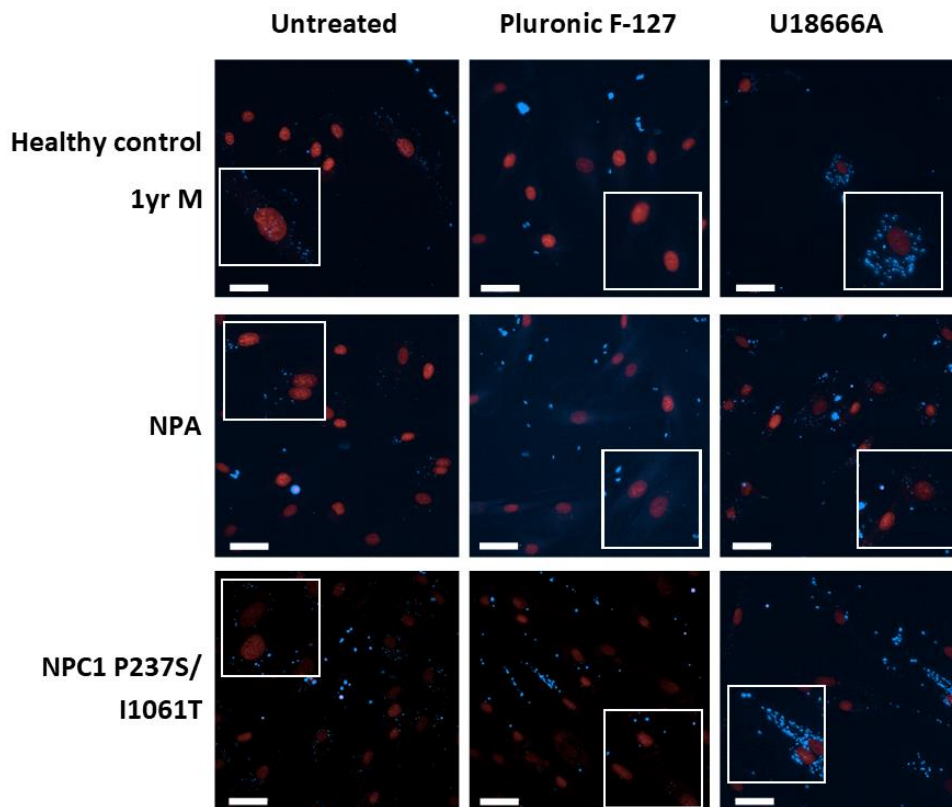


***Figure 4.4. Pluronic F-127 reduces cells with TSQ puncta fluorescence***

*In (a) the percentage of cells with TSQ puncta are shown in three cell lines, when untreated or treated with U18666A. Also shown is a comparison of when untreated cells were probed with TSQ that had been supplemented with Pluronic F-127. All data is n=1. Scale bars represent 50 $\mu$ m.*

### 4.2.3 Zinc storage in Niemann-Pick disease cell lines

Previous data from the Lloyd-Evans laboratory showed that zinc storage is a phenotype of Niemann-Pick disease cells (Maguire 2017). Therefore, TSQ was used to evaluate whether free  $Zn^{2+}$  is elevated in all Niemann-Pick disease cell lines. As we had hypothesised that reducing  $Zn^{2+}$  storage would be beneficial in NPC, we required confirmation of elevated  $Zn^{2+}$  in Niemann-Pick, particularly the NPC1 P237S/I1061T cell line, which was to be used in the screen.

NPA, and both NPC1 cell lines tested had significantly elevated free  $Zn^{2+}$  when compared to two control fibroblasts (*Figure 4.5*). No free zinc storage is observed in the NPB cell line, with  $Zn^{2+}$  puncta being comparable to that of healthy controls. In NPA and NPC disease cell lines, an approximate two-fold increase in the number of puncta was observed.

These findings supported previously produced data from the Lloyd-Evans laboratory and showed that free  $Zn^{2+}$  storage is a phenotype of NPC1 P237S/I1061T cells. Therefore, with a two-fold increase in zinc puncta in NPC1 P237S/I1061T cells over healthy control, there was a suitable signal window in which compounds that reduced free  $Zn^{2+}$  storage in NPC cells could be identified.

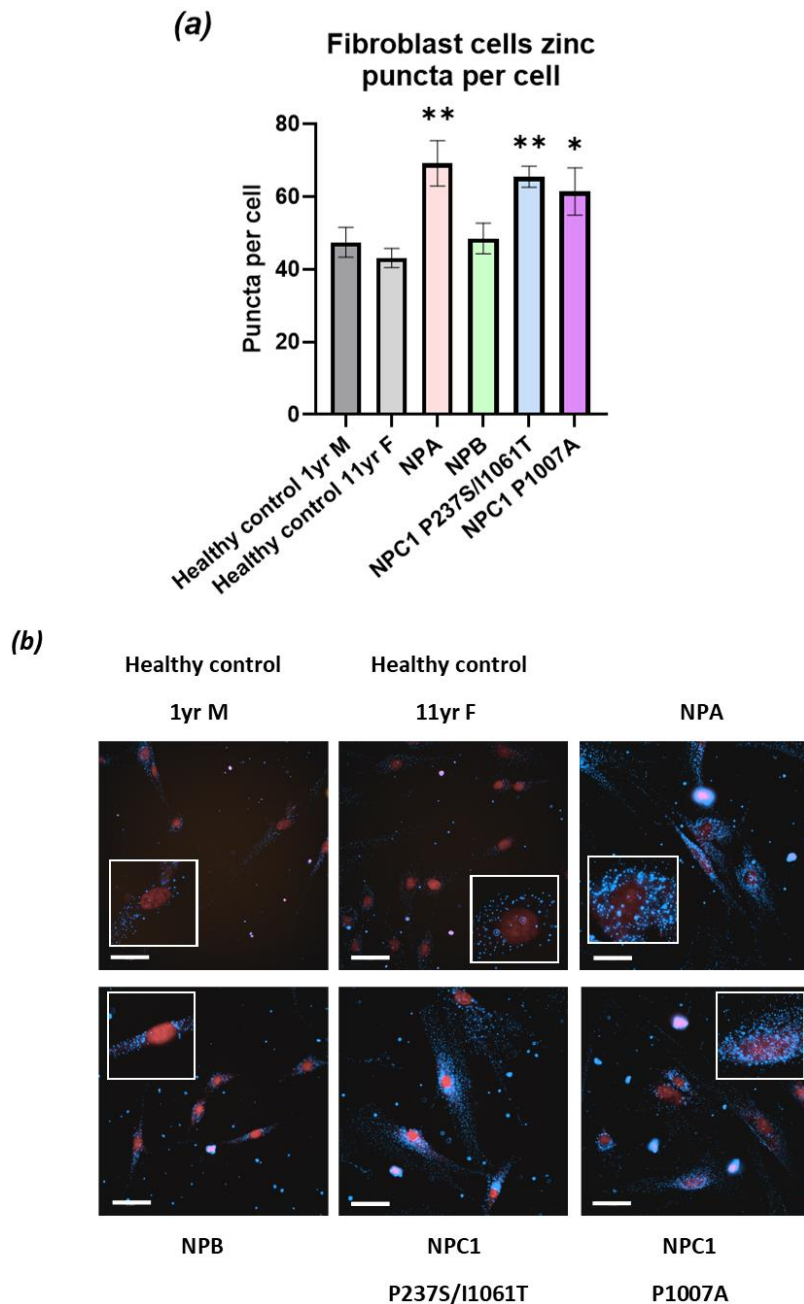


**Figure 4.5. Elevated zinc storage is observed in Niemann-Pick disease cell lines**

In (a) the mean number of puncta per cell is shown, with significance shown when compared to both healthy control cell lines. In (b) reference images for each cell line are shown. Statistical significance was determined using a One-way ANOVA with post hoc Tukey test  $*=p<0.05$ ,  $**=p<0.01$ ,  $***=p<0.001$ ,  $****=p<0.0001$ , data shown is  $n=3$  with error bars being mean  $\pm$  SD. Scale bars represent  $50\mu\text{m}$ .

#### 4.2.4 Plate uniformity testing

Once the Zn<sup>2+</sup> imaging probe had been determined, and the concentration of the probe optimised, the next step was to determine if the probe was suitable for screening. To do this, we wanted to determine if plate patternation would occur if the probe was used, as well as the variability of the probe when analysis was carried out.

Plate uniformity testing was required to ensure that data between wells on a plate was consistent, and that no effects were observed either from the time course or the plate itself used during the assay. Examples of time course effects can include things such as changes in fluorescence (increase or decrease) from the first well to the last well, potentially skewing the data generated. Another potential issue can arise from the layout on the plate and the plate map used. Examples of potential issues from the well layout on the plate includes effects in the edge wells (edge effect), or bleed through from adjacent wells.

From the data in *Figure 4.6*, no discernible plate patternation occurs, with good uniformity across each of the analysis parameters. In two of the analysis parameters to be used in the zinc HTS (puncta per cell & total puncta area) no plate patternation was observed across the plate. Additionally, the data appeared to be precise, with limited variability between wells. No significant variation was observed in the number of cells identified or the percentage of cells with staining, with each both having one two outlier values per plate.

Based on this data, there is no issue with using 100µM TSQ on fixed NPC1 P237S/I1061T cells for a phenotypic screening assay. Therefore, these conditions were taken forward for use in the HTS.

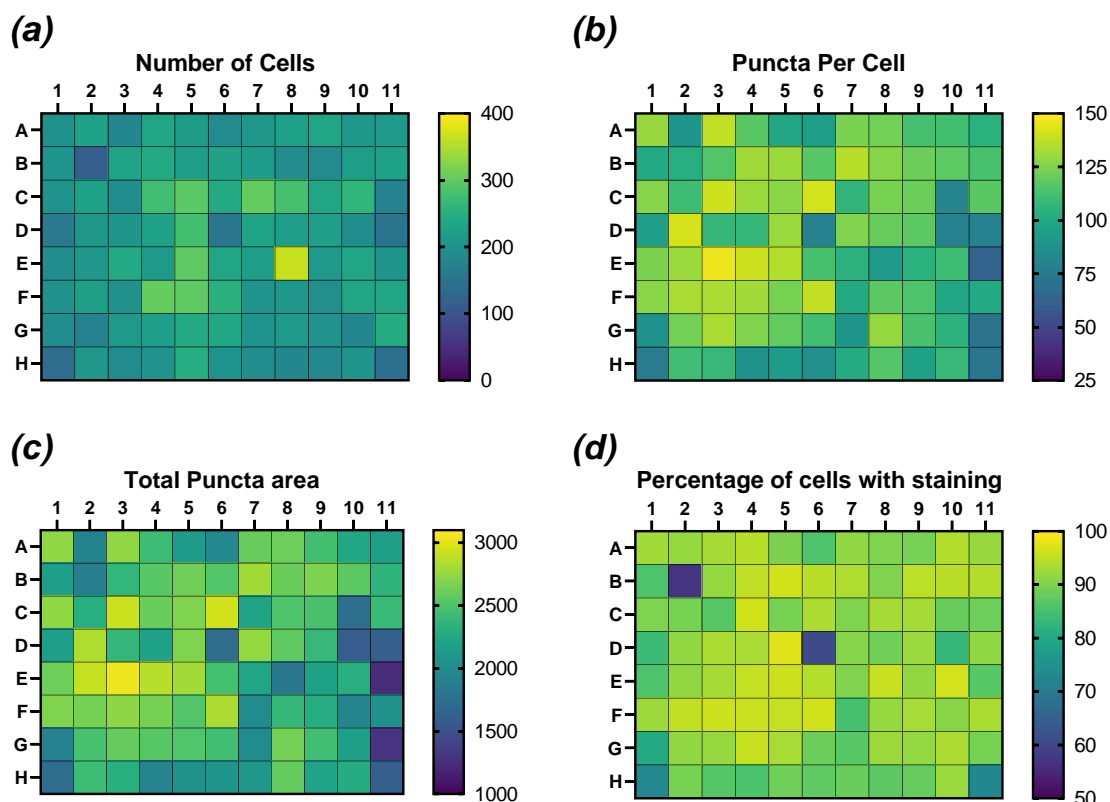


**Figure 4.6. No plate patterning effects are observed with TSQ**

Fixed NPC1 P237S/I1061T fibroblasts were stained with TSQ and imaged using an Operetta CLS to check if plate patterning effects could be observed. Four analysis parameters for the data produced was analysed using Harmony are shown in (a-d). Data is n=1.

#### 4.2.5 DMSO concentration effects on TSQ assay

As the TSQ assay would be used to screen compounds dissolved in DMSO, we assayed the effect of DMSO concentration upon the assay. The maximum concentration planned for the assay was 1%, however a range from 20% to 0.1% was tested.

Concentrations of DMSO over 2% led to significant reductions in both puncta number and in cell viability. Increasing concentrations beyond 2% did not further significantly reduce the number of puncta. However, increasing DMSO concentrations above 2% led to further reductions in cell viability. From this assay, it is clear that 2% DMSO can be tolerated without adverse effects, however concentrations of 1% DMSO or below are preferable.

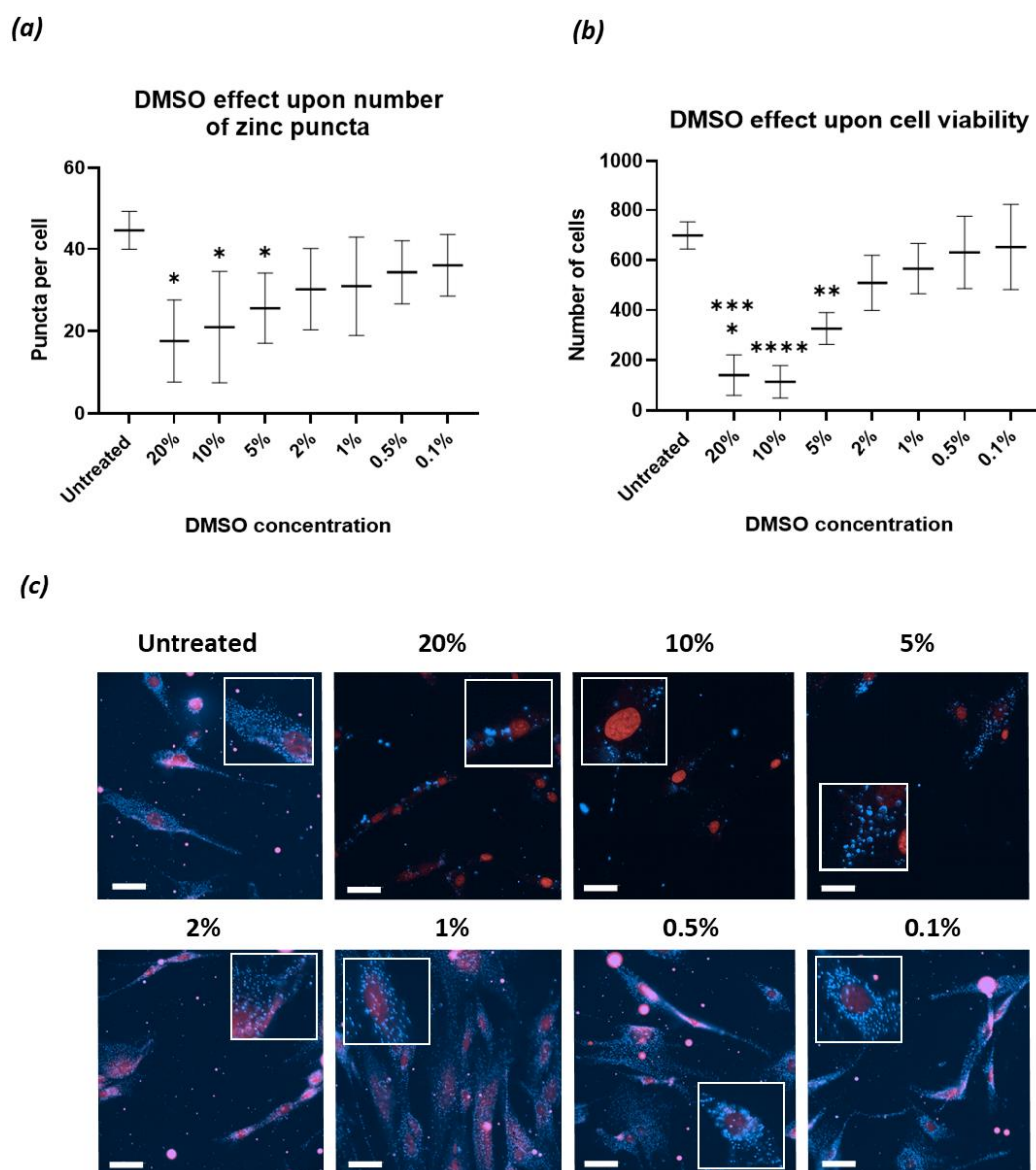


**Figure 4.7. High DMSO concentrations reduce zinc puncta and induce cellular toxicity**

NPC1 P237S/11061T cells were treated overnight with a range of DMSO concentrations from 20% to 0.1% prior to being fixed. In (a) the number of puncta per cell is shown, with corresponding cell number in (b). Representative images are shown in (c). Statistical significance was determined using a One-way ANOVA with post hoc Tukey test  $*=p<0.05$ ,  $**=p<0.01$ ,  $***=p<0.001$ ,  $****=p<0.0001$ , data shown is  $n=3$  with error bars being mean  $\pm$  SD. Scale bars represent  $50\mu\text{m}$

#### 4.2.6 Tool compound identification

To ensure that the data being produced in a HTS is robust, positive and negative controls are required. Thus, tool compounds are required to either increase or decrease free  $\text{Zn}^{2+}$  storage. In this section a range of potential tool compounds are evaluated for their use as either a negative or positive control.

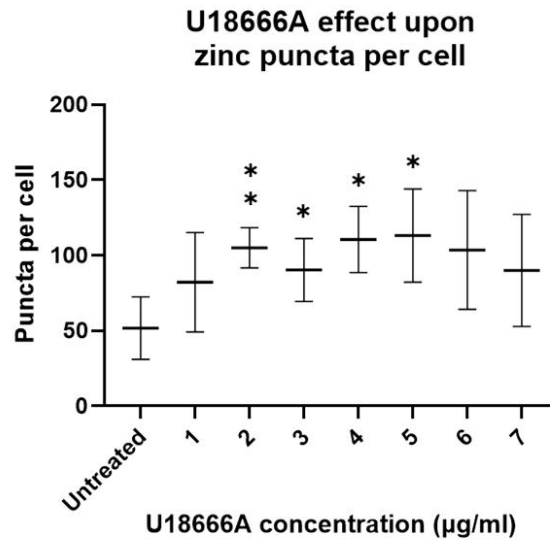
#### 4.2.6.1 U18666A

U18666A can be used to induce an NPC-like phenotype in healthy control cells. We evaluated the effect of U18666A treatment on free Zn<sup>2+</sup> storage in healthy control cells, to assess the molecule as a potential positive control for healthy control cells.

In healthy control cells, U18666A increased free Zn<sup>2+</sup> puncta at all concentrations. At 2µg/ml, over a twofold increase in the number of free Zn<sup>2+</sup> puncta was detected compared to untreated control cells. Further increasing the U18666A concentration did not increase the number of puncta of free zinc further, and beyond 5µg/ml began to induce cellular toxicity.

Based on the data, 2µg/ml U18666A was selected as the concentration to be used. This is consistent with other assays, whereby 2µg/ml U18666A induces an NPC1 like phenotype, with associated cholesterol storage, and increased lysosomal volume. As U18666A inhibits NPC1, the molecule is not suitable for use as a tool compound in NPC disease cells as no effect would be observed. However, U18666A can be used as a positive control for healthy control cells.

(a)



(b)

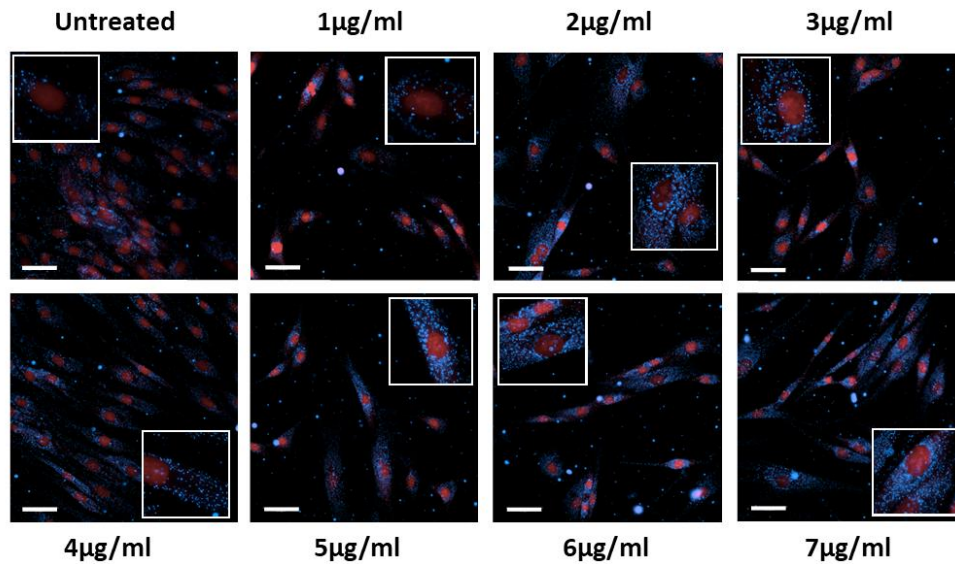


**Figure 4.8. U18666A increases free zinc puncta in healthy control cells**

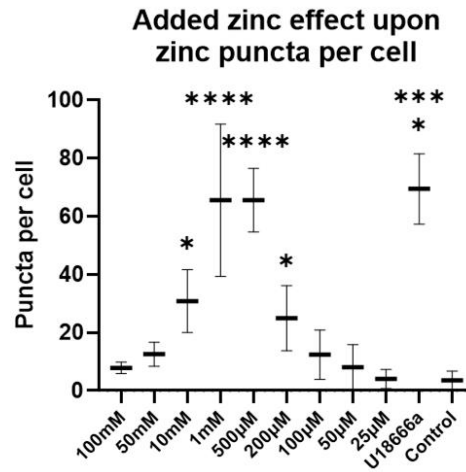
Healthy cells were treated overnight with varying concentrations of U18666A and fixed the next day. Free zinc was visualised using TSQ, with nuclei staining using TO-PRO3. In (a) puncta per cell for each concentration is shown, with representative images in (b). All data is  $n=3$  error bars are mean with standard deviation. Statistical significance was determined using a One-way ANOVA with post hoc Tukey test  $*=p<0.05$ ,  $**=p<0.01$ ,  $***=p<0.001$ ,  $****=p<0.0001$ . Scale bars represent  $50\mu\text{m}$ .

#### 4.2.6.2 Zinc

As we had shown that U18666A could be used to induce free  $Zn^{2+}$  storage in healthy control cells, we needed to identify a suitable positive control for use with the NPC cells, for both further assay development, and as a positive control for the HTS.

From the literature, it appeared that anywhere from 100 $\mu$ M to 1mM zinc chloride induces  $Zn^{2+}$  storage. Therefore, a range of zinc chloride concentrations were tested both above and below this range to ensure that we could detect induced zinc storage. From the data in *Figure 4.9*, it is clear that increasing zinc chloride concentrations up to 1mM leads to increased free  $Zn^{2+}$  storage, and thus TSQ puncta. Beyond 10mM zinc chloride, cellular toxicity is observed, and TSQ staining became diffuse. Based on these observations 500 $\mu$ M zinc chloride was identified as the optimal concentration to be used as a positive control with the NPC cells in the HTS.

(a)



(b)

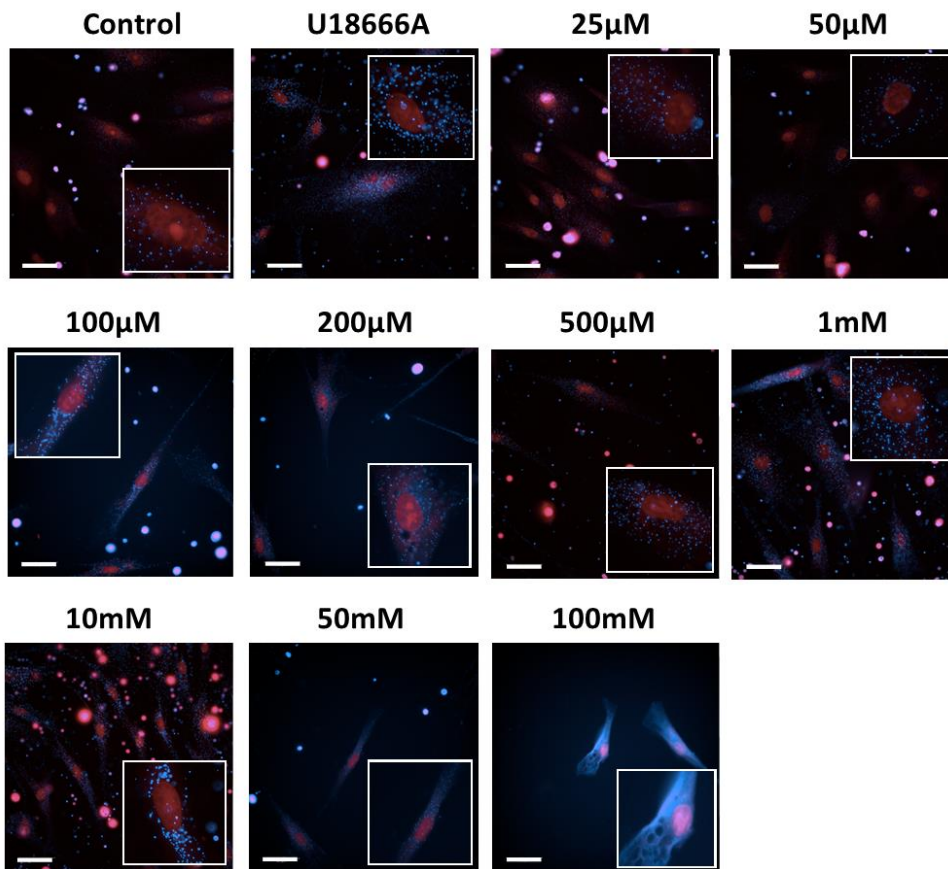


**Figure 4.9. Effect of zinc concentrations upon TSQ puncta**

Healthy control fibroblasts were treated with varying zinc concentrations from 25µM to 200mM, or with U18666A overnight. Free zinc was visualised using 100µM TSQ, with DRAQ5 as a nuclei marker. In (a) the number of puncta per cell for each condition is shown, with corresponding representative images in (b). All data is  $n=3$ , error bars are mean with standard deviation. Statistical significance was determined using a One-way ANOVA with post hoc Tukey test  $*=p<0.05$ ,  $**=p<0.01$ ,  $***=p<0.001$ ,  $****=p<0.0001$ . Scale bars represent 50µm.

#### 4.2.6.3 TPEN

To identify a potential negative control compound, first a metal chelator TPEN was evaluated. TPEN, whilst binding to free  $Zn^{2+}$ , is not  $Zn^{2+}$  specific, and will also chelate other metal ions. Based on the literature, a low micromolar concentration range was selected to test the effects of TPEN upon  $Zn^{2+}$  puncta.

Treating patient derived fibroblasts with TPEN did not significantly affect free  $Zn^{2+}$  puncta in either healthy control or NPC cells. Additionally, cells that were treated with  $10\mu M$  TPEN had over 90% cellular death, so the data was not included in *Figure 4.10*. High cellular toxicity from the ability of TPEN to bind to a range of secondary transition metal ions beyond zinc, is likely the driver of cellular death observed.

Based on these findings, TPEN is not a suitable tool compound for use in a lysosomal zinc modulating assay and was not used in subsequent assays.

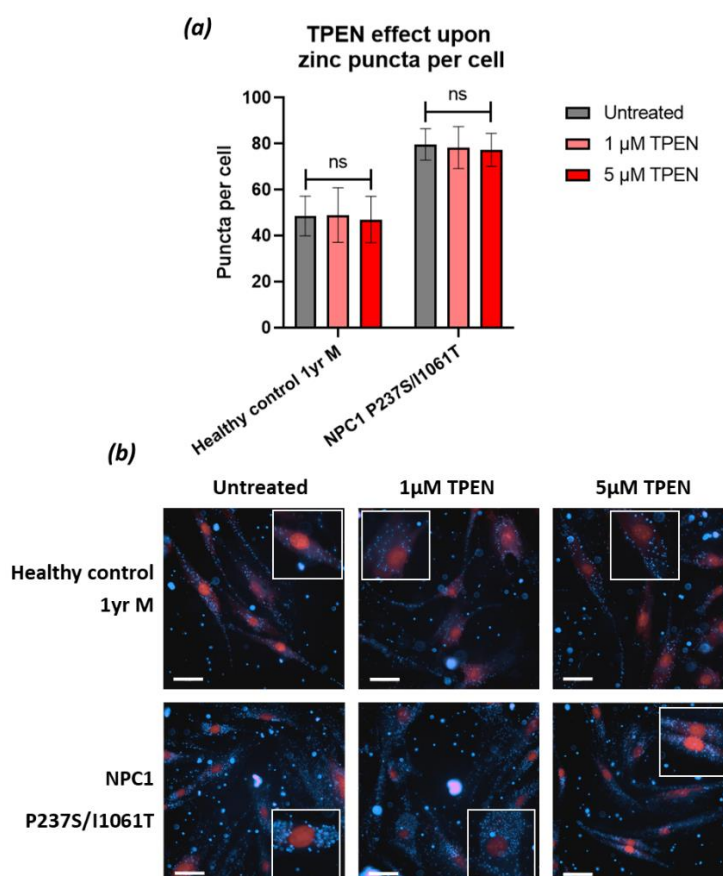


***Figure 4.10. TPEN treatment does not affect intracellular free zinc storage***

*Cells were treated overnight with varying TPEN concentrations prior to fixation. Free zinc puncta were visualised using TSQ, with TO-PRO3 used as a nuclei stain. In (a) mean puncta per cell is shown, with reference images in (b). All data is  $n=3$ , with error bars representing mean with standard deviation. Statistical significance was determined using a One-way ANOVA with post-hoc Tukey test. Scale bars represent  $50\mu m$ .*

### 4.2.7 Imidazole

As TPEN proved unsuitable, we also evaluated another metal chelator imidazole for use as a tool compound to reduce zinc puncta. Unlike TPEN imidazole does not induce cell death at the concentrations tested.

Treating cells with imidazole showed a cell line dependant effect. In the healthy controls, treating with imidazole at any concentration used led to a significant increase in the number of puncta of free  $Zn^{2+}$ . However, in the NPC cells, treating with imidazole did not produce significant changes in puncta of free  $Zn^{2+}$ .

Therefore, imidazole is not suitable for use as a tool compound to reduce  $Zn^{2+}$ , as there was no change in NPC disease cells.

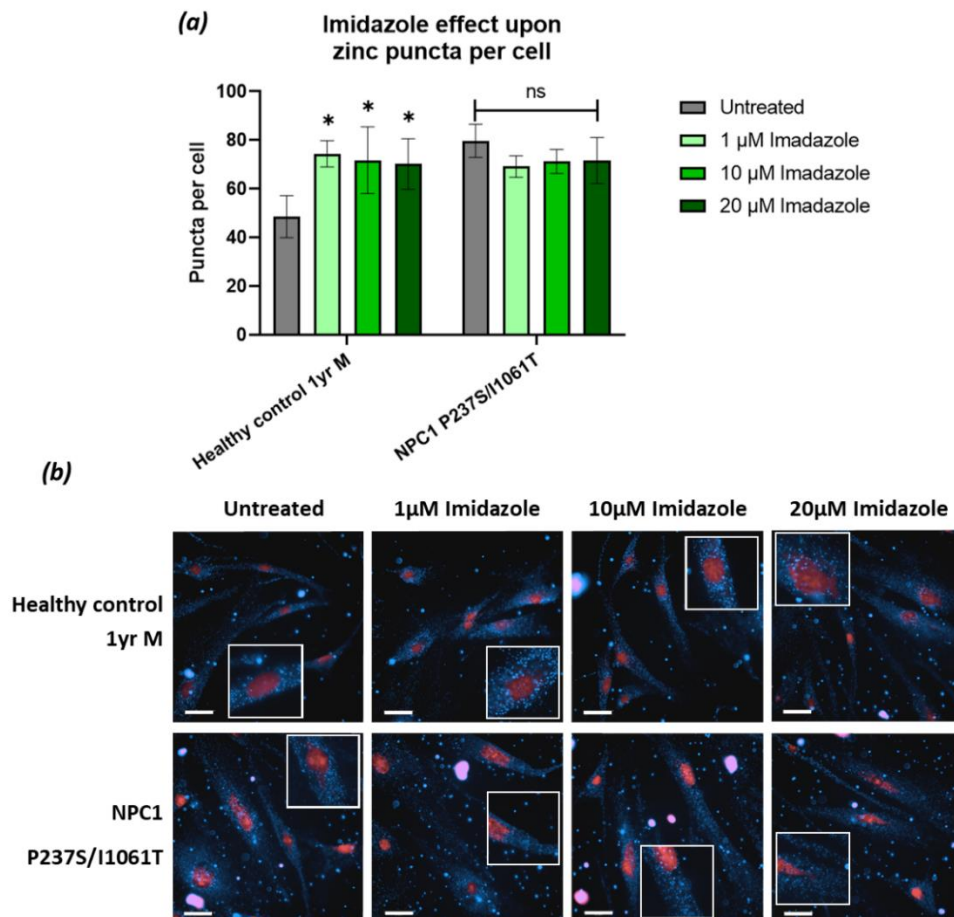


**Figure 4.11. Imidazole increases free zinc puncta in healthy control cells**

Healthy control and NPC1 disease cells were treated with varying concentrations of imidazole overnight prior to being fixed. Free zinc was probed with TSQ. In (a) mean free zinc puncta per cell is shown for two cell lines, with corresponding reference images in (b). Statistical significance was determined using a Two-way ANOVA with post hoc Tukey test  $*=p<0.05$ ,  $**=p<0.01$ ,  $***=p<0.001$ ,  $****=p<0.0001$ , data shown is  $n=3$  with error bars being mean  $\pm$  SD. Scale bars represent  $50\mu\text{m}$ .

#### 4.2.7.1 *Clioquinol*

As no recognised zinc chelator sufficiently reduced free zinc puncta, we evaluated ionophores for use as a potential negative control. Clioquinol is a known zinc ionophore, however high concentrations can also lead to cell death.

Treating both healthy control and NPC cells with clioquinol reduced the number of puncta of free Zn<sup>2+</sup> detected. Both cell lines showed a similar response to clioquinol treatment, with no significant difference between the cell lines when treated. Clioquinol effects appeared consistent irrespective of the concentration used, with a small increase at 10µM, however most concentrations, had approximately 10 puncta per cell. For the healthy control cells this corresponded to a two-fold decrease in puncta number upon treatment, whereas the NPC cells had a six-fold decrease in puncta number.

Therefore, clioquinol is a suitable tool compound, and can be used as a negative control for both healthy control and NPC cells. A concentration of 100µM clioquinol was selected for future assay set up work, and in the HTS.

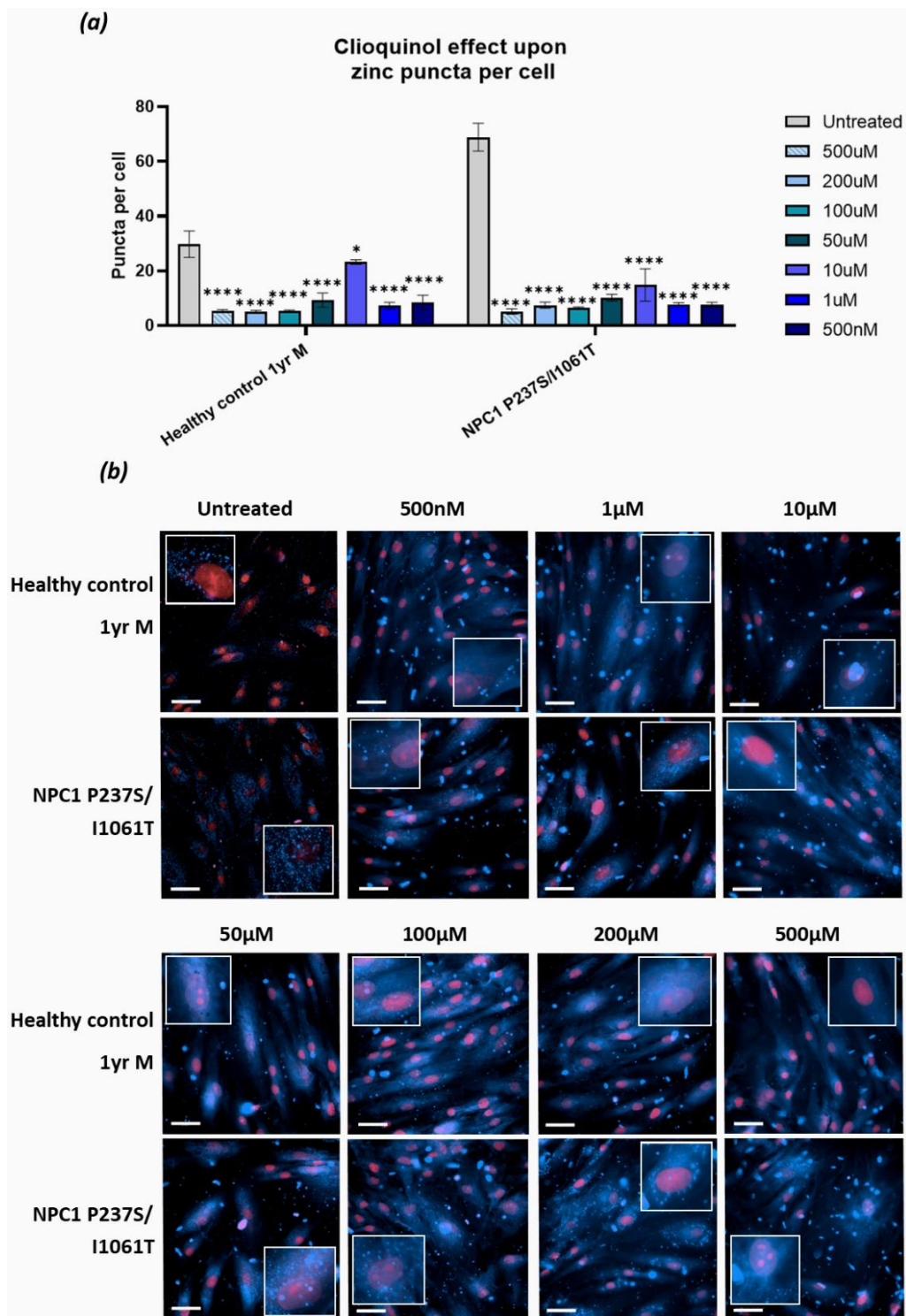


**Figure 4.12. Clioquinol reduces zinc puncta**

Cells were treated with a range of clioquinol concentrations overnight and fixed the following day. Free zinc was imaged using TSQ. Statistical significance was determined using a Two-way ANOVA with post hoc Tukey test  $*=p<0.05$ ,  $**=p<0.01$ ,  $***=p<0.001$ ,  $****=p<0.0001$ , data shown is  $n=3$  with error bars being mean  $\pm$  SD. Scale bars represent  $50\mu\text{m}$ .

#### 4.2.8 *Testing a potential Niemann-Pick therapeutic with zinc modulatory effects*

Phytic acid is naturally occurring in plants; being abundant in grains and seeds. Phytic acid is known to chelate positively charged divalent atoms, primarily: zinc, calcium, and iron.

Previous work within the Lloyd-Evans laboratory identified that phytic acid, a known zinc chelator, reduced lysosomal volume and cholesterol storage in NPC disease cells.

Therefore, we decided to determine if phytic acid reduces free zinc puncta or reduces LBPA, and thus lysosomal volume in patient derived fibroblasts.

##### 4.2.8.1 *TSQ staining*

In both healthy control and NPC disease fibroblasts, at certain concentrations, phytic acid increases the number of zinc puncta. In the healthy control cells, the number of puncta peaks at the mid micromolar range, however in the NPC1 cell line, increasing the phytic acid beyond micromolar concentrations continues to increase the number of zinc puncta.

In Niemann-Pick disease fibroblasts, phytic acid produces a biphasic effect upon total zinc puncta area. Concentrations below 1mM of phytic acid reduces, although not significantly, the total puncta area. Increasing the phytic acid beyond 1mM leads to significant increase in the total zinc staining area within the cell, and thus accumulation of zinc. In the healthy control cells, increasing phytic acid concentration leads to increased total puncta area, with significant increases observed from 1mM to 5mM.

Therefore, despite phytic acid being a zinc chelator, and reducing the free  $Zn^{2+}$ , treatment with phytic acid led to more puncta of zinc being identified. At higher phytic acid concentrations it is probable that the cells are endocytosing zinc to compensate for that chelated with phytic acid. With the increased number of puncta, and total puncta area, it is probable that TSQ can bind to the free  $Zn^{2+}$  that is chelated by phytic acid. This data showed that molecules that can increase the number of puncta or total puncta area of zinc may also be of therapeutic benefit.

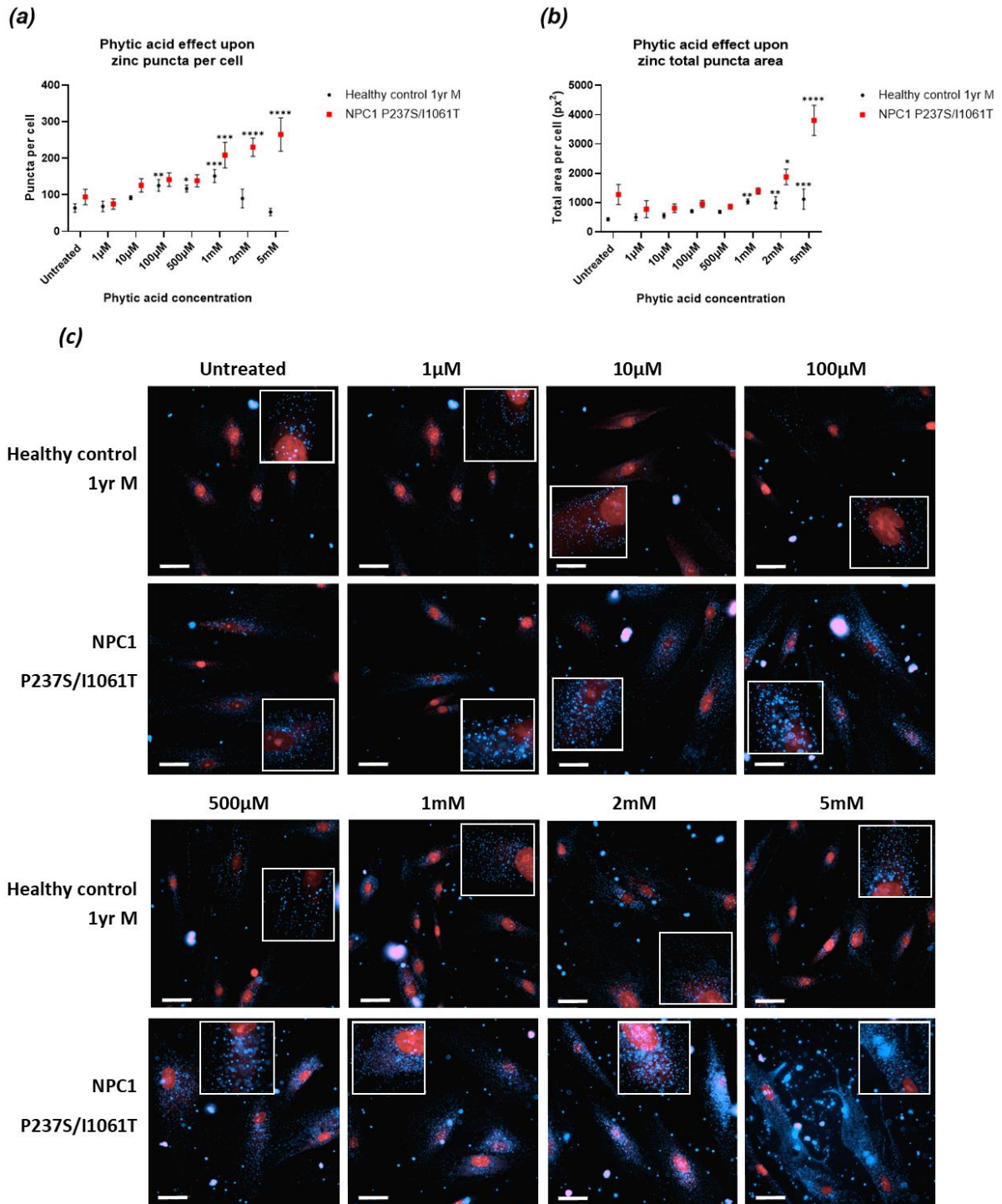


**Figure 4.13. Phytic acid increases intracellular zinc puncta**

Cells were treated with various concentrations of phytic acid for 24 hours, prior to fixation. Free zinc was probed using TSQ, with the number of puncta shown in (a) and the total puncta area per cell in (b). Representative images are shown in (c). Statistical significance was determined using a One-way ANOVA with post hoc Tukey test with each treatment being compared to the corresponding untreated control.  $*=p<0.05$ ,  $**=p<0.01$ ,  $***=p<0.001$ ,  $****=p<0.0001$ , data shown is  $n=3$  with error bars being mean  $\pm$  SD. Scale bars represent  $50\mu\text{m}$ .

#### 4.2.8.2 LBPA staining

As we had seen in 4.2.8.1, that phytic acid modulates zinc puncta *in vitro*, we wanted to determine if these changes in zinc puncta corresponded to changes in lysosome number or total lysosome area. As TSQ staining was carried out on fixed cells, neither LysoTracker nor AQ7 were suitable probes to determine the effects upon cellular lysosomal volume. Instead, to evaluate changes in both number of lysosomes and total lysosomal area, we stained LysoBisphosphatidic acid (LBPA), a phospholipid, which is a major constituent of late endosome and lysosome membranes.

With puncta per cell, concentrations above 1mM of phytic acid led to significant reductions in the number of puncta per cell in the NPC cell line. In control cells, no significant change in the number of puncta of LBPA was observed at any phytic acid concentration.

All concentrations of phytic acid reduced the total LBPA area in the NPC cells, however, only the 1mM-5mM concentrations showed a statistically significant reduction in area. In the healthy control cell lines, no significant change was observed at any concentration, however at higher concentrations (2mM-5mM) there is a trend of increasing LBPA area per cell.

This data shows that phytic acid is reducing LBPA, and thus lysosome number and total lysosomal area per cell in Niemann-Pick disease fibroblasts. No change is observed in the healthy control cells, suggesting that phytic acid is reducing lipid storage, likely through reducing free  $Zn^{2+}$ .

Of note is how LBPA and TSQ staining data shows opposing results. High phytic acid concentrations lead to increased TSQ and thus zinc staining, however these concentrations also lead to a reduction in LBPA, and thus lysosomal area in the NPC fibroblasts.

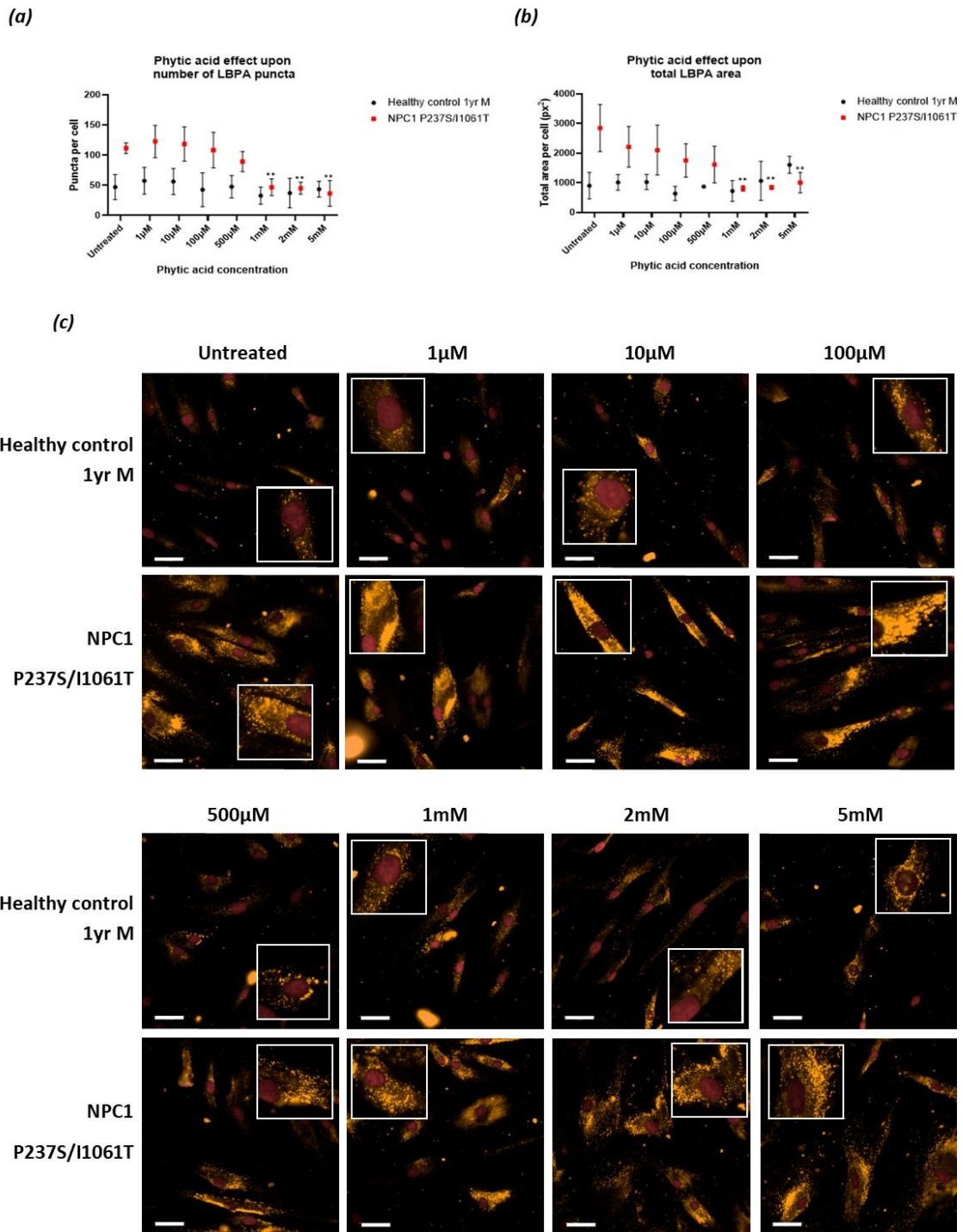


**Figure 4.14. Phytic acid reduces LBPA staining in Niemann-Pick disease**

Analysis of LBPA accumulation was carried out on cells that had been treated with various concentrations of phytic acid for 24 hours, prior to fixation. An LBPA specific antibody was used, with a corresponding species specific Alexaflour 568 conjugated second antibody. The mean number of puncta of LBPA is shown in (a) and the total puncta area per cell in (b). Representative images are shown in (c). Statistical significance was determined using a One-way ANOVA with post hoc Tukey test with each treatment being compared to the corresponding untreated control.  $*=p<0.05$ ,  $**=p<0.01$ ,  $***=p<0.001$ ,  $****=p<0.0001$ , data shown is  $n=3$  with error bars being mean  $\pm$  SD. Scale bars represent  $50\mu\text{m}$ .

#### 4.2.9 *Testing HDAC inhibitors with known benefit in Niemann-Pick cells in vitro*

Several HDAC inhibitors have been trialled in Niemann-Pick disease, however none has been granted FDA approval for use. As well as working as primarily being HDAC inhibitors, some HDAC inhibitors, also possess a region within their structure with the ability to chelate metal ions. Two HDAC inhibitors were tested, vorinostat, which underwent clinical trial in Niemann-Pick, and panobinostat, a molecule which has been suggested as a potential therapeutic in Niemann-Pick.

##### 4.2.9.1 *NPC1 P237S/I1061T*

###### 4.2.9.1.1 Zinc storage

Both panobinostat and vorinostat showed similar effects upon the number of zinc puncta. Vorinostat significantly reduced the number of zinc puncta at concentrations below 2.5 $\mu$ M, and panobinostat significantly reduced zinc puncta at concentrations below 10 $\mu$ M. Neither molecule significantly effected zinc puncta at 20 $\mu$ M.

A similar pattern was observed with the total puncta area per cell with both molecules significantly reducing the total zinc puncta area at concentrations below 1 $\mu$ M. Both molecules had very similar effects upon the total zinc puncta area per cell, with no significant differences between either molecule at any concentration.

This data clearly shows that both panobinostat and vorinostat are leading to modulation of intracellular zinc storage in NPC1 P237S/I1061T, surprisingly lower concentrations of both molecules led to more significant decreases in zinc puncta. Both molecules show similar effects at the same concentrations, with no significant differences between molecules at any concentration for either analysis parameter used.

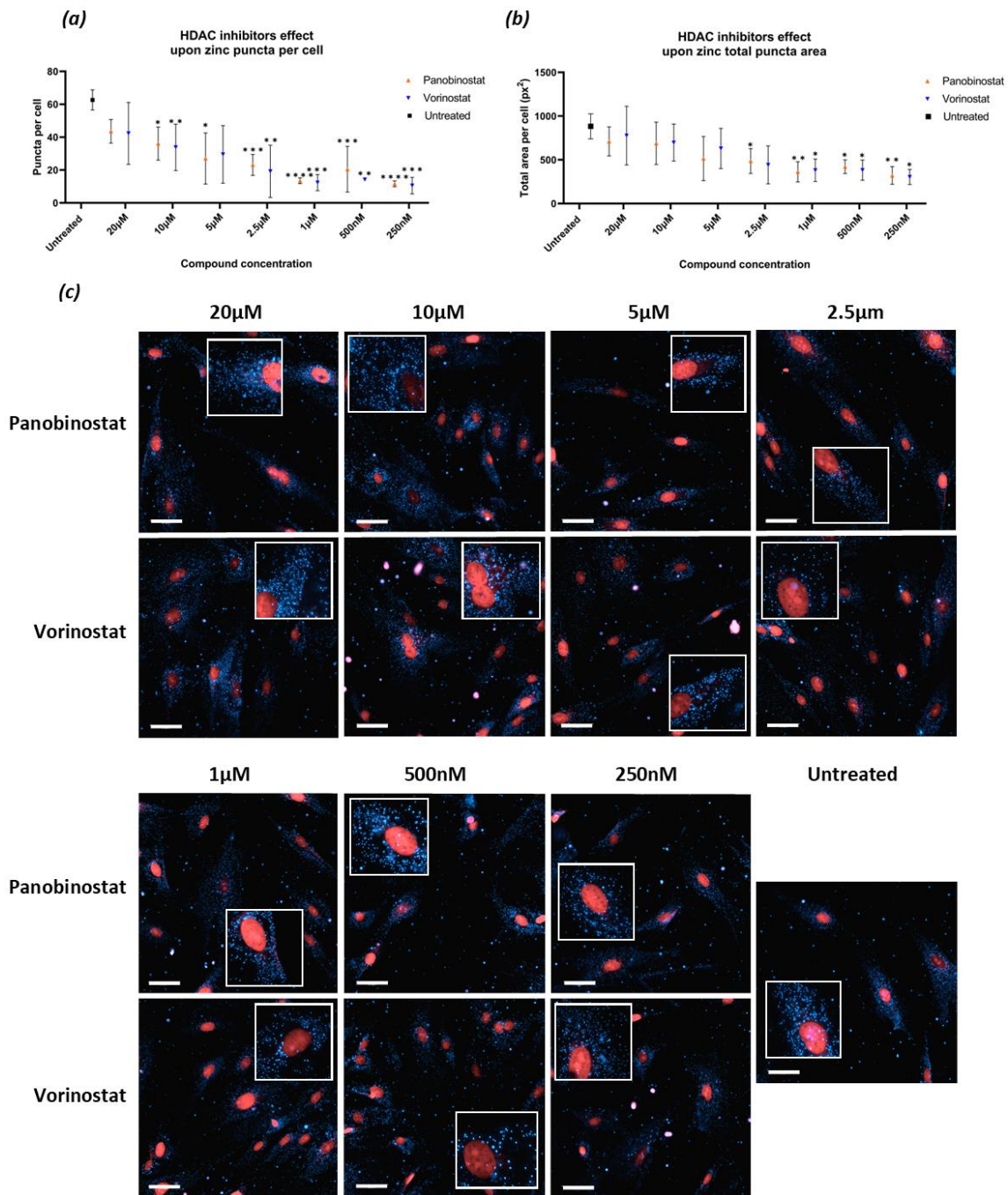


**Figure 4.15. Zinc puncta are reduced upon HDAC inhibitor treatment in classical NPC fibroblasts**  
 Analysis of the effects of HDAC inhibitors in NPC1 P237S/I1061T cells upon zinc puncta. Cells were treated with a range of panobinostat or vorinostat concentrations for 24 hours prior to fixation. Zinc puncta was probed with TSQ. The mean number of puncta of zinc is shown in (a) and the total puncta area per cell in (b). Representative images are shown in (c). Statistical significance was determined using a One-way ANOVA with post hoc Tukey test with each treatment being compared to the corresponding untreated control. \*= $p < 0.05$ , \*\*= $p < 0.01$ , \*\*\*= $p < 0.001$ , \*\*\*\*= $p < 0.0001$ , data shown is  $n=3$  with error bars being mean  $\pm$  SD. Scale bars represent 50µm.

## 4.2.10 Zinc modulator screening

### 4.2.10.1 TSQ Screen

The DiscoveryProbe™ compound library from APExBio was used for screening, with all compounds being FDA approved. This library contains 1499 compounds, covering a range of targets, including kinases and a range of receptor types.

The NPC1 P237/I1061T mutant cell line was selected as this cell line has a mutation in both alleles, with the I1061T mutation also being the most common single mutation in NPC. We had also demonstrated in 4.2.2.1 that the NPC1 P237S/I1061T line had zinc storage, approximately 50% greater when compared to healthy control cell lines.

As we had identified previously, ZnCl<sub>2</sub> can be used to induce additional zinc storage and was used as a positive control, with clioquinol being used as a negative control on each plate. Four wells of untreated cells were used to calculate the fold change in the analysis parameters used. All compounds were used at 10µM concentration and treated for 24 hours.

To identify hits, three analysis parameters were used, the first was the TSQ puncta fluorescence intensity, also used were the number of puncta identified and the total zinc puncta area per cell. Compounds that were either able to reduce the zinc storage or led to increased zinc storage were to be selected for further analysis. In addition to selecting compounds that reduced zinc storage, we also identified compounds that increased zinc storage as we had seen that phytic acid, whilst reducing lysosomal volume, increased zinc puncta.

For each plate, the Z' score was recorded with the plates having Z' scores ranging from 0.39 to 0.61, which are within the tolerated range for screening plates and assays.

For each analysis parameter, the top 100 hits that increased or decreased each of the analysis parameter were identified; approximately 250 each for reduction of zinc and increase of zinc. Any compound that ranked in the top 100 for two or more analysis parameters was selected to be screened further to determine if the molecule could improve lysosomal storage in NPC1 P237S/I1061T fibroblasts. The remaining compounds were selected by being the highest ranked compounds in a single analysis parameter; this was

carried out until 80 compounds that increased zinc and 80 that reduced zinc had been identified.

From the screen, 33 compounds induced severe toxicity, with a 10-fold decrease in cell viability. A further 200 compounds showed a 2-fold decrease in cell viability. Compounds showing high cellular toxicity were discounted and were not selected for further analysis.

Only minor changes were observed in puncta fluorescence intensity, with only two compounds having a two-fold or greater increase in puncta fluorescence brightness. No compound tested led to a two-fold decrease in fluorescence intensity, with the strongest effect being a 1.9-fold decrease.

When analysing number of zinc puncta, one compound led to a 20-fold reduction in puncta of zinc (lenalidomide). A further 25 compounds led to a 10-fold or greater decrease in zinc puncta, with a further 100 compounds having at least a 5-fold decrease in zinc puncta per cell. Three compounds tested led to at least a four-fold increase in zinc puncta number: clobetasol propionate, dyclonine, and dipyrindamole. An additional 51 compounds that were tested, showed at least a 2-fold increase in the number of zinc puncta per cell.

Larger differences were observed when analysing the total zinc puncta area per cell. Five compounds led to at least a five-fold increase in total zinc puncta area: romidepsin, elacridar, ponatinib, ispinesib, and ABT-787. A further 50 compounds led to at least a 2-fold increase in the total zinc puncta area per cell. Seven compounds, including lenalidomide, had at least an 8-fold decrease in the total zinc puncta area per cell. Over 100 compounds showed at least a two-fold decrease in the total zinc puncta area per cell.

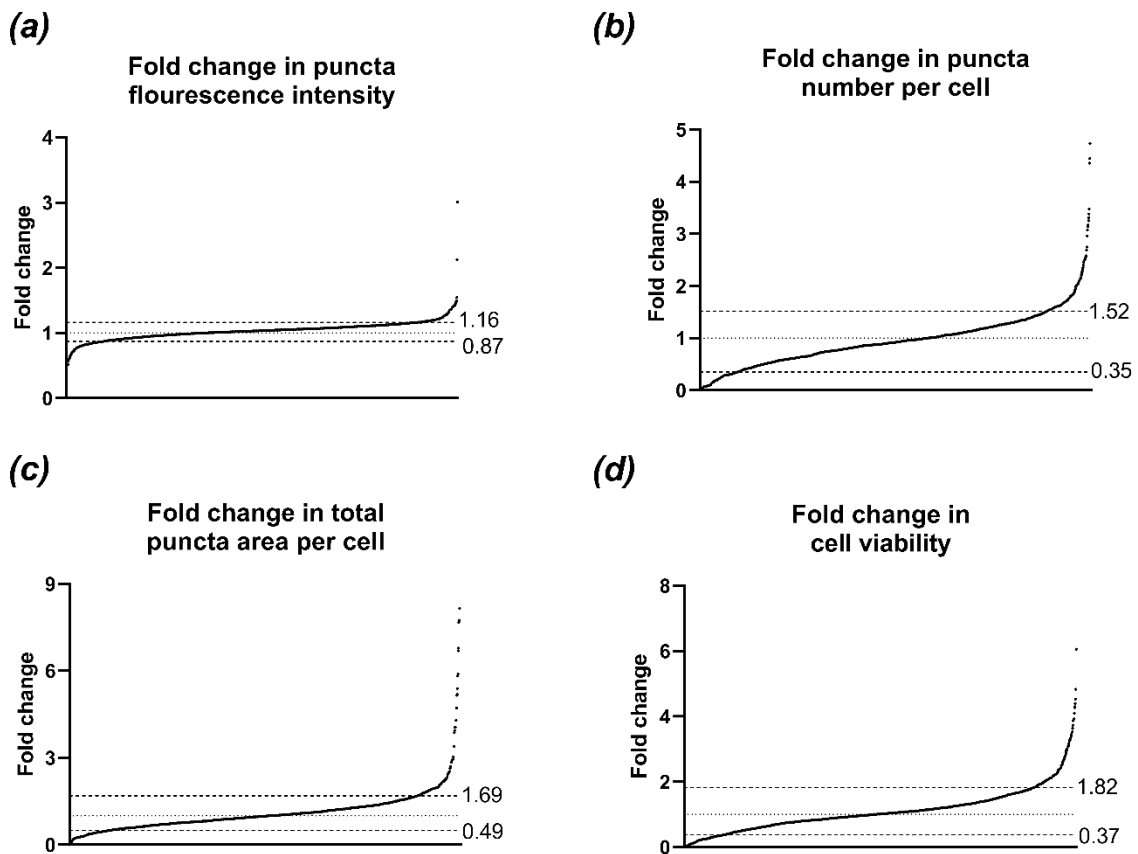


***Figure 4.16. Compound library effects upon zinc in NPC1 P237S/1061T fibroblasts***

1499 compounds were screened using TSQ assay in NPC1 P237S/1061T cells. Positive controls were 200 $\mu$ M ZnCl<sub>2</sub> and a negative control was 100 $\mu$ M clioquinol. Fold change was calculated against untreated NPC1 P237S/1061T cells. Dotted line on graph represents the one-fold change, with the dashed lines representing the top 5% and bottom 5% of compounds, with the numbers corresponding to the fold change. All data is n=1.

#### 4.2.11 *Hit screening*

Once hits that modulated zinc storage had been identified, we needed to determine if they had any effect upon the disease phenotype. To do this, LysoTracker Deep Red was used to visualise lysosomal storage and to determine if any compounds reduced lysosomal volume in NPC P237S/I1061T cells.

##### 4.2.11.1 *Zinc raising compounds*

80 compounds that showed the greatest effect in raising intracellular zinc were taken forward for further evaluation. These were screened using LysoTracker Deep Red to determine the effect upon lysosomal volume. For analysis, four parameters were determined, however, to evaluate the efficacy of each molecule only total puncta area was used.

12 compounds led to at least 0.1-fold increase in total LysoTracker staining area, however 34 compounds showed between a 0.1-fold and 0.2-fold decrease in total LysoTracker staining area. A further 6 compounds showed a 0.3-fold to-0.4-fold decrease in total LysoTracker area, with the compound showing the largest decrease, 0.39-fold, being nintedanib.

Despite removing compounds that showed toxicity in the initial zinc screening assay, of the 80 compounds tested 48 showed a 0.1-fold decrease in cell viability, compared to the untreated controls.

From this data the top 10 hits that most reduced LysoTracker Deep Red staining, without inducing cellular toxicity were identified.

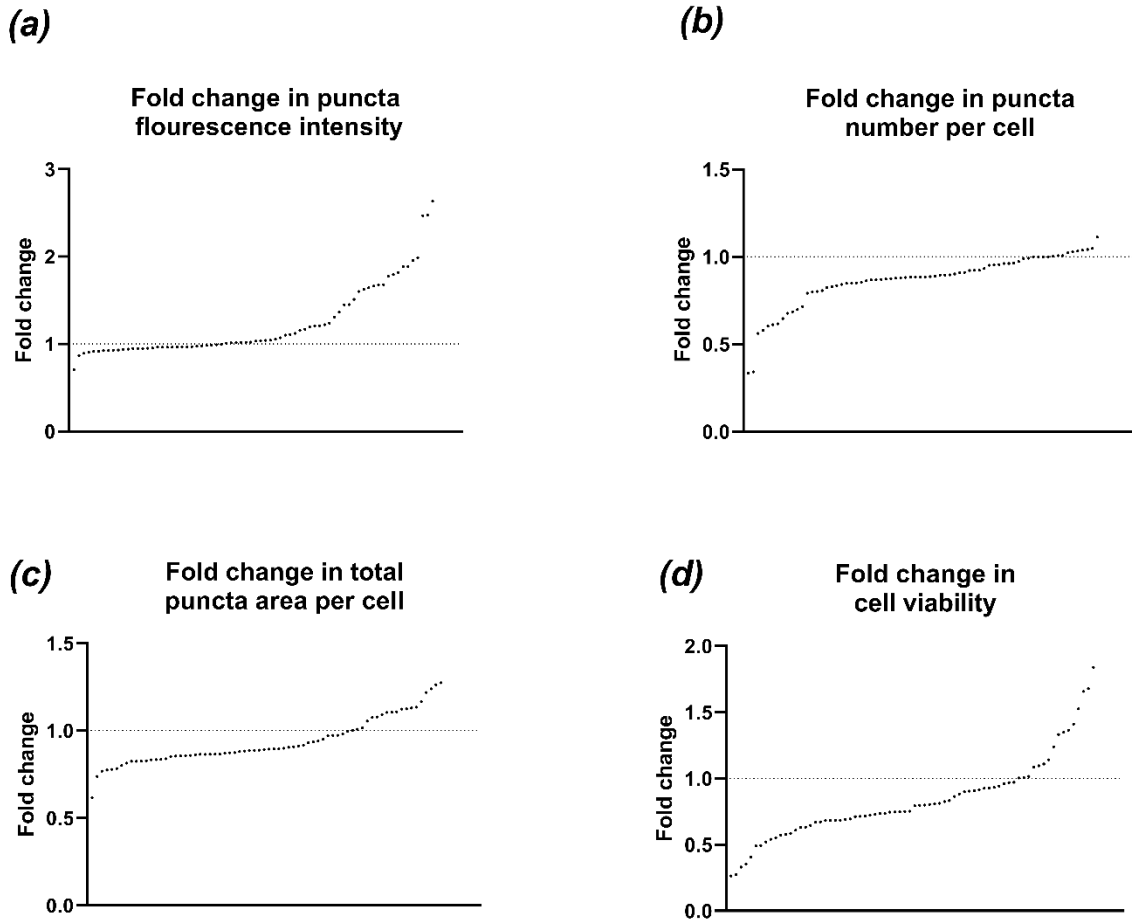


**Figure 4.17. Effect of zinc raising compounds upon LysoTracker Deep Red fluorescence in NPC1 cells**  
 Compounds shown to increase intracellular zinc were screened to determine effects upon lysosomal volume. NPC1 P237S/I1061T cells were treated with compound at 10 $\mu$ M overnight. Cells were then probed with LysoTracker Deep Red. Data plotted is mean, with fold change being calculated using untreated cells. All data is n=3.

#### *4.2.11.2 Zinc lowering compounds*

The 80 compounds that showed the greatest reduction in intracellular zinc were secondary screened with LysoTracker Deep Red to identify any molecules reducing lysosomal volume.

Only 10 compounds led to a reduction in LysoTracker fluorescence, and only 4 of these was the fold change less than 0.1, with the highest being clofazimine which showed a 0.45-fold decrease. Of note was that 36 out of the 80 compounds led to at least 0.2-fold in puncta fluorescence.

17 compounds tested showed at least a 0.1-fold increase in the number of puncta of LysoTracker, however this is compared to the 32 compounds that reduced the puncta number by 0.1-fold or more. 21 of these compounds led to an at least 0.2-fold decrease and 12 at least a 0.4-fold decrease in number of puncta.

When analysing total puncta area, 20 compounds led to at least a 0.1-fold decrease in total puncta area. Of these compounds 4 led to at least a 0.4-fold decrease, with the largest decrease being observed with doxofylline treatment.

Of the zinc lowering compounds 33 led to a reduction of 0.5-fold in cell viability when compared to the untreated control. A further 15 compounds saw an increase in cell viability over 0.1-fold, with 7 compounds having at least a 2-fold increase.

From this data the top 10 hits that most reduced LysoTracker Deep Red total puncta area, without inducing cellular toxicity were identified.

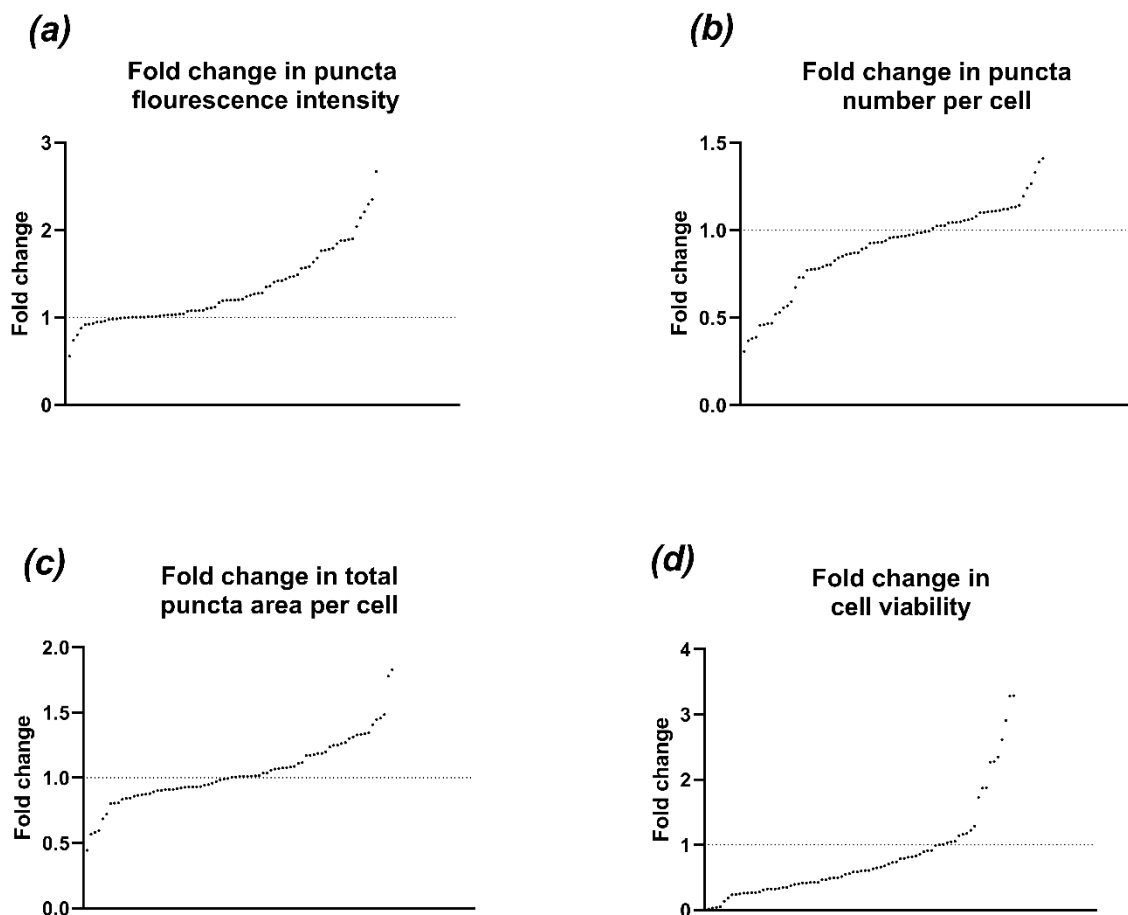


**Figure 4.18. Effects of zinc lowering compounds upon LysoTracker Deep Red fluorescence in NPC1 cells.**

Compounds shown to reduce intracellular zinc were screened to determine effects upon lysosomal volume. NPC1 P237S/I1061T cells were treated with compound at 10 $\mu$ M overnight. Cells were then probed with LysoTracker Deep Red. Data plotted is mean, with fold change being calculated using untreated cells. All data is n=3.

## 4.2.12 Hit analysis

### 4.2.12.1 Zinc raising compounds

**Table 4.1. Compounds that increased zinc storage and reduced lysosomal volume**

<b>Name</b>	<b>Target</b>	<b>Previous link to Niemann-Pick</b>	<b>Effect on free zinc area</b>	<b>Effect on lysosomal area</b>
Nintedanib	VEGFR/PDGFR/FGFR inhibitor	X	+95%	-39%
Doxorubicin	Topo II inhibitor (Antibiotic)	X	+30%	-27%
Azaguanine-8	Purine analog (Antineoplastic)	X	+79%	-24%
Chlormethine	DNA synthesis inhibitor (Antineoplastic)	X	+74% in puncta No.	-22%
Dipyridamole	PDE inhibitor	Yes	+340%	-22%
Brexpiprazole	5-HT <sub>2A</sub> , $\alpha$ 1B/ $\alpha$ 2C receptor antagonist	X	+97%	-21%
Letrozole	Non-steroidal aromatase inhibitor	X	+15% in fluorescence intensity	-20%
Clobetasol propionate	Glucocorticoid receptor agonist	X	+63%	-19%
Pancuronium dibromide	AChR antagonist	X	+77% in puncta No.	-17%
Triamcinolone	Anti-inflammatory steroid	X	+43%	-17%

Of the 10 compounds identified that raised zinc storage, but reduced lysosomal volume, only dipyridamole has been directly linked to beneficial effects in Niemann-Pick. It is believed that dipyridamole leads to activation of the adenosine A<sub>2A</sub>R receptor subtype after the increased levels of extracellular adenosine due to the inhibition of ENT1. This in turn leads to significantly reduced cholesterol storage and reduced mitochondrial defects (Pepponi et al. 2022). However, it is unclear what cellular pathway changes are leading to significant increases in zinc staining area upon treatment, as this is unlikely to be driven solely by ENT1 inhibition.

The other hits identified cover a broad range of targets, however it is of note that three of the molecules are steroidal, being: clobetasol propionate, pancuronium dibromide, and triamcinolone. One hit compound that is likely to not see further work is chlormethine, as

this molecule is part of the mustard gas family and would not be able to undergo series development.

#### 4.2.12.2 Zinc lowering compounds

**Table 4.2. Compounds that reduced zinc storage and reduced lysosomal volume**

<b>Name</b>	<b>Target</b>	<b>Previous link to Niemann-Pick</b>	<b>Effect on free zinc area</b>	<b>Effect on lysosomal area</b>
Doxofylline	PDE inhibitor	X	-78%	-45%
Clofazimine	Tuberculosis drug	X	-85%	-42%
Proadifen (SKF 525)	Cytochrome P (CYP)450 inhibitor	X	-29%	-41%
Nilotinib	Bcr-Abl kinase inhibitor	Yes	-90% in puncta No.	-28%
Pelitinib (EKB-569)	EGFR inhibitor	X	-32%	-19%
Bazedoxifene acetate	Estrogen receptor modulator	X	-95% in puncta No.	-19%
Bivalirudin Trifluoroacetate	Thrombin inhibitor	X	-65%	-19%
Methazolamide	Carbonic anhydrase inhibitor	X	-37%	-17%
Sulfaphenazole	CYP2C9 inhibitor	X	-56%	-13%
Macitentan	Endothelin receptor antagonist	X	-59%	-13%

The 10 hit compounds that both reduced zinc storage and reduced LysoTracker staining area cover a wide range of therapeutic uses. Some of the hits in *Table 4.2*, despite affecting zinc storage differently share similar targets to the hits identified in *Table 4.2*, including kinases and PDE.

One molecule, nilotinib has been linked to Niemann-Pick disease use. Nilotinib is a kinase inhibitor that targets c-Abl, which is linked to lysosomal and autophagy defects (Contreras et al. 2020).

Long term treatment *In vivo* with nilotinib has been shown to improve autophagy, likely driven through upregulation of nuclear localisation of TFEB driven by c-ABL inhibition. The

increased nuclear localisation of TFEB leads to upregulation in gene transcription and increased lysosomal biogenesis through the CLEAR pathway. Niemann-Pick disease mice treated with nilotinib have an increased life span and take longer to initiate neurodegeneration (Marín et al. 2022).

Of note, as also observed in *Table 4.1*, several of the molecule identified and included in *Table 4.2* are steroidal and are thus likely affecting intracellular cholesterol homeostasis.

## ***4.3 Discussion***

### ***4.3.1 Aims of chapter***

The aims covered in this chapter were to develop an imaging-based zinc assay suitable for screening. Once a zinc screening assay was developed, it was to be used to screen a compound library.

#### ***4.3.1.1 Identify a suitable zinc imaging probe for live or fixed cell imaging***

The first aim of the chapter was to identify a suitable zinc probe. Three probes were trialed: Zinquin, Flou-Zin 3 and TSQ. Of these only TSQ was shown to be able to distinguish between untreated and zinc treated cells. Therefore, TSQ was selected as the zinc probe to be used.

#### ***4.3.1.2 Optimise zinc probe concentration, and determine if live or fixed cells are to be used***

Experiments on fixed cells showed that at 100µM TSQ there was an observable difference between healthy control and NPC P237S/I1061T cells. However, when cells were imaged with TSQ it was clear that the probe was either quenching or dissociating from the free Zn<sup>2+</sup> leading to loss of ability to visualise zinc puncta. This occurred in both live and fixed cells and was only alleviated through leaving TSQ on the cells for the duration of imaging. Fixed cells appeared to be less prone to TSQ quenching, and the decrease observed when TSQ was removed was more gradual, and therefore fixed cells were to be used.

#### ***4.3.1.3 Identify tool compounds that increase and decrease zinc storage***

We needed to find two molecules, the first was one that led to increased zinc storage and could be used as a positive control, and the second, a compound that reduced the zinc puncta and could be used as a negative control. A positive control was identified in ZnCl<sub>2</sub>, which produced a concentration dependant increase in zinc puncta. From the data 500µM zinc was selected as a positive control and was used on all screening plates. Identification of a negative control proved more challenging, as metal chelators tested did not decrease the

number of zinc puncta, instead some metal chelators increased the number of zinc puncta. However, clioquinol, an ionophore, led to a significant decrease in the number of zinc puncta. From the data produced, 100µM clioquinol was identified as the concentration to be used as a negative control for screening.

#### *4.3.1.4 Test assay to determine if the assay can identify known zinc modulators*

Using phytic acid we were able to detect cell line-specific changes in zinc puncta. However, upon phytic acid treatment, particularly in the NPC1 P237S/I1061T cells, the number of zinc puncta increased significantly, suggesting that the assay could detect chelated zinc as well as free Zn<sup>2+</sup>. We also evaluated two molecules that have shown therapeutic benefit in Niemann-Pick disease, panobinostat and vorinostat, which may also have zinc chelating properties. Both panobinostat and vorinostat showed concentration dependant reductions in zinc puncta in NPC1 P237S/I1061T.

#### *4.3.1.5 Screen a compound library with NPC cells to identify hit compounds*

As we had shown that the assay was sensitive enough to detect modulation of intracellular zinc with known modulators, the assay was deemed to be robust enough for compound screening, with a Z' score of 0.48 when a trial plate was run. The Discovery Probe™ library was used, which contained approximately 1,500 compounds, of which all were clinically approved molecules, with most being molecules no longer covered by patents. The library included molecules that covered a range of targets, including kinases, antibiotics and HDAC inhibitors.

Compounds were all screened at 10µM, in NPC1 P237S/I1061T fibroblasts. Each plate comprised 80 compounds, 4 wells of untreated cells, 2 wells of positive control (ZnCl<sub>2</sub>) and 2 wells of a negative control (clioquinol). Effectiveness of a molecule was determined through identifying hit molecules effect upon puncta fluorescence intensity, the number of puncta and the total puncta area. To determine the efficacy of a molecule the fold change was calculated in each analysis parameter when compared to the untreated controls. Compounds that showed high toxicity, identified by a reduction in the number of cells detected, were also identified, and excluded from being taken forward.

The 80 compounds that increased zinc storage the most and the 80 compounds that led to the largest reduction in zinc were selected for further investigation. The compounds

covered a range of targets and had a broad range of chemical structures, however several molecules clustered together, including PDE inhibitors and steroid-like molecules.

#### **4.3.1.6 *Test hit compounds in a LysoTracker based assay to identify if molecules decrease lysosomal storage.***

The 80 hit molecules that either increased or decreased zinc the most were triaged using LysoTracker Deep Red in NPC1 P2237S/I1061T cells to determine the effects upon lysosomal volume. To determine the effectiveness of a compound, the fold change in total puncta area was analysed, determined through comparing to untreated control NPC1 P237/I1061T. The top 10 compounds for compounds that increased and decreased zinc were identified. Of these 20 compounds, 2 have been shown benefit *in vitro* for treating Niemann-Pick disease, therefore it is likely that the other 18 molecules identified do have disease improving effects, and that some could be potential chemical starting point for the creation of chemical series.

### **4.3.2 *Analysis of hit compounds***

Of the 20 hit compounds, 2 have been shown to be beneficial to Niemann-Pick disease *in vitro*, with 18 having no currently published direct link to Niemann Pick. Some of the molecules with potential mechanisms of actions in Niemann-Pick are discussed below:

#### **4.3.2.1 *Dipyridamole***

Dipyridamole activates the adenosine A<sub>2A</sub>R receptor, a known therapeutic target in Niemann-Pick disease. Dipyridamole significantly reduced cholesterol accumulation in Niemann-Pick Type C fibroblasts and reversed mitochondrial deficits (Pepponi et al. 2022). Dipyridamole is linked to the activation of the adenosine receptors due to the inhibition of ENT1, which helps to restore intracellular adenosine homeostasis (Pepponi et al. 2022)

#### **4.3.2.2 *Nilotinib***

Nilotinib, which has been shown to be beneficial in Niemann-Pick, targets the c-Abl protein (kinase), whereby inhibition of c-Abl leads to TFEB activation and lysosomal biogenesis, and improvements in autophagy.

#### **4.3.2.3 *Nintedanib***

Nintedanib is also a tyrosine kinase inhibitor, has also been reported that the molecule leads to upregulation in autophagy via TFEB. It is therefore likely that nintedanib is upregulating the CLEAR pathway, promoting lysosome, and lysosomal enzyme biogenesis, which may be

reducing lipid storage similarly to nilotinib (Hegedüs et al. 2022). Nintedanib has also been reported to reduce oxidised-LDL, as well as reducing the intracellular free cholesterol (Li et al. 2022). It is unclear if this effect is in addition to TFEB activation or is because of the upregulation of lysosomal biogenesis and improvements in autophagy.

#### 4.3.2.4 *Bazedoxifene*

Another hit compound with cholesterol reducing effects through modulation of LDL is bazedoxifene. It is known that bazedoxifene functions as an estrogen agonist in lipid metabolism, which leads to a decrease in both total and LDL cholesterol levels (Sexton and Gherman 2001).

#### 4.3.2.5 *Doxorubicin*

Doxorubicin, like nintedanib and bazedoxifene leads to reduction in intracellular cholesterol, in addition to reducing LDL derived cholesterol. Doxorubicin is a (HMG-CoA) reductase (HMGR) inhibitor, HMG-CoA is a key regulatory enzyme in the *de novo* synthesis of cholesterol. When cells were treated with doxorubicin, downregulation of HMG-CoA was observed, coordinated with reduction in cholesterol and lipid levels (Yun et al. 2019).

#### 4.3.2.6 *Letrozole*

Letrozole treatment in breast cancer cells has been shown to decrease expression of several proteins related to cholesterol synthesis, including aromatase and HMGR (Danila and Federico 2023). The inhibition of HMGR would lead to a decrease in *de novo* cholesterol synthesis through blocking the first step of the mevalonate pathway. Therefore, with *de novo* cholesterol synthesis inhibited, this should lead to reduced intracellular cholesterol. Of note is that aromatase contains a pocket structurally similar to NPC2, therefore potential off target effects could also be observed with aromatase inhibitors.

#### 4.3.2.7 *Proadifen*

Proadifen has been shown to inhibit cholesterol 7 $\alpha$ -hydroxylase (CYP7A1) activity by 98% (Schwartz and Margolis 1983). However human fibroblasts do not possess CYP7A1, so it is unclear how proadifen is having an effect. It is possible that proadifen is also inhibiting another enzyme involved in cholesterol metabolism leading to the reduction in lysosomal storage that we observed.

#### 4.3.2.8 *Clobetasol*

Clobetasol is known to interact with Sonic Hedgehog signalling and is believed to be an agonist of smoothened (Porcu et al. 2015). *In vivo* clobetasol has been shown to lead to re myelination of neurons (Yao et al. 2016). Clobetasol treatment is known to lead to modulation of cholesterol metabolism pathways through SREBP activation (Del Giovane and Ragnini-Wilson 2018). SREBP activation is known to have cross talk with mTOR, and thus it is possible that clobetasol is leading to upregulation of TFEB and lysosome biogenesis (Porstmann et al. 2008).

#### 4.3.2.9 *Triamcinolone*

Surprisingly some of the hit molecules identified have been shown to cause elevated cholesterol, such as triamcinolone, which leads to increases in both total and free cholesterol when administered in a rat model (Mitamura 1987). Triamcinolone also has been shown to inhibit protein kinase C *in vitro*, however treatment did not reduce aSMase activity (Sosnowski et al. 1997).

#### 4.3.2.10 *Clofazimine*

Clofazimine, unlike triamcinolone, has been shown to function as an aSMase inhibitor (Kornhuber et al. 2011). However other publications have suggested that clofazimine increases lysosomal enzyme activity (Sarracent and Finlay 1982,1984). With increased lysosomal enzyme activity, activation of TFEB is likely a possible driver, and may explain how despite inhibition of aSMase total lysosomal volume was reduced.

### 4.3.3 *Technical limitations*

#### 4.3.3.1 *Issues with Zinc probe*

Whilst TSQ was suitable for use in screening, it possesses limitations. The biggest issue with TSQ was that the probe dissociated or quenched when removed from the staining solution for imaging. Therefore, this required that TSQ be left on the cells whilst imaging, causing high fluorescence background, and aggregates of TSQ to form within the wells with high fluorescence. Additionally, despite aliquoting TSQ, in multiple assays, the probe did not always bind to zinc instead showing diffuse weak staining. If future zinc screens were to be carried out, further evaluation of other zinc probe options should be carried out.

One potential option is SpiroZin2, which is a far-red zinc binding probe (Han et al. 2018). Additionally, TSQ identified zinc that was stored outside of lysosomes, and therefore the

ability to differentiate between lysosomal zinc and zincosomes, would be beneficial. A range of new zinc probes have been produced that not only bind to zinc, but are also pH sensitive (Bazzicalupi et al. 2010; Berezin et al. 2011; Zhang et al. 2023). Should any of these molecules become commercially available, then they should have distinct advantages over TSQ.

Additionally, genetically encoded zinc probes have shown promise in visualising intracellular zinc (Pratt et al. 2021). Many of the genetically encoded zinc sensors exploit FRET, and thus can be used as ratiometric zinc sensors. An advantage of live cell encoded zinc probes is that they can be used to monitor zinc in real time, and are unlikely to induce artifacts associated with the use of fluorescence zinc probes (Park and Palmer 2014).

#### *4.3.3.2 Number of compounds*

The Discovery Probe™ library used contained approximately 1500 compounds, however larger private screening libraries can contain over 1 million compounds. Whilst it wouldn't have been possible to screen a library of that size in-house, it would have been possible to screen 10,000-20,000 compounds if the assay had been miniaturised into 384 well plate format. With a larger compound library, the probability of finding hit molecules that had stronger effects upon both zinc accumulation and reducing LysoTracker would be increased. Therefore, if zinc screening is to be undertaken again in future, increasing the library size should be a primary factor to be considered.

#### *4.3.4 Future work*

Future work should be focused primarily on assaying the hits from the screen to assess their validity. The next step should be to assay how the molecule affects cholesterol and sphingomyelin storage. Reduction of either molecule could suggest possible mechanisms of action for the molecules, some of which have no obvious cause for reducing lysosomal area.

Following this, carrying out a dose response curve with hit molecules and either LysoTracker or cholesterol staining to determine if the molecules induce a concentration dependant effect and could be used to assess potency of each molecule. If one molecule is identified as being potent and reducing lipid storage, then the next step should be to assess other structurally similar molecules to determine whether they possess the same effects upon lysosomal storage and may possible be able to suggest a putative mechanism of action.

#### 4.4 Conclusion

In conclusion, we have established a zinc phenotypic assay. This assay has proved to be robust enough to be suitable for high throughput screening. We also identified tool compounds that could be used to evaluate modulation of zinc, as well as testing compounds with known zinc modulatory effects.

We have run successfully the first zinc phenotypic screen for a lysosomal storage disorder, and thus Niemann-Pick disease. For the screening, we have taken a 1500 compound library and identified 20 hit compounds that modulate zinc and show at least a 15% reduction in lysosomal volume in NPC1 P237/I1061T cells. Encouragingly, 2 of the hits, dipyridamole and nilotinib, have been shown to have disease modifying effects in pre-clinical models of Niemann-Pick by other groups, which confirms the validity of the screen and the hits that have been identified.

# 5 Investigation into cannabidiol and copaiba oil as potential therapeutics in Niemann-Pick

## *5.1 Introduction*

Despite Niemann-Pick type C (NPC) disease being primarily characterised by loss of NPC1 activity (or rarely NPC2), a range of secondary enzymatic defects are also observed. In NPC, there is a 40-60% reduction in acid sphingomyelinase (aSMase) activity. Loss of aSMase activity is also the underlying driver of Niemann-Pick disease type A (NPA) and Niemann-Pick disease type B (NPB).

Finding an activator for aSMase, has therapeutic potential to partially alleviate lysosomal storage of sphingomyelin, thus likely to provide improved lysosomal health and offer a treatment option for NPA and NPB, as well as a secondary therapy for NPC. No small molecule activators of aSMase exist, however research has shown that treating patient derived fibroblasts with cannabidiol can all but remove sphingomyelin storage.

### *5.1.1 aSMase regulation in LSD's/NPD*

Whilst loss of function of aSMase is most closely associated with NPA and NPB, significant knockdown in aSMase is observed in NPC disease, amongst others including a-mannosidosis, I Cell, CLN5, and Gaucher disease. In NPC, aSMase activity is reduced by approximately 50%, coinciding with accumulation and mis-localisation of sphingomyelin (Vanier et al. 1991). This significant decrease in aSMase activity in NPC, leads in part to the secondary sphingomyelin storage associated with the 'classical' presentation of NPC and may lead to some of disease pathology.

The exact reason underpinning the decrease in aSMase activity in NPC is not fully understood, however two probable causes have been suggested. The first is due to cholesterol accumulation, which leads to downregulation of aSMase activity through post-translational modification, whereby it was suggested that cholesterol mediates disruption of

a folding or sorting event leading to improper maturation of active aSMase (Reagan et al. 2000). The cholesterol post translational modification was suggested as a mechanism of action as *Reagan et al (2000)* showed that, whilst increasing cholesterol concentration did not affect the quantity of aSMase within cells, it did reduce the activity significantly.

The second cause for a reduction in aSMase activity is due to reduced protein kinase C (PKC) activity in NPC disease. Increased lysosomal sphingosine concentrations, as observed in NPC leads to decreased PKC activity; and may cause some of the associated endocytic defects through downregulation of Rab9 (Walter et al. 2009). PKC is known to be a positive regulator of aSMase activity, therefore if PKC activity is decreased in Niemann-Pick, aSMase activity will also be decreased. (Rodriguez-Lafrasse and Vanier 1999; Zeidan and Hannun 2007b).

### ***5.1.2 Cannabidiol***

Cannabidiol (CBD) is a phytocannabinoid, usually isolated from *Cannabis sativa*. Extracts from *Cannabis sativa* have been shown to have over 500 compounds, of which at least 120 are phytocannabinoids. Cannabidiol is one of the major constituents of *Cannabis sativa* extract, which along with  $\Delta^9$ -Tetrahydrocannabinol (THC) make up to 40% of the crude extract. However, whilst THC is known to produce psychoactivity, no psychoactivity is associated with cannabidiol (Martínez et al. 2020). Data from several pre-clinical studies suggests that cannabidiol has potential therapeutic uses, with evidence suggesting positive effects including: anti-inflammatory, anticonvulsant, antipsychotic, and antiemetic (Pertwee 2006).

#### ***5.1.2.1 Cannabidiol Mechanism of Action***

Cannabidiol is known to interact with several receptors, the most well characterised being the cannabinoid receptors (CB). Cannabidiol functions as an indirect antagonist of CB<sub>1</sub> and CB<sub>2</sub> receptors, by antagonising CB<sub>1</sub> and CB<sub>2</sub> receptor agonists, with a K<sub>d</sub> in the low nanomolar range, however more recent research has suggested that cannabidiol may also function as a negative allosteric modulator (NAM) of CB<sub>1</sub> (Davidson et al. 2016). The antagonism of CB<sub>1</sub> and CB<sub>2</sub> by cannabidiol prevents anandamide hydrolysis, leading to increased endogenous anandamide signalling, potentially leading to antipsychotic effects (Leweke et al. 2012). In addition to acting on CB receptors, cannabidiol is a known agonist

of both TRPV1 and 5-HT1A receptors, with the antagonistic effect on the latter receptor likely to be driving cannabidiol's anxiolytic effects (Peres et al. 2018).

Cannabidiol is currently undergoing, or has undergone, a range of clinical trials for various conditions, including: pain management, bipolar disorder, psychosis, and epilepsy. However, no trials concerning the use of cannabidiol as a treatment option in lysosomal storage disease has been carried out; one clinical trial is testing cannabidiol for pain management in Fabry disease.

### 5.1.3 *Cannabidiol in Niemann-Pick*

Work carried out in the 1980's demonstrated that treating patient derived fibroblasts (healthy control and NPA) with cannabidiol, led to decreased intracellular sphingomyelin levels (Burstein et al. 1984). The authors demonstrated that treating NPA cells with cannabidiol for 24 hours led to a 77% decrease in sphingomyelin levels, compared to a 17% decrease in healthy control fibroblasts. Of note was that cannabidiol, but not THC treatment produced significantly decreased sphingomyelin levels.

Whilst the Burstein paper showed that cannabidiol significantly reduced sphingomyelin levels, no mechanism of action was suggested. However, later work demonstrated that cannabinoids, including cannabidiol, can activate PKC (Hillard and Auchampach 1994). The activation of several lysosomal enzymes, including aSMase is PKC phosphorylation dependant, therefore PKC activation directly regulates aSMase activity (Zeidan and Hannun 2007a).

*Charytoniuk et al (2022)* suggested possible secondary mechanisms for decreased cellular sphingomyelin levels, whereby treating rats with cannabidiol decreased de-novo ceramide synthesis, by downregulating the ceramide synthesis pathway (Charytoniuk et al. 2022). Reducing lysosomal ceramide levels should lead to increased production of aSMase to restore lysosomal ceramide homeostasis.

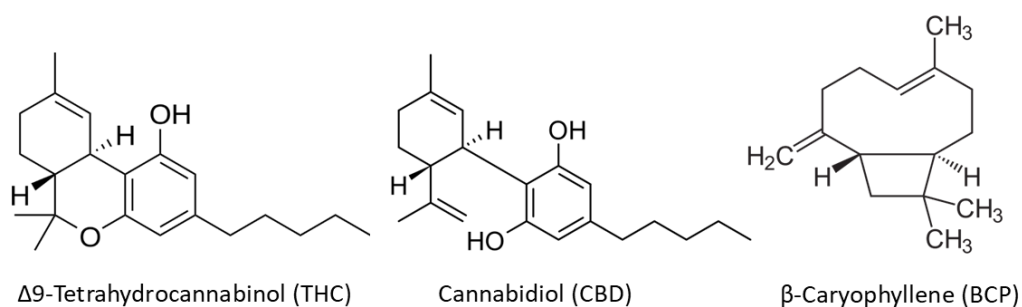


**Figure 5.1. Chemical structures of three significant members of the cannabinoid family**  
 THC forms the principal psychoactive component of cannabis, in addition to being a CB1 receptor agonist. Cannabidiol, whilst being structurally similar molecule to THC is not psychoactive and functions as a CB1 receptor antagonist, directly opposed to THC. BCP is the major cannabinoid present in copaiba, and a known CB2 receptor agonist.

### 5.1.4 Copaiba

Copaiba oil is derived from balsam obtained by tapping the trunk of trees from several species in the genus *Copaifera*. The copaiba balsam is then steam distilled to give a crude extract, copaiba oil. Due to the natural origins of copaiba oil, the resulting product is highly heterogenous, with many different chemical constituents, including over 60 different terpenes alone. Of these terpenes, 5 are responsible for up to 75% of the total terpenes content in copaiba, and a significant overall percentage of overall copaiba oil. Outlined in Table 1. Below are the major terpene constituents of copaiba oil (Urasaki et al. 2020).

**Table 5.1. Major terpene constituents of copaiba oil based on data from Urasaki et al. 2020**

Name	Percentage of copaiba oil terpenes (%)	Range (+/-)
β-Caryophyllene	52	±8%
α-Copaene	8	±3%
α-Bergamotene	7	±1%
α-Humulene	6	±2%
Germacrene D	5	±3%
B-Bisabolene	3	±2%
Δ-Cadinene	3	±1%
γ-Elemene	2	±1%
trans-Cadina1(6),4-Diene	2	±1%
α-Cubebene	2	±1%
β-Elemene	2	±1%

#### 5.1.4.1 Copaiba Pharmacokinetics

Initial research using copaiba oil, showed anti-inflammatory and pain reducing effects (Dalenogare et al. 2019; Menezes et al. 2022). Further research into these effects, has

suggested that that the primary terpene in copaiba, the cannabinoid  $\beta$ -caryophyllene (BCP) is likely to be mediating the therapeutic effects.

#### 5.1.4.2 *Copaiba Mechanism of Action*

The main putative mechanism of action of copaiba, and therefore BCP, is through interaction with CB<sub>2</sub> receptors. BCP has been shown to have low nanomolar binding affinity for CB<sub>2</sub> receptor functioning as a selective agonist (Gertsch et al. 2008). Upon BCP binding to CB<sub>2</sub>, this leads to inhibition of adenylate cyclase, which leads to intracellular Ca<sup>2+</sup> transients and further activates the signalling pathways mediated by Erk1/2 and p38 (Gertsch 2008).

Of note is that BCP shows binding exclusively to CB<sub>2</sub> *in vitro*, unlike cannabidiol and THC that bind both receptors (Pertwee 2008). *In silico* modelling has shown a binding pocket for BCP in the CB<sub>2</sub> receptor, which is at the same loci as a putative THC binding pocket (Gertsch et al. 2008). Unlike other cannabinoid agonists and antagonists, BCP does not elicit the GABAergic or NMDA receptor mediated activities, associated with other CB receptor modulating anti-anxiety therapies (Galdino et al. 2012).

BCP has also been demonstrated to increase lysosomal membrane integrity, preventing lysosomal rupture (Meeran et al. 2021). Despite preventing lysosomal damage, BCP was shown to reduce cytosolic release of lipid degrading enzymes including  $\beta$ -Glu, and  $\beta$ -Gal, with no change to lysosomal enzyme activity, however no analysis of aSMase levels was made, so it unclear what effects, if any, BCP will have upon LSD cell lines.

To date no research has been carried out on copaiba oil on lysosomal activity or on lysosomal storage disorders. Therefore, it is unclear what effects if any copaiba oil has on lysosomes, or on lipid accumulation associated with lysosomal storage disorders such as Niemann-Pick disease. Additionally, the effect of copaiba oil on PKC signalling is not known. However, work on CB<sub>2</sub> receptors has shown that activation of CB<sub>2</sub> receptors decreases cell surface levels of HMGB1, reducing cellular degradation through the autophagy-lysosome pathway (Zhou et al. 2020).

### 5.1.5 Chapter aims

There is a better need to understand how cannabidiol and copaiba may bring about therapeutic benefits in Niemann-Pick disease beyond their use as anticonvulsants. This chapter will determine what effects cannabidiol and copaiba have on lysosomal function, how they mediate those effects upon the cell, and whether there is a potential therapeutic use for these compounds in treating the lipid storage associated with Niemann-Pick disease.

Therefore, the following aims were determined:

1. Determine maximum concentration of both cannabidiol and copaiba, which cells can be treated with over a 72-hour time period to avoid toxicity.
2. Determine if cannabidiol or copaiba can reduce lysosomal volume in patient derived fibroblasts.
3. Compare lipid storage in cells treated with cannabidiol and copaiba to see how specific lysosomal lipid levels change.
4. Perform aSMase enzyme assays to determine whether cannabidiol and copaiba lead to changes in aSMase activity.
5. Analyse how cannabidiol and copaiba change protein expression levels of several potentially modulated proteins.
6. Analyse TFE3 localisation to determine how cannabidiol and copaiba may be affecting aSMase synthesis.

## 5.2 Results

### 5.2.1 *aSMase activity in Niemann-Pick disease fibroblasts*

Sphingomyelin accumulates within lysosomes in all forms of Niemann-Pick disease, due to loss of aSMase activity, which is most significant in NPA and NPB (Vanier et al. 1980) and a combination of: reduced aSMase activity, aSMase mis-localisation, and trapping of SM by cholesterol in NPC (Tamura et al. 2006; Lee et al. 2013). As cannabidiol has been reported to reduce SM accumulation, *Figure 5.2* shows aSMase activity in Niemann-Pick disease patient fibroblasts. Both healthy control fibroblasts have similar aSMase activity, being higher than any disease cell line, with the 1yr male cell line having aSMase activity of 10.9 +/- 1.1  $\mu\text{mol/hr}/\mu\text{g}$  protein, whilst the 11yr female cell line had aSMase activity of 10.4 +/- 2.1  $\mu\text{mol/hr}/\mu\text{g}$  protein. The activity in NPA cells was reduced ~90% to 1.2 +/- 0.2  $\mu\text{mol/hr}/\mu\text{g}$  (p

< 0.0001), consistent with previous reports (Poulos et al. 1983). aSMase activity in NPB is approximately 40% of healthy controls (3.6 +/- 0.8  $\mu\text{mol/hr}/\mu\text{g}$  ( $p < 0.0001$ )), consistent with the less severe phenotype associated with NPB. Activity is also reduced by 40-60% ( $p < 0.0001$ ) in NPC1 fibroblasts, ranging between 5-6.5  $\mu\text{mol/hr}/\mu\text{g}$ , consistent with previous reports (van Diggelen et al. 2005). Of note is that no statistically significant difference is observed in aSMase activity between the three NPC disease cell lines tested, despite 2 cell lines being 'classical' NPC and one being 'variant' form of the disease.

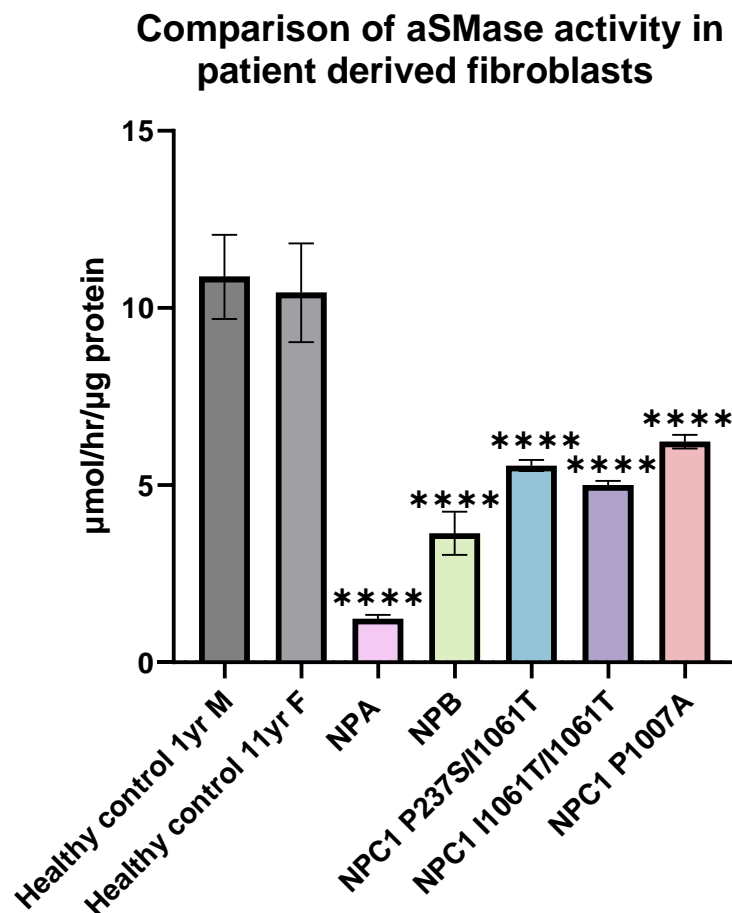


**Figure 5.2. Comparison of acid sphingomyelinase activity in Niemann-Pick disease patient derived fibroblasts and healthy control fibroblasts**

aSMase activity assay in patient fibroblasts was determined using a fluorescent substrate plate-based assay as outlined by van Diggelen et al. 2005 and in 2.4.1.2. Statistical significance was calculated with a one-way ANOVA and a post-hoc Tukey's multiple comparison test. All statistical significance shown is when compared to both healthy control samples.  $N=3$  for all experiments, data shown is mean  $\pm$  SD. \*= $p < 0.05$ , \*\*= $p < 0.01$ , \*\*\*= $p < 0.001$ , \*\*\*\*= $p < 0.0001$ .  $N=3$  for all experiments,

## 5.2.2 Toxicity of cannabidiol and copaiba oil

### 5.2.2.1 Cannabidiol LC50 determination in patient derived fibroblasts

Cells were treated with a range of concentrations of cannabidiol, and the viability recorded at: 24, 48, and 72 hours. In all cell lines it was observed that cellular viability decreased as time elapsed, with all cell lines having an LC50 in the 50 $\mu$ M to 150 $\mu$ M range, as shown in *Figure 5.3(f)*.

Compared to healthy control cells, classical NPC (P237S/I1061T and I1061T/I1061T) were more resistant to cannabidiol-induced toxicity at 48h and 72h, with the P237S/I1061T cell line having an LC50 of 107 $\mu$ M +/- 7 $\mu$ M ( $p=0.0061$ ) and 82 $\mu$ M +/- 5 $\mu$ M ( $p=0.0013$ ) respectively. The NPC1 I1061T homozygous cells had an LC50 of 104 $\mu$ M +/- 15 $\mu$ M ( $p=0.0008$ ) and LC50 of 81 $\mu$ M +/- 5 $\mu$ M ( $p=0.0004$ ). NPA cells were shown to be more resistant at 48h 90 $\mu$ M +/- 18 $\mu$ M ( $p=0.032$ ). Variant (P1007A) NPC cells were more susceptible to cannabidiol-induced toxicity at 24h with an LC50 of 76 $\mu$ M +/- 6 $\mu$ M ( $p=0.045$ ) but not different at longer incubation times.

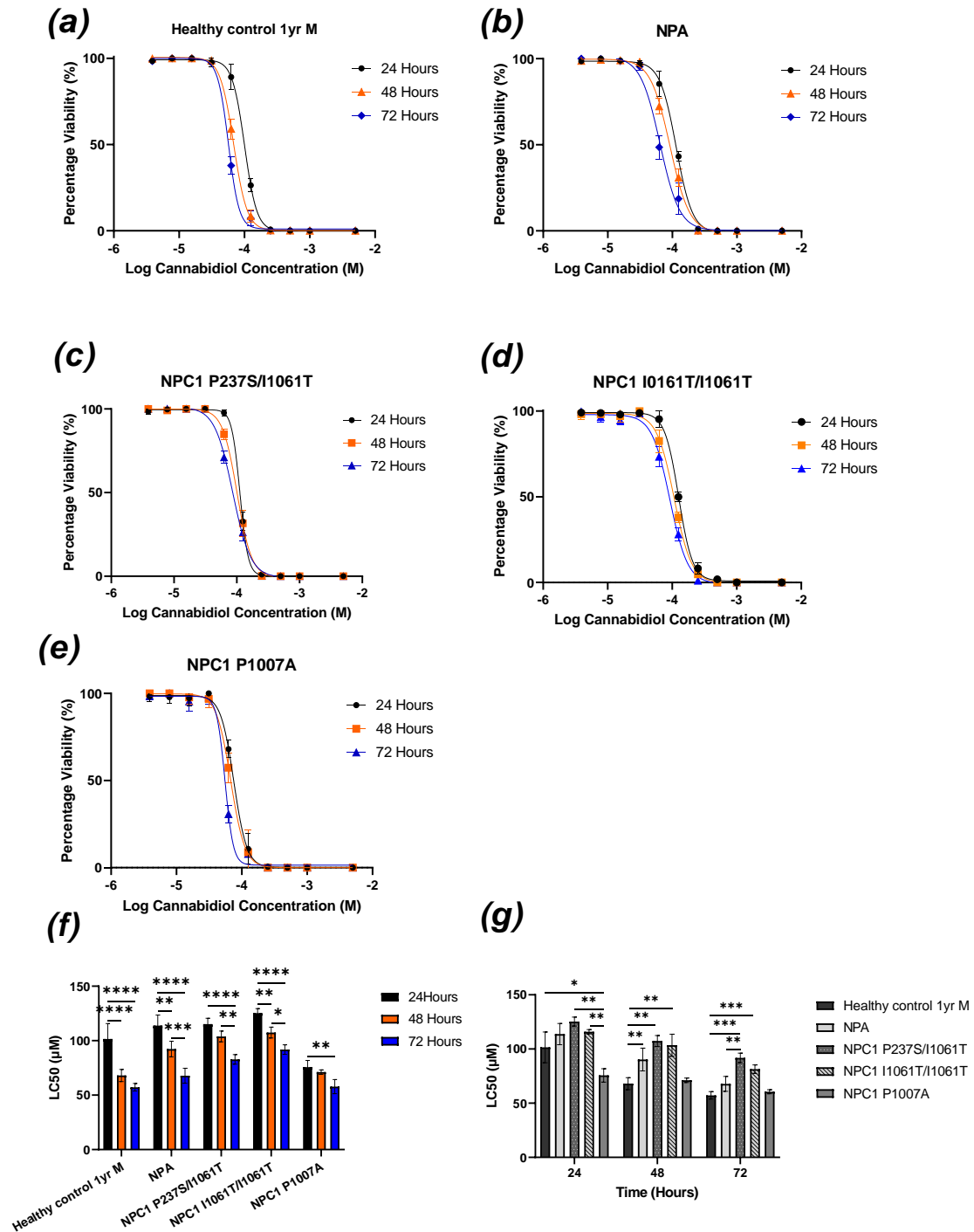


**Figure 5.3. Cell viability assay for Niemann-Pick disease patient derived fibroblasts treated with cannabidiol**

In (a-e) healthy control cells and Niemann-Pick disease fibroblasts were treated with a range of cannabidiol concentrations and the cell viability recorded at 24, 48 and 72 hours. Percentage viability was determined by comparison with untreated cells and cells which had been killed through ethanol exposure. (f) LC50 is compared between time points for each cell line individually. (g) Comparison of LC50 between cell lines at 24 hours, 48 hours and 72 hours. Significance was calculated with a two-way ANOVA and a post-hoc Tukey's multiple comparison test.  $*$ = $p < 0.05$ ,  $**$ = $p < 0.01$ ,  $***$ = $p < 0.001$ ,  $****$ = $p < 0.0001$ .  $N=3$  for all experiments, data shown is mean  $\pm$  SD.

#### 5.2.2.2 *Copaiba LC50 determination*

As only limited research had been carried out on copaiba oil, first the LC50 needed to be determined in both healthy control and Niemann-Pick disease cell lines. As the potential active constituent(s) of copaiba oil was not known, concentrations could only be determined using the mass of copaiba oil. In all cell lines except NPC P1007A, where viability decreased with time elapsed, there was no change in cellular viability with longer treatments, with all cell lines having an LC50 in the 20-40ug/ml range (*Figure 5.4(f)*). There was no difference in susceptibility in disease cell lines compared to healthy controls except the NPC1 P1007A cell line.

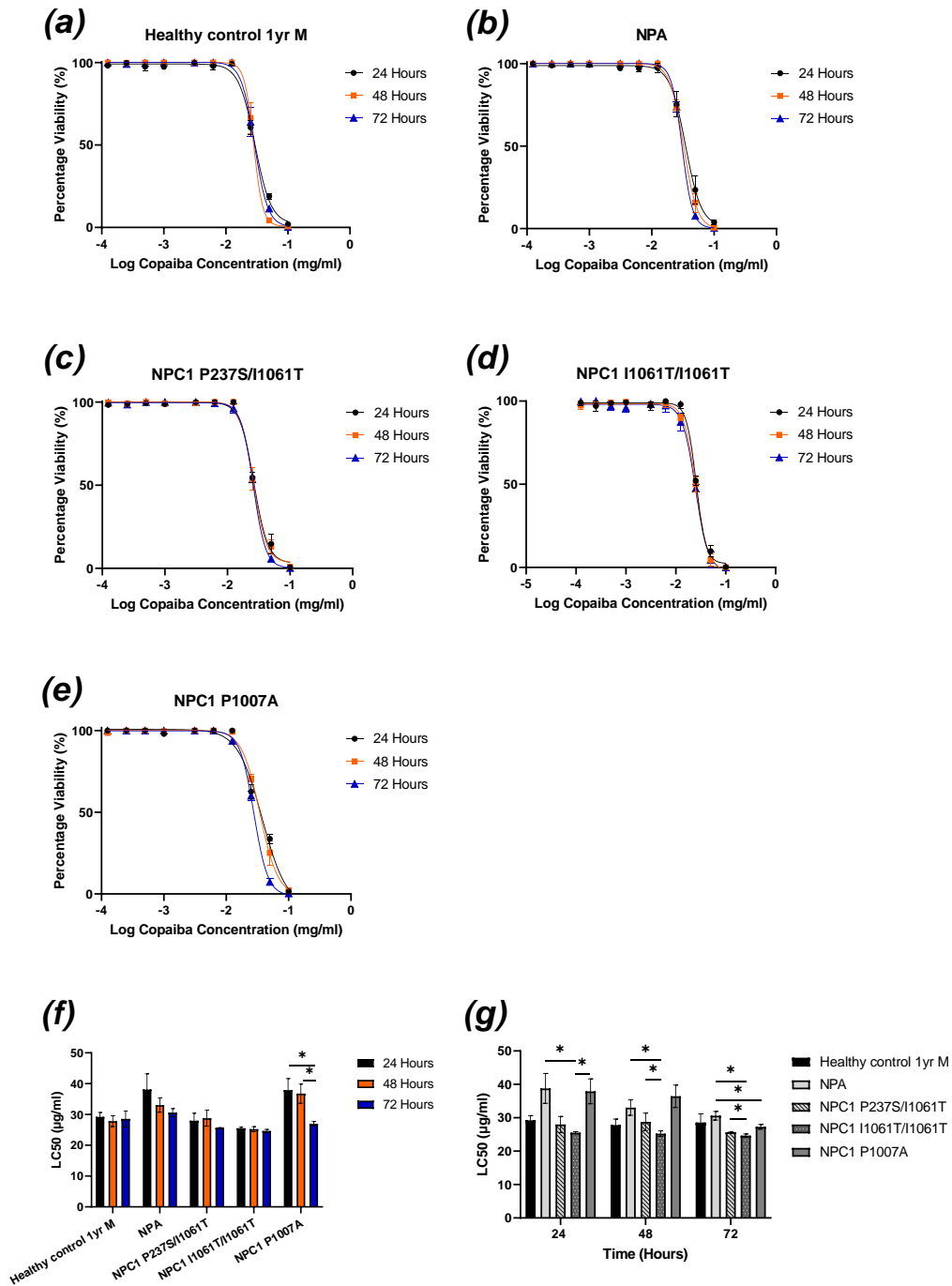


**Figure 5.4. Cell viability assay for Niemann-Pick disease patient derived fibroblasts treated with copaiba**

(In (a-e) healthy control cells and Niemann-Pick disease fibroblasts were treated with a range of copaiba oil concentrations and the cell viability recorded at 24, 48 and 72 hours. Percentage viability was determined by comparison with untreated cells and cells which had been killed through ethanol exposure. (f) LC50 is compared between time points for each cell line individually. (g) Comparison of LC50 between cell lines at 24 hours, 48 hours and 72 hours. Significance was calculated with a two-way ANOVA and a post-hoc Tukey's multiple comparison test.  $*=p<0.05$ ,  $**=p<0.01$ ,  $***=p<0.001$ ,  $****=p<0.0001$ .  $N=3$  for all experiments, data shown is mean  $\pm$  SD.

### *5.2.3 Effect of cannabidiol and copaiba upon lysosomal storage in Niemann-Pick disease*

Previous investigation by Burstein *et al* (1984) reported reduced SM storage in NPA cells treated with cannabidiol. To determine whether this effect is specific to SM, or whether cannabinoids can effect a more general reduction in lipid storage, we conducted a comprehensive characterisation of the effects of cannabidiol and copaiba on lysosomal lipid storage in patient derived Niemann-Pick cells. Concentrations and incubation times for cannabidiol and copaiba, and use of a single batch of cannabidiol, were chosen following toxicity studies (9.3.2.2).

#### *5.2.3.1 Lysosomal volume changes in cannabidiol treated cells using a plate-based assay*

Analysis of lysosomal volume by LysoTracker Green and plate reader analysis, showed that cannabidiol reduced LysoTracker Green fluorescence in all Niemann-Pick disease cell lines (*Figure 5.5(a)*). The biggest effect was observed in NPA cells, where treatment with 15 $\mu$ M cannabidiol reduced the LysoTracker fluorescence by approximately 25% to comparable levels with the healthy control cell lines. LysoTracker values were also normalised in NPB, NPC P237S/I1061T and NPC P1007A cells, following reductions of 15, 10 and 10% respectively, and reduced by 10% in NPC I1061T/I1061T cells.

Comparisons of fold decrease in LysoTracker fluorescence, showed that only the NPA and NPB had a significantly increased change in LysoTracker Green fluorescence when compared to the healthy control cell lines. Whilst all NPC cell lines showed a decrease in LysoTracker fluorescence upon cannabidiol treatment, none of the cell lines showed a significant reduction in fluorescence when compared to the healthy control cell lines.

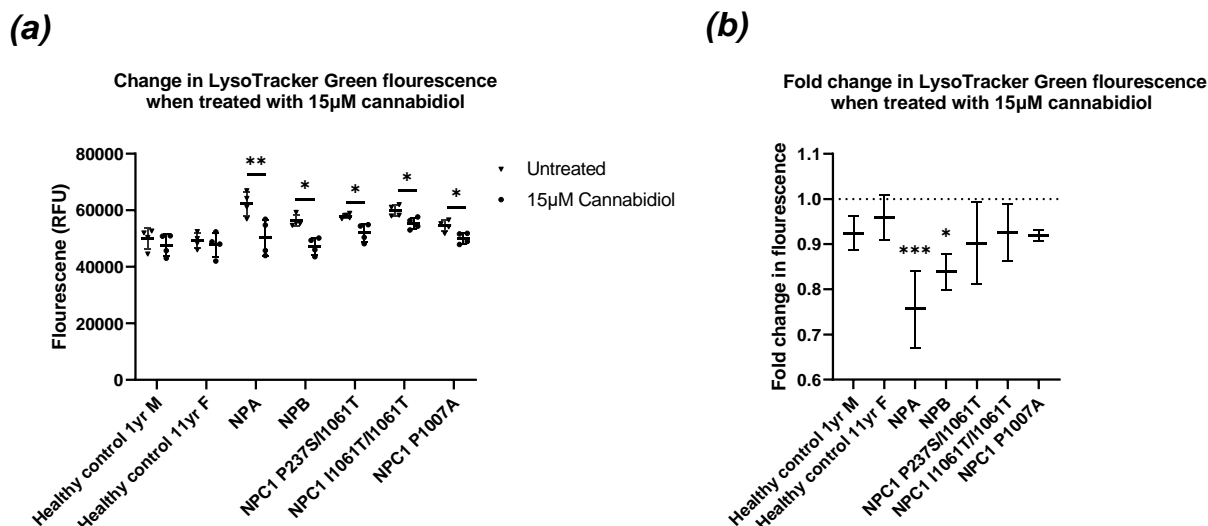


**Figure 5.5. Comparison of LysoTracker Green fluorescence before and after cannabidiol treatment**

In (a) fluorescence values comparing untreated cells and cells treated with 15µM cannabidiol for 48 hours. Cells were treated with 200nM LysoTracker green for 15 minutes and the plate read on a plate reader with a filter set with an excitation of 485nm and emission at 520nm. (b) Fold change comparison in lysotracker fluorescence, between untreated cells, and cells treated with 15µM cannabidiol. Statistical significance was calculated with a one-way ANOVA and a post-hoc Tukey's multiple comparison test.  $*=p<0.05$ ,  $**=p<0.01$ ,  $***=p<0.001$ ,  $****=p<0.0001$ .  $N=4$  for all experiments, data shown is mean  $\pm$  SD.

### 5.2.3.2 Copaiba effect upon lysosomal volume in Niemann-Pick disease

The plate reader based lysosomal expansion assay using LysoTracker, showed that treating some Niemann-Pick disease cells with copaiba oil reduced fluorescence, and thus lysosomal volume.

The NPA cells showed the most pronounced response to treatment with 10µg/ml copaiba, where fluorescence was decreased ~16%, but not returned to control levels. The NPB cells also showed a significant reduction, and normalisation to control levels, in LysoTracker fluorescence upon copaiba treatment, with an 8% reduction in fluorescence. There was no significant reduction in NPC cell fluorescence following copaiba treatment.

The only cell line to show a significantly different response to the control cell lines when treated with copaiba, was the NPA cell line, which also showed a statistically different response to both the NPB and NPC lines in fold change in LysoTracker Green fluorescence (Figure 5.6(b)). No difference was observed between either the NPB or any of the NPC1 mutant cell lines, when the fold change in fluorescence was compared to the healthy control cell lines.

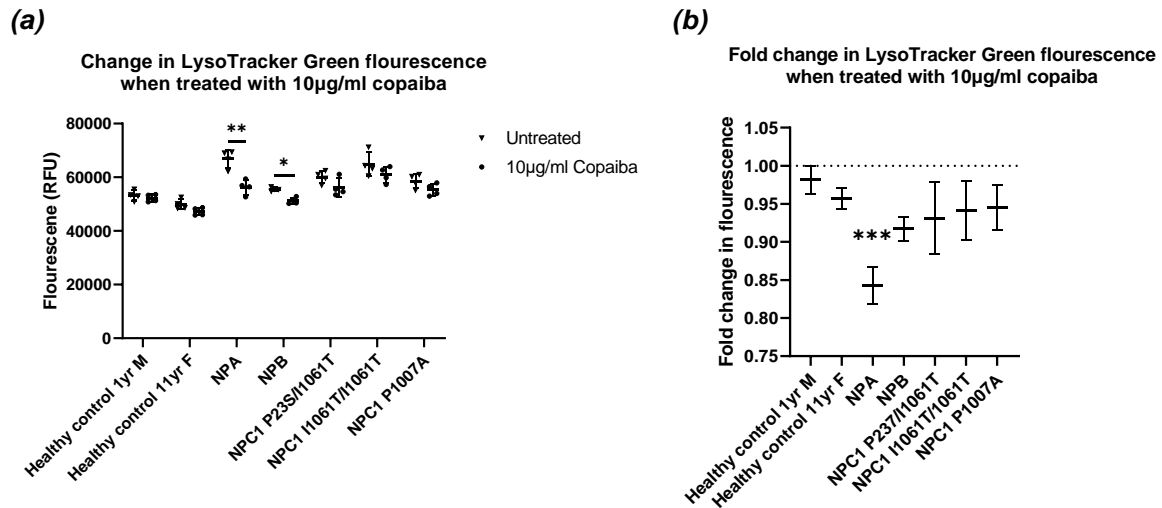


**Figure 5.6. Change in LysoTracker Green fluorescence when healthy control and Niemann-Pick fibroblasts are treated with copaiba**

In (a) LysoTracker Green fluorescence values comparing untreated cells and cells treated with 10µg/ml copaiba oil for 48 hours. Cells were treated with 200nM LysoTracker green for 15 minutes and the plate read on a plate reader with a filter set with an excitation of 485nm and emission at 520nm. (b) Fold change comparison in LysoTracker fluorescence, between untreated cells, and cells treated with 15µM copaiba. Statistical significance was calculated with a one-way ANOVA and a post-hoc Tukey's multiple comparison test. \*= $p < 0.05$ , \*\*= $p < 0.01$ , \*\*\*= $p < 0.001$ , \*\*\*\*= $p < 0.0001$ .  $N=4$  for all experiments, data shown is mean  $\pm$  SD.

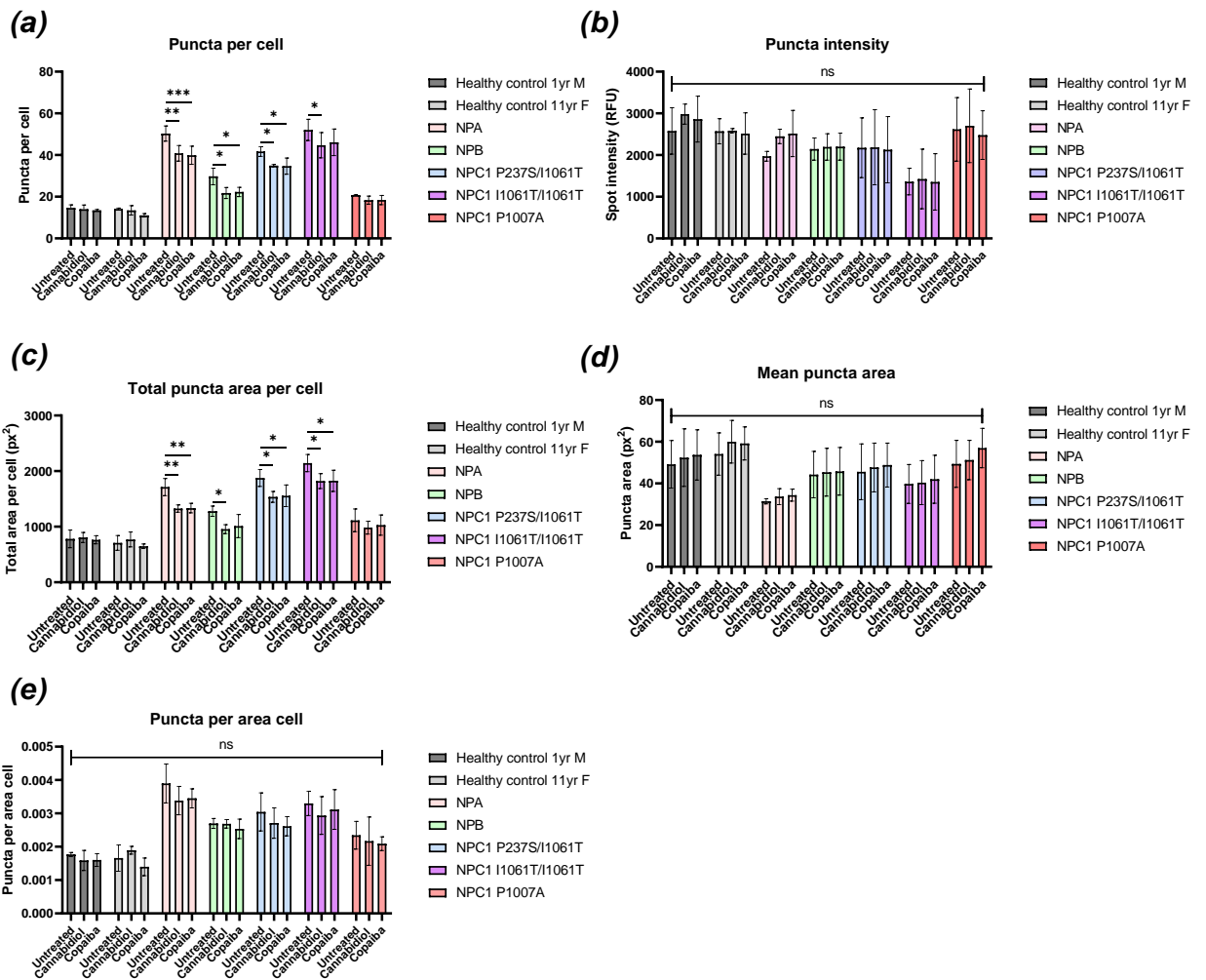
### 5.2.3.3 Cannabidiol and Copaiba both reduce lysosome number and total puncta area in Niemann-Pick disease fibroblasts

As we had shown that some of the Niemann-Pick disease cell lines saw reduction in LysoTracker Green fluorescence when treated with cannabidiol and copaiba, we decided to further analyse the effects of cannabidiol and copaiba using a LysoTracker Red imaging-based assay. Unlike the plate reader-based assay, the imaging assay allowed for the analysis of several parameters when the cells were imaged.

From the data in Figure 5.7, both cannabidiol and copaiba induce similar effects upon LysoTracker Red staining. Both NPA and NPB fibroblasts show significant reductions in the number of puncta of LysoTracker Red when treated with cannabidiol and copaiba, as do NPC1 P237S/I1061T fibroblasts. NPC1 I1061T/I1061T showed a significant decrease in puncta number when treated with cannabidiol, but not copaiba, while puncta number was unchanged in NPC1 P1007A fibroblasts following treatment with cannabidiol or copaiba.

Changes in total puncta area per cell closely resemble the changes observed in puncta number, with significant decreases being observed with the: NPA, NPB, and both NPC1

I1061T fibroblasts following cannabidiol treatment, but no change in P1007A. Copaiba treatment reduced total puncta area per cell in NPA and both NPC I1061T mutant fibroblast cell lines. No significant change was observed in puncta fluorescence, nor mean puncta area or puncta per area cell in any of the cell line upon treatment with cannabidiol or copaiba.



(f)

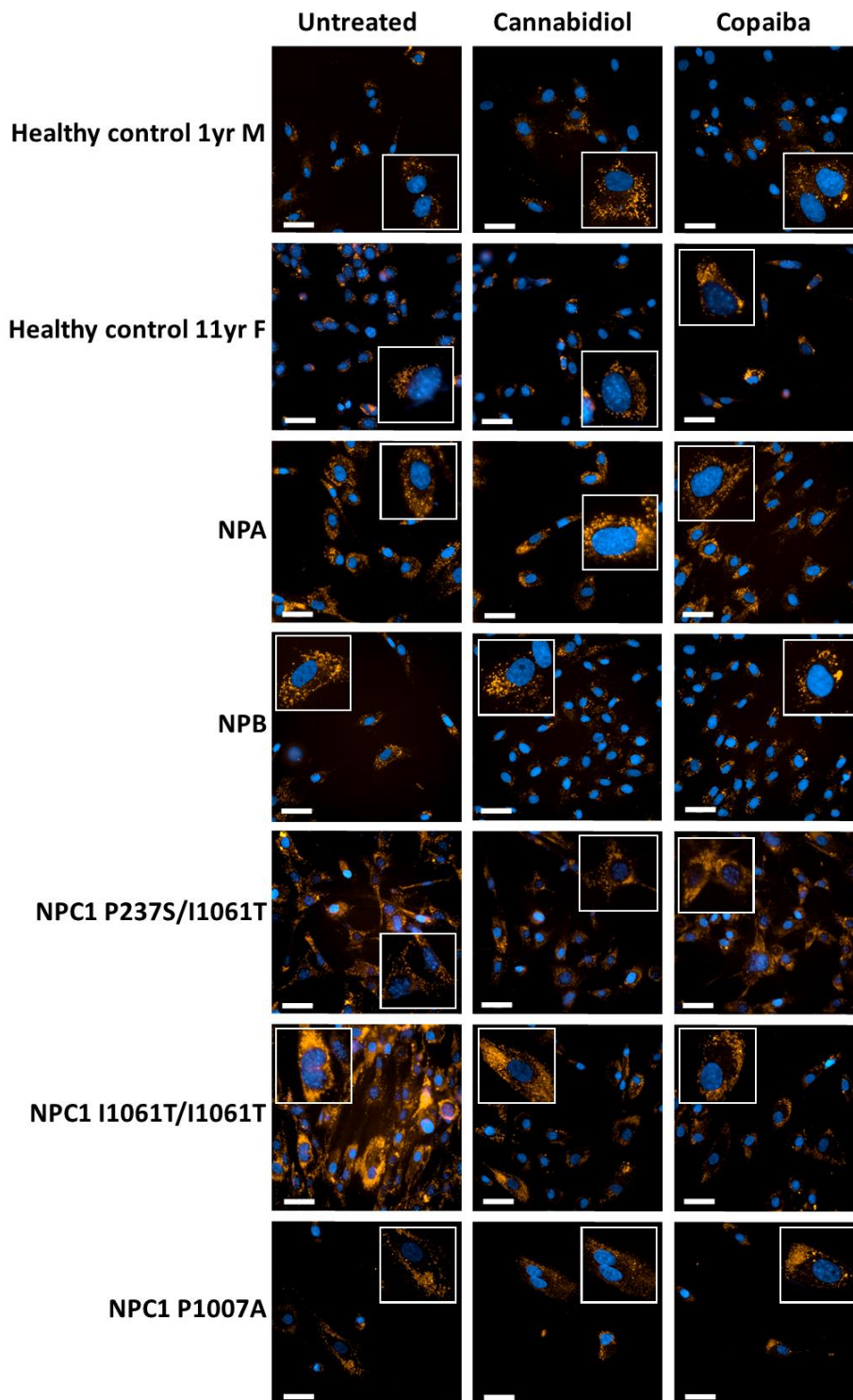


***Figure 5.7. Cannabidiol and copaiba treatment reduces number of puncta and total puncta area in most Niemann-Pick disease fibroblasts when probed with LysoTracker Red***

*In (a-e) various analysis parameters are shown after healthy control and Niemann-Pick disease fibroblasts were treated with cannabidiol and copaiba for 48 hours before being probed with LysoTracker Red. In (f) representative images for each cell line, with each treatment are shown. Statistical significance was calculated with a one-way ANOVA and a post-hoc Tukey's multiple comparison test. \*= $p < 0.05$ , \*\*= $p < 0.01$ , \*\*\*= $p < 0.001$ , \*\*\*\*= $p < 0.0001$ .  $N=3$  for all experiments, data shown is mean  $\pm$  SD. Scale bars represent  $50\mu\text{m}$ .*

*5.2.3.4 Cannabidiol and Copaiba reduce lysosome number when probed with AQ7.* Knowing that LysoTracker Red could detect changes in lysosomal volume in Niemann-Pick cells, confirmation using a second lysosomal probe, AQ7, was used. Whilst both molecules can identify late endosomes/lysosomes, AQ7 unlike LysoTracker Red requires the molecule to be trafficked into the cell, therefore allowing for potential differences in staining.

Number of puncta was reduced in both NPA and NPB cell lines and NPC1 I1061T mutant cell lines when treated with cannabidiol and copaiba. No change was observed in either the healthy control lines or the NPC1 P1007A mutant cell line. Similar changes were observed in the total puncta area per cell; however the effect was less significant for most cell lines and treatments, and there was no reduction in NPB cells treated with copaiba. No change in puncta intensity, mean puncta area or puncta per area of cytoplasm were observed in any of the cell lines when treated with cannabidiol or copaiba.

Across all cell lines, cannabidiol and copaiba induced broadly similar changes in puncta, with no significant differences observed between cannabidiol and copaiba in any of the cell lines, across all the analysis parameters.

Data from AQ7 was consistent with LysoTracker Red, which further suggests that AQ7 is suitable for use as a lysosomal probe.



(f)

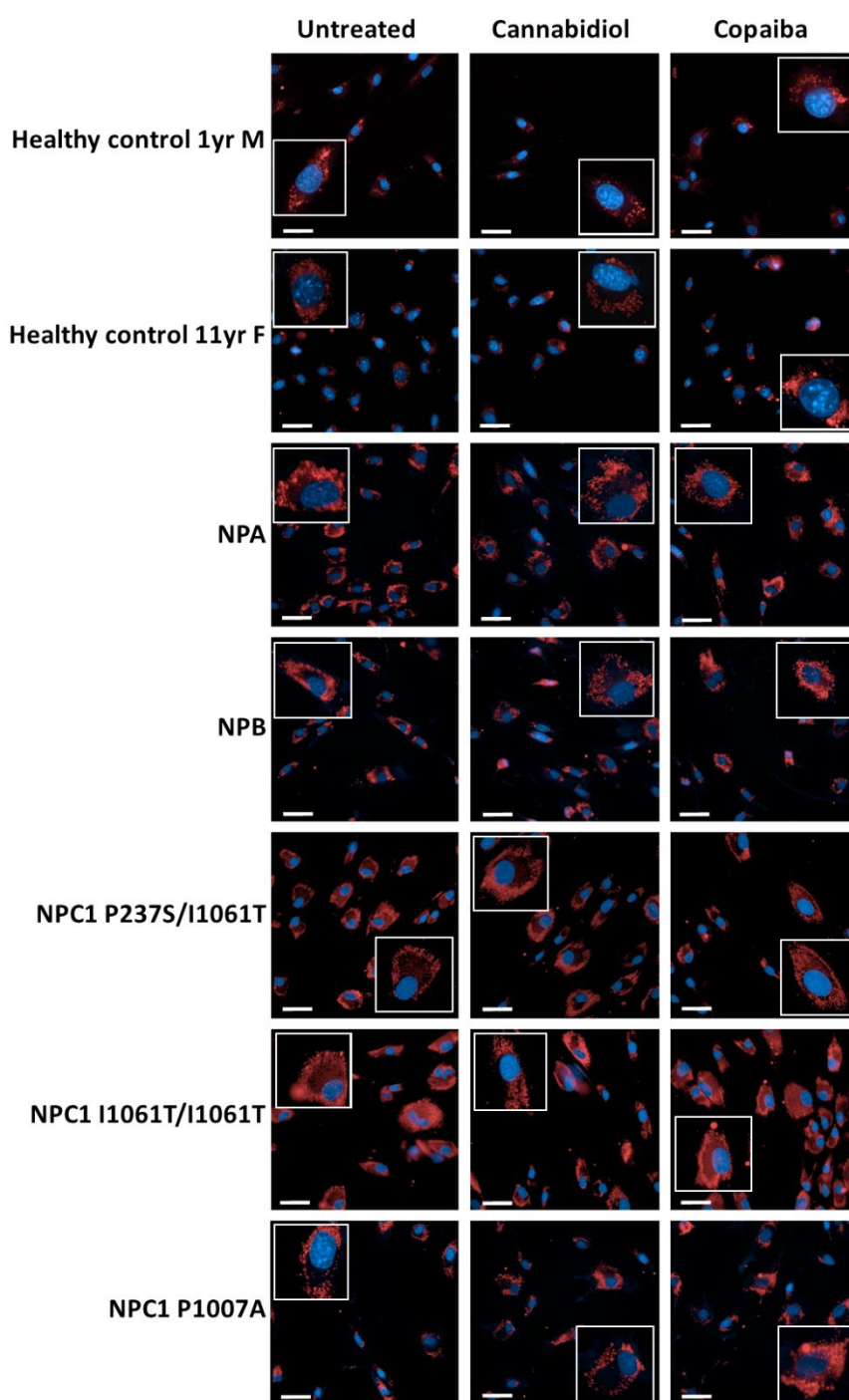


***Figure 5.8. Cannabidiol and copaiba treatment recues lysosomal volume in most Niemann-Pick disease fibroblasts when probed with AQ7***

*In (a-e) five analysis parameters are shown after healthy control and Niemann-Pick disease fibroblasts were treated with cannabidiol and copaiba for 48 hours, before being probed with AQ7. Significant differences were observed in both the number of puncta and the total puncta area when cells were treated with cannabidiol or copaiba, however no significant differences were observed in the other parameters analysed. In (f) representative images for each cell line, with each treatment are shown. Statistical significance was calculated with a one-way ANOVA and a post-hoc Tukey's multiple comparison test. \*= $p < 0.05$ , \*\*= $p < 0.01$ , \*\*\*= $p < 0.001$ , \*\*\*\*= $p < 0.0001$ . N=3 for all experiments, data shown is mean  $\pm$  SD. Scale bars represent 50 $\mu$ m.*

## 5.2.4 Effects of cannabidiol and copaiba on specific lysosomal lipid storage

### 5.2.4.1 Sphingomyelin

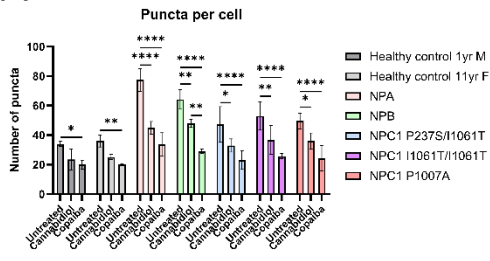
As reductions in sphingomyelin have previously been reported in NPA fibroblasts following cannabidiol treatment, we investigated whether this is also the case for other forms of Niemann-Pick disease. Sphingomyelin storage is a primary phenotypic marker in NPA and NPB disease; whilst sphingomyelin storage is a secondary marker in classical NPC phenotypes. To probe sphingomyelin storage, recombinant European lysenin was used.

Treatment with cannabidiol and copaiba showed significant decreases and normalisation to control levels in number of puncta per cell in all Niemann-Pick disease cell lines, with a larger decrease being observed in the copaiba treated cells (*Figure 5.9(a)*). A decrease in the puncta fluorescence intensity, indicating reduced sphingomyelin within puncta, was observed in NPA when cells were treated with both cannabidiol and copaiba, and in NPB and NPC1 I1061T/I1061T cells treated with copaiba. The mean puncta area was increased in NPA, NPB, and NPC1 P1007A cells when treated with cannabidiol. Whilst the mean puncta area was increased for NPA and NPB when treated with cannabidiol, the total overall puncta area was significantly decreased in both cell lines. Similar significant decreases in sphingomyelin were observed in both NPC1 I1061T cells. Copaiba led to a significant reduction in total puncta area in all Niemann-Pick disease cells.

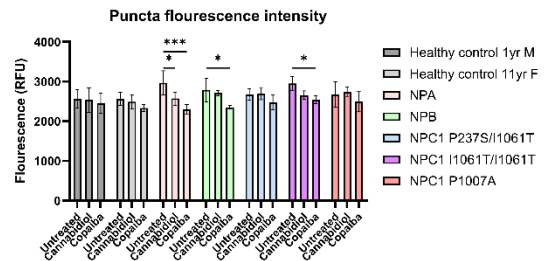
A significant reduction in puncta of sphingomyelin per area cell was observed in all cell lines, with cannabidiol leading to reductions in both NPA and NPB disease cells. In all cell lines copaiba significantly reduced the puncta per area cell of sphingomyelin.

Imaging sphingomyelin using a plate reader produced data consistent with the imaging assay (*Figure 5.9 (f)*), supporting the validity of the results obtained. Data from the plate reader showed that cannabidiol reduced total sphingomyelin in NPA and both NPC1 I1061T mutant cell lines. Copaiba treatment led to reduced sphingomyelin staining in NPA, NPB and NPC1 I1061T mutant cell lines.

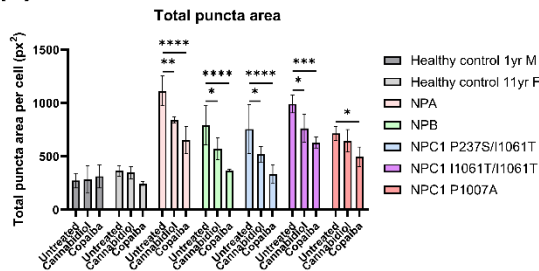
(a)



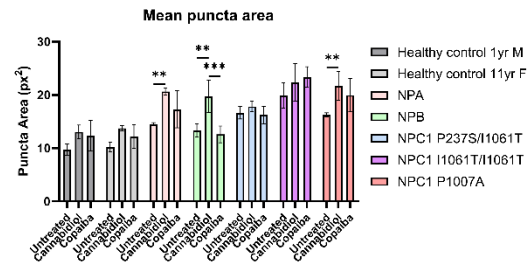
(b)



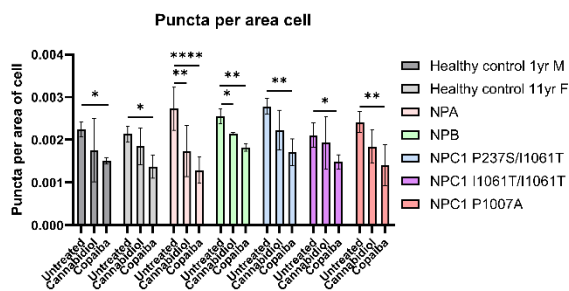
(c)



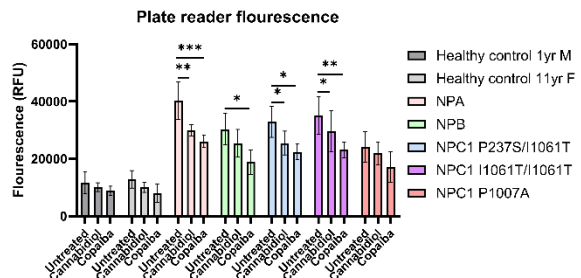
(d)



(e)



(f)



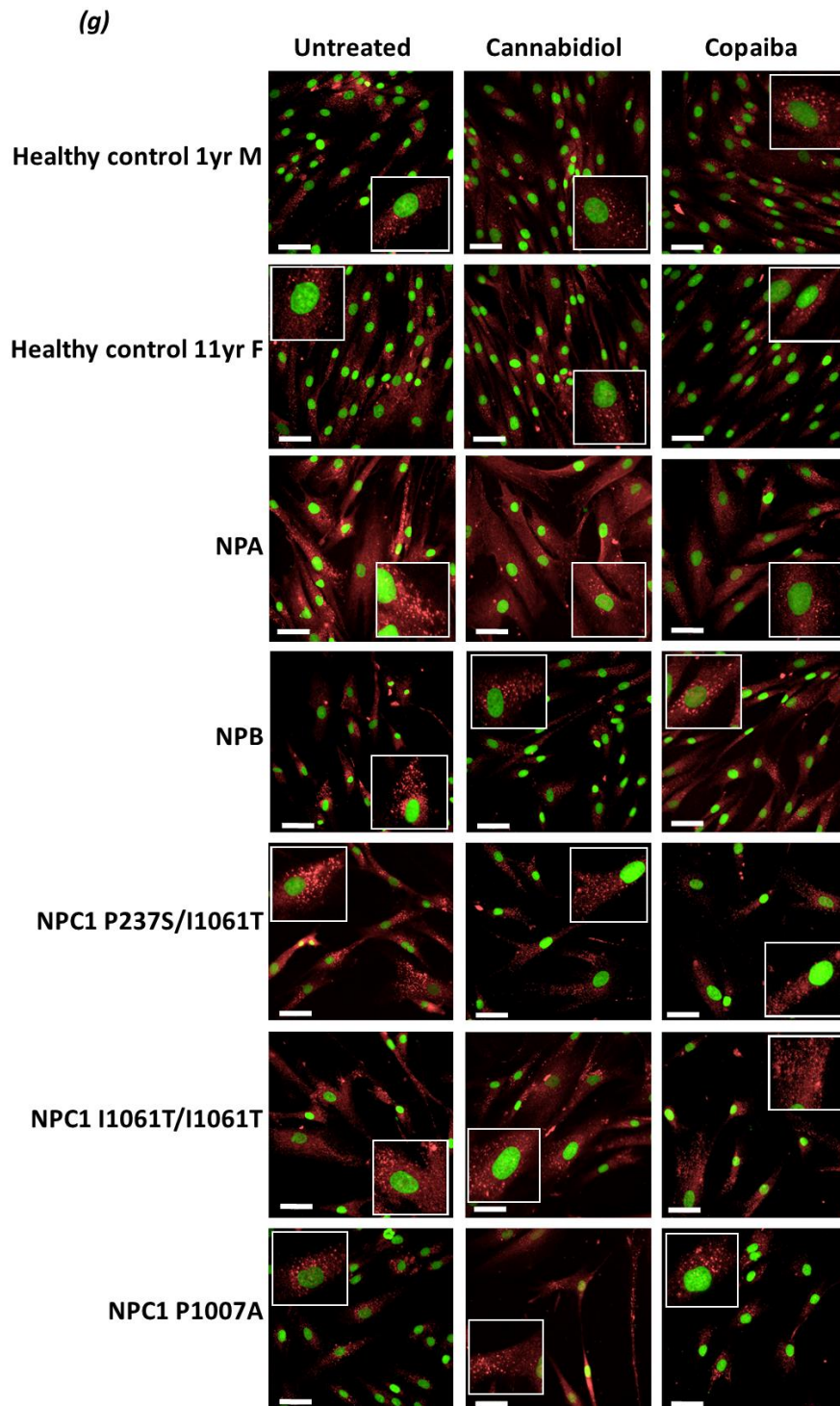


**Figure 5.9. Sphingomyelin storage is reduced in Niemann-Pick cells with cannabidiol or copaiba treatment**

Sphingomyelin storage in Niemann-Pick disease was probed using recombinant lysenin, followed by staining with an Anti-His Tag. In (a-e) various analysis parameters are shown when cells were imaged using an Operetta CLS. In (f) sphingomyelin storage was assessed using a plate reader to detect lysenin fluorescence. Representative images for each cell line and treatment are shown in (g). Statistical significance was calculated with a one-way ANOVA and a post-hoc Tukey's multiple comparison test.  $*=p<0.05$ ,  $**=p<0.01$ ,  $***=p<0.001$ ,  $*****=p<0.0001$ .  $N=3$  for all experiments, data shown is mean  $\pm$  SD. Scale bars represent  $50\mu\text{m}$ .

#### 5.2.4.2 Cholesterol

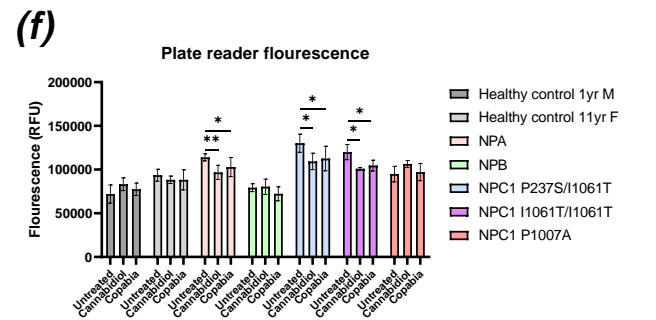
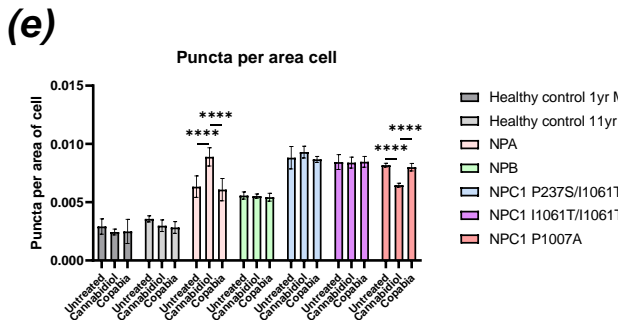
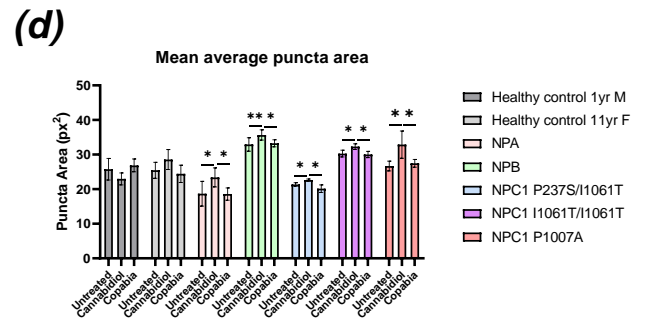
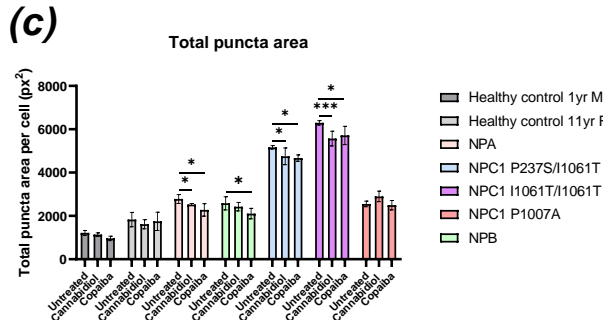
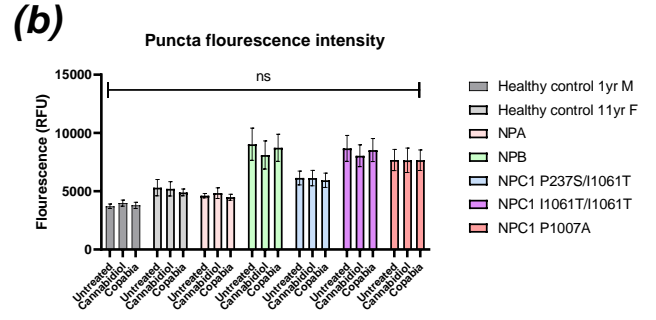
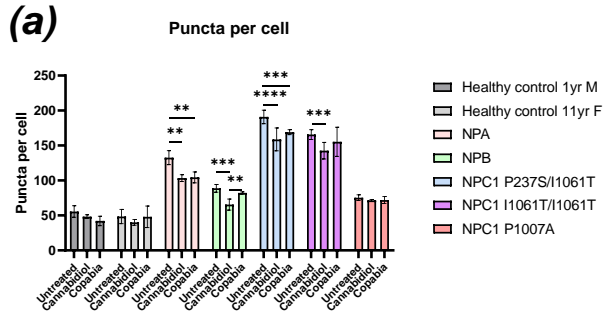
Cannabidiol and copaiba reduced the number of cholesterol puncta in NPA, NPB, and both NPC1 I1061T fibroblasts (*Figure 5.10(a)*). In the cell lines that showed an effect, cannabidiol reduced the number of puncta further than copaiba treatment. No change in the number of puncta was observed in either of the healthy controls, or NPC1 P1007A. Treatment with cannabidiol and copaiba does not lead to any significant changes in puncta fluorescence intensity, suggesting no change in the density of cholesterol in each puncta. Fluorescence intensity was highest in both NPC1 I1061T mutant cell lines, consistent with the known storage of cholesterol in the disease (*Figure 5.10(b)*).

Total area of cholesterol staining per cell was reduced in NPA and both NPC1 I1061T cells when treated with cannabidiol. Treating with copaiba reduced the total cholesterol staining in: NPA, NPB, and NPC1 I1061T fibroblasts (*Figure 5.10(c)*). Total cholesterol staining was highest in both NPC1 I1061T mutant cell lines, consistent with published data. No significant changes in cholesterol staining were observed in either of the healthy controls or the NPC1 P1007A.

Analysis of the mean puncta of cholesterol showed that cannabidiol treatment significantly increased mean puncta area in all Niemann-Pick disease cells but not controls (*Figure 5.10(d)*). No change in mean puncta area of cholesterol was observed when cells were treated with copaiba.

Comparison of the density of cholesterol puncta within the cell showed that cannabidiol treatment led to a significant increase in density of cholesterol in NPA (*Figure 5.10(e)*). Treatment of the NPC1 P1007A variant phenotype cells with cannabidiol led to a significant reduction in the density of cholesterol staining, when compared to both untreated and copaiba treated.

The plate reader data showed a significant decrease in cholesterol in NPA, and both NPC1 I1061T mutant cell lines, but not NPB or NPC1 P1007A, largely supportive of the imaging assay data. Both cannabidiol and copaiba produced similar decreases in filipin fluorescence, and thus cholesterol, in NPA and NPC1 I1061T mutant cell lines (*Figure 5.10(f)*).



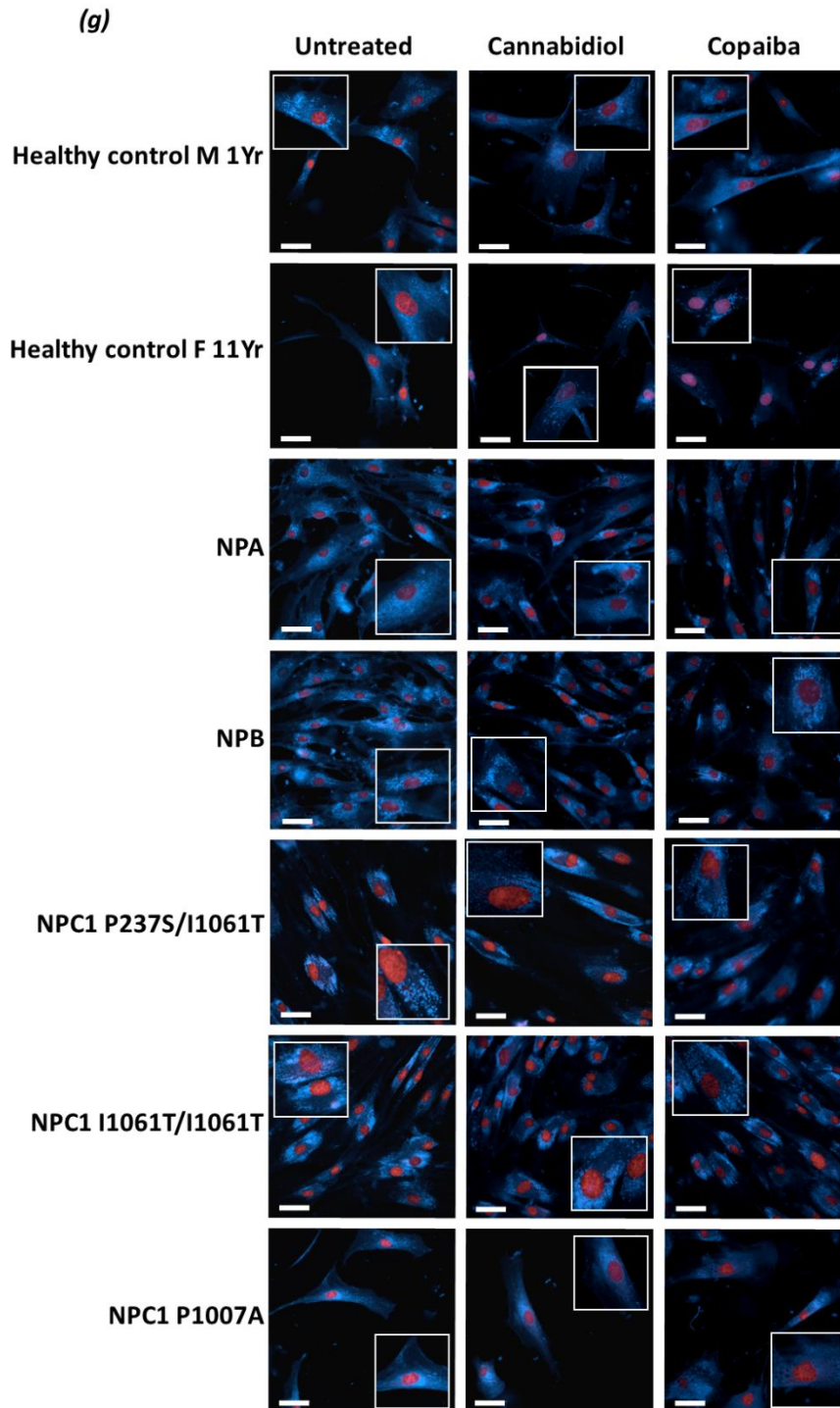


**Figure 5.10. Cannabidiol and copaiba reduces cholesterol storage in Niemann-Pick disease cells**

Cells were probed for cholesterol using filipin, a cholesterol specific probe. In (a-e) an Operetta CLS was used to generate data, with a Pherastar FSX used to generate data shown in (f). In (a) the mean puncta of cholesterol staining is shown, with corresponding puncta fluorescence intensity in (b). In (c) mean total puncta area of cholesterol per cell is shown, with the mean puncta area of region of cholesterol staining in (d). The density of cholesterol staining per cell is shown in (e). In (f) filipin staining was analysed using a plate reader to determine total cholesterol staining. In (g) reference images for each cell line, with each treatment method is shown. Statistical significance was calculated with a one-way ANOVA and a post-hoc Tukey's multiple comparison test.  $*=p<0.05$ ,  $**=p<0.01$ ,  $***=p<0.001$ ,  $****=p<0.0001$ .  $N=3$  for all experiments, data shown is mean  $\pm$  SD. Scale bars represent  $50\mu\text{m}$ .

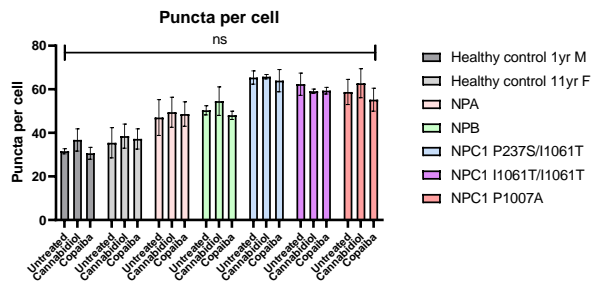
#### 5.2.4.3 Gangliosides GM1

Cellular GM1 localisation was probed using Cholera Toxin subunit B, conjugated to an Alexa Flour 594 fluorophore. No significant change in number of puncta of GM1 was observed in any of the cell lines when treated with cannabidiol or copaiba (*Figure 5.11(a)*). However, compared to untreated cells, puncta fluorescence intensity was increased following cannabidiol treatment in NPA in both NPC I1061T cell lines.

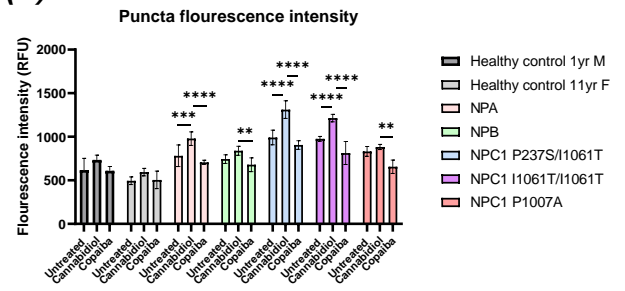
Cannabidiol increased significantly the total puncta area in both NPA and NPB cell lines, however no significant changes were observed in any of the NPC disease cell lines (*Figure 5.11(c)*). Treating NPC1 I1061T fibroblast lines with copaiba showed a significantly decreased total puncta area, corresponding with a decrease in mean puncta area, observed in NPA, NPB and both NPC1 I1061T mutant cell lines (*Figure 5.11(d)*).

No significant change in the density of GM1 puncta was observed in any of the cell lines when treated with cannabidiol or copaiba (*Figure 5.11(e)*). Comparison of total puncta area to plate reader fluorescence shows a reduction in the differences observed when the data is generated using a plate reader. When GM1 staining is analysed using a plate reader, only copaiba treatment of NPC1 I1061T mutants showed a significant reduction (*Figure 5.11(f)*).

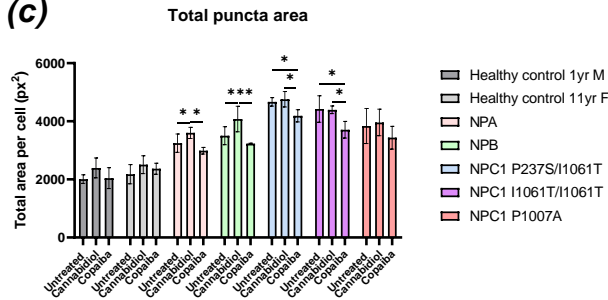
(a)



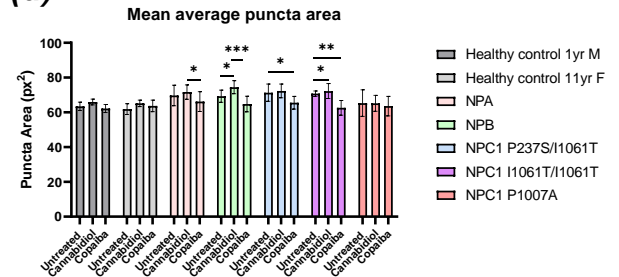
(b)



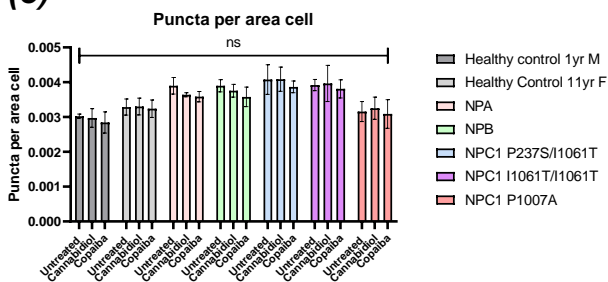
(c)



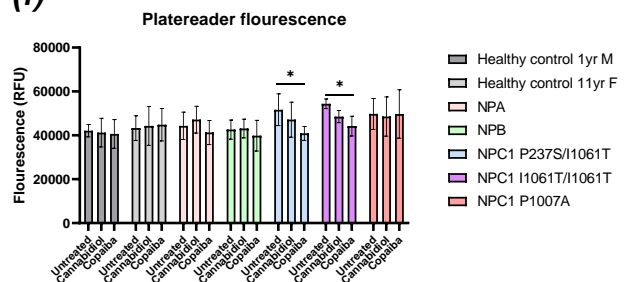
(d)



(e)



(f)



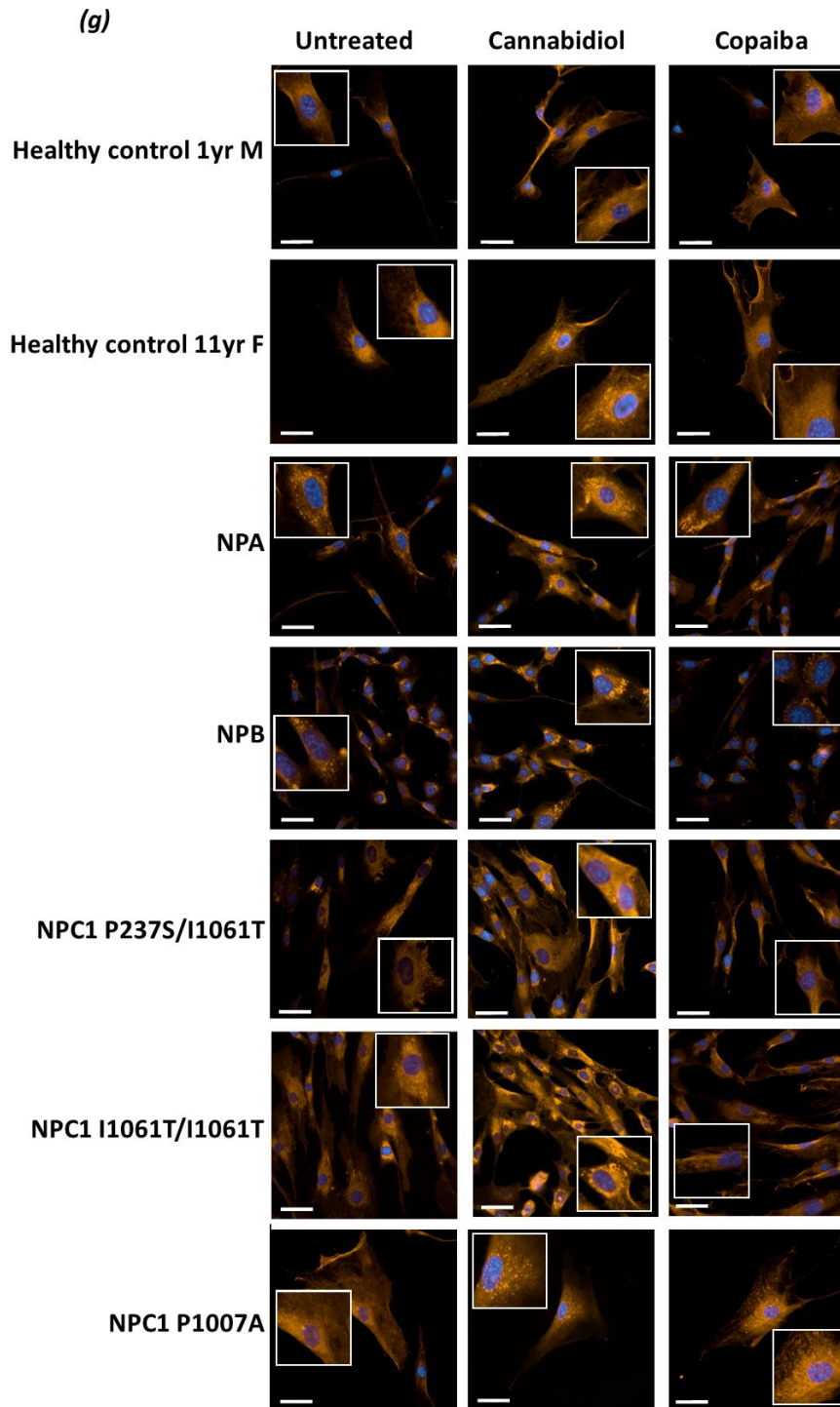


**Figure 5.11. Changes in GM1 staining with cannabidiol and copaiba are Niemann-Pick disease mutation dependant**

Cells were probed with CTxB to identify ganglioside GM1 localisation. Data in panels (a-e) were generated using an Operetta CLS, with panel (f) being generated using a Pherastar FSX. Mean number of puncta per cell is shown in (a), with the corresponding puncta fluorescence intensity shown in (b). The total puncta area of GM1 staining per cell is shown in (c), with the average area of GM1 puncta is shown in (d). The density of GM1 staining per cell is shown in (e). In (f) the total GM1 staining is shown as determined using a plate reader. In (g) reference images for each cell line with each treatment are shown. Statistical significance was calculated with a one-way ANOVA and a post-hoc Tukey's multiple comparison test.  $*=p<0.05$ ,  $**=p<0.01$ ,  $***=p<0.001$ ,  $****=p<0.0001$ .  $N=3$  for all experiments, data shown is mean  $\pm$  SD. Scale bars represent  $50\mu\text{m}$ .

#### 5.2.4.4 LBPA

LBPA, a lysosomal membrane lipid, is found only in late endosomes and lysosomes, and is a marker of lysosomal storage. For puncta per cells, cannabidiol led to a significant reduction in both NPA and NPB cell lines, however no change was observed in NPC fibroblasts.

Copaiba only showed a significant reduction in NPA fibroblasts (*Figure 5.12a*).

Treatment with cannabidiol significantly increased puncta fluorescence intensity across all cell lines, including both healthy controls and NPC1 P1007A (*Figure 5.12b*). Treatment with cannabidiol led to significant reductions in the total puncta area of LBPA staining in both NPA and NPB, but not NPC cells. Treatment with copaiba only led to a significant reduction in total puncta area in NPA fibroblasts (*Figure 5.12c*).

No significant change in the mean puncta area was observed in any of the cell lines when treated with either cannabidiol or copaiba (*Figure 5.12d*). A similar lack of change was also observed in the density of LBPA staining, as no change was observed in any of the cell lines, when treated with cannabidiol or copaiba (*Figure 5.12e*).

Analysis of LBPA staining by plate reader showed a similar pattern to that of the imaging data. Similar to the total puncta area data, the only significant change in the plate reader data was that treating NPA cells with cannabidiol significantly reduced LBPA staining (*Figure 5.12(f)*).



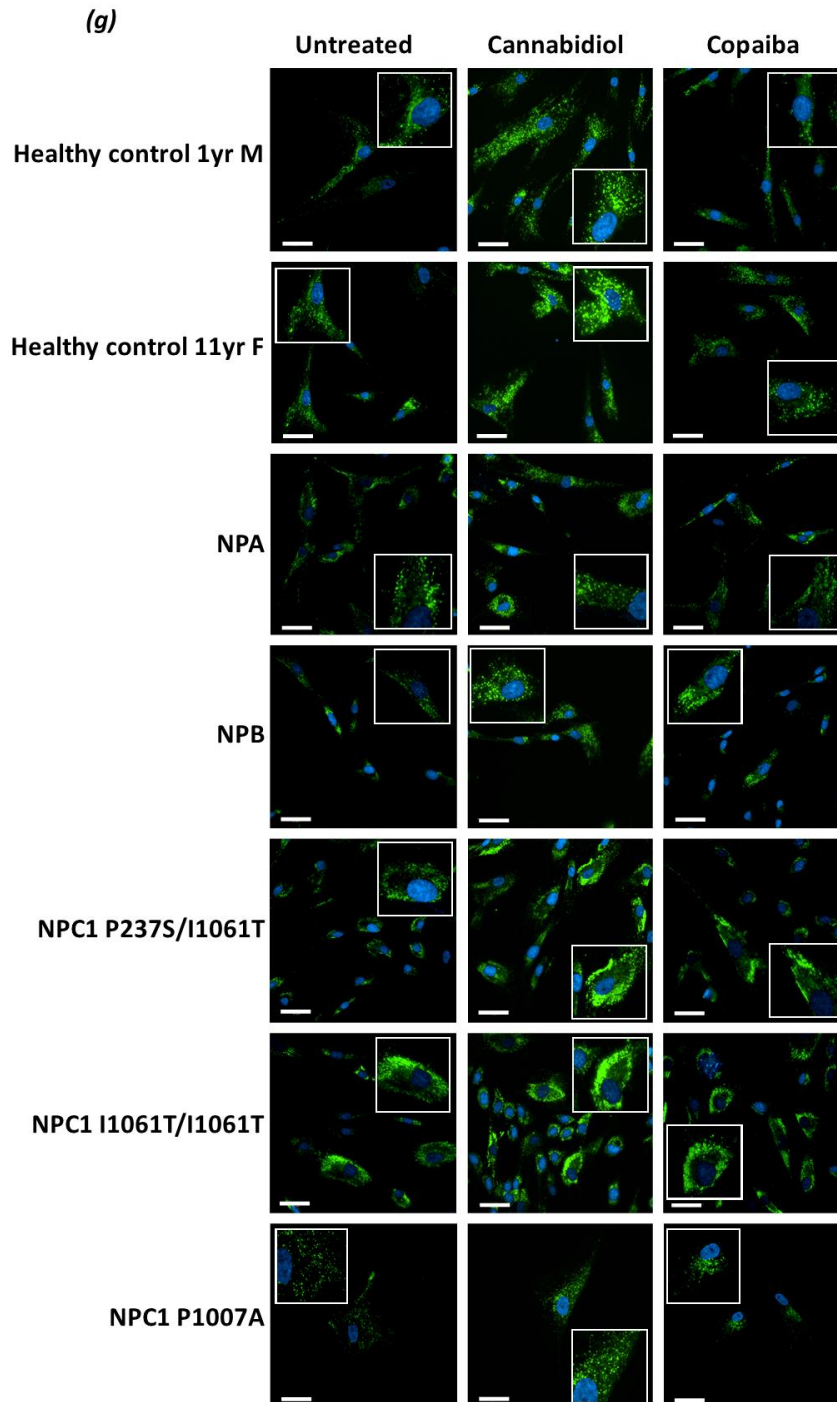


**Figure 5.12. Cannabidiol and copaiba treatment decreases LBPA staining In Niemann-Pick disease Type A & B fibroblasts**

LBPA localisation was probed with an anti-LBPA antibody, in conjunction with the corresponding Alexaflour 488 secondary antibody. Data shown in (a-e) was generated using an Operetta CLS, with data in (f) being generated using a Pherastar FSX. In (a) the mean number of puncta of LBPA per cell is shown for each cell line, with (b) showing the corresponding puncta fluorescence intensity. In (c) the total area of LBPA staining is shown, with the mean puncta area of LBPA staining shown in (d). In (e) the density of LBPA per staining, (f) shows the total LBPA staining when analysed using a plate reader. Images in (g) show reference images for each cell line and treatment. Statistical significance was calculated with a one-way ANOVA and a post-hoc Tukey's multiple comparison test.  $*=p<0.05$ ,  $**=p<0.01$ ,  $***=p<0.001$ ,  $*****=p<0.0001$ .  $N=3$  for all experiments, data shown is mean  $\pm$  SD. Scale bars represent  $50\mu\text{m}$ .

## *5.2.5 Effects of cannabidiol and copaiba upon aSMase activity*

### *5.2.5.1 Stimulation of aSMase activity in Niemann-Pick disease fibroblasts by cannabidiol*

To determine whether reductions in sphingomyelin storage are due to increased aSMase activity, cells were treated with cannabidiol for 48 hours and aSMase activity assessed as described in section 2.4.1.2.

In all cell lines, except NPC1 P1007A where there was a decrease in aSMase activity, cannabidiol treatment increased aSMase activity (*Figure 5.13*). This increase was concentration dependent and followed a bell-shaped curve, with the highest increase observed at 15uM.

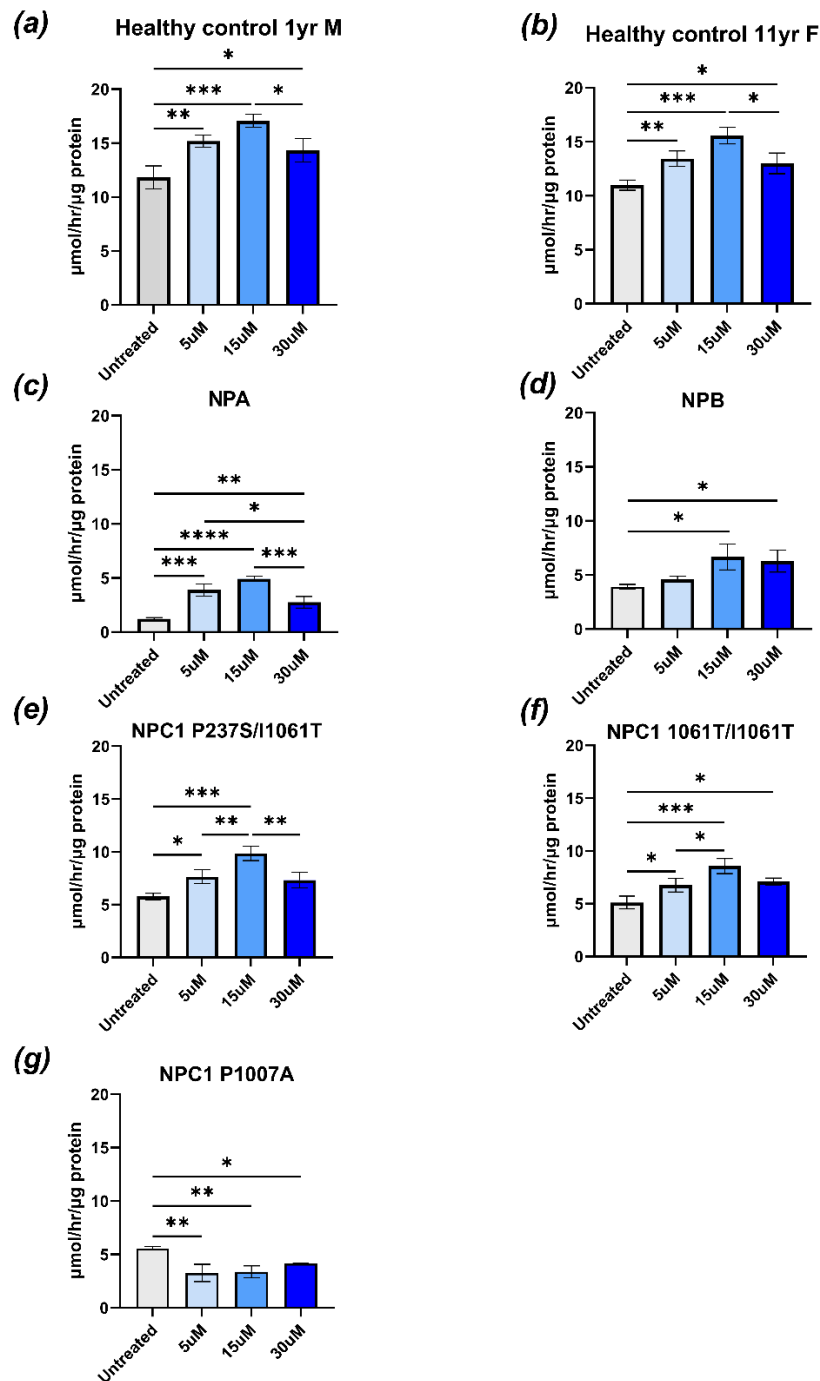


**Figure 5.13. Comparison of acid sphingomyelinase activity in Niemann-Pick disease patient derived fibroblasts and healthy control fibroblasts cell lines treated with cannabidiol**

In (a-g) cells were treated with a range of cannabidiol concentrations for 48 hours. Cells were homogenised, and aSMase activity determined by a biochemical fluorogenic substrate based aSMase activity assay, as outlined in 2.4.1.2. Statistical significance was calculated with a one-way ANOVA and a post-hoc Tukey's multiple comparison test. \*= $p < 0.05$ , \*\*= $p < 0.01$ , \*\*\*= $p < 0.001$ , \*\*\*\*= $p < 0.0001$ .  $N=3$  for all experiments, data shown is mean  $\pm$  SD.

### 5.2.5.2 Comparison of change in aSMase activity when fibroblasts are treated with cannabidiol

Comparison of the fold change in aSMase in cells treated with 15 $\mu$ M compared to untreated cells showed significant differences between disease cells. Both healthy controls showed a small increase in aSMase with the 1-year-old male having a 1.4-fold increase and the 11-year-old female a 1.3-fold increase.

NPA cells showed the most significant increase in aSMase activity with a 4-fold increase in aSMase activity, compared to the 2-fold increase observed in NPB cells. The classical phenotype NPC cells showed a similar response to cannabidiol treatment with the P237S/I1061T cell line having a 1.7-fold increase and the I1061T/I1061T cell line a 1.7-fold increase. The NPC1 P1007A cell line was the only cell line to show a decrease in aSMase activity with a 0.5-fold change.

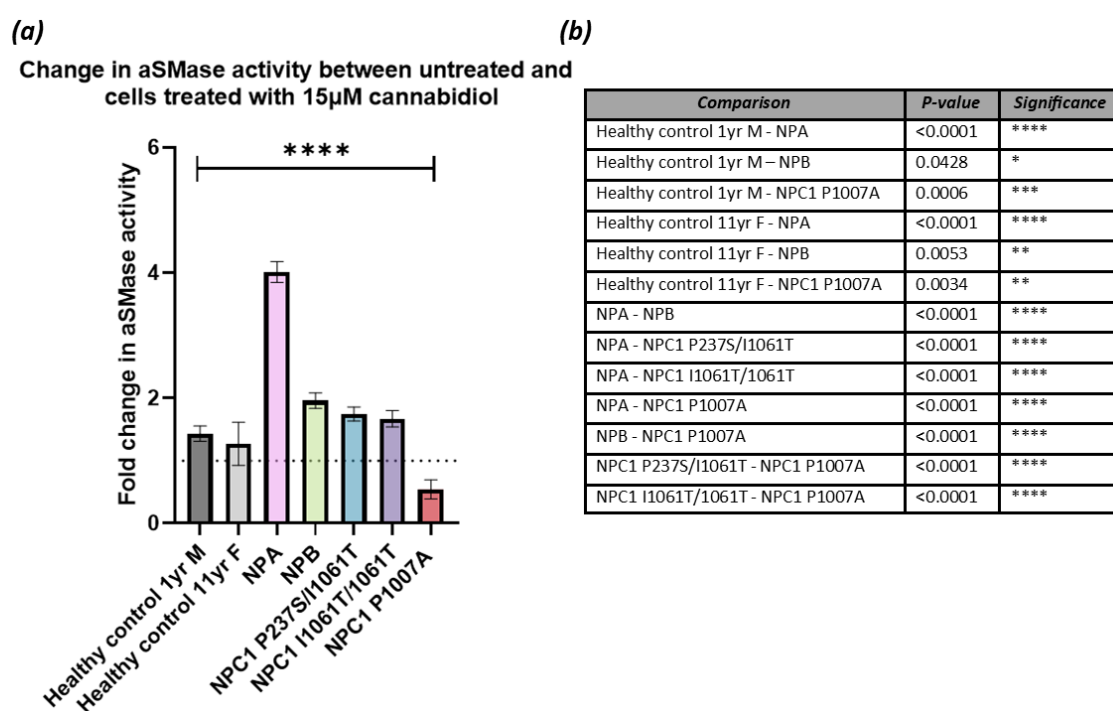


**Figure 5.14. Comparison of the fold change in acid sphingomyelinase activity between untreated and cells treated with 15 $\mu$ M cannabidiol**

(a) Fold change in aSMase activity at 15 $\mu$ M cannabidiol compared to untreated control for the corresponding cell line. In (b) a table of all statistical significance between cell lines is shown. Cells were treated for 48 hours followed by homogenisation, and aSMase activity determined by a biochemical fluorogenic substrate based aSMase activity assay, as outlined in 2.4.1. Statistical significance was calculated with a one-way ANOVA and a post-hoc Tukey's multiple comparison test. \*= $p$ <0.05, \*\*= $p$ <0.01, \*\*\*= $p$ <0.001, \*\*\*\*= $p$ <0.0001.  $N=3$  for all experiments, data shown is mean  $\pm$  SD.

### 5.2.5.3 Treating Niemann-Pick fibroblasts with copaiba increases aSMase activity

Cells treated with copaiba showed differing effects based on genotype. The healthy controls did not show any change in aSMase activity after being treated with any of the copaiba concentrations (*Figure 5.15(a&b)*).

NPA cells (*Figure 5.15(c)*) showed a stepwise increase in aSMase activity with increasing copaiba concentrations, from a baseline activity of 3  $\mu\text{mol/hr}/\mu\text{g}$  to an activity of 7  $\mu\text{mol/hr}/\mu\text{g}$  at 10  $\mu\text{g/ml}$  of copaiba. NPB cells (*Figure 5.15(d)*) showed a less pronounced effect upon copaiba treatment than the NPA cell line, with a significant increase only observed at 10  $\mu\text{g/ml}$ .

NPC I1061T cells (*Figure 5.15(e&f)*) show a similar trend to NPA, with increasing concentrations of copaiba leading to increased aSMase activity. However, only the increase in aSMase activity at 10  $\mu\text{g/ml}$  was significant. Copaiba treatment did not alter aSMase activity in NPC1 P1007A cells (*Figure 5.15(g)*).

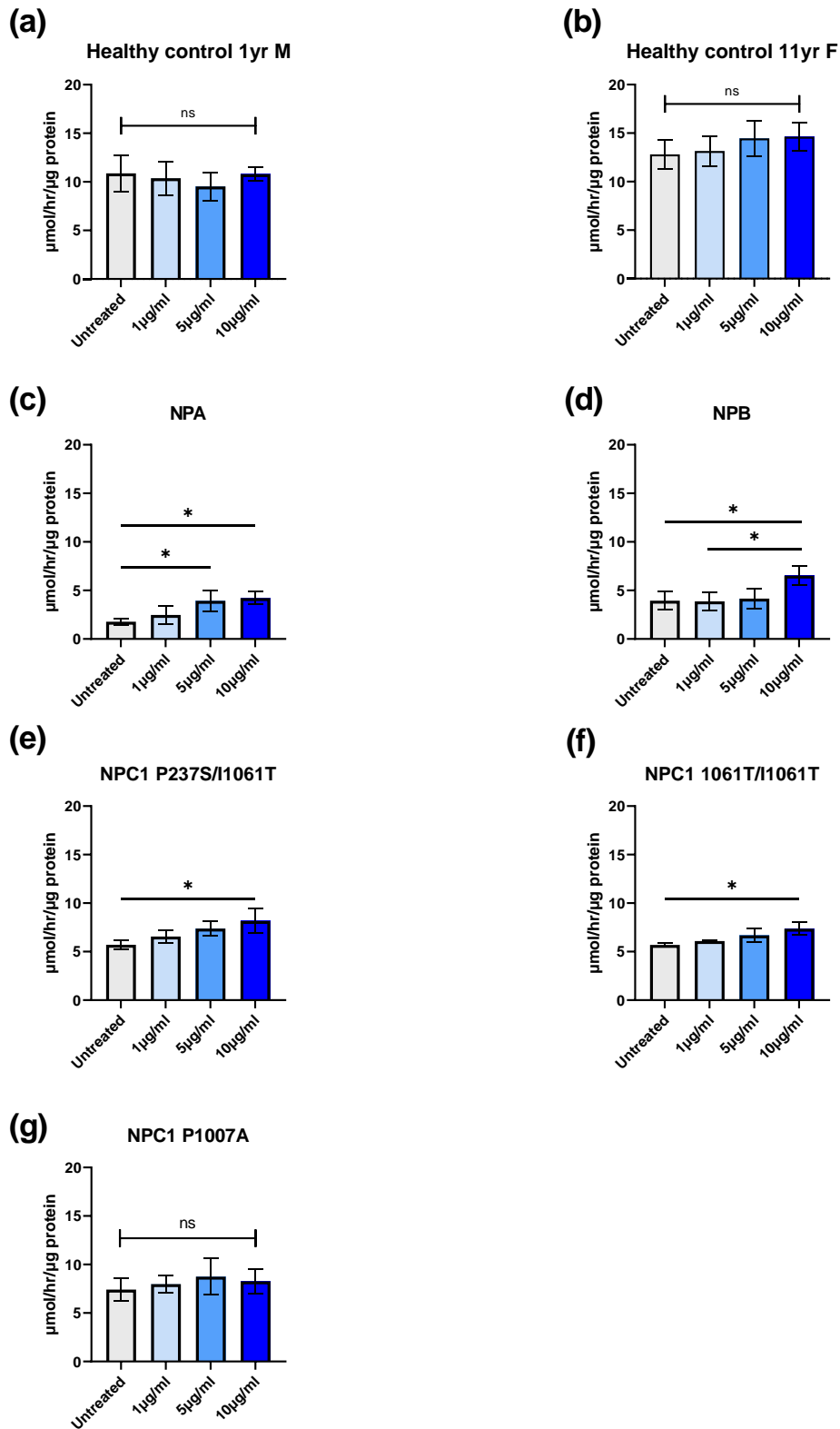


**Figure 5.15. Comparison of acid sphingomyelinase activity in Niemann-Pick disease patient derived fibroblasts and healthy control fibroblasts treated with copaiba oil for 48-hours**

In (a-g) aSMase activity assay was determined after fibroblasts were treated with varying concentrations of copaiba oil for 48 hours, prior to homogenisation. aSMase activity was determined using a plate-based assay as outlined in 2.4.1.2. Statistical significance was calculated with a one-way ANOVA and a post-hoc Tukey's multiple comparison test. \*= $p < 0.05$ , \*\*= $p < 0.01$ , \*\*\*= $p < 0.001$ , \*\*\*\*= $p < 0.0001$ .  $N=3$  for all experiments, data shown is mean  $\pm$  SD.

#### 5.2.5.4 Comparison of change in aSMase activity between fibroblast cell lines when treated with copaiba

The comparison of the fold change in aSMase activity, following treatment with copaiba showed that in healthy cells copaiba has minimal effect upon aSMase activity (Figure 5.16). In the 1-year male, copaiba had no effect upon aSMase activity, and in the 11-year-old female, a 1.15-fold increase was observed. However, copaiba led to a 2.5-fold increase in aSMase activity in NPA cells when treated with 10µg/ml copaiba, and a 1.4-fold increase in NPB. Both NPC1 I1061T mutants showed an approximately 1.3-fold increase in aSMase activity, higher than the 1.1-fold increase observed in the NPC1 P1007A cell line. Of the Niemann-Pick disease cells, an increase in fold change in activity compared to controls was only seen for NPA.

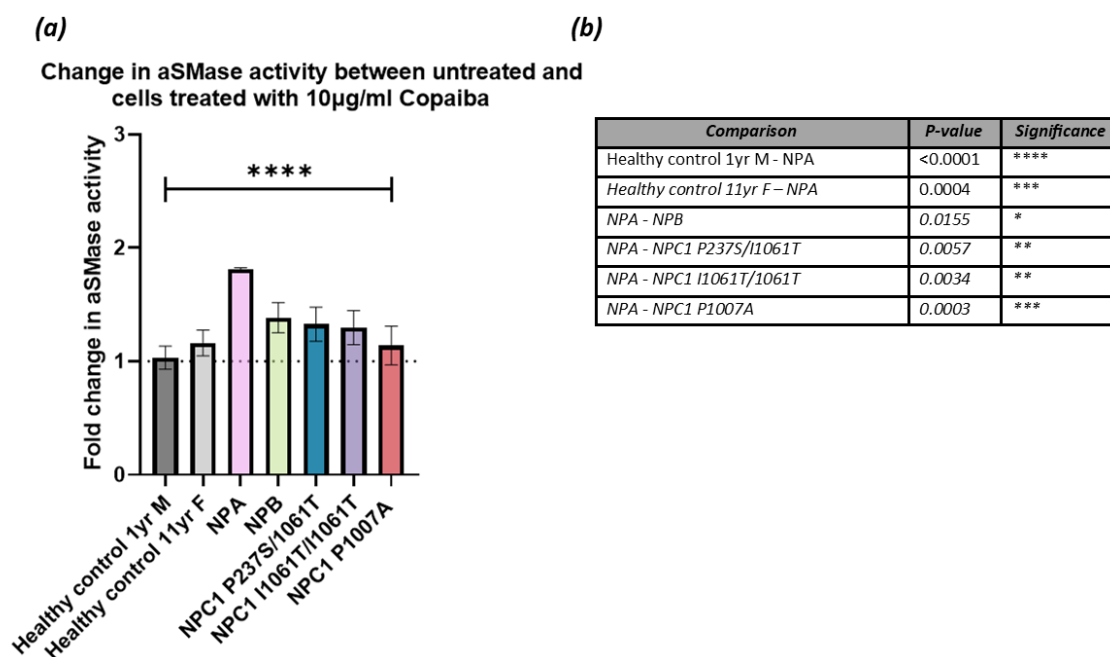


**Figure 5.16. Treatment of cells with copaiba oil leads to increased acid sphingomyelinase activity when compared to an untreated control.**

(a) Fold change in aSMase activity at 10µg/ml copaiba compared to untreated control for the corresponding cell line. In (b) a table of all statistical significance between cell lines is shown. Cells were treated for 48 hours followed by homogenisation, and aSMase activity determined by a biochemical fluorogenic substrate based aSMase activity assay, as outlined in 2.4.1.2. Statistical significance was calculated with a one-way ANOVA and a post-hoc Tukey's multiple comparison test. \*=p<0.05, \*\*=p<0.01, \*\*\*=p<0.001, \*\*\*\*=p<0.0001. N=3 for all experiments, data shown is mean ± SD.

## *5.2.6 Treatment of cell homogenate with cannabidiol and copaiba*

### *5.2.6.1 Treatment of cell homogenate with cannabidiol does not lead to the same increase in aSMase activity as treating live cells with cannabidiol*

As we had shown in section 3.6 that when cells are treated with cannabidiol, aSMase activity was increased, we next decided to determine whether cannabidiol was acting directly on aSMase or activating intracellular pathways leading to its increased activity. To assess this, cell homogenate was treated with 15 $\mu$ M cannabidiol for 1 hour and aSMase activity assessed.

The data shown in *Figure 5.17* clearly shows that whilst treating cells with cannabidiol increases aSMase activity, treating cell homogenate with cannabidiol does not increase aSMase activity. Therefore, it can be surmised that cannabidiol is not directly acting on aSMase, instead modulating pathways that lead to the effects observed.

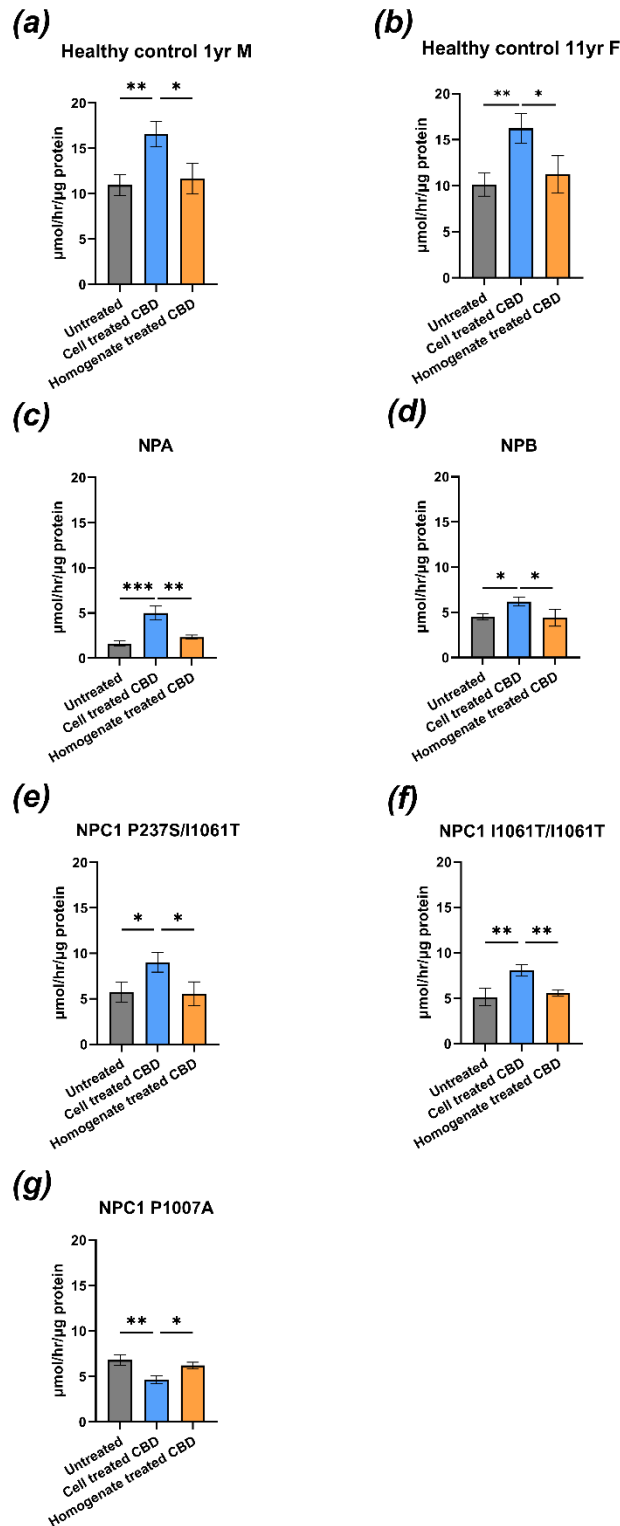


**Figure 5.17. Treatment of cell pellets with cannabidiol does not cause an increase in acid sphingomyelinase activity.**

In (a-g) cell lines were treated with cannabidiol both before and after homogenisation. For the cell treated with cannabidiol samples, cells were incubated with cannabidiol for 48 hours and subsequently homogenised, whereas for the homogenate treated samples, untreated cell pellets were treated with cannabidiol for 1 hour after homogenisation. Statistical significance was calculated with a one-way ANOVA and a post-hoc Tukey's multiple comparison test.  $*$ = $p<0.05$ ,  $**$ = $p<0.01$ ,  $***$ = $p<0.001$ ,  $****$ = $p<0.0001$ .  $N=3$  for all experiments, data shown is mean  $\pm$  SD.

### 5.2.6.2 *Treating cell homogenate with copaiba does not increase aSMase activity*

As we had shown in 5.2.5.2 that when Niemann-Pick disease fibroblasts are treated with copaiba, there is a significant increase in aSMase activity, we wanted to determine if copaiba is directly acting on aSMase or on upstream pathways. To do this, aSMase activity was compared between cells treated with copaiba and untreated cell homogenate that was incubated with copaiba.

The data in *Figure 5.18* clearly shows that treating cell homogenate with copaiba does not increase aSMase activity in any of the cells tested indicating that there is no direct effect on aSMase.

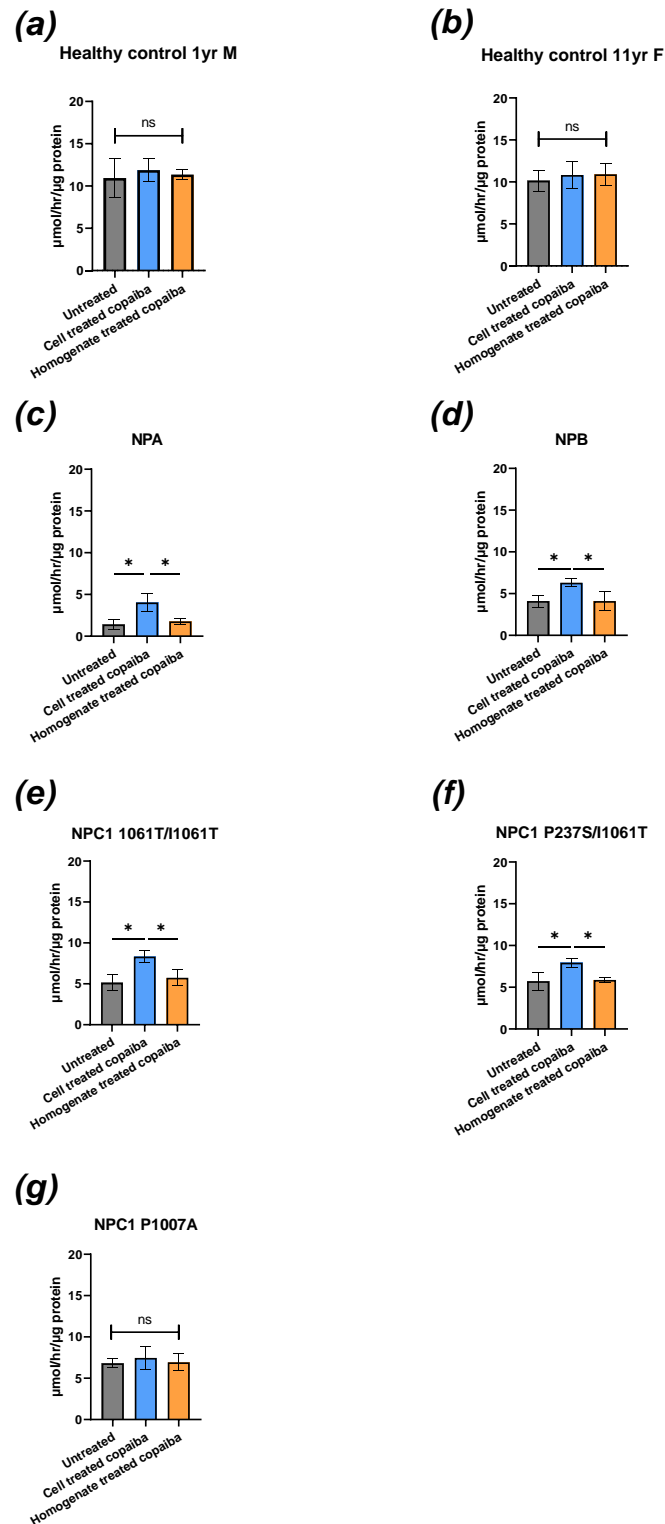


**Figure 5.18. Treating cell homogenate with copaiba does not produce the same increase in acid sphingomyelinase activity as treating cells with copaiba**

In (a-g) cell lines were treated with copaiba both before and after homogenisation. For the cell treated with copaiba samples, cells were incubated with copaiba for 48 hours and subsequently homogenised, whereas for the homogenate treated samples, untreated cell pellets were treated with copaiba for 1 hour after homogenisation. Statistical significance was calculated with a one-way ANOVA and a post-hoc Tukey's multiple comparison test. \*= $p < 0.05$ , \*\*= $p < 0.01$ , \*\*\*= $p < 0.001$ , \*\*\*\*= $p < 0.0001$ .  $N=3$  for all experiments, data shown is mean  $\pm$  SD.

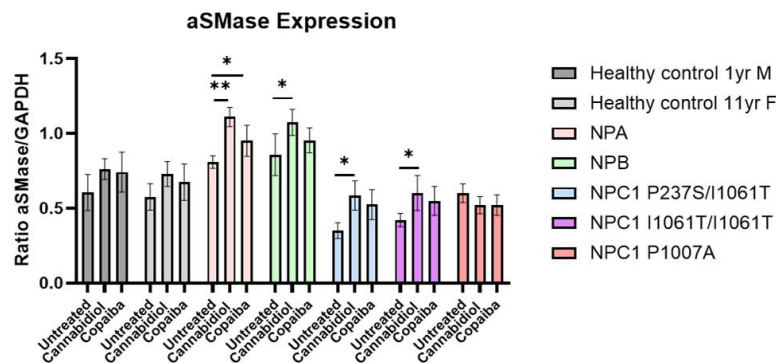
## 5.2.7 Analysis of protein expression upon cannabidiol and copaiba treatment

### 5.2.7.1 Acid Sphingomyelinase

As we had shown that aSMase activity was increasing aSMase activity, whilst not acting on the enzyme directly, we hypothesised that cannabidiol and copaiba were increasing aSMase expression.

No significant changes in aSMase expression were observed in either healthy control cell lines following treatment. For the Niemann-Pick cells, cannabidiol treatment increased aSMase expression in all cells except NPC1 P1007A. The biggest increase was observed in NPC1 I106T, with an approximate 50% elevation in aSMase levels in both cell lines. Copaiba treatment increased aSMase levels only in NPA. These data are consistent with the effects of cannabidiol and copaiba on aSMase activity in treated cells, suggesting that increased expression is responsible for the observed increases in activity.

(a)



(b)

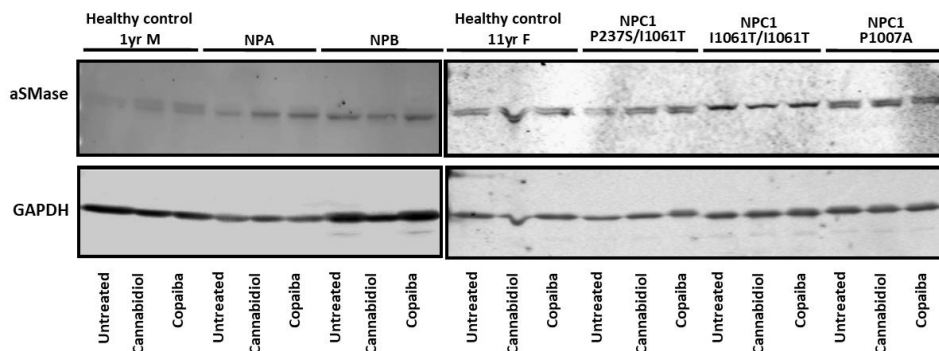


**Figure 5.19. Cannabidiol significantly increases acid sphingomyelinase expression in Niemann-Pick disease cells**

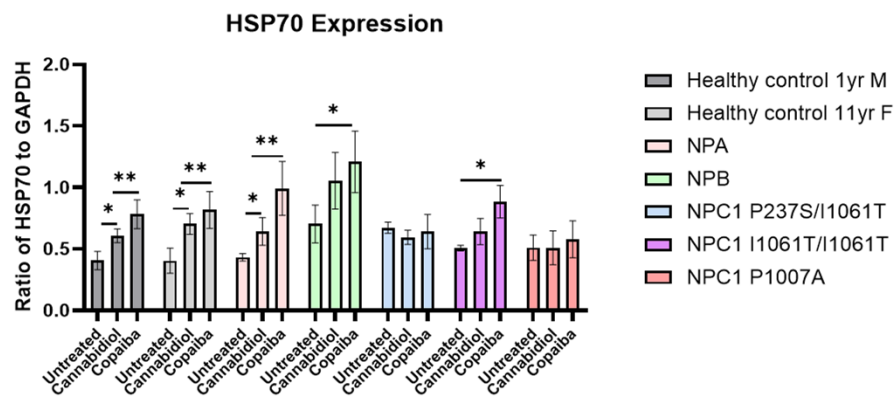
aSMase expression in fibroblasts treated with cannabidiol or copaiba for 48 hours and probed with an aSMase antibody and GAPDH Species specific fluorophore secondary antibodies were used, and membranes imaged using a LI-COR Odyssey CLx. Statistical significance was calculated with a one-way ANOVA and post-hoc Tukey's multiple comparison test.  $*=p<0.05$ ,  $**=p<0.01$ ,  $***=p<0.001$   $****=p<0.0001$ .  $N=3$  for all experiments, data shown is mean  $\pm$  SD.

### 5.2.7.2 Heat shock protein 70

Heat shock proteins (HSP) upregulation is known to reduce sphingomyelin storage, through improving lysosomal stability by recruiting LBPA to the lysosome. It is also possible that HSP proteins may be chaperoning aSMase to the lysosome, thus increasing the amount of partially functional aSMase within the lysosome in NPA and NPB.

Cannabidiol significantly increased expression of HSP70 in both healthy controls, and NPA. Whilst not significant a similar trend is observed in NPB and NPC1 I1061T. Copaiba significantly increased the expression of HSP in both healthy control cell lines, NPA, NPB and the NPC1 I1061T/I106T mutant cell lines. Copaiba also led to a higher level of HSP70 expression in cells when compared to cannabidiol. Of note is the NPC1 P237S/I1061T did not show a significant change in HSP70 expression. The change in HSP70 expression does not correlate with the observed increases in aSMase activity, meaning that a chaperone effect is an unlikely explanation.

(a)



(b)

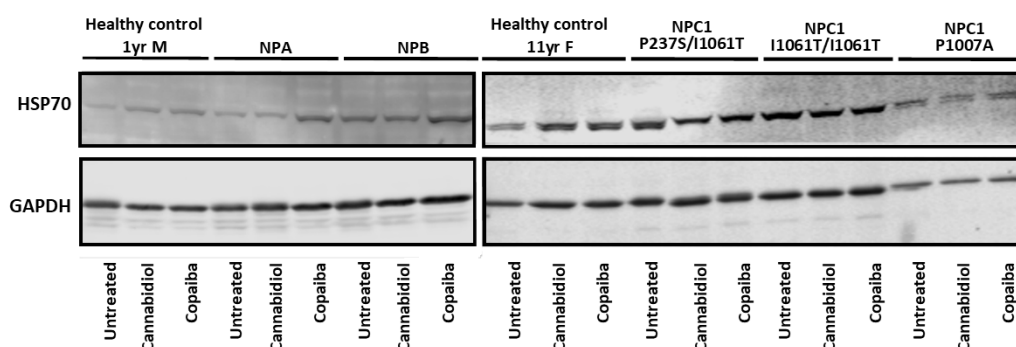


**Figure 5.20. Heat shock protein 70 expression is increased by cannabidiol or copaiba treatment**

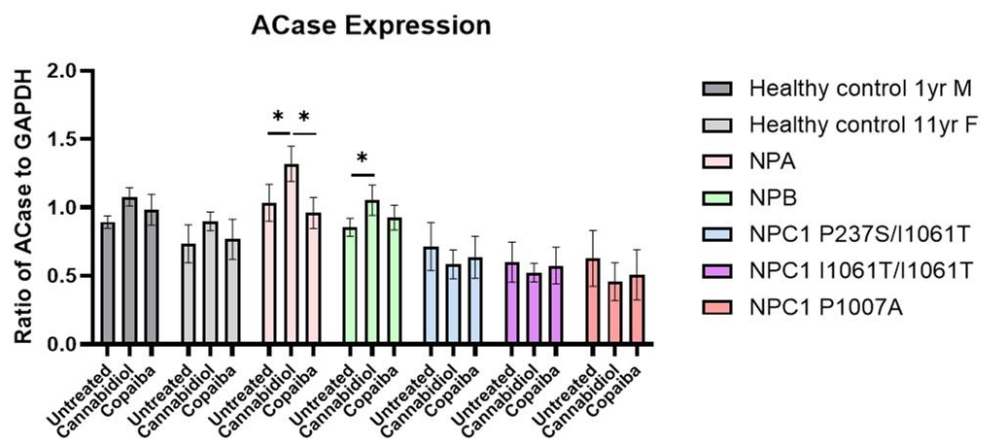
Expression of HSP70 was probed using western blotting. HSP70 and GAPDH specific antibodies were used with fluorophore conjugated species-specific secondary antibodies. Membranes were imaged using a LI-COR Odyssey CLx. Statistical significance was calculated with a one-way ANOVA and a post-hoc Tukey's multiple comparison test. \*= $p < 0.05$ , \*\*= $p < 0.01$ , \*\*\*= $p < 0.001$ , \*\*\*\*= $p < 0.0001$ .  $N=3$  for all experiments, data shown is mean  $\pm$  SD.

### 5.2.7.3 Acid Ceramidase

As acid ceramidase (ACase) is the next enzyme in the sphingomyelin degradation pathway after acid sphingomyelinase, it is possible that restoring aSMase activity through cannabidiol or copaiba treatment may alter ACase activity or expression.

Only NPA and NPB showed a significant difference (increase) in ACase expression when treated with cannabidiol. No significant change in ACase expression was observed when any cell line tested was treated with copaiba. It is possible that the increased ACase expression in NPA and NPB may be to compensate for the increase in ceramide being produced by the increase in aSMase activity upon cannabidiol treatment.

(a)



(b)

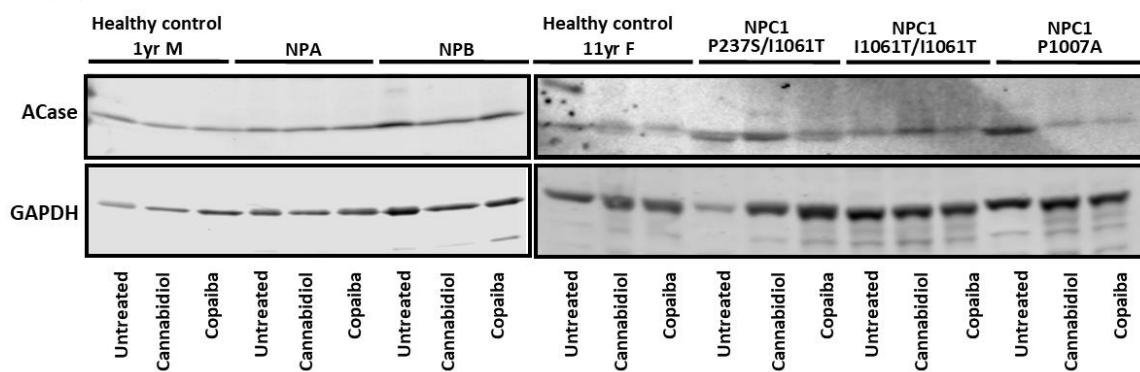


**Figure 5.21. Cannabidiol increases acid ceramidase expression in acid sphingomyelinase deficient cell lines**

Expression of ACCase was probed through western blotting, with specific ACCase antibody, and GAPDH, used as a standardisation loading control. Species specific fluorophore conjugated species-specific secondary antibodies were used. Membranes were imaged using a LI-COR Odyssey CLx. Statistical significance was calculated with a one-way ANOVA and a post-hoc Tukey's multiple comparison test. \*= $p < 0.05$ , \*\*= $p < 0.01$ , \*\*\*= $p < 0.001$ , \*\*\*\*\*= $p < 0.0001$ .  $N=3$  for all experiments, data shown is mean  $\pm$  SD.

## 5.2.8 Cannabidiol and copaiba effects upon transcription in Niemann-Pick

### 5.2.8.1 TFE3 Nuclei localisation

We have shown that both aSMase activity and aSMase expression was increased when treated with cannabidiol or copaiba. SMPD1, the gene responsible for aSMase, forms part of the CLEAR network, thus is regulated by the TFEB family of transcription factors.

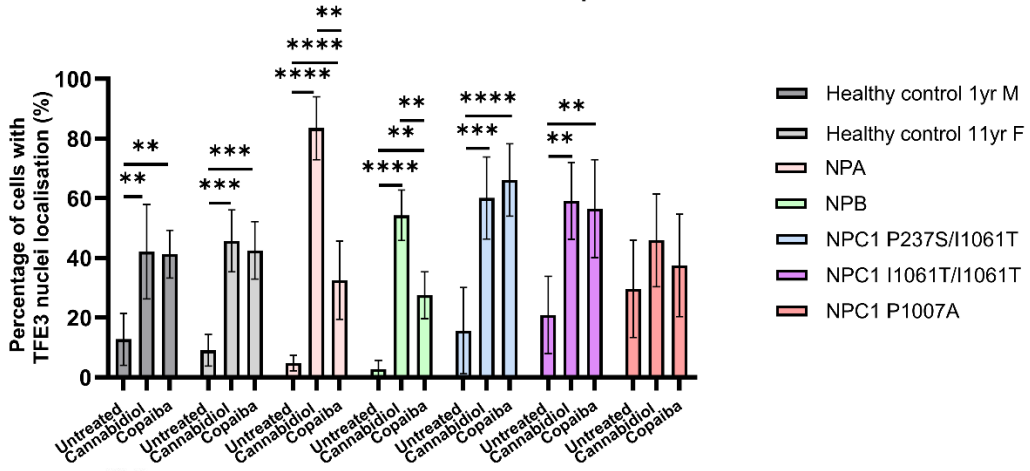
One of the most abundant TFEB transcription factors in fibroblast cells is TFE3, which under periods of no lysosome biogenesis or autophagy, can be found diffusely distributed within the cytosol. However, under times of lysosomal biogenesis, TFE3 localised to the nuclei, leading to upregulated transcription of several lysosomal genes, including those of the CLEAR network. Thus, cells showing nuclear TFE3 localisation can be postulated to be upregulating the expression of aSMase.

The data in *Figure 5.22* shows that cannabidiol increases TFE3 nuclear translocation. Cannabidiol led to a significant increase in all cells, except NPC P1007A; probably due to constitutively high TFE3 nuclear localisation. NPA cells showed the most significant change, with TFE3 nuclear localisation increasing from a baseline of 5% up to 85% upon cannabidiol treatment.

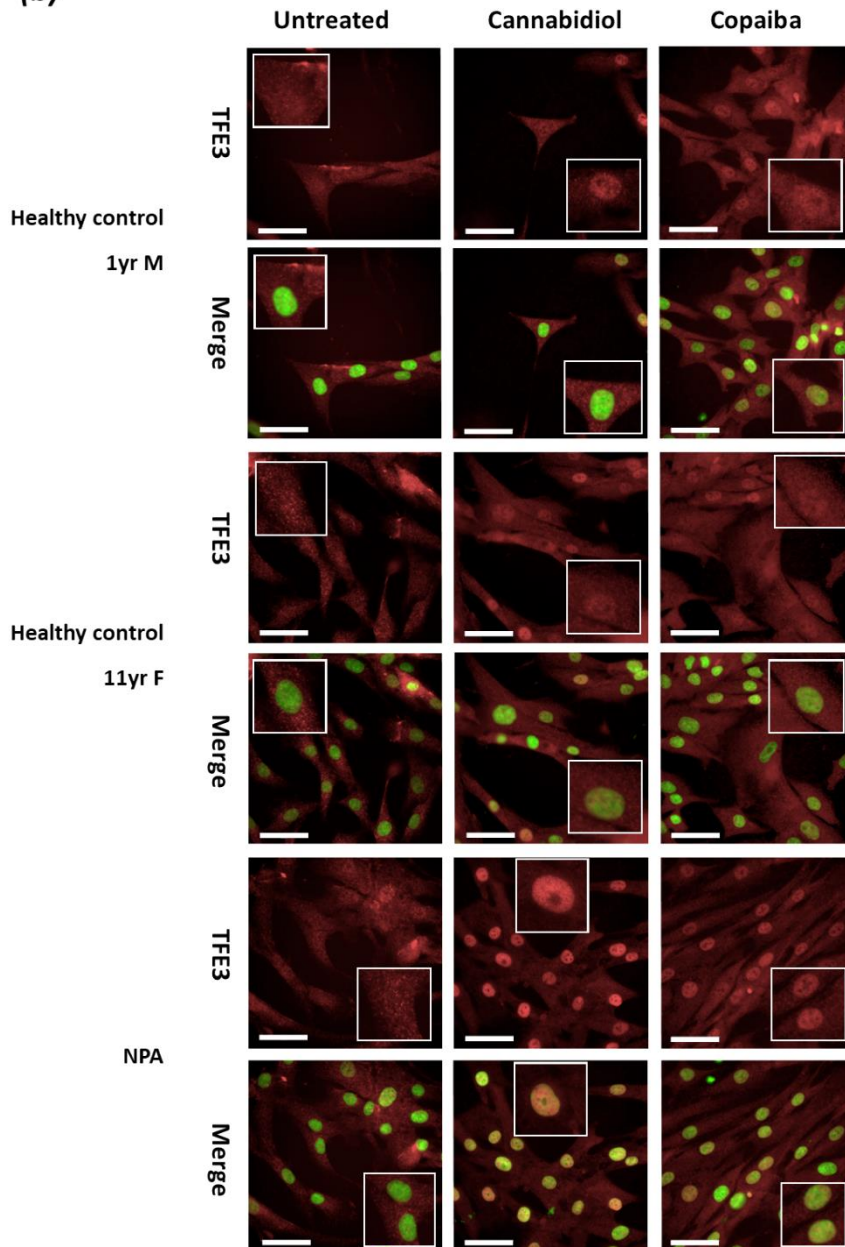
Copaiba also showed a significant increase in TFE3 nuclei localisation in all cells, except NPC P1007A. Copaiba increased the TFE3 nuclei localisation in the NPC1 P237S/I1061T from a baseline of 15% up to 65%. However, compared to cannabidiol, copaiba treatment led to smaller increase of TFE3 nuclear localisation, with significant differences between the two in the NPA and NPB. Furthermore, whilst cannabidiol induced the strongest effect in the NPA and NPB, copaiba was most effective in NPC1 I1061T mutant cell lines.

(a)

Percentage of cells with TFE3 nuclei localisation when treated with cannabidiol or copaiba



(b)



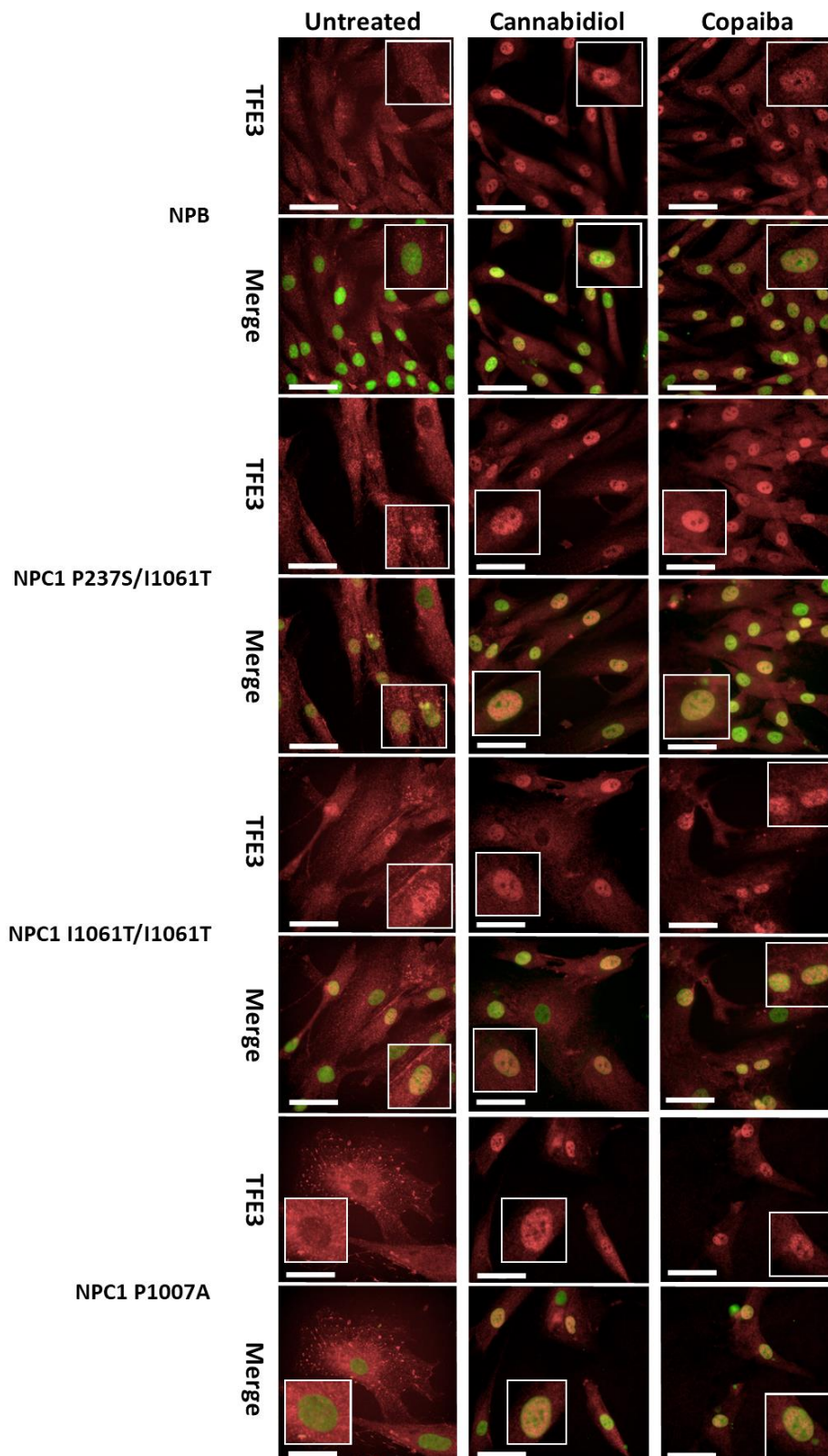


**Figure 5.22. Cannabidiol and copaiba promotes TFE3 nuclei localisation**

Cells were incubated with either cannabidiol or copaiba for 48 hours before fixing and probing with a TFE3 specific antibody. Nuclei staining was achieved with Sytox green. Cells were imaged at 40x magnification, and percentage TFE3 nuclei localisation analysed using Harmony software. Statistical significance was calculated with a one-way ANOVA and a post-hoc Tukey's multiple comparison test. \*= $p < 0.05$ , \*\*= $p < 0.01$ , \*\*\*= $p < 0.001$ , \*\*\*\*= $p < 0.0001$ .  $N=3$  for all experiments, data shown is mean  $\pm$  SD. Scale bars represent 50 $\mu$ m.

### **5.3 Discussion**

#### **5.3.1 *Cellular tolerance to cannabidiol and copaiba treatments***

The assays carried out showed significant differences in toxicity between batches of cannabidiol, which initially affected the ability to determine the LC50. However, once a suitable batch of cannabidiol was identified, then it was possible to determine both the LC50, and a concentration, which would not adversely affect cell viability.

All cell lines showed an LC50 to cannabidiol in the low micromolar range, which offers a wide therapeutic window. as plasma cannabidiol levels are usually observed in the low nanomolar range. The data generated also showed that cells were not affected by cannabidiol at doses up to 50µM, which match the data by Burstein *et al* (1984), where they treated cells with up to 60µM cannabidiol for 48 hours. The currently FDA approved formulation of cannabidiol, Epidiolex, can reach plasma concentrations as high as 5µM, which is within the range of cannabidiol concentrations used for the assays.

A similar therapeutic window was observed with copaiba oil, with LC50 values in the low µg/ml range, and no adverse effects being observed at 5g/kg in a rodent model; suggesting that copaiba oil is unlikely to cause toxic effects in humans at the concentrations used in these assays.

#### **5.3.2 *Reduced lysosomal volume in cells treated with cannabidiol and copaiba***

When change in lysosomal volume is measured using the LysoTracker Green plate-based assay, significant decreases in all Niemann-Pick disease cell lines were observed when treated with cannabidiol. Treatment with copaiba only led to significant reductions in the NPA and NPB.

However, analysis using the Operetta CLS showed that there was no significant decrease in lysosomal volume in the NPC1 P1007A cell line when treated with cannabidiol. Direct comparison of cannabidiol and copaiba treatments showed that a similar decrease in the total lysosomal volume was achieved with both therapeutics. This pattern was also observed when AQ7 was used instead of LysoTracker Red.

Therefore, with both plate reader based and Operetta CLS showing reductions in total lysosomal volume, it is postulated that the increase in aSMase activity observed in the enzyme assays is directly leading to reduction in the total lysosomal volume in Niemann-Pick disease cell lines.

### *5.3.3 Reduction in lysosomal lipid storage*

With the decreased lysosomal volume when treated with cannabidiol and copaiba, a corresponding decrease in lipid staining was observed. Both the puncta per cell and total lysosomal volume were reduced in: sphingomyelin, cholesterol, and LBPA, but not in ganglioside GM1 in nearly all Niemann-Pick cell lines. Consistent with the known lipids that accumulate between: NPA, NPB, and NPC, sphingomyelin was most significantly reduced in NPA and NPB, with the most significant reductions in cholesterol being observed in NPC1 I1061T mutant cell lines. It is probable that the restoration of aSMase activity is driving the improvement in lysosomal health that is leading to the corresponding reduction in cholesterol, as cholesterol and sphingomyelin trap each other within lysosomes (Wanikawa et al. 2020). However, it is surprising that despite a reduction in both sphingomyelin and cholesterol storage, that a reduction in LBPA staining was not observed in NPC disease cell lines.

It is unclear why cannabidiol increases total ganglioside GM1 area in most Niemann-Pick disease cells. This may be due to improved trafficking of the molecule, as each corresponding puncta of GM1 also has a higher concentration of GM1, with corresponding fluorescence intensity. However, it is possible that cannabidiol is improving the internalisation of GM1 from the plasma membrane, which is increasing the lysosomal concentration of GM1 (Sugimoto et al. 2001). Surprisingly, no increase is seen GM1 in copaiba treated cells, therefore cannabidiol must be affecting distinct pathways from the compounds in copaiba oil.

### *5.3.4 Activation of aSMase in vitro by cannabidiol and copaiba*

Despite the lack of research into cannabidiol and copaiba in lysosomal storage disorders, particularly Niemann-Pick disease, one previous study has demonstrated reduction in sphingomyelin in NPA cells following cannabidiol treatment, Burstein et al (1984). In this

study, both cannabidiol and copaiba improve aSMase activity leading to reduced lysosomal sphingomyelin levels.

Of the two, cannabidiol offers a bigger therapeutic effect; as demonstrated by the corresponding aSMase enzyme assays on treated cell homogenate. NPA disease fibroblasts showed a significant response to 15 $\mu$ M cannabidiol and 10 $\mu$ g/ml copaiba treatment, with cannabidiol leading to a 4-fold increase in aSMase activity, and copaiba leading to a 2.5-fold increase in activity.

Significant differences between 'classical' and 'variant' phenotype NPC cells response to cannabidiol and copaiba were observed. The classical phenotype (I1061T mutant) cells showed a moderate increase in aSMase activity, whereas the variant phenotype (P1007A mutant) cells showed a 45% decrease in aSMase activity (cannabidiol) or no change (copaiba).

This difference may be due to the differences in underlying mutation in the NPC1 protein. Recent work has shown that classical and variant NPC cells have differing sphingosine storage levels, with variant phenotype cells having increased sphingosine storage compared to the classical NPC cells in the patient fibroblasts analysed (Brodden et al. 2020). If sphingosine storage is higher in the P1007A cells than the I1061T cells, then it is likely that the P1007A cells will be tightly controlling aSMase activity, and probably downregulating aSMase activity to prevent further excess sphingosine synthesis and storage. With cannabidiol increasing aSMase activity in all but the P1007A cell lines, it is possible that this cell line is actively downregulating aSMase to prevent increased sphingosine synthesis and reduce storage as the NPC variant cells are the least capable cells to clear excess lysosomal sphingosine.

Neither cannabidiol nor copaiba are direct modulators of aSMase activity, as when cell homogenate was treated with each, no significant changes in aSMase activity was observed. Therefore, both molecules must be inducing their therapeutic effect by promoting the synthesis of aSMase.

### *5.3.5 Changes in protein expression and localisation*

As we had shown that cannabidiol and copaiba were indirectly increasing aSMase activity, it was confirmed that both increased the abundance of aSMase within cells, with cannabidiol producing a more significant increase in aSMase expression across the cell lines.

Both cannabidiol and copaiba led to increases in the heat shock pathway activation, with increases observed in both healthy control and Niemann-Pick disease cell lines. Whilst increases in HSP has been reported in cancer cells treated with cannabidiol, this data is the first that shows that cannabidiol activates the heat shock pathway in healthy control and Niemann-Pick disease cells. However, our data shows that the increased pattern of HSP70 expression, does not correlate directly to increased aSMase activity or reduction in sphingomyelin storage, therefore it is unlikely that the chaperone effect of HSP70 is leading to the improvements in phenotype.

Conflicting data is published on the oxidative effects of cannabidiol and BCP of copaiba oil (Pereira et al. 2021), however based on these data, cannabidiol and copaiba appear to be increasing oxidative stress, driving an increase in expression of HSP70. It is also possible that increased synthesis of incorrectly folded aSMase or NPC1 is driving the increase of HSP70 as HSP90 is known to be upregulated in the presence of unfolded proteins (Zou et al. 1998). Of note was that copaiba oil induced a stronger response than cannabidiol in all cell lines, however it is not clear if this is being driven by BCP or another compound present in copaiba oil.

Changes in expression of ACase closely mirror aSMase in healthy control and NPA/NPB disease cell lines. However, surprisingly, no change in ACase expression is observed in the NPC I1061T mutant disease fibroblasts, especially as aSMase expression is increased in these cell lines. Decreased ACase expression may be a compensatory measure from the cell to prevent an accumulation of sphingosine, and thus prevent cytotoxicity.

### *5.3.6 Cannabidiol and copaiba lead to nuclei localisation and thus activation of TFE3*

The increase in expression of lysosomal enzymes can be linked directly to the increase in TFE3 staining observed with cannabidiol and copaiba treatment. Whilst TFE3 activation is known to activate the CLEAR network, there must be secondary control mechanisms

controlling specific lysosomal enzyme expression, as both the genes for aSMase (SMPD1) and ACase (ASAH1) are controlled by CLEAR, but differences in protein expression is observed for each. It is unclear if the proteins are being produced and quickly degraded when not needed, or if translation of specific genes are being downregulated. It is known that aSMase is regulated by PKC, and PKC is known to be regulated by intracellular levels of ceramide, therefore ACase expression and activity is going to be a driver of PKC activity (Rodriguez-Lafrasse et al. 1997; Zeidan and Hannun 2007a).

#### **5.4 Conclusion**

We have found a safe concentration of cannabidiol and copaiba for treating cells for 72 hours without inducing cellular toxicity. Using this toxicity data, it has been possible to treat Niemann-Pick disease fibroblasts with cannabidiol and copaiba, and assay aSMase function after a 48-hour incubation.

Data from the enzyme assays showed a disease dependant response to cannabidiol, with NPA and classical form of NPC responding best to cannabidiol treatment. Treatment with copaiba showed increases in aSMase activity, however the effects were less significant using cannabidiol. Cannabidiol and copaiba also showed significant decreases in lysosomal volume in NPA and NPC cells. We have shown that cannabidiol and copaiba do not act directly on aSMase, instead inducing effects upstream that promote nuclear translocation of TFE3 and thus upregulation of the CLEAR control network.

We have also shown that cannabidiol and copaiba treatment can reduce lysosomal volume in Niemann-Pick disease cell lines and identified specific lipid species that are reduced in each cell line. Furthermore, we have shown that these changes in lipid storage are being improved by increased aSMase and modulation of ACase expression.

Further work, such as determining the effects of cannabidiol and copaiba upstream of TFE3 would be useful to better understand their mechanisms of action. This would also being beneficial to determine whether the effects observed by cannabidiol and copaiba are mTOR dependant or independent. Additionally, further work could include analysing the storage in patient derived neurons, or determining if calcium homeostasis is being restored, which would help further to evaluate the potential benefit of either cannabidiol or copaiba oil.

## 6 General Discussion

### 6.1 Summary

This thesis aimed to identify through screening, novel molecules with therapeutic effects in Niemann-Pick disease. In chapter 3, we assessed the potential of a range of novel anthraquinone derivatives, to determine if they could function as an NPC1 substrate for use in a transporter assay. Despite the lack of trafficking by NPC1, AQ7 was identified as a novel cell permeant long-lived lysosomal probe; with limited effects upon lysosomal function. In chapter 4, we developed an imaging-based zinc phenotypic assay. This assay was then used to screen a compound library to identify compounds able to modulate intracellular zinc in Niemann-Pick type C. In chapter 5, we evaluated 2 potential therapeutics, cannabidiol and copaiba oil, to determine whether these molecules have a therapeutic effect, and attempt to understand the mechanisms underpinning them.

### 6.2 AQ7 is a novel lysosome specific probe.

We had intended to develop an NPC1 trafficking assay, utilising an AQ2 analogue as an NPC1 specific substrate, however, despite previous work showing that AQ2 was an NPC1 substrate, none of the tested AQ2 analogues were trafficked from the lysosome by NPC1.

The current lack of understanding and clearly defined roles for NPC1, has hampered development of NPC1-specific probes. Whilst NPC1 has been believed to be a cholesterol transporter, based on loss of function analysis, no direct evidence for NPC1 transport of cholesterol has been observed; and thus it is hard to determine an NPC1 specific substrate (Ory 2000). Therefore, to be able to design NPC1 specific probes, more basic biology of NPC1 will need to be carried out, particularly in determining how molecules are trafficked through NPC1, as it currently not clear how this is facilitated (Pfeffer 2019).

Acriflavine is known to be an NPC1 substrate, however it shows poor fluorescent properties, making it unsuitable for a transport assay (Davies et al. 2000). AQ2, and AQ7, whilst broadly structurally similar to acriflavine sharing a tricyclic ring structure, share similarity to another molecule with an anthraquinone backbone Pt-1C3, which was shown to show lysosome specific localisation, due to the addition of a platinum containing side group preventing trafficking to the nucleus (Alderden et al. 2006).

It is likely that the addition of the side group to the molecule has prevented its lysosomal export, similar to the side group on AQ7 preventing lysosomal export. Thus, through changing of the side groups on anthraquinones it may be possible to develop an NPC1 substrate, however without structural data, such as Cryo-EM of the trafficking by NPC1, there is nothing to guide the design.

As there are currently no suitable NPC1 activity probes, measures of changes in number of lysosomes and lysosomal area are frequently used to assess NPC1 activity. Thus, the creation of new lysosome specific probes are the most likely option to further our understanding of Niemann-Pick disease and other LSDs. The most used commercial series of lysosomal dyes, the LysoTracker family have known issues, the most impactful being the deacidifying effect of the molecules upon lysosomes, and thus cannot be used for prolonged imaging assays. Therefore, the creation of dyes that have minimal effect upon lysosomal function and do not lead to de-acidification are desirable. AQ7 has shown that it does not produce the de-acidification effects, observed with LysoTracker dyes, and cells can be imaged for up to 48 hours, without observing toxicity.

A range of new lysosomal dyes have been created, which also comprise pH sensing capabilities. A range of Bodipy-derived molecules have been developed, which show high fluorescence sensitivity, suitable for detecting changes in lysosomal pH (Ruan et al. 2022). Should these probes become commercially available, it is likely that they will supersede the commercially available LysoTracker family of dyes.

Whilst screening assays have been developed for Niemann-Pick disease before, they utilised LysoTracker Red, and it possible that using newer dyes, such as AQ7 or the pH sensitive BODIPY derivatives as a primary screen in conjunction with a large library to identify compounds responsible for reduction of lysosomal volume, would lead to the development of more effective therapies.

### **6.3 Disease phenotype reducing compounds can be identified through zinc screening.**

As we had not been able to develop an NPC1 activity assay for screening using AQ7, we evaluated other potential phenotypic markers in NPC, with previous work within the Lloyd-Evans laboratory identifying zinc storage as a biomarker in Niemann-Pick.

Despite a range of small molecules showing zinc modulating effects in pre-clinical or clinical trials, no screens have been published looking at metal dyshomeostasis in Niemann-Pick. Therefore, we developed an assay suitable for HTS that could identify changes in zinc dyshomeostasis. This assay was used to screen a commercially available compound library to identify zinc modulators in NPC disease fibroblasts. The top 80 zinc reducing and zinc raising compounds were subsequently screened using LysoTracker to identify which of these compounds were able to reduce lysosomal volume. From these top 80 zinc compounds, 20 compounds were identified, and encouragingly two of the compounds had been found to have beneficial effects in NPC by other research groups. Therefore, this confirms that using zinc modulation to carry out an initial screen is a valid way of identifying potential hit compounds in NPC.

The results of our screen of zinc modulators have shown that whilst some molecules shared structural similarity, such as some compounds being steroid derivatives, the majority of compounds, show very limited structural similarity. This is encouraging, as it suggests several different receptors and pathways are being targeted by these molecules. Additional evaluation of the molecule's effects upon intracellular pathways, would allow further triage of compounds, to identify the compound that possess the most desirable intracellular effects, and those with the least off target effects, which leads to reduction in lysosomal volume.

Due to the lack of similarity in structure between the hits, it will be necessary to generate structure-activity relationships through medicinal chemistry to determine any compound with potential to be taken forward for Niemann-Pick.

As well as zinc, several other transition metals, including: manganese, iron, and copper are known to be dysregulated in NPC disease (Hung et al. 2014). All of these metal ions are therefore valid biomarkers that could be used to screen compounds for modulatory effects in NPC. As well as NPC, metal dyshomeostasis, has been reported in a range of lysosomal storage disorders (Yu et al. 2003; Kanninen et al. 2013; Baguña Torres et al. 2019).

Therefore, for lysosomal diseases where transition metal ion dyshomeostasis occurs, screening for modulators of any of the metals that are dysregulated using suitable probes, could be used to identify novel compounds for the disease with therapeutic effects. The

availability of ever-expanding compound libraries also improves the probability of hit molecules that are able to reduce the disease phenotype, and be able to progress *in vivo*. However, the current commercially available fluorescent probes for transition metals are limited and are likely to be the limiting factor in being able to screen for changes in other transition metals in an imaging-based assay.

#### **6.4 Cannabidiol and copaiba increase aSMase activity in vitro and reduce NPA disease phenotype.**

Despite the lack of research into either cannabidiol, or any of the main compounds present within copaiba oil in Niemann-Pick, both showed positive effects. Cannabidiol had previously been shown to reduce sphingomyelin storage, however no research into any of constituents of copaiba oil in Niemann-Pick had been carried out. However, anecdotal evidence from the families of Niemann-Pick patients and the ability of some of the constituents to interact with cannabinoid receptors, warranted further investigation. Both molecules activated aSMase, primarily through upregulation of TFE3 and the CLEAR pathway, leading to increased aSMase expression. However, it is possible that the molecules are also acting on different pathways, as differing effects were seen. This is probable as copaiba oil contains a range of terpenes, and whilst it is postulated that  $\beta$ -caryophyllene is driving the effects, it is possible that other molecules present at lower concentrations are driving other effects.

However, to identify which molecule, or molecules are the active constituents of copaiba oil, each constituent would have to be assayed individually to. With over 120 different compounds, and at least 60 different terpenes, this is not a minor undertaking (Urasaki et al. 2020). If one of the more minor constituents of copaiba oil was found to be modulating aSMase expression, then it would possess high receptor binding affinity for its activity to be detected as cells were treated with 10 $\mu$ g/ml copaiba, and therefore may be a more attractive molecule for further investigation and development.

Storage of sphingomyelin has been shown to lead to impairments in autophagy, thus activating TFEB/TFE3 is a potential therapeutic target. In NPA and NPB cells, cannabidiol was more effective than copaiba oil at inducing the nuclear localisation, and thus activation, of TFE3. However, this is surprising as copaiba oil appeared to lead to the largest decrease in sphingomyelin staining in cells. Thus, the reduction in sphingomyelin staining does not

directly correlate to the increase in TFE3 activation, suggesting that copaiba oil must possess an additional mechanism of action. However, the activation of TFE3 leading to aSMase upregulation, does show that therapeutics that lead to activation of TFE3 can reduce lipid storage in NPC. Therefore, molecules that lead to upregulation of TFE3 do have therapeutic potential for both NPA/B and NPC. However, prolonged treatment with molecules will likely see cells compensate by attempting to prevent prolonged CLEAR pathway activation. In addition, this would not be unique to TFE3/TFEB activations, as compensation methods are required to attempt to counteract this. With HDACi such as vorinostat, the treatment is given in a set number of days on and off of the therapeutic. However, it is unclear how well this treatment strategy works, as no published data from the phase I/II study of vorinostat in Niemann-Pick has been reported.

## 7 Conclusion

In this thesis it has been shown that AQ7 is not a suitable substrate for NPC1, but is a novel lysosome probe, with the ability to be used for time course assays, without inducing lysosomal de-acidification. The inability to develop a trafficking assay led us to develop a zinc imaging-based assay. Screening of compounds that modulated zinc led to identification of hit compounds that also reduced lysosomal area, by up to as much as 45% after a 24-hour treatment period. This 45% reduction is much larger than the reduction that miglustat had upon 24-hour treatment, however miglustat continued to reduce lysosomal volume for 200 days, and by the end had led to a 6-fold reduction in lysosomal volume (Lachmann et al. 2004).

Evaluation of cannabidiol and copaiba oil has shown that both reduce disease phenotype *in vitro*, with both treatment and concentration dependant effects, with greater effects being observed in NPA/B over NPC. Of the two tested, cannabidiol produced more significant effects, however copaiba oil still reduced lysosomal volume and activated TFE3. Future work should include characterising the hits from the zinc screen, to identify the pathways being modulated to determine if these molecules can be chemical starting points for therapies for Niemann-Pick. For cannabidiol and copaiba oil, moving into disease relevant models, such as zebrafish or mouse Niemann-Pick models would determine whether either molecule has therapeutic potential in the management of Niemann-Pick disease.

## 8 Bibliography

Abed Rabbo, M., Khodour, Y., Kaguni, L. S. and Stiban, J. 2021. Sphingolipid lysosomal storage diseases: from bench to bedside. *Lipids in health and disease* 20(1), pp. 44-44. doi: 10.1186/s12944-021-01466-0

Ahmad, I. et al. 2005. Allopregnanolone treatment, both as a single injection or repetitively, delays demyelination and enhances survival of Niemann-Pick C mice. *Journal of neuroscience research* 82(6), pp. 811-821. doi: 10.1002/jnr.20685

Alderden, R. A., Mellor, H. R., Modok, S., Hambley, T. W. and Callaghan, R. 2006. Cytotoxic efficacy of an anthraquinone linked platinum anticancer drug. *Biochemical pharmacology* 71(8), pp. 1136-1145. doi: 10.1016/j.bcp.2005.12.039

Allison, A. C. and Mallucci, L. 1964. Uptake of Hydrocarbon Carcinogens by Lysosomes. *Nature (London)* 203(4949), pp. 1024-1027. doi: 10.1038/2031024b0

Altmann, S. W. et al. 2004. Niemann-Pick C1 like 1 Protein Is Critical for Intestinal Cholesterol Absorption. *Science (American Association for the Advancement of Science)* 303(5661), pp. 1201-1204. doi: 10.1126/science.1093131

Alvi, N. K., Rizvi, R. Y. and Hadi, S. M. 1985. Interaction of intercalating and non-intercalating agents with DNA: use of hydroxyapatite chromatography and S1 nuclease. *Chemico-biological interactions* 53(1-2), pp. 219-231. doi: 10.1016/S0009-2797(85)80098-3

Anes, J., McCusker, M. P., Fanning, S. and Martins, M. 2015. The ins and outs of RND efflux pumps in *Escherichia coli*. *Frontiers in microbiology* 6, pp. 587-587. doi: 10.3389/fmicb.2015.00587

Appelmans, F., Wattiaux, R. and De Duve, C. 1955. Tissue fractionation studies. 5. The association of acid phosphatase with a special class of cytoplasmic granules in rat liver. *Biochemical journal* 59(3), pp. 438-445. doi: 10.1042/bj0590438

Arenas, F., Garcia-Ruiz, C. and Fernandez-Checa, J. C. 2017. Intracellular Cholesterol Trafficking and Impact in Neurodegeneration. *Frontiers in molecular neuroscience* 10, pp. 382-382. doi: 10.3389/fnmol.2017.00382

Argüello, G. et al. 2021. Genistein Activates Transcription Factor EB and Corrects Niemann-Pick C Phenotype. *International journal of molecular sciences* 22(8), p. 4220. doi: 10.3390/ijms22084220

Arvio, M. and Mononen, I. 2016. Aspartylglycosaminuria: a review. *Orphanet journal of rare diseases* 11(1), pp. 162-162. doi: 10.1186/s13023-016-0544-6

Auer, I. A. et al. 1995. Paired helical filament tau (PHFtau) in Niemann-Pick type C disease is similar to PHFtau in Alzheimer's disease. *Acta neuropathologica* 90(6), pp. 547-551.

Aydemir, T. B., Liuzzi, J. P., McClellan, S. and Cousins, R. J. 2009. Zinc transporter ZIP8 (SLC39A8) and zinc influence IFN- $\gamma$  expression in activated human T cells. *Journal of leukocyte biology* 86(2), pp. 337-348. doi: 10.1189/jlb.1208759

Azbill, R. D., Mu, X. and Springer, J. E. 2000. Riluzole increases high-affinity glutamate uptake in rat spinal cord synaptosomes. *Brain research* 871(2), pp. 175-180. doi: 10.1016/S0006-8993(00)02430-6

Baguña Torres, J. et al. 2019. Imaging of changes in copper trafficking and redistribution in a mouse model of Niemann-Pick C disease using positron emission tomography. *Biometals* 32(2), pp. 293-306. doi: 10.1007/s10534-019-00185-5

Bai, Y. et al. 2016. Essential Metals Zinc, Selenium, and Strontium Protect against Chromosome Damage Caused by Polycyclic Aromatic Hydrocarbons Exposure. *Environmental science & technology* 50(2), pp. 951-960. doi: 10.1021/acs.est.5b03945

Balber, A. E. 2011. Concise Review: Aldehyde Dehydrogenase Bright Stem and Progenitor Cell Populations from Normal Tissues: Characteristics, Activities, and Emerging Uses in Regenerative Medicine. *Stem cells (Dayton, Ohio)* 29(4), pp. 570-575. doi: 10.1002/stem.613

Baltaci, A. K. and Yuce, K. 2018. Zinc Transporter Proteins. *Neurochemical research* 43(3), pp. 517-530. doi: 10.1007/s11064-017-2454-y

Bazzicalupi, C. et al. 2010. A highly pH-sensitive Zn(II) chemosensor. *Dalton transactions : an international journal of inorganic chemistry* 39(30), pp. 7080-7090. doi: 10.1039/c0dt00126k

Beevers, C. S., Long, C., Lei, L. I. U., Yan, L. U. O., Webster, N. J. G. and Shile, H. 2009. Curcumin Disrupts the Mammalian Target of Rapamycin-Raptor Complex. *Cancer research (Chicago, Ill.)* 69(3), pp. 1000-1008. doi: 10.1158/0008-5472.CAN-08-2367

Bendellaa, M., Lelièvre, P., Coll, J. L., Sancey, L., Deniaud, A. and Busser, B. 2024. Roles of zinc in cancers: From altered metabolism to therapeutic applications. *International journal of cancer* 154(1), pp. 7-20. doi: 10.1002/ijc.34679

Berezin, Mikhail Y. et al. 2011. Near-Infrared Fluorescence Lifetime pH-Sensitive Probes. *Biophysical journal* 100(8), pp. 2063-2072. doi: 10.1016/j.bpj.2011.02.050

Berruti, G. and Martegani, E. 1984. Dansylalanyllysylchloromethyl ketone as a fluorescent probe for localization of acrosin activity in boar and human spermatozoa. *The journal of histochemistry and cytochemistry* 32(5), pp. 526-530. doi: 10.1177/32.5.6371133

Besser, L., Chorin, E., Sekler, I., Silverman, W. F., Atkin, S., Russell, J. T. and Hershfinkel, M. 2009. Synaptically Released Zinc Triggers Metabotropic Signaling via a Zinc-Sensing Receptor in the Hippocampus. *The Journal of neuroscience* 29(9), pp. 2890-2901. doi: 10.1523/JNEUROSCI.5093-08.2009

Biederbick, A., Kern, H. F. and Elsasser, H. P. 1995. Monodansylcadaverine (MDC) is a specific in vivo marker for autophagic vacuoles. *European Journal of Cell Biology* 66(1), pp. 3-14.

Bienias, K., Fiedorowicz, A., Sadowska, A., Prokopiuk, S. and Car, H. 2016. Regulation of sphingomyelin metabolism. *Pharmacological reports* 68(3), pp. 570-581. doi: 10.1016/j.pharep.2015.12.008

Bilmen, J. G., Khan, S. Z., Javed, M. H. and Michelangeli, F. 2001. Inhibition of the SERCA Ca<sup>2+</sup> pumps by curcumin. Curcumin putatively stabilizes the interaction between the nucleotide-binding and phosphorylation domains in the absence of ATP. *European journal of biochemistry* 268(23), pp. 6318-6327. doi: 10.1046/j.0014-2956.2001.02589.x

Binder, C. J. et al. 2003. Pneumococcal vaccination decreases atherosclerotic lesion formation: molecular mimicry between *Streptococcus pneumoniae* and oxidized LDL. *Nature medicine* 9(6), pp. 736-743. doi: 10.1038/nm876

Bissig, C. and Gruenberg, J. 2013. Lipid sorting and multivesicular endosome biogenesis. *Cold Spring Harbor perspectives in biology* 5(10), pp. a016816-a016816. doi: 10.1101/cshperspect.a016816

Blackburn, E. H., Epel, E. S. and Lin, J. 2015. Human telomere biology: A contributory and interactive factor in aging, disease risks, and protection. *Science (American Association for the Advancement of Science)* 350(6265), pp. 1193-1198. doi: 10.1126/science.aab3389

Blaho, V. A. and Hla, T. 2011. Regulation of Mammalian Physiology, Development, and Disease by the Sphingosine 1-Phosphate and Lysophosphatidic Acid Receptors. *Chemical reviews* 111(10), pp. 6299-6320. doi: 10.1021/cr200273u

Blom, T. et al. 2010. FTY720 Stimulates 27-Hydroxycholesterol Production and Confers Atheroprotective Effects in Human Primary Macrophages. *Circulation research* 106(4), pp. 720-729. doi: 10.1161/CIRCRESAHA.109.204396

Bonesso, L., Piraud, M., Caruba, C., Van Obberghen, E., Mengual, R. and Hinault, C. 2014. Fast urinary screening of oligosaccharidoses by MALDI-TOF/TOF mass spectrometry. *Orphanet journal of rare diseases* 9(1), pp. 19-19. doi: 10.1186/1750-1172-9-19

Bonney, D. K. et al. 2010. Successful allogeneic bone marrow transplant for Niemann–Pick disease type C2 is likely to be associated with a severe ‘graft versus substrate’ effect. *Journal of inherited metabolic disease* 33(S3), pp. 171-173. doi: 10.1007/s10545-010-9060-3

Borbon, I. A., Hillman, Z., Duran, E., Kiela, P. R., Frautschy, S. A. and Erickson, R. P. 2012. Lack of efficacy of curcumin on neurodegeneration in the mouse model of Niemann–Pick C1. *Pharmacology, biochemistry and behavior* 101(1), pp. 125-131. doi: 10.1016/j.pbb.2011.12.009

Bosomworth, H. J., Thornton, J. K., Coneyworth, L. J., Ford, D. and Valentine, R. A. 2012. Efflux function, tissue-specific expression and intracellular trafficking of the Zn transporter ZnT10 indicate roles in adult Zn homeostasis. *Metallomics* 4(8), pp. 771-779. doi: 10.1039/c2mt20088k

Bras, J. M. 2013. Lysosomal Storage Disorders and Iron. *International Review of Neurobiology* 110, pp. 251-275. doi: 10.1016/B978-0-12-410502-7.00012-0

Braulke, T. and Bonifacino, J. S. 2009. Sorting of lysosomal proteins. *Biochimica et biophysica acta. Molecular cell research* 1793(4), pp. 605-614. doi: 10.1016/j.bbamcr.2008.10.016

Breiden, B. and Sandhoff, K. 2021. Acid sphingomyelinase, a lysosomal and secretory phospholipase c, is key for cellular phospholipid catabolism. *International journal of molecular sciences* 22(16), p. 9001. doi: 10.3390/ijms22169001

Bremova-Ertl, T. et al. 2021. Efficacy and safety of N-acetyl-L-leucine in Niemann-Pick disease type C. *Journal of neurology* 1(12), doi: 10.1007/s00415-021-10717-0

Brogden, G., Shamma, H., Walters, F., Maalouf, K., Das, A. M., Naim, H. Y. and Rizk, S. 2020. Different Trafficking Phenotypes of Niemann-Pick C1 Gene Mutations Correlate with Various Alterations in Lipid Storage, Membrane Composition and Miglustat Amenability. *International journal of molecular sciences* 21(6), p. 2101. doi: 10.3390/ijms21062101

Brook, P. F., Lawry, J., Cooke, I. D. and Barratt, C. L. 1996. Measurement of intracellular pH in human spermatozoa by flow cytometry with the benzo[c]xanthene dye SNAFL-1: a novel, single excitation, dual emission, molecular probe. *Molecular human reproduction* 2(1), pp. 18-25. doi: 10.1093/molehr/2.1.18

Brunkhorst, R., Vutukuri, R. and Pfeilschifter, W. 2014. Fingolimod for the treatment of neurological diseases-state of play and future perspectives. *Frontiers in cellular neuroscience* 8, pp. 283-283. doi: 10.3389/fncel.2014.00283

Burstein, S., Hunter, S. A. and Renzulli, L. 1984. Stimulation of sphingomyelin hydrolysis by cannabidiol in fibroblasts from a Niemann-Pick patient. *Biochemical and biophysical research communications* 31(121), pp. 168-173.

Canonico, P. G. and John, W. C. B. 1969. The Use of Acridine Orange as a Lysosomal Marker in Rat Skeletal Muscle. *The Journal of cell biology* 43(2), pp. 367-371. doi: 10.1083/jcb.43.2.367

Casado, M., Ferrer-López, I., Ruiz-Sala, P., Pérez-Cerdá, C. and Artuch, R. 2017. Urine oligosaccharide tests for the diagnosis of oligosaccharidoses. *Reviews in analytical chemistry* 36(3), pp. 221-227. doi: 10.1515/revac-2016-0019

Chandler, R. J. et al. 2017. Systemic AAV9 gene therapy improves the lifespan of mice with Niemann-Pick disease, type C1. *Human molecular genetics* 26(1), pp. 52-64. doi: 10.1093/hmg/ddw367

- Charytoniuk, T., Sztolsztener, K., Bielawiec, P., Chabowski, A., Konstantynowicz-Nowicka, K. and Harasim-Symbor, E. 2022. Cannabidiol Downregulates Myocardial de Novo Ceramide Synthesis Pathway in a Rat Model of High-Fat Diet-Induced Obesity. *International journal of molecular sciences* 23(4), p. 2232. doi: 10.3390/ijms23042232
- Chausmer, A. B. 1998. Zinc, Insulin and Diabetes. *Journal of the American College of Nutrition* 17(2), pp. 109-115. doi: 10.1080/07315724.1998.10718735
- Chen, L. et al. 2017. Fasting-induced hormonal regulation of lysosomal function. *Cell research* 27(6), pp. 748-763. doi: 10.1038/cr.2017.45
- Chen, P., Miah, M. R. and Aschner, M. 2016. Metals and Neurodegeneration. *F1000 research* 5, p. 366. doi: 10.12688/f1000research.7431.1
- Chen, S.-H., Lin, K.-Y., Chang, C.-C., Fang, C.-L. and Lin, C.-P. 2007. Aloe-emodin-induced apoptosis in human gastric carcinoma cells. *Food and chemical toxicology* 45(11), pp. 2296-2303. doi: 10.1016/j.fct.2007.06.005
- Chen, Y. and Cao, Y. 2017. The sphingomyelin synthase family: proteins, diseases, and inhibitors. *Biological chemistry* 398(12), pp. 1319-1325. doi: 10.1515/hsz-2017-0148
- Chimienti, F., Favier, A. and Seve, M. 2005. ZnT-8, a pancreatic beta-cell-specific zinc transporter. *Biometals* 18(4), pp. 313-317. doi: 10.1007/s10534-005-3687-9
- Choi, D. W., Yokoyama, M. and Koh, J. 1988. Zinc neurotoxicity in cortical cell culture. *Neuroscience* 24(1), pp. 67-79. doi: 10.1016/0306-4522(88)90312-0
- Coleman, J. E. 1998. Zinc enzymes. *Current opinion in chemical biology* 2(2), pp. 222-234. doi: 10.1016/S1367-5931(98)80064-1
- Colvin, R. A., Bush, A. I., Volitakis, I., Fontaine, C. P., Thomas, D., Kikuchi, K. and Holmes, W. R. 2008. Insights into Zn<sup>2+</sup> homeostasis in neurons from experimental and modeling studies. *American Journal of Physiology: Cell Physiology* 294(3), p. C726. doi: 10.1152/ajpcell.00541.2007
- Contreras, P. S. et al. 2020. c-Abl Inhibition Activates TFEB and Promotes Cellular Clearance in a Lysosomal Disorder. *iScience* 23(11), pp. 101691-101691. doi: 10.1016/j.isci.2020.101691
- Cook, N. R., Row, P. E. and Davidson, H. W. 2004. Lysosome Associated Membrane Protein 1 (Lamp1) Traffics Directly from the TGN to Early Endosomes. *Traffic (Copenhagen, Denmark)* 5(9), pp. 685-699. doi: 10.1111/j.1600-0854.2004.00212.x

- Cougnoux, A. et al. 2021. Reduction of glutamate neurotoxicity: A novel therapeutic approach for Niemann–Pick disease, type C1. *Molecular genetics and metabolism* 134(4), pp. 330-336. doi: 10.1016/j.ymgme.2021.11.008
- Coutinho, M. F., Santos, J. I. and Alves, S. 2016. Less Is More: Substrate Reduction Therapy for Lysosomal Storage Disorders. *International Journal of Molecular Sciences* 17(7), pp. 1065-1065. doi: 10.3390/ijms17071065
- Cox, T. et al. 2000. Novel oral treatment of Gaucher's disease with N-butyldeoxynojirimycin (OGT 918) to decrease substrate biosynthesis. *The Lancet (British edition)* 355(9214), pp. 1481-1485. doi: 10.1016/S0140-6736(00)02161-9
- Craddock, T. J. A., Tuszynski, J. A., Chopra, D., Casey, N., Goldstein, L. E., Hameroff, S. R. and Tanzi, R. E. 2012. The zinc dyshomeostasis hypothesis of Alzheimer's disease. *PloS one* 7(3), pp. e33552-e33552. doi: 10.1371/journal.pone.0033552
- Cuajungco, M. P. et al. 2014. Cellular Zinc Levels Are Modulated by TRPML1–TMEM163 Interaction. *Traffic (Copenhagen, Denmark)* 15(11), pp. 1247-1265. doi: 10.1111/tra.12205
- Czaplinska, B., Spaczynska, E. and Musiol, R. 2018. Quinoline Fluorescent Probes for Zinc - from Diagnostic to Therapeutic Molecules in Treating Neurodegenerative Diseases. *Medicinal chemistry (Shp-sariqah, United Arab Emirates)* 14(1), pp. 19-33. doi: 10.2174/1573406413666171002121817
- D'Souza, R. S. et al. 2014. Danon disease: clinical features, evaluation, and management. *Circulation. Heart failure* 7(5), pp. 843-849. doi: 10.1161/CIRCHEARTFAILURE.114.001105
- Dalenogare, D. P. et al. 2019. Antinociceptive activity of *Copaifera officinalis* Jacq. L oil and kaurenoic acid in mice. *Inflammopharmacology* 27(4), pp. 829-844. doi: 10.1007/s10787-019-00588-3
- Danila, C. and Federico, A. 2023. Cholesterol de novo biosynthesis: a promising target to overcome the resistance to aromatase inhibitors in postmenopausal patients with estrogen receptor-positive breast cancer. *Exploration of medicine* 4(6), pp. 1079-1093. doi: 10.37349/emed.2023.00196
- Davidson, C. D. et al. 2009. Chronic cyclodextrin treatment of murine Niemann–Pick C disease ameliorates neuronal cholesterol and glycosphingolipid storage and disease progression. *PloS one* 4(9), p. e6951. doi: 10.1371/journal.pone.0006951
- Davidson, C. D. et al. 2016. Efficacy and ototoxicity of different cyclodextrins in Niemann–Pick C disease. *Annals of clinical and translational neurology* 3(5), pp. 366-380. doi: 10.1002/acn3.306
- Davies, J. P., Chen, F. W. and Ioannou, Y. A. 2000. Transmembrane Molecular Pump Activity of Niemann–Pick C1 Protein. *Science (American Association for the Advancement of Science)* 290(5500), pp. 2295-2298. doi: 10.1126/science.290.5500.2295

- Deegan, P. B. and Cox, T. M. 2012. Imiglucerase in the treatment of Gaucher disease: a history and perspective. *Drug design, development and therapy* 6(default), pp. 81-106. doi: 10.2147/DDDT.S14395
- Deffieu, M. S. and Pfeffer, S. R. 2011. Niemann—Pick type C 1 function requires luminal domain residues that mediate cholesterol-dependent NPC2 binding. *Proceedings of the National Academy of Sciences - PNAS* 108(47), pp. 18932-18936. doi: 10.1073/pnas.1110439108
- Deibert, E., Gentry, T., Foster, S. J., Kurtzberg, J. and Balber, A. E. 2007. 23: Early hematopoietic cells, including megakaryocyte progenitors, are recovered in ALDH bright cell populations isolated by cell sorting from previously frozen umbilical cord blood. *Biology of blood and marrow transplantation* 13(2), pp. 11-11. doi: 10.1016/j.bbmt.2006.12.026
- Del Giovane, A. and Ragnini-Wilson, A. 2018. Targeting Smoothed as a New Frontier in the Functional Recovery of Central Nervous System Demyelinating Pathologies. *International journal of molecular sciences* 19(11), p. 3677. doi: 10.3390/ijms19113677
- Dell'Osso, L., Del Grande, C., Gesi, C., Carmassi, C. and Musetti, L. 2016. A new look at an old drug: neuroprotective effects and therapeutic potentials of lithium salts. *Neuropsychiatric disease and treatment* 12, pp. 1687-1703. doi: 10.2147/NDT.S106479
- Dhami, R., Xingxuan, H. E., Gordon, R. E. and Schuchman, E. H. 2001. Analysis of the Lung Pathology and Alveolar Macrophage Function in the Acid Sphingomyelinase-Deficient Mouse Model of Niemann-Pick Disease. *Laboratory investigation* 81(7), pp. 987-999. doi: 10.1038/labinvest.3780311
- Diaz, G. A. et al. 2021. One-year results of a clinical trial of olipudase alfa enzyme replacement therapy in pediatric patients with acid sphingomyelinase deficiency. *Genetics in medicine*,
- Doble, A. 1996. The pharmacology and mechanism of action of riluzole. *Neurology* 47(6), pp. S233-S241. doi: 10.1212/WNL.47.6\_Suppl\_4.233S
- Dringen, R. 2000. Metabolism and functions of glutathione in brain. *Progress in neurobiology* 62(6), pp. 649-671. doi: 10.1016/S0301-0082(99)00060-X
- Du, W. et al. 2021. Lysosomal Zn<sup>2+</sup> release triggers rapid, mitochondria-mediated, non-apoptotic cell death in metastatic melanoma. *Cell reports (Cambridge)* 37(3), pp. 109848-109848. doi: 10.1016/j.celrep.2021.109848
- Duffy, J. Y., Miller, C. M., Rutschilling, G. L., Ridder, G. M., Clegg, M. S., Keen, C. L. and Daston, G. P. 2001. A decrease in intracellular zinc level precedes the detection of early indicators of apoptosis in HL-60 cells. *Apoptosis (London)* 6(3), pp. 161-172. doi: 10.1023/A:1011380508902
- Eichelsdoerfer, J. L., Evans, J. A., Slaugenhaupt, S. A. and Cuajungco, M. P. 2010. Zinc Dyshomeostasis Is Linked with the Loss of Mucopolipidosis IV-associated TRPML1 Ion Channel. *The Journal of biological chemistry* 285(45), pp. 34304-34308. doi: 10.1074/jbc.C110.165480

Elmacken, M. et al. 2015. A pilot trial of unmatched human placental derived stem cells (HPDSC) infusion in conjunction with unrelated cord blood transplantation (UCBT) in children and young adults with malignant and non-malignant diseases. *Cytotherapy (Oxford, England)* 17(6), pp. S64-S65. doi: 10.1016/j.jcyt.2015.03.527

Endo, Y., Furuta, A. and Nishino, I. 2015. Danon disease: a phenotypic expression of LAMP-2 deficiency. *Acta neuropathologica* 129(3), pp. 391-398. doi: 10.1007/s00401-015-1385-4

Errington, R. J. et al. 2018. Probing cytochrome P450 bioactivation and fluorescent properties with morpholinyl-tethered anthraquinones. *Bioorganic & medicinal chemistry letters* 28(8), pp. 1274-1277. doi: 10.1016/j.bmcl.2018.03.040

Escobar, A., Styrpejko, D. J., Ali, S. and Cuajungco, M. P. 2022. Transmembrane 163 (TMEM163) protein interacts with specific mammalian SLC30 zinc efflux transporter family members. *Biochemistry and biophysics reports* 32, pp. 101362-101362. doi: 10.1016/j.bbrep.2022.101362

Eskes, E. C. B., Sjouke, B., Vaz, F. M., Goorden, S. M. I., van Kuilenburg, A. B. P., Aerts, J. M. F. G. and Hollak, C. E. M. 2020. Biochemical and imaging parameters in acid sphingomyelinase deficiency: Potential utility as biomarkers. *Molecular genetics and metabolism* 130(1), pp. 16-26. doi: 10.1016/j.ymgme.2020.02.002

Fanani, M. L. and Maggio, B. 2017. The many faces (and phases) of ceramide and sphingomyelin I – single lipids. *Biophysical reviews* 9(5), pp. 589-600. doi: 10.1007/s12551-017-0297-z

Farmer, C. A., Thurm, A., Farhat, N., Bianconi, S., Keener, L. A. and Porter, F. D. 2019. Long-Term Neuropsychological Outcomes from an Open-Label Phase I/IIa Trial of 2-Hydroxypropyl- $\beta$ -Cyclodextrins (VTS-270) in Niemann-Pick Disease, Type C1. *CNS drugs* 33(7), pp. 677-683. doi: 10.1007/s40263-019-00642-2

Feng, D., Ohlsson, L. and Duan, R.-D. 2010a. Curcumin inhibits cholesterol uptake in Caco-2 cells by down-regulation of NPC1L1 expression. *Lipids in health and disease* 9(1), pp. 40-40. doi: 10.1186/1476-511X-9-40

Feng, X. et al. 2019. Determination of the Pathological Features of NPC1 Variants in a Cellular Complementation Test. *International journal of molecular sciences* 20(20), p. 5185. doi: 10.3390/ijms20205185

Feng, Y., Hartig, S. M., Bechill, J. E., Blanchard, E. G., Caudell, E. and Corey, S. J. 2010b. The Cdc42-interacting Protein-4 (CIP4) Gene Knock-out Mouse Reveals Delayed and Decreased Endocytosis. *The Journal of biological chemistry* 285(7), pp. 4348-4354. doi: 10.1074/jbc.M109.041038

Fernández-Pereira, C. et al. 2021. Therapeutic Approaches in Lysosomal Storage Diseases. *Biomolecules (Basel, Switzerland)* 11(12), p. 1775. doi: 10.3390/biom11121775

Fields, T. et al. 2021. A master protocol to investigate a novel therapy acetyl-L-leucine for three ultra-rare neurodegenerative diseases: Niemann-Pick type C, the GM2 gangliosidosis, and ataxia telangiectasia. *Trials* 22(1), pp. 84-84. doi: 10.1186/s13063-020-05009-3

Fierke, C. A. and Thompson, R. B. 2001. Fluorescence-based biosensing of zinc using carbonic anhydrase. *Biometals* 14(3-4), pp. 205-222. doi: 10.1023/A:1012980628412

Fog, C. K. et al. 2018. The heat shock protein amplifier arimoclomol improves refolding, maturation and lysosomal activity of glucocerebrosidase. *EBioMedicine* 38, pp. 142-153. doi: 10.1016/j.ebiom.2018.11.037

Folts, C. J., Scott-Hewitt, N., Pröschel, C., Mayer-Pröschel, M. and Noble, M. 2016. Lysosomal Re-acidification Prevents Lysosphingolipid-Induced Lysosomal Impairment and Cellular Toxicity. *PLoS biology* 14(12), p. e1002583. doi: 10.1371/journal.pbio.1002583

Frederickson, C. 2003. Imaging zinc: old and new tools. *Science's signal transduction knowledge environment (STKE)* 2003(182), pp. pe18-pe18. doi: 10.1126/stke.2003.182.pe18

Frederickson, C. J., Kasarskis, E. J., Ringo, D. and Frederickson, R. E. 1987. A quinoline fluorescence method for visualizing and assaying the histochemically reactive zinc (bouton zinc) in the brain. *Journal of neuroscience methods* 20(2), pp. 91-103. doi: 10.1016/0165-0270(87)90042-2

Freundt, E. C., Czapiga, M. and Lenardo, M. J. 2007. Photoconversion of LysoTracker Red to a green fluorescent molecule. *Cell research* 17(11), pp. 956-958. doi: 10.1038/cr.2007.80

Frimurer, T. M. et al. 2017. Model-Based Discovery of Synthetic Agonists for the Zn<sup>2+</sup>-Sensing G-Protein-Coupled Receptor 39 (GPR39) Reveals Novel Biological Functions. *Journal of medicinal chemistry* 60(3), pp. 886-898. doi: 10.1021/acs.jmedchem.6b00648

Fu, R. et al. 2013. Efficacy of N-acetylcysteine in phenotypic suppression of mouse models of Niemann-Pick disease, type C1. *Human molecular genetics* 22(17), pp. 3508-3523. doi: 10.1093/hmg/ddt206

Galdino, P. M. et al. 2012. The anxiolytic-like effect of an essential oil derived from *Spiranthera odoratissima* A. St. Hil. leaves and its major component,  $\beta$ -caryophyllene, in male mice. *Progress in neuro-psychopharmacology & biological psychiatry* 38(2), pp. 276-284. doi: 10.1016/j.pnpbp.2012.04.012

Gamsjaeger, R., Liew, C. K., Loughlin, F. E., Crossley, M. and Mackay, J. P. 2007. Sticky fingers: zinc-fingers as protein-recognition motifs. *Trends in biochemical sciences (Amsterdam. Regular ed.)* 32(2), pp. 63-70. doi: 10.1016/j.tibs.2006.12.007

Gault, C. R., Obeid, L. M. and Hannun, Y. A. 2010. An Overview of Sphingolipid Metabolism: From Synthesis to Breakdown. *Advances in experimental medicine and biology* 688, pp. 1-23. doi: 10.1007/978-1-4419-6741-1\_1

Geberhiwot, T. et al. 2018. Consensus clinical management guidelines for Niemann-Pick disease type C. *Orphanet journal of rare diseases* 13(1), pp. 50-50. doi: 10.1186/s13023-018-0785-7

Geisow, M. J. 1984. Fluorescein conjugates as indicators of subcellular pH : A critical evaluation. *Experimental Cell Research* 150(1), pp. 29-35. doi: 10.1016/0014-4827(84)90698-0

Gentry, T., Deibert, E., Foster, S. J., Haley, R., Kurtzberg, J. and Balber, A. E. P. 2007. Isolation of early hematopoietic cells, including megakaryocyte progenitors, in the ALDH-bright cell population of cryopreserved, banked UC blood. *Cytotherapy (Oxford, England)* 9(6), pp. 569-576. doi: 10.1080/14653240701466347

Gertsch, J. 2008. Antiinflammatory cannabinoids in diet - towards a better understanding of CB2 receptor action?: Towards a better understanding of CB2 receptor action? *Communicative & integrative biology* 1(1), pp. 26-28. doi: 10.4161/cib.1.1.6568

Gertsch, J. et al. 2008. Beta-Caryophyllene Is a Dietary Cannabinoid. *Proceedings of the National Academy of Sciences - PNAS* 105(26), pp. 9099-9104. doi: 10.1073/pnas.0803601105

Geuze, H. J., Slot, J. W. and Schwartz, A. L. 1987. Membranes of Sorting Organelles Display Lateral Heterogeneity in Receptor Distribution. *The Journal of cell biology* 104(6), pp. 1715-1723. doi: 10.1083/jcb.104.6.1715

Ghisaidoobe, A. T. et al. 2014. Identification and Development of Biphenyl Substituted Iminosugars as Improved Dual Glucosylceramide Synthase/Neutral Glucosylceramidase Inhibitors. *Journal of medicinal chemistry* 57(21), pp. 9096-9104. doi: 10.1021/jm501181z

Glunde, K., Guggino, S. E., Ichikawa, Y. and Bhujwalla, Z. M. 2003. A novel method of imaging lysosomes in living human mammary epithelial cells. *Molecular imaging* 2(1), pp. 24-36. doi: 10.1162/153535003765276264

Gordon, P. F. and Gregory, P. 1987. Anthraquinone Dyes. *Organic Chemistry in Colour*. Berlin: Springer, pp. 163-199.

Goñi, F. M. and Alonso, A. 2002. Sphingomyelinases: enzymology and membrane activity. *FEBS Letters* 531(1), pp. 38-46. doi: 10.1016/S0014-5793(02)03482-8

Grant, B. D. and Donaldson, J. G. 2009. Pathways and mechanisms of endocytic recycling. *Nature reviews. Molecular cell biology* 10(9), pp. 597-608. doi: 10.1038/nrm2755

Grant, C. C. et al. 2021. Acetylation turns leucine into a drug by membrane transporter switching. *Scientific reports* 11(1), pp. 15812-15812. doi: 10.1038/s41598-021-95255-5

Greer, W. L. et al. 1998. The Nova Scotia (type D) form of Niemann-Pick disease is caused by a G3097→T transversion in NPC1. *American journal of human genetics* 63(1), pp. 52-54. doi: 10.1086/301931

Grievink, H. W. et al. 2020. The Effect of a 13-Valent Conjugate Pneumococcal Vaccine on Circulating Antibodies Against Oxidized LDL and Phosphorylcholine in Man, A Randomized Placebo-Controlled Clinical Trial. *Biology (Basel, Switzerland)* 9(11), p. 345. doi: 10.3390/biology9110345

Griffin, L. D., Gong, W., Verot, L. and Mellon, S. H. 2004. Niemann-Pick type C disease involves disrupted neurosteroidogenesis and responds to allopregnanolone. *Nature medicine* 10(7), pp. 704-711. doi: 10.1038/nm1073

Griñán-Ferré, C. et al. 2021. Inhibition of Soluble Epoxide Hydrolase Ameliorates Phenotype and Cognitive Abilities in a Murine Model of Niemann Pick Type C Disease. *International journal of molecular sciences* 22(7), p. 3409. doi: 10.3390/ijms22073409

Guatibonza Moreno, P. et al. 2023. At a glance: the largest Niemann-Pick type C1 cohort with 602 patients diagnosed over 15 years. *European journal of human genetics : EJHG* 31(10), pp. 1108-1116. doi: 10.1038/s41431-023-01408-7

Guerinot, M. L. 2000. The ZIP family of metal transporters. *BBA - Biomembranes* 1465(1), pp. 190-198. doi: 10.1016/S0005-2736(00)00138-3

Guo, R.-M. et al. 2018. In Vivo Assessment of Neurodegeneration in Type C Niemann-Pick Disease by IDEAL-IQ. *Korean journal of radiology* 19(1), pp. 93-100. doi: 10.3348/kjr.2018.19.1.93

Guérard, N., Morand, O. and Dingemans, J. 2017. Lucerastat, an iminosugar with potential as substrate reduction therapy for glycolipid storage disorders: safety, tolerability, and pharmacokinetics in healthy subjects. *Orphanet journal of rare diseases* 12(1), p. 9. doi: 10.1186/s13023-017-0565-9

Gèze, M., Morlière, P., Mazière, J. C., Smith, K. M. and Santus, R. 1993. Lysosomes, a key target of hydrophobic photosensitizers proposed for photochemotherapeutic applications. *Journal of photochemistry and photobiology. B, Biology* 20(1), pp. 23-35. doi: 10.1016/1011-1344(93)80128-V

Haase, H. and Beyersmann, D. 1999. Uptake and intracellular distribution of labile and total Zn(II) in C6 rat glioma cells investigated with fluorescent probes and atomic absorption. *Biometals* 12(3), pp. 247-254. doi: 10.1023/A:1009232311677

Hallows, J. L., Iosif, R. E., Biasell, R. D. and Vincent, I. 2006. p35/p25 Is Not Essential for Tau and Cytoskeletal Pathology or Neuronal Loss in Niemann-Pick Type C Disease. *The Journal of neuroscience* 26(10), pp. 2738-2744. doi: 10.1523/JNEUROSCI.4834-05.2006

Han, S. et al. 2021. Potential Disease-Modifying Effects of Lithium Carbonate in Niemann-Pick Disease, Type C1. *Frontiers in pharmacology* 12, pp. 667361-667361. doi: 10.3389/fphar.2021.667361

Han, Y., Goldberg, J. M., Lippard, S. J. and Palmer, A. E. 2018. Superiority of SpiroZin2 Versus FluoZin-3 for monitoring vesicular Zn<sup>2+</sup> allows tracking of lysosomal Zn<sup>2+</sup> pools. *Scientific reports* 8(1), pp. 1-15. doi: 10.1038/s41598-018-33102-w

Hastings, C. et al. 2019. Expanded access with intravenous hydroxypropyl- $\beta$ -cyclodextrin to treat children and young adults with Niemann-Pick disease type C1: a case report analysis. *Orphanet journal of rare diseases* 14(1), pp. 228-228. doi: 10.1186/s13023-019-1207-1

Hawiger, J. and Timmons, S. 1973. Dynamic changes in the membrane of leukocyte lysosomes detected with fluorescent probe and accompanied by release of lysosomal enzymes. *Biochemical and Biophysical Research Communications* 55(4), pp. 1278-1284.

Hegedüs, L. et al. 2022. Nintedanib and Dasatinib Treatments Induce Protective Autophagy as a Potential Resistance Mechanism in MPM Cells. *Frontiers in cell and developmental biology* 10, pp. 852812-852812. doi: 10.3389/fcell.2022.852812

Heins-Marroquin, U., Jung, P. P., Cordero-Maldonado, M. L., Crawford, A. D. and Linster, C. L. 2019. Phenotypic assays in yeast and zebrafish reveal drugs that rescue ATP13A2 deficiency. *Brain communications* 1(1), pp. fc019-fc019. doi: 10.1093/braincomms/fcz019

Heitner, R., Elstein, D., Aerts, J., Weely, S. v. and Zimran, A. 2002. Low-Dose N-Butyldeoxynojirimycin (OGT 918) for Type I Gaucher Disease. *Blood cells, molecules, & diseases* 28(2), pp. 127-133. doi: 10.1006/bcmd.2002.0497

Heitz, C., Epelbaum, S. and Nadjar, Y. 2017. Cognitive impairment profile in adult patients with Niemann pick type C disease. *Orphanet journal of rare diseases* 12(1), pp. 166-166. doi: 10.1186/s13023-017-0714-1

Helenius, A. and Aebi, M. 2001. Intracellular Functions of N-Linked Glycans. *Science (American Association for the Advancement of Science)* 291(5512), pp. 2364-2369. doi: 10.1126/science.291.5512.2364

Hillard, C. J. and Auchampach, J. A. 1994. In vitro activation of brain protein kinase C by the cannabinoids. *Biochimica et biophysica acta. Molecular cell research* 1220(2), pp. 163-170. doi: 10.1016/0167-4889(94)90131-7

Holopainen, J. M., Saarikoski, J., Kinnunen, P. K. J. and Järvelä, I. 2001. Elevated lysosomal pH in neuronal ceroid lipofuscinoses (NCLs). *European journal of biochemistry* 268(22), pp. 5851-5856. doi: 10.1046/j.0014-2956.2001.02530.x

Horgan, C., Watts, K., Ram, D., Rust, S., Hutton, R., Jones, S. and Wynn, R. 2023. A retrospective cohort study of Libmeldy (atidarsagene autotemcel) for MLD : What we have accomplished and what opportunities lie ahead. *JIMD reports* 64(5), pp. 346-352. doi: 10.1002/jmd2.12378

Howes, M. T. et al. 2010. Clathrin-independent carriers form a high capacity endocytic sorting system at the leading edge of migrating cells. *The Journal of cell biology* 190(4), pp. 675-691. doi: 10.1083/jcb.201002119

Hu, J. et al. 2021a. Clinical, biochemical, and genotype-phenotype correlations of 118 patients with Niemann-Pick disease Types A/B. *Human mutation* 42(5), pp. 614-625. doi: 10.1002/humu.24192

Hu, M., Yang, F., Huang, Y., You, X., Liu, D., Sun, S. and Sui, S. F. 2021b. Structural insights into the mechanism of human NPC1L1-mediated cholesterol uptake. *Science advances* 7(29), doi: 10.1126/sciadv.abg3188

Hu, Y.-B., Dammer, E. B., Ren, R.-J. and Wang, G. 2015. The endosomal-lysosomal system: from acidification and cargo sorting to neurodegeneration. *Translational neurodegeneration* 4(1), pp. 18-18. doi: 10.1186/s40035-015-0041-1

Huang, L. and Tepasamorndech, S. 2013. The SLC30 family of zinc transporters – A review of current understanding of their biological and pathophysiological roles. *Molecular aspects of medicine* 34(2-3), pp. 548-560. doi: 10.1016/j.mam.2012.05.008

Hughes, M. P. et al. 2018. AAV9 intracerebroventricular gene therapy improves lifespan, locomotor function and pathology in a mouse model of Niemann-Pick type C1 disease. *Human molecular genetics* 27(17), pp. 3079-3098. doi: 10.1093/hmg/ddy212

Huitema, K., van den Dikkenberg, J., Brouwers, J. F. H. M. and Holthuis, J. C. M. 2004. Identification of a family of animal sphingomyelin synthases. *The EMBO journal* 23(1), pp. 33-44. doi: 10.1038/sj.emboj.7600034

Hung, Y. H. et al. 2014. Altered transition metal homeostasis in Niemann-Pick disease, type C1. *Metallomics* 6(3), pp. 542-553. doi: 10.1039/c3mt00308f

Imrie, J., Heptinstall, L., Knight, S. and Strong, K. 2015. Observational cohort study of the natural history of Niemann-Pick disease type C in the UK: a 5-year update from the UK clinical database. *BMC neurology* 15(1), pp. 257-257. doi: 10.1186/s12883-015-0511-1

Infante, R. E. et al. 2008. Purified NPC1 protein: II. Localization of sterol binding to a 240-amino acid soluble luminal loop. *The Journal of biological chemistry* 283(2), pp. 1064-1075.

Ingemann, L. and Kirkegaard, T. 2014. Lysosomal storage diseases and the heat shock response: convergences and therapeutic opportunities. *Journal of lipid research* 55(11), pp. 2198-2210. doi: 10.1194/jlr.R048090

- Iravani, M., Nedaeifard, L., Alimoghaddam, K., Mousavi, A., Karimi, M. and Ghavamzadeh, A. 2006. Bone marrow transplantation in a child with type C of niemann-pick disease (second case in the world). *Biology of blood and marrow transplantation* 12(2), pp. 129-129. doi: 10.1016/j.bbmt.2005.11.396
- Ishiguro, K., Ando, T. and Goto, H. 2008. Novel application of 4-nitro-7-(1-piperazinyl)-2,1,3-benzoxadiazole to visualize lysosomes in live cells. *BioTechniques* 45(4), pp. 465-468. doi: 10.2144/000112912
- Ishikawa, M. and Numakunai, T. 1972. Changes in the activity of acid phosphatase and the appearance of metamorphosing potencies of the larvae of the Ascidian halocynthia Rozetzi. *Development, growth & differentiation* 14(1), pp. 75-84. doi: 10.1111/j.1440-169X.1972.00075.x
- Janahmadi, M., Goudarzi, I., Kaffashian, M. R., Behzadi, G., Fathollahi, Y. and Hajizadeh, S. 2009. Co-treatment with riluzole, a neuroprotective drug, ameliorates the 3-acetylpyridine-induced neurotoxicity in cerebellar Purkinje neurones of rats: Behavioural and electrophysiological evidence. *Neurotoxicology (Park Forest South)* 30(3), pp. 393-402. doi: 10.1016/j.neuro.2009.02.014
- Jenkins, R. W. et al. 2010. Regulated secretion of acid sphingomyelinase: implications for selectivity of ceramide formation. *The Journal of biological chemistry* 285(46), pp. 35706-35718. doi: 10.1074/jbc.M110.125609
- Jenkins, R. W. et al. 2011. A novel mechanism of lysosomal acid sphingomyelinase maturation: requirement for carboxyl-terminal proteolytic processing. *The Journal of biological chemistry* 286(5), pp. 3777-3788. doi: 10.1074/jbc.M110.155234
- Jeurissen, M. L. J. et al. 2016. Prevention of oxLDL uptake leads to decreased atherosclerosis in hematopoietic NPC1-deficient Ldlr  $-/-$  mice. *Atherosclerosis* 255, pp. 59-65. doi: 10.1016/j.atherosclerosis.2016.10.038
- Jia, L., Betters, J. L. and Yu, L. 2011. Niemann-Pick C1-Like 1 (NPC1L1) protein in intestinal and hepatic cholesterol transport. *Annual review of physiology* 73(1), pp. 239-259. doi: 10.1146/annurev-physiol-012110-142233
- Johansson, E., Lindh, U., Westermarck, T., Heiskala, H. and Santavuori, P. 1990. Altered elemental profiles in neuronal ceroid lipofuscinosis. *Journal of trace elements and electrolytes in health and disease* 4(3), p. 139.
- Kahali, S., Sarcar, B., Fang, B., Williams, E. S., Koomen, J. M., Tofilon, P. J. and Chinnaiyan, P. 2010. Activation of the Unfolded Protein Response Contributes toward the Antitumor Activity of Vorinostat. *Neoplasia (New York, N.Y.)* 12(1), pp. 80-86. doi: 10.1593/neo.91422
- Kambe, T., Suzuki, T., Nagao, M. and Yamaguchi-Iwai, Y. 2006. Sequence Similarity and Functional Relationship Among Eukaryotic ZIP and CDF Transporters. *Genomics, proteomics & bioinformatics* 4(1), pp. 1-9. doi: 10.1016/S1672-0229(06)60010-7

Kambe, T., Tsuji, T., Hashimoto, A. and Itsumura, N. 2015. The Physiological, Biochemical, and Molecular Roles of Zinc Transporters in Zinc Homeostasis and Metabolism. *Physiological reviews* 95(3), pp. 749-784. doi: 10.1152/physrev.00035.2014

Kamizono, A., Nishizawa, M., Teranishi, Y., Murata, K. and Kimura, A. 1989. Identification of a gene conferring resistance to zinc and cadmium ions in the yeast *Saccharomyces cerevisiae*. *Molecular & general genetics* 219(1-2), pp. 161-167. doi: 10.1007/BF00261172

Kang, I. et al. 2018. Stem cell-secreted 14,15- epoxyeicosatrienoic acid rescues cholesterol homeostasis and autophagic flux in Niemann-Pick-type C disease. *Experimental & molecular medicine* 50(11), pp. 1-14. doi: 10.1038/s12276-018-0176-0

Kanninen, K. M. et al. 2013. Increased zinc and manganese in parallel with neurodegeneration, synaptic protein changes and activation of Akt/GSK3 signaling in ovine CLN6 neuronal ceroid lipofuscinosis. *PLoS one* 8(3), pp. e58644-e58644. doi: 10.1371/journal.pone.0058644

Karim, M. R. and Petering, D. H. 2016. Newport Green, a fluorescent sensor of weakly bound cellular Zn<sup>2+</sup>: competition with proteome for Zn<sup>2+</sup>. Electronic supplementary information (ESI) available. See DOI: 10.1039/c5mt00167f. 8(2), pp. 21-21. doi: 10.1039/c5mt00167f

Keam, S. J. 2022. Olipudase Alfa: First Approval. *Drugs (New York, N.Y.)* 82(8), pp. 941-947. doi: 10.1007/s40265-022-01727-x

Keilin, D. and Mann, T. 1985. Carbonic Anhydrase. Purification And Nature Of The Enzyme. *Nutrition reviews* 43(5), pp. 150-152. doi: 10.1111/j.1753-4887.1985.tb06896.x

Kidnapillai, S. et al. 2019. Drugs used in the treatment of bipolar disorder and their effects on cholesterol biosynthesis - A possible therapeutic mechanism. *The world journal of biological psychiatry* 20(10), pp. 766-777. doi: 10.1080/15622975.2019.1669823

Kim, M. P. et al. 2011. ALDH activity selectively defines an enhanced tumor-initiating cell population relative to CD133 expression in human pancreatic adenocarcinoma. *PLoS one* 6(6), pp. e20636-e20636. doi: 10.1371/journal.pone.0020636

Kim, S.-J., Lee, B.-H., Lee, Y.-S. and Kang, K.-S. 2007. Defective cholesterol traffic and neuronal differentiation in neural stem cells of Niemann–Pick type C disease improved by valproic acid, a histone deacetylase inhibitor. *Biochemical and biophysical research communications* 360(3), pp. 593-599. doi: 10.1016/j.bbrc.2007.06.116

Kimura, T. and Kambe, T. 2016. The Functions of Metallothionein and ZIP and ZnT Transporters: An Overview and Perspective. *International journal of molecular sciences* 17(3), pp. 336-336. doi: 10.3390/ijms17030336

Kirkegaard, T. et al. 2016. Heat shock protein-based therapy as a potential candidate for treating the sphingolipidoses. *Science translational medicine* 8(355), pp. 355ra118-355ra118. doi: 10.1126/scitranslmed.aad9823

Kirkegaard, T. et al. 2010. Hsp70 stabilizes lysosomes and reverts Niemann-Pick disease-associated lysosomal pathology. *Nature (London)* 463(7280), pp. 549-553. doi: 10.1038/nature08710

Kitatani, K., Idkowiak-Baldys, J. and Hannun, Y. A. 2008. The sphingolipid salvage pathway in ceramide metabolism and signaling. *Cellular signalling* 20(6), pp. 1010-1018. doi: 10.1016/j.cellsig.2007.12.006

Klionsky, D. J., Eskelinen, E.-L. and Deretic, V. 2014. Autophagosomes, phagosomes, autolysosomes, phagolysosomes, autophagolysosomes... Wait, I'm confused. *Autophagy* 10(4), pp. 549-551. doi: 10.4161/auto.28448

Koenig, H. 1963. Intravital staining of lysosomes by basic dyes and metallic ions. *The journal of histochemistry and cytochemistry* 11(1), pp. 120-121. doi: 10.1177/11.1.120

Kollmann, K. et al. 2012. Lysosomal dysfunction causes neurodegeneration in mucopolidosis II 'knock-in' mice. *Brain (London, England : 1878)* 135(Pt 9), pp. 2661-2675. doi: 10.1093/brain/aws209

Kolter, T. and Sandhoff, K. 2005. Principles of lysosomal membrane digestion: stimulation of sphingolipid degradation by sphingolipid activator proteins and anionic lysosomal lipids. *Annual review of cell and developmental biology* 21(1), pp. 81-103. doi: 10.1146/annurev.cellbio.21.122303.120013

Kornfeld, S., Ghosh, P. and Dahms, N. M. 2003. Mannose 6-phosphate receptors: new twists in the tale. *Nature reviews. Molecular cell biology* 4(3), pp. 202-213. doi: 10.1038/nrm1050

Kornhuber, J. et al. 2011. Identification of novel functional inhibitors of acid sphingomyelinase. *PloS one* 6(8), pp. e23852-e23852. doi: 10.1371/journal.pone.0023852

Krezel, A. and Maret, W. 2006. Zinc-buffering capacity of a eukaryotic cell at physiological pZn. *Journal of biological inorganic chemistry* 11(8), pp. 1049-1062. doi: 10.1007/s00775-006-0150-5

Kucic, I., Lee, J. K., Coblentz, J., Kelleher, S. L. and Kiselyov, K. 2013. Zinc-dependent lysosomal enlargement in TRPML1-deficient cells involves MTF-1 transcription factor and ZnT4 (Slc30a4) transporter. *Biochemical journal* 451(2), pp. 155-163. doi: 10.1042/bj20121506

Kumar, N., Gross, J. J. B. and Ahlskog, J. E. 2004. Copper deficiency myelopathy produces a clinical picture like subacute combined degeneration. *Neurology* 63(1), p. 33. doi: 10.1212/01.WNL.0000132644.52613.FA

Kumar, P. et al. 2011. SREBP2 mediates the modulation of intestinal NPC1L1 expression by curcumin. *American Journal of Physiology - Gastrointestinal and Liver Physiology* 301(1), pp. 148-155. doi: 10.1152/ajpgi.00119.2011

Kumari, S., Swetha, M. G. and Mayor, S. 2010. Endocytosis unplugged : multiple ways to enter the cell. *Cell research* 20(3), pp. 256-275. doi: 10.1038/cr.2010.19

Kurtzberg, J. et al. 2015. Preclinical characterization of DUOC-01, a cell therapy product derived from banked umbilical cord blood for use as an adjuvant to umbilical cord blood transplantation for treatment of inherited metabolic diseases. *Cytotherapy (Oxford, England)* 17(6), pp. 803-815. doi: 10.1016/j.jcyt.2015.02.006

Kwon, H. J., Abi-Mosleh, L., Wang, M. L., Deisenhofer, J., Goldstein, J. L., Brown, M. S. and Infante, R. E. 2009. Structure of N-Terminal Domain of NPC1 Reveals Distinct Subdomains for Binding and Transfer of Cholesterol. *Cell (Cambridge)* 137(7), pp. 1213-1224. doi: 10.1016/j.cell.2009.03.049

Kölzer, M., Ferlinz, K., Bartelsen, O., Hoops, S. L., Lang, F. and Sandhoff, K. 2004. Functional characterization of the postulated intramolecular sphingolipid activator protein domain of human acid sphingomyelinase. *Biological chemistry* 385(12), pp. 1193-1195. doi: 10.1515/BC.2004.154

La Spina, M., Contreras, P. S., Rissone, A., Meena, N. K., Jeong, E. and Martina, J. A. 2021. MIT/TFE Family of Transcription Factors: An Evolutionary Perspective. *Frontiers in cell and developmental biology* 8, pp. 609683-609683. doi: 10.3389/fcell.2020.609683

Labrecque, M., Touma, L., Bhérer, C., Duquette, A. and Tétreault, M. 2021. Estimated prevalence of Niemann-Pick type C disease in Quebec. *Scientific reports* 11(1), pp. 22621-22621. doi: 10.1038/s41598-021-01966-0

Lachmann, R. H. 2011. Enzyme replacement therapy for lysosomal storage diseases. *Current opinion in pediatrics* 23(6), pp. 588-593. doi: 10.1097/MOP.0b013e32834c20d9

Lachmann, R. H., Diaz, G. A., Wasserstein, M. P., Armstrong, N. M., Yarramaneni, A., Kim, Y. and Kumar, M. 2023. Olipudase alfa enzyme replacement therapy for acid sphingomyelinase deficiency (ASMD): sustained improvements in clinical outcomes after 6.5 years of treatment in adults. *Orphanet journal of rare diseases* 18(1), pp. 94-94. doi: 10.1186/s13023-023-02700-x

Lachmann, R. H. et al. 2004. Treatment with miglustat reverses the lipid-trafficking defect in Niemann-Pick disease type C. *Neurobiology of disease* 16(3), pp. 654-658. doi: 10.1016/j.nbd.2004.05.002

Lampe, M., Vassilopoulos, S. and Merrifield, C. 2016. Clathrin coated pits, plaques and adhesion. *Journal of structural biology* 196(1), pp. 48-56. doi: 10.1016/j.jsb.2016.07.009

Lamri, A., Pigeyre, M., Garver, W. S. and Meyre, D. 2018. The Extending Spectrum of NPC1-Related Human Disorders: From Niemann–Pick C1 Disease to Obesity. *Endocrine reviews* 39(2), pp. 192-220. doi: 10.1210/er.2017-00176

Lazzarino, D. A. and Gabel, C. A. 1989. Mannose Processing Is an Important Determinant in the Assembly of Phosphorylated High Mannose-type Oligosaccharides. *The Journal of biological chemistry* 264(9), pp. 5015-5023. doi: 10.1016/S0021-9258(18)83692-4

Lee, C. A. and Blackstone, C. 2020. ER morphology and endo-lysosomal crosstalk: Functions and disease implications. *Biochimica et biophysica acta. Molecular and cell biology of lipids* 1865(1), pp. 158544-158544. doi: 10.1016/j.bbalip.2019.158544

Lee, C. Y. P., Ruel, I. P., Denis, M. P., Genest, J. M. D. and Kiss, R. S. P. 2013. Cholesterol trapping in Niemann–Pick disease type B fibroblasts can be relieved by expressing the phosphotyrosine binding domain of GULP. *Journal of clinical lipidology* 7(2), pp. 153-164. doi: 10.1016/j.jacl.2012.02.006

Lee, H. et al. 2014. Pathological roles of the VEGF/SphK pathway in Niemann–Pick type C neurons. *Nature communications* 5(1), pp. 5514-5514. doi: 10.1038/ncomms6514

Leweke, F. M. et al. 2012. Cannabidiol enhances anandamide signaling and alleviates psychotic symptoms of schizophrenia. *Translational psychiatry* 2(3), pp. e94-e94. doi: 10.1038/tp.2012.15

Li, F. and Zhang, H. 2019. Lysosomal Acid Lipase in Lipid Metabolism and Beyond. *Arteriosclerosis, thrombosis, and vascular biology* 39(5), pp. 850-856. doi: 10.1161/ATVBAHA.119.312136

Li, L., Chen, Y. and Shi, C. 2022. Nintedanib ameliorates oxidized low-density lipoprotein -induced inflammation and cellular senescence in vascular endothelial cells. *Bioengineered* 13(3), pp. 6196-6207. doi: 10.1080/21655979.2022.2036913

Li, X., Wang, J., Coutavas, E., Shi, H., Hao, Q. and Blobel, G. 2016. Structure of human Niemann–Pick C1 protein. *Proceedings of the National Academy of Sciences - PNAS* 113(29), pp. 8212-8217. doi: 10.1073/pnas.1607795113

Liao, G., Cheung, S., Galeano, J., Ji, A. X., Qin, Q. and Bi, X. 2009. Allopregnanolone treatment delays cholesterol accumulation and reduces autophagic/lysosomal dysfunction and inflammation in Npc1–/– mouse brain. *Brain research* 1270, pp. 140-151. doi: 10.1016/j.brainres.2009.03.027

Liu, X., Zhao, P., Wang, X., Wang, L., Zhu, Y., Song, Y. and Gao, W. 2019. Celastrol mediates autophagy and apoptosis via the ROS/JNK and Akt/mTOR signaling pathways in glioma cells. *Journal of experimental & clinical cancer research* 38(1), pp. 184-184. doi: 10.1186/s13046-019-1173-4

Liuzzi, J. P. and Cousins, R. J. 2004. Mammalian zinc transporters. *Annual review of nutrition* 24(1), pp. 151-172. doi: 10.1146/annurev.nutr.24.012003.132402

- Lloyd-Evans, E. et al. 2008. Niemann-Pick disease type C1 is a sphingosine storage disease that causes deregulation of lysosomal calcium. *Nature medicine* 14(11), pp. 1247-1255. doi: 10.1038/nm.1876
- Logan-Smith, M. J., Lockyer, P. J., East, J. M. and Lee, A. G. 2001. Curcumin, a Molecule That Inhibits the Ca<sup>2+</sup>-ATPase of Sarcoplasmic Reticulum but Increases the Rate of Accumulation of Ca<sup>2+</sup>. *The Journal of biological chemistry* 276(50), pp. 46905-46911. doi: 10.1074/jbc.M108778200
- Luzio, J. P., Pryor, P. R. and Bright, N. A. 2007. Lysosomes: fusion and function. *Nature reviews. Molecular cell biology* 8(8), pp. 622-632. doi: 10.1038/nrm2217
- Maguire, E. 2017. Investigating ion dyshomeostasis in Niemann-Pick disease type C, both in vitro and in vivo.
- Marchesini, N. and Hannun, Y. A. 2004. Acid and neutral sphingomyelinases: roles and mechanisms of regulation. *Biochemistry and cell biology* 82(1), pp. 27-44. doi: 10.1139/o03-091
- Maret, W. 2009. Fluorescent probes for the structure and function of metallothionein. *Journal of chromatography. B, Analytical technologies in the biomedical and life sciences* 877(28), pp. 3378-3383. doi: 10.1016/j.jchromb.2009.06.014
- Maret, W. 2013. Zinc Biochemistry: From a Single Zinc Enzyme to a Key Element of Life. *Advances in nutrition (Bethesda, Md.)* 4(1), pp. 82-91. doi: 10.3945/an.112.003038
- Martínez, V., Iriondo De-Hond, A., Borrelli, F., Capasso, R., Del Castillo, M. D. and Abalo, R. 2020. Cannabidiol and Other Non-Psychoactive Cannabinoids for Prevention and Treatment of Gastrointestinal Disorders: Useful Nutraceuticals? *International journal of molecular sciences* 21(9), p. 3067. doi: 10.3390/ijms21093067
- Marín, T. et al. 2014. Vitamin E dietary supplementation improves neurological symptoms and decreases c-Abl/p73 activation in Niemann-Pick C mice. *Nutrients* 6(8), pp. 3000-3017. doi: 10.3390/nu6083000
- Marín, T. et al. 2022. c-Abl Activation Linked to Autophagy-Lysosomal Dysfunction Contributes to Neurological Impairment in Niemann-Pick Type A Disease. *Frontiers in cell and developmental biology* 10, pp. 844297-844297. doi: 10.3389/fcell.2022.844297
- Matsuo, M. et al. 2014. Effects of intracerebroventricular administration of 2-hydroxypropyl- $\beta$ -cyclodextrin in a patient with Niemann-Pick Type C disease. *Molecular genetics and metabolism reports* 1(C), pp. 391-400. doi: 10.1016/j.ymgmr.2014.08.004
- Matsuo, M. et al. 2013. Effects of cyclodextrin in two patients with Niemann-Pick Type C disease. *Molecular genetics and metabolism* 108(1), pp. 76-81. doi: 10.1016/j.ymgme.2012.11.005

Mayor, S., Presley, J. F. and Maxfield, F. R. 1993. Sorting of Membrane Components from Endosomes and Subsequent Recycling to the Cell Surface Occurs by a Bulk Flow Process. *The Journal of cell biology* 121(6), pp. 1257-1269. doi: 10.1083/jcb.121.6.1257

Maywald, M. and Rink, L. 2022. Zinc in Human Health and Infectious Diseases. *Biomolecules (Basel, Switzerland)* 12(12), p. 1748. doi: 10.3390/biom12121748

Mazein, A., Watterson, S., Hsieh, W.-Y., Griffiths, W. J. and Ghazal, P. 2013. A comprehensive machine-readable view of the mammalian cholesterol biosynthesis pathway. *Biochemical pharmacology* 86(1), pp. 56-66. doi: 10.1016/j.bcp.2013.03.021

McGovern, M. M., Lipka, N., Bagiella, E., Schuchman, E. H., Desnick, R. J. and Wasserstein, M. P. 2013. Morbidity and mortality in type B Niemann-Pick disease. *Genetics in medicine* 15(8), pp. 618-623. doi: 10.1038/gim.2013.4

McKay Bounford, K. and Gissen, P. 2014. Genetic and laboratory diagnostic approach in Niemann Pick disease type C. *Journal of neurology* 261(S2), pp. 569-575. doi: 10.1007/s00415-014-7386-8

McMahon, H. T. and Schmid, E. M. 2007. Integrating molecular and network biology to decode endocytosis. *Nature (London)* 448(7156), pp. 883-888. doi: 10.1038/nature06031

Meeran, M. F. N. et al. 2021.  $\beta$ -Caryophyllene, a natural bicyclic sesquiterpene attenuates  $\beta$ -adrenergic agonist-induced myocardial injury in a cannabinoid receptor-2 dependent and independent manner. *Free radical biology & medicine* 167, pp. 348-366. doi: 10.1016/j.freeradbiomed.2021.01.046

Meikle, P. J., Hopwood, J. J., Clague, A. E. and Carey, W. F. 1999. Prevalence of Lysosomal Storage Disorders. *JAMA : the journal of the American Medical Association* 281(3), pp. 249-254. doi: 10.1001/jama.281.3.249

Mendoza, A. D. et al. 2024. Lysosome-related organelles contain an expansion compartment that mediates delivery of zinc transporters to promote homeostasis. *Proceedings of the National Academy of Sciences - PNAS* 121(7), pp. e2307143121-e2307143121. doi: 10.1073/pnas.2307143121

Menezes, A. C. d. S., Alves, L. D. B., Goldemberg, D. C., de Melo, A. C. and Antunes, H. S. 2022. Anti-inflammatory and wound healing effect of Copaiba oleoresin on the oral cavity: A systematic review. *Heliyon* 8(2), pp. e08993-e08993. doi: 10.1016/j.heliyon.2022.e08993

Merza, H., Sood, N. and Sood, R. 2015. Idiopathic hyperzincemia with associated copper deficiency anemia: a diagnostic dilemma. *Clinical case reports* 3(10), pp. 819-822. doi: 10.1002/ccr3.344

Mettlen, M., Chen, P.-H., Srinivasan, S., Danuser, G. and Schmid, S. L. 2018. Regulation of Clathrin-Mediated Endocytosis. *Annual review of biochemistry* 87(1), pp. 871-896. doi: 10.1146/annurev-biochem-062917-012644

Millat, G., Bailo, N., Molinero, S., Rodriguez, C., Chikh, K. and Vanier, M. T. 2005. Niemann–Pick C disease: Use of denaturing high performance liquid chromatography for the detection of NPC1 and NPC2 genetic variations and impact on management of patients and families. *Molecular genetics and metabolism* 86(1), pp. 220-232. doi: 10.1016/j.ymgme.2005.07.007

Millat, G. et al. 1999. Niemann-Pick C1 Disease: The I1061T Substitution Is a Frequent Mutant Allele in Patients of Western European Descent and Correlates with a Classic Juvenile Phenotype. *American journal of human genetics* 65(5), pp. 1321-1329. doi: 10.1086/302626

Miller, J., McLachlan, A. D. and Klug, A. 1985. Repetitive zinc-binding domains in the protein transcription factor IIIA from *Xenopus oocytes*. *The EMBO journal* 4(6), pp. 1609-1614. doi: 10.1002/j.1460-2075.1985.tb03825.x

Milstien, S. and Spiegel, S. 2003. Sphingosine-1-phosphate: an enigmatic signalling lipid. *Nature reviews. Molecular cell biology* 4(5), pp. 397-407. doi: 10.1038/nrm1103

Minckley, T. F., Zhang, C., Fudge, D. H., Dischler, A. M., LeJeune, K. D., Xu, H. and Qin, Y. 2019. Sub-nanomolar sensitive GZnP3 reveals TRPML1-mediated neuronal Zn<sup>2+</sup> signals. *Nature communications* 10(1), pp. 1-14. doi: 10.1038/s41467-019-12761-x

Mistry, P. K., Kishnani, P. S., Balwani, M., Charrow, J. M., Hull, J., Weinreb, N. J. and Cox, T. M. 2023. The Two Substrate Reduction Therapies for Type 1 Gaucher Disease Are Not Equivalent. Comment on Hughes et al. Switching between Enzyme Replacement Therapies and Substrate Reduction Therapies in Patients with Gaucher Disease: Data from the Gaucher Outcome Survey (GOS). *J. Clin. Med.* 2022, 11, 5158. *Journal of clinical medicine* 12(9), p. 3269. doi: 10.3390/jcm12093269

Mitamura, T. 1987. Glucocorticoid-induced elevation of serum high-density lipoprotein-cholesterol and its reversal by adrenocorticotropin in the rat. *Biochimica et biophysica acta. Lipids and lipid metabolism* 917(1), pp. 121-130. doi: 10.1016/0005-2760(87)90292-X

Mitroi, D. N., Pereyra-Gómez, G., Soto-Huelin, B., Senovilla, F., Kobayashi, T., Esteban, J. A. and Ledesma, M. D. 2019. NPC1 enables cholesterol mobilization during long-term potentiation that can be restored in Niemann–Pick disease type C by CYP46A1 activation. *EMBO reports* 20(11), pp. e48143-n/a. doi: 10.15252/embr.201948143

Mitsche, M. A., McDonald, J. G., Hobbs, H. H. and Cohen, J. C. 2015. Flux analysis of cholesterol biosynthesis in vivo reveals multiple tissue and cell-type specific pathways. *eLife* 4, pp. e07999-e07999. doi: 10.7554/elife.07999

Mocchegiani, E., Giacconi, R. and Malavolta, M. 2008. Zinc signalling and subcellular distribution: emerging targets in type 2 diabetes. *Trends in molecular medicine* 14(10), pp. 419-428. doi: 10.1016/j.molmed.2008.08.002

Moskot, M. et al. 2014. The Phytoestrogen Genistein Modulates Lysosomal Metabolism and Transcription Factor EB (TFEB) Activation. *The Journal of biological chemistry* 289(24), pp. 17054-17069. doi: 10.1074/jbc.M114.555300

Mu, T.-W., Ong, D. S. T., Wang, Y.-J., Balch, W. E., Yates, J. R., Segatori, L. and Kelly, J. W. 2008. Chemical and Biological Approaches Synergize to Ameliorate Protein-Folding Diseases. *Cell* 134(5), pp. 769-781. doi: 10.1016/j.cell.2008.06.037

Mullard, A. 2024. FDA approves gene therapy for metachromatic leukodystrophy, the tenth for a genetic disease and the priciest yet. *Nature reviews. Drug discovery*,

Mullen, T. D., Hannun, Y. A. and Obeid, L. M. 2012. Ceramide synthases at the centre of sphingolipid metabolism and biology. *Biochemical journal* 441(3), pp. 789-802. doi: 10.1042/BJ20111626

Nakasone, N., Nakamura, Y. S., Higaki, K., Oumi, N., Ohno, K. and Ninomiya, H. 2014. Endoplasmic reticulum-associated degradation of Niemann-Pick C1: evidence for the role of heat shock proteins and identification of lysine residues that accept ubiquitin. *The Journal of biological chemistry* 289(28), pp. 19714-19725. doi: 10.1074/jbc.M114.549915

Newrzella, D. and Stoffel, W. 1992. Molecular Cloning of the Acid Sphingomyelinase of the Mouse and the Organization and Complete Nucleotide Sequence of the Gene. *Biological Chemistry* 373(12), pp. 1233-1238.

Newton, J. et al. 2017. FTY720/fingolimod increases NPC1 and NPC2 expression and reduces cholesterol and sphingolipid accumulation in Niemann-Pick type C mutant fibroblasts. *The FASEB journal* 31(4), pp. 1719-1730. doi: 10.1096/fj.201601041R

Newton, J., Milstien, S. and Spiegel, S. 2018. Niemann-Pick type C disease: The atypical sphingolipidosis. *Advances in biological regulation* 70, pp. 82-88. doi: 10.1016/j.jbior.2018.08.001

Newton, J. et al. 2020. Targeting defective sphingosine kinase 1 in Niemann–Pick type C disease with an activator mitigates cholesterol accumulation. *The Journal of biological chemistry* 295(27), pp. 9121-9133. doi: 10.1074/jbc.RA120.012659

Nikaido, H. 2018. RND transporters in the living world. *Research in microbiology* 169(7-8), pp. 363-371. doi: 10.1016/j.resmic.2018.03.001

Nittari, G., Tomassoni, D., Roy, P., Martinelli, I., Tayebati, S. K. and Amenta, F. 2023. Batten disease through different in vivo and in vitro models: A review. *Journal of neuroscience research* 101(3), pp. 298-315. doi: 10.1002/jnr.25147

Nobutaka, O., Dennis, C. K., Matthew, T., Matthew, P. S., Catherine, C. Y. C., Ta-Yuan, C. and Vagelos, P. R. 2004. Binding between the Niemann-Pick C1 Protein and a Photoactivatable Cholesterol Analog Requires a Functional Sterol-Sensing Domain. *Proceedings of the National Academy of Sciences - PNAS* 101(34), pp. 12473-12478. doi: 10.1073/pnas.0405255101

Nunes, M. J. et al. 2024. Cholesterol redistribution triggered by CYP46A1 gene therapy improves major hallmarks of Niemann-Pick type C disease but is not sufficient to halt neurodegeneration. *Biochimica et biophysica acta. Molecular basis of disease* 1870(3), pp. 166993-166993. doi: 10.1016/j.bbadis.2023.166993

Ogawa, K., Mizuno, N. and Okamoto, M. 1961. Lysosomes in cultured cells. *The journal of histochemistry and cytochemistry* 9(2), pp. 202-202. doi: 10.1177/9.2.202

Ohgane, K., Karaki, F., Dodo, K. and Hashimoto, Y. 2013. Discovery of Oxysterol-Derived Pharmacological Chaperones for NPC1: Implication for the Existence of Second Sterol-Binding Site. *Chemistry & biology* 20(3), pp. 391-402. doi: 10.1016/j.chembiol.2013.02.009

Ohkuma, S. and Poole, B. 1978. Fluorescence Probe Measurement of the Intralysosomal pH in Living Cells and the Perturbation of pH by Various Agents. *Proceedings of the National Academy of Sciences - PNAS* 75(7), pp. 3327-3331. doi: 10.1073/pnas.75.7.3327

Ory, D. S. 2000. Niemann-Pick type C: A disorder of cellular cholesterol trafficking. *BBA - Molecular and Cell Biology of Lipids* 1529(1), pp. 331-339. doi: 10.1016/S1388-1981(00)00158-X

Ottinger, E. A. et al. 2014. Collaborative Development of 2-Hydroxypropyl- $\beta$ -Cyclodextrin for the Treatment of Niemann-Pick Type C1 Disease. *Current topics in medicinal chemistry* 14(3), pp. 330-339. doi: 10.2174/1568026613666131127160118

Pak, J. E. et al. 2013. Structures of intermediate transport states of ZneA, a Zn(II)/proton antiporter. *Proceedings of the National Academy of Sciences - PNAS* 110(46), pp. 18484-18489. doi: 10.1073/pnas.1318705110

Palmieri, M., Impey, S., Kang, H., di Ronza, A., Pelz, C., Sardiello, M. and Ballabio, A. 2011. Characterization of the CLEAR network reveals an integrated control of cellular clearance pathways. *Human molecular genetics* 20(19), pp. 3852-3866. doi: 10.1093/hmg/ddr306

Palmiter, R. D., Cole, T. B. and Findley, S. D. 1996a. ZnT-2, a mammalian protein that confers resistance to zinc by facilitating vesicular sequestration. *The EMBO journal* 15(8), pp. 1784-1791. doi: 10.1002/j.1460-2075.1996.tb00527.x

Palmiter, R. D., Cole, T. B., Quaife, C. J. and Findley, S. D. 1996b. ZnT-3, a Putative Transporter of Zinc into Synaptic Vesicles. *Proceedings of the National Academy of Sciences - PNAS* 93(25), pp. 14934-14939. doi: 10.1073/pnas.93.25.14934

Palmiter, R. D. and Findley, S. D. 1995. Cloning and functional characterization of a mammalian zinc transporter that confers resistance to zinc. *The EMBO journal* 14(4), pp. 639-649. doi: 10.1002/j.1460-2075.1995.tb07042.x

- Park, J. G. and Palmer, A. E. 2014. Quantitative Measurement of Ca<sup>2+</sup> and Zn<sup>2+</sup> in Mammalian Cells Using Genetically Encoded Fluorescent Biosensors. *Fluorescent Protein-Based Biosensors* 1071, pp. 29-47. doi: 10.1007/978-1-62703-622-1\_3
- Park, M., Koh, K. N., Seo, J. J. and Im, H. J. 2011. Clinical implications of chimerism after allogeneic hematopoietic stem cell transplantation in children with non-malignant diseases. *Korean journal of hematology* 46(4), pp. 258-264. doi: 10.5045/kjh.2011.46.4.258
- Pastores, G. M. 2012. Miglustat: Substrate Reduction Therapy for Lysosomal Storage Disorders Associated with Primary Central Nervous System Involvement. *Recent patents on CNS drug discovery* 1(1), pp. 77-82. doi: 10.2174/1574889810601010077
- Patterson, M. C. et al. 1993. The effect of cholesterol-lowering agents on hepatic and plasma cholesterol in Niemann-Pick disease type C. *Neurology* 43(1), pp. 61-64. doi: 10.1212/wnl.43.1\_part\_1.61
- Patterson, M. C. F., Vecchio, D., Prady, H., Abel, L. P. and Wraith, J. E. F. 2007. Miglustat for treatment of Niemann-Pick C disease: a randomised controlled study. *Lancet neurology* 6(9), pp. 765-772. doi: 10.1016/S1474-4422(07)70194-1
- Patton, W. F., Pande, P., Xiang, Y., Li, Z., Donegan, J. L. and Rabbani, E. 2016. *Fluorochromes for organelle tracing and multi-color imaging*. [Patent].
- Peake, K. B. and Vance, J. E. 2012. Normalization of Cholesterol Homeostasis by 2-Hydroxypropyl- $\beta$ -cyclodextrin in Neurons and Glia from Niemann-Pick C1 (NPC1)-deficient Mice. *Journal of Biological Chemistry* 287(12), pp. 9290-9298. doi: 10.1074/jbc.M111.326405
- Pepponi, R. et al. 2022. Repurposing Dipyridamole in Niemann Pick Type C Disease: A Proof of Concept Study. *International journal of molecular sciences* 23(7), p. 3456. doi: 10.3390/ijms23073456
- Pereira, Sónia R., Hackett, B., O'Driscoll, David N., Sun, Melody C. and Downer, Eric J. 2021. Cannabidiol modulation of oxidative stress and signalling. *Neuronal signaling* 5(3), pp. NS20200080-NS20200080. doi: 10.1042/NS20200080
- Peres, F. F., Lima, A. C., Hallak, J. E. C., Crippa, J. A., Silva, R. H. and Abílio, V. C. 2018. Cannabidiol as a Promising Strategy to Treat and Prevent Movement Disorders? *Frontiers in pharmacology* 9, pp. 482-482. doi: 10.3389/fphar.2018.00482
- Pertwee, R. G. 2006. The pharmacology of cannabinoid receptors and their ligands: an overview. *International Journal of Obesity* 30(S1), pp. S13-S18. doi: 10.1038/sj.ijo.0803272
- Pertwee, R. G. 2008. The diverse CB1 and CB2 receptor pharmacology of three plant cannabinoids: delta9-tetrahydrocannabinol, cannabidiol and delta9-tetrahydrocannabivarin. *British journal of pharmacology* 153(2), pp. 199-215.

Pfeffer, S. R. 2019. NPC intracellular cholesterol transporter 1 (NPC1)-mediated cholesterol export from lysosomes. *The Journal of biological chemistry* 294(5), pp. 1706-1709. doi: 10.1074/jbc.TM118.004165

Pinto, R. et al. 2004. Prevalence of lysosomal storage diseases in Portugal. *European journal of human genetics : EJHG* 12(2), pp. 87-92. doi: 10.1038/sj.ejhg.5201044

Piotrowska, E., Jakobkiewicz-Banecka, J., Baranska, S., Tyłki-Szymanska, A., Czartoryska, B., Wegrzyn, A. and Wegrzyn, G. 2006. Genistein-mediated inhibition of glycosaminoglycan synthesis as a basis for gene expression-targeted isoflavone therapy for mucopolysaccharidoses. *European journal of human genetics : EJHG* 14(7), pp. 846-852. doi: 10.1038/sj.ejhg.5201623

Pipalia, N. H. et al. 2017. Histone deacetylase inhibitors correct the cholesterol storage defect in most Niemann-Pick C1 mutant cells. *Journal of lipid research* 58(4), pp. 695-708. doi: 10.1194/jlr.M072140

Platt, F. M. 2014. Sphingolipid lysosomal storage disorders. *Nature (London)* 510(7503), pp. 68-75. doi: 10.1038/nature13476

Platt, F. M., d'Azzo, A., Davidson, B. L., Neufeld, E. F. and Tiffit, C. J. 2018. Lysosomal storage diseases. *Nature reviews. Disease primers* 4(1), pp. 27-27. doi: 10.1038/s41572-018-0025-4

Platt, F. M., Neises, G. R., Dwek, R. A. and Butters, T. D. 1994. N-butyldeoxynojirimycin is a novel inhibitor of glycolipid biosynthesis. *The Journal of biological chemistry* 269(11), pp. 8362-8365. doi: 10.1016/S0021-9258(17)37202-2

Pohlmann, R., Nagel, G., Hille, A., Wendland, M., Waheed, A., Bräulke, T. and von Figura, K. 1989. Mannose 6-phosphate specific receptors: structure and function. *Biochemical Society transactions* 17(1), pp. 15-16. doi: 10.1042/bst0170015

Ponting, C. P. 1994. Acid sphingomyelinase possesses a domain homologous to its activator proteins: Saposins B and D. *Protein science* 3(2), pp. 359-361. doi: 10.1002/pro.5560030219

Porcu, G. et al. 2015. Clobetasol and Halcinonide Act as Smoothed Agonists to Promote Myelin Gene Expression and ROR $\gamma$  Receptor Activation. *PLoS one* 10(12), pp. e0144550-e0144550. doi: 10.1371/journal.pone.0144550

Porstmann, T. et al. 2008. SREBP Activity Is Regulated by mTORC1 and Contributes to Akt-Dependent Cell Growth. *Cell metabolism* 8(3), pp. 224-236. doi: 10.1016/j.cmet.2008.07.007

Poulos, A., Shankaran, P., Jones, C. S. and Callahan, J. W. 1983. Enzymatic hydrolysis of sphingomyelin liposomes by normal tissues and tissues from patients with niemann-pick disease. *Biochimica et biophysica acta. Lipids and lipid metabolism* 751(3), pp. 428-431. doi: 10.1016/0005-2760(83)90302-8

Prakash, A., Bharti, K. and Majeed, A. B. A. 2015. Zinc: indications in brain disorders. *Fundamental & clinical pharmacology* 29(2), pp. 131-149. doi: 10.1111/fcp.12110

Prasad, A. S. 2012. Discovery of human zinc deficiency: 50 years later. *Journal of trace elements in medicine and biology* 26(2-3), pp. 66-69. doi: 10.1016/j.jtemb.2012.04.004

Prasad, A. S., Miale, J. A., Farid, Z., Sandstead, H. H. and Schulert, A. R. 1990. Clinical and experimental. Zinc metabolism in patients with the syndrome of iron deficiency anemia, hepatosplenomegaly, dwarfism, and hypogonadism. 1963. *The Journal of laboratory and clinical medicine* 116(5), pp. 737-749.

Prasad, A. S., Rabbani, P., Abbasii, A., Bowersox, E. and Fox, M. R. 1978. Experimental zinc deficiency in humans. *Annals of internal medicine* 89(4), pp. 483-490. doi: 10.7326/0003-4819-89-4-483

Pratt, E. P. S., Damon, L. J., Anson, K. J. and Palmer, A. E. 2021. Tools and techniques for illuminating the cell biology of zinc. *Biochimica et biophysica acta. Molecular cell research* 1868(1), pp. 118865-118865. doi: 10.1016/j.bbamcr.2020.118865

Puertollano, R., Ferguson, S. M., Brugarolas, J. and Ballabio, A. 2018. The complex relationship between TFEB transcription factor phosphorylation and subcellular localization. *The EMBO journal* 37(11), p. n/a. doi: 10.15252/emj.201798804

Pugach, E. K., Feltes, M., Kaufman, R. J., Ory, D. S. and Bang, A. G. 2018. High-content screen for modifiers of Niemann-Pick type C disease in patient cells. *Human molecular genetics* 27(12), pp. 2101-2112. doi: 10.1093/hmg/ddy117

Qin, Y., Dittmer, P. J., Park, J. G., Jansen, K. B., Palmer, A. E. and Valentine, J. S. 2011. Measuring steady-state and dynamic endoplasmic reticulum and Golgi Zn<sup>2+</sup> with genetically encoded sensors. *Proceedings of the National Academy of Sciences - PNAS* 108(18), pp. 7351-7356. doi: 10.1073/pnas.1015686108

Qin, Y., Miranda, J. G., Stoddard, C. I., Dean, K. M., Galati, D. F. and Palmer, A. E. 2013. Direct Comparison of a Genetically Encoded Sensor and Small Molecule Indicator: Implications for Quantification of Cytosolic Zn<sup>2+</sup>. *ACS chemical biology* 8(11), pp. 2366-2371. doi: 10.1021/cb4003859

Qiu, H. et al. 2003. Activation of Human Acid Sphingomyelinase through Modification or Deletion of C-terminal Cysteine. *The Journal of biological chemistry* 278(35), pp. 32744-32752. doi: 10.1074/jbc.M303022200

Qiu, Y. et al. 2020. Genome-Wide Analysis Reveals Zinc Transporter ZIP9 Regulated by DNA Methylation Promotes Radiation-Induced Skin Fibrosis via the TGF- $\beta$  Signaling Pathway. *Journal of investigative dermatology* 140(1), pp. 94-102. doi: 10.1016/j.jid.2019.04.027

Qureshi, K., Abdulmajeed, Z. G., Saleem, S., Tariq, J. and Iqbal, M. 2022. Niemann-Pick Disease Type A: A Rare Disease With a Fatal Outcome. *Curēus (Palo Alto, CA)* 14(2), p. e21955.

Raas-Rothschild, A. et al. 2000. Molecular basis of variant pseudo-hurler polydystrophy (mucopolidosis IIIC). *The Journal of clinical investigation* 105(5), pp. 673-681. doi: 10.1172/jci5826

Raben, N. and Puertollano, R. 2016. TFEB and TFE3: Linking Lysosomes to Cellular Adaptation to Stress. *Annual review of cell and developmental biology* 32(1), pp. 255-278. doi: 10.1146/annurev-cellbio-111315-125407

Rappaport, J., Garnacho, C. and Muro, S. 2014. Clathrin-Mediated Endocytosis Is Impaired in Type A–B Niemann–Pick Disease Model Cells and Can Be Restored by ICAM-1-Mediated Enzyme Replacement. *Molecular pharmaceuticals* 11(8), pp. 2887-2895. doi: 10.1021/mp500241y

Reagan, J. W., Hubbert, M. L. and Shelness, G. S. 2000. Posttranslational Regulation of Acid Sphingomyelinase in Niemann-Pick Type C1 Fibroblasts and Free Cholesterol-enriched Chinese Hamster Ovary Cells. *The Journal of biological chemistry* 275(48), pp. 38104-38110. doi: 10.1074/jbc.M005296200

Reddy, J. V., Ganley, I. G. and Pfeffer, S. R. 2006. Clues to neuro-degeneration in Niemann-Pick type C disease from global gene expression profiling. *PLoS one* 1(1), pp. e19-e19. doi: 10.1371/journal.pone.0000019

Rommel, N., Locatelli-Hoops, S., Breiden, B., Schwarzmann, G. and Sandhoff, K. 2007. Saposin B mobilizes lipids from cholesterol-poor and bis(monoacylglycerol)phosphate-rich membranes at acidic pH. Unglycosylated patient variant saposin B lacks lipid-extraction capacity. *The FEBS journal* 274(13), pp. 3405-3420. doi: 10.1111/j.1742-4658.2007.05873.x

Ribeiro, I., Marcão, A., Amaral, O., Sá Miranda, M. C., Vanier, M. T. and Millat, G. 2001. Niemann-Pick type C disease: NPC1 mutations associated with severe and mild cellular cholesterol trafficking alterations. *Human genetics* 109(1), pp. 24-32. doi: 10.1007/s004390100531

Roberts, R. 2005. Lysosomal cysteine proteases: structure, function and inhibition of cathepsins. *Drug news & perspectives* 18(10), p. 605. doi: 10.1358/dnp.2005.18.10.949485

Rodriguez-Lafrasse, C., Rousson, R., Valla, S., Antignac, P., Louisot, P. and Vanier, M. T. 1997. Modulation of protein kinase C by endogenous sphingosine: inhibition of phorbol dibutyrate binding in Niemann-Pick C fibroblasts. *Biochemical journal* 325 ( Pt 3)(3), pp. 787-791. doi: 10.1042/bj3250787

Rodriguez-Lafrasse, C. and Vanier, M. T. 1999. Sphingosylphosphorylcholine in Niemann-Pick Disease Brain: Accumulation in Type A But Not in Type B. *Neurochemical research* 24(2), pp. 199-205. doi: 10.1023/A:1022501702403

Rowland, T. J., Sweet, M. E., Mestroni, L. and Taylor, M. R. G. 2016. Danon disease - dysregulation of autophagy in a multisystem disorder with cardiomyopathy. *Journal of cell science* 129(11), pp. 2135-2143. doi: 10.1242/jcs.184770

Ruan, L., Bai, J., Ji, X., Zhao, W. and Dong, X. 2022. A series of meso amide BODIPY based lysosome-targeting fluorescent probe with high photostability and sensitivity. *Analytica chimica acta* 1205, pp. 339771-339771. doi: 10.1016/j.aca.2022.339771

Saha, A. et al. 2016. A cord blood monocyte-derived cell therapy product accelerates brain remyelination. *JCI insight* 1(13), pp. e86667-e86667. doi: 10.1172/jci.insight.86667

Sakane, H., Urabe, J., Nakahira, S., Hino, K., Miyata, N. and Akasaki, K. 2020. Involvement of lysosomal integral membrane protein-2 in the activation of autophagy. *Biochemical and biophysical research communications* 533(4), pp. 976-982. doi: 10.1016/j.bbrc.2020.09.114

Samaranch, L. et al. 2019. Adeno-associated viral vector serotype 9-based gene therapy for Niemann-Pick disease type A. *Science translational medicine* 11(506), p. eaat3738. doi: 10.1126/scitranslmed.aat3738

Sandvig, K., Pust, S., Skotland, T. and van Deurs, B. 2011. Clathrin-independent endocytosis: mechanisms and function. *Current opinion in cell biology* 23(4), pp. 413-420. doi: 10.1016/j.ceb.2011.03.007

Sarracent, J. and Finlay, C. M. 1982. The action of Clofazimine on the level of lysosomal enzymes of cultured macrophages. *Clinical and experimental immunology* 48(1), pp. 261-267.

Sarracent, J. and Finlay, C. M. 1984. In vivo effect of clofazimine in the lysosomal enzyme level and immune complex phagocytosis of mouse peritoneal macrophages. *International journal of leprosy and other mycobacterial diseases* 52(2), p. 154.

Sasisekharan, R., Raman, R. and Prabhakar, V. 2006. Glycomics approach to structure-function relationships of glycosaminoglycans. *Annual review of biomedical engineering* 8(1), pp. 181-231. doi: 10.1146/annurev.bioeng.8.061505.095745

Schiffmann, R. et al. 2023. Venglustat combined with imiglucerase for neurological disease in adults with Gaucher disease type 3: the LEAP trial. *Brain (London, England : 1878)* 146(2), pp. 461-474. doi: 10.1093/brain/awac379

Schmid, S. L. 2017. Reciprocal regulation of signaling and endocytosis: Implications for the evolving cancer cell. *The Journal of cell biology* 216(9), pp. 2623-2632. doi: 10.1083/jcb.201705017

Schneiderman, J., Thormann, K. and Kletzel, M. 2005. Niemann-Pick type B: Successful allogeneic hematopoietic stem cell transplantation with correction of enzyme levels. *Biology of blood and marrow transplantation* 11(2), pp. 81-81. doi: 10.1016/j.bbmt.2004.12.239

Schuchman, E. H. and Desnick, R. J. 2017. Types A and B Niemann-Pick disease. *Molecular genetics and metabolism* 120(1-2), pp. 27-33. doi: 10.1016/j.ymgme.2016.12.008

Schuchman, E. H., Suchi, M., Takahashi, T., Sandhoff, K. and Desnick, R. J. 1991. Human acid sphingomyelinase. Isolation, nucleotide sequence and expression of the full-length and alternatively spliced cDNAs. *The Journal of biological chemistry* 266(13), pp. 8531-8539. doi: 10.1016/S0021-9258(18)93007-3

Schwartz, M. A. and Margolis, S. 1983. Effects of drugs and sterols on cholesterol 7 alpha-hydroxylase activity in rat liver microsomes. *Journal of lipid research* 24(1), pp. 28-33. doi: 10.1016/S0022-2275(20)38021-4

Scott, C. C., Vacca, F. and Gruenberg, J. 2014. Endosome maturation, transport and functions. *Seminars in cell & developmental biology* 31, pp. 2-10. doi: 10.1016/j.semcdb.2014.03.034

Sendelbach, L. E. 1989. A review of the toxicity and carcinogenicity of anthraquinone derivatives. *Toxicology (Amsterdam)* 57(3), pp. 227-240. doi: 10.1016/0300-483X(89)90113-3

Settembre, C. et al. 2013. TFEB controls cellular lipid metabolism through a starvation-induced autoregulatory loop.(Correction notice). *Nature cell biology* 15(8), p. 1016. doi: 10.1038/ncb2814

Settembre, C. and Perera, R. M. 2024. Lysosomes as coordinators of cellular catabolism, metabolic signalling and organ physiology. *Nature reviews. Molecular cell biology* 25(3), pp. 223-245. doi: 10.1038/s41580-023-00676-x

Sexton, M. J. and Gherman, R. B. 2001. Selective estrogen receptor modulators: the ideal estrogen replacement? *Primary care update for Ob/Gyns* 8(1), pp. 25-30. doi: 10.1016/S1068-607X(00)00066-4

Shah, A. J., Kapoor, N., Crooks, G. M., Parkman, R., Weinberg, K. I., Wilson, K. and Kohn, D. B. 2005. Successful Hematopoietic Stem Cell Transplantation for Niemann-Pick Disease Type B. *Pediatrics (Evanston)* 116(4), pp. 1022-1025. doi: 10.1542/peds.2005-0867

Shammas, H., Kuech, E.-M., Rizk, S., Das, A. M. and Naim, H. Y. 2019. Different Niemann-Pick C1 Genotypes Generate Protein Phenotypes that Vary in their Intracellular Processing, Trafficking and Localization. *Scientific reports* 9(1), pp. 5292-5292. doi: 10.1038/s41598-019-41707-y

Sharpe, L. J. and Brown, A. J. 2013. Controlling Cholesterol Synthesis beyond 3-Hydroxy-3-methylglutaryl-CoA Reductase (HMGCR). *The Journal of biological chemistry* 288(26), pp. 18707-18715. doi: 10.1074/jbc.R113.479808

Shayman, J. A. 2018. Targeting Glucosylceramide Synthesis in the Treatment of Rare and Common Renal Disease. *Seminars in nephrology* 38(2), pp. 183-192. doi: 10.1016/j.semnephrol.2018.01.007

Sigel, A., Sigel, H. and Sigel, R. K. O. 2013. Zinc and Human Disease. *Interrelations Between Essential Metal Ions and Human Diseases* 13, pp. 389-414. doi: 10.1007/978-94-007-7500-8\_12

Simm, C., Luan, C.-H., Weiss, E. and O'Halloran, T. 2011. High-throughput screen for identifying small molecules that target fungal zinc homeostasis. *PLoS one* 6(9), pp. e25136-e25136. doi: 10.1371/journal.pone.0025136

Singhal, A., Krystofiak, E. S., Jerome, W. G. and Song, B. 2020. 2-Hydroxypropyl-gamma-cyclodextrin overcomes NPC1 deficiency by enhancing lysosome-ER association and autophagy. *Scientific reports* 10(1), pp. 8663-8663. doi: 10.1038/s41598-020-65627-4

Singhal, A., Szente, L., Hildreth, J. E. K. and Song, B. 2018. Hydroxypropyl-beta and -gamma cyclodextrins rescue cholesterol accumulation in Niemann-Pick C1 mutant cell via lysosome-associated membrane protein 1. *Cell death & disease* 9(10), pp. 1019-1013. doi: 10.1038/s41419-018-1056-1

Soga, M. et al. 2015. HPGCD Outperforms HPBCD as a Potential Treatment for Niemann-Pick Disease Type C During Disease Modeling with iPSCs. *Stem cells (Dayton, Ohio)* 33(4), pp. 1075-1088. doi: 10.1002/stem.1917

Sorkin, A. and von Zastrow, M. 2009. Endocytosis and signalling: intertwining molecular networks. *Nature reviews. Molecular cell biology* 10(9), pp. 609-622. doi: 10.1038/nrm2748

Sosnowski, J., Stetter-Neel, C., Cole, D., Durham, J. P. and Mawhinney, M. G. 1997. Protein Kinase C Mediated Anti-Proliferative Glucocorticoid-Sphinganine Synergism in Cultured Pollard III Prostate Tumor Cells. *The Journal of urology* 158(1), pp. 269-274. doi: 10.1097/00005392-199707000-00084

Soyombo, A. A., Tjon-Kon-Sang, S., Rbaibi, Y., Bashllari, E., Bisceglia, J., Muallem, S. and Kiselyov, K. 2006. TRP-ML1 Regulates Lysosomal pH and Acidic Lysosomal Lipid Hydrolytic Activity. *The Journal of biological chemistry* 281(11), pp. 7294-7301. doi: 10.1074/jbc.M508211200

Stahl, A., Pletzer, D., Mehmood, A. and Ullrich, M. S. 2015. *Marinobacter adhaerens* HP15 harbors two CzcCBA efflux pumps involved in zinc detoxification. *Antonie van Leeuwenhoek* 108(3), pp. 649-658. doi: 10.1007/s10482-015-0520-5

Stepien, K. M., Ciara, E. and Jezela-Stanek, A. 2020. Fucosidosis—Clinical Manifestation, Long-Term Outcomes, and Genetic Profile—Review and Case Series. *Genes* 11(11), p. 1383. doi: 10.3390/genes11111383

Subramanian, K., Hutt, D. M., Scott, S. M., Gupta, V., Mao, S. and Balch, W. E. 2020. Correction of Niemann-Pick type C1 trafficking and activity with the histone deacetylase inhibitor valproic acid. *The Journal of biological chemistry* 295(23), pp. 8017-8035. doi: 10.1074/jbc.RA119.010524

Sugimoto, Y., Ninomiya, H., Ohsaki, Y., Higaki, K., Davies, J. P., Ioannou, Y. A. and Ohno, K. 2001. Accumulation of Cholera Toxin and GM1 Ganglioside in the Early Endosome of Niemann-Pick C1-Deficient Cells. *Proceedings of the National Academy of Sciences - PNAS* 98(22), pp. 12391-12396. doi: 10.1073/pnas.221181998

Sun, A. 2018. Lysosomal storage disease overview. *Annals of translational medicine* 6(24), pp. 476-476. doi: 10.21037/atm.2018.11.39

Sun, J., Kurtzberg, J., Prasad, V. K., Parikh, S., Page, K. and Saha, A. 2016. Augmentation of Allogenic Cord Blood (CB) Transplantation for Inherited Metabolic Diseases with CB-Derived Intrathecal Cellular Therapy, Duoc-01. *Biology of blood and marrow transplantation* 23(3), pp. S132-S133. doi: 10.1016/j.bbmt.2017.01.051

Szewczyk, B. 2013. Zinc homeostasis and neurodegenerative disorders. *Frontiers in aging neuroscience* 5, p. 33. doi: 10.3389/fnagi.2013.00033

Szymańska, M. and Majerz, I. 2021. Effect of Substitution of Hydrogen Atoms in the Molecules of Anthrone and Anthraquinone. *Molecules (Basel, Switzerland)* 26(2), p. 502. doi: 10.3390/molecules26020502

Tafesse, F. G. et al. 2007. Both Sphingomyelin Synthases SMS1 and SMS2 Are Required for Sphingomyelin Homeostasis and Growth in Human HeLa Cells. *The Journal of biological chemistry* 282(24), pp. 17537-17547. doi: 10.1074/jbc.M702423200

Tamura, H., Takahashi, T., Ban, N., Torisu, H., Ninomiya, H., Takada, G. and Inagaki, N. 2006. Niemann–Pick type C disease: Novel NPC1 mutations and characterization of the concomitant acid sphingomyelinase deficiency. *Molecular genetics and metabolism* 87(2), pp. 113-121. doi: 10.1016/j.ymgme.2005.07.025

Tan, E. Y., Boelens, J. J., Jones, S. A. and Wynn, R. F. 2019. Hematopoietic Stem Cell Transplantation in Inborn Errors of Metabolism. *Frontiers in pediatrics* 7, pp. 433-433. doi: 10.3389/fped.2019.00433

Thiadens, A. A. H. J., Slingerland, N. W. R., Florijn, R. J., Visser, G. H., Riemsdag, F. C. and Klaver, C. C. W. 2012. Cone-rod dystrophy can be a manifestation of Danon disease. *Graefe's archive for clinical and experimental ophthalmology* 250(5), pp. 769-774. doi: 10.1007/s00417-011-1857-8

Thomas, C. A., Garner, D. L., DeJarnette, J. M. and Marshall, C. E. 1997. Fluorometric assessments of acrosomal integrity and viability in cryopreserved bovine spermatozoa. *Biology of reproduction* 56(4), pp. 991-998. doi: 10.1095/biolreprod56.4.991

Thompson, R. B. 2005. Studying zinc biology with fluorescence: ain't we got fun? *Current opinion in chemical biology* 9(5), pp. 526-532. doi: 10.1016/j.cbpa.2005.08.020

Ting, Y. U., Chan, C., Dongbiao, S., Haoxing, X. U. and Lieberman, A. P. 2012. Ryanodine receptor antagonists adapt NPC1 proteostasis to ameliorate lipid storage in Niemann–Pick type C disease fibroblasts. *Human molecular genetics* 21(14), pp. 3205-3214. doi: 10.1093/hmg/dds145

Todd, W. R., Elvehjem, C. A. and Hart, E. B. 1980. ZINC IN THE NUTRITION OF THE RAT. *Nutrition reviews* 38(4), pp. 151-154. doi: 10.1111/j.1753-4887.1980.tb05879.x

Torres, S. et al. 2017. Mitochondrial GSH replenishment as a potential therapeutic approach for Niemann Pick type C disease. *Redox biology* 11, pp. 60-72. doi: 10.1016/j.redox.2016.11.010

Treiber-Held, S., Distl, R., Meske, V., Albert, F. and Ohm, T. G. 2003. Spatial and temporal distribution of intracellular free cholesterol in brains of a Niemann-Pick type C mouse model showing hyperphosphorylated tau protein. Implications for Alzheimer's disease. *The Journal of pathology* 200(1), pp. 95-103. doi: 10.1002/path.1345

Tucci, F., Scaramuzza, S., Aiuti, A. and Mortellaro, A. 2021. Update on Clinical Ex Vivo Hematopoietic Stem Cell Gene Therapy for Inherited Monogenic Diseases. *Molecular therapy* 29(2), pp. 489-504. doi: 10.1016/j.ymthe.2020.11.020

Tängemo, C., Weber, D., Theiss, S., Mengel, E. and Runz, H. 2011. Niemann-Pick Type C disease: characterizing lipid levels in patients with variant lysosomal cholesterol storage. *Journal of lipid research* 52(4), pp. 813-825. doi: 10.1194/jlr.P013524

Urano, Y. et al. 2009. *Selective molecular imaging of viable cancer cells with pH-activatable fluorescence probes*. *Nature Medicine* 15(1), pp. 104-109. doi: 10.1038/nm.1854

Urasaki, Y., Beaumont, C., Workman, M., Talbot, J. N., Hill, D. K. and Le, T. T. 2020. Fast-Acting and Receptor-Mediated Regulation of Neuronal Signaling Pathways by Copaiba Essential Oil. *International journal of molecular sciences* 21(7), p. 2259. doi: 10.3390/ijms21072259

Vacca, F. et al. 2019. Cyclodextrin triggers MCOLN1-dependent endo-lysosome secretion in Niemann-Pick type C cells[S]. *Journal of lipid research* 60(4), pp. 832-843. doi: 10.1194/jlr.M089979

Valli, D., Gruszka, A. M. and Alcalay, M. 2020. Has Drug Repurposing Fulfilled Its Promise in Acute Myeloid Leukaemia? *Journal of clinical medicine* 9(6), p. 1892. doi: 10.3390/jcm9061892

van Diggelen, O. P. et al. 2005. A new fluorimetric enzyme assay for the diagnosis of Niemann–Pick A/B, with specificity of natural sphingomyelinase substrate. *Journal of inherited metabolic disease* 28(5), pp. 733-741. doi: 10.1007/s10545-005-0105-y

Van Wart, H. E. and Birkedal-Hansen, H. 1990. The Cysteine Switch: A Principle of Regulation of Metalloproteinase Activity with Potential Applicability to the Entire Matrix Metalloproteinase Gene Family. *Proceedings of the National Academy of Sciences - PNAS* 87(14), pp. 5578-5582. doi: 10.1073/pnas.87.14.5578

Vanier, M. and Millat, G. 2003. Niemann-Pick disease type C. *Clinical genetics* 64(4), pp. 269-281. doi: 10.1034/j.1399-0004.2003.00147.x

Vanier, M. T., Revol, A. and Fichet, M. 1980. Sphingomyelinase activities of various human tissues in control subjects and in Niemann-Pick disease — development and evaluation of a microprocedure. *Clinica chimica acta* 106(3), pp. 257-267. doi: 10.1016/0009-8981(80)90309-5

Vanier, M. T. et al. 1991. Type C Niemann-Pick disease: spectrum of phenotypic variation in disruption of intracellular LDL-derived cholesterol processing. *Biochimica et biophysica acta. Molecular basis of disease* 1096(4), pp. 328-337. doi: 10.1016/0925-4439(91)90069-L

Vult von Steyern, F., Josefsson, J. O. and Tagerud, S. 1996. Rhodamine B, a fluorescent probe for acidic organelles in denervated skeletal muscle. *The journal of histochemistry and cytochemistry* 44(3), pp. 267-274. doi: 10.1177/44.3.8648087

Vázquez, M. C., Balboa, E., Alvarez, A. R. and Zanlungo, S. 2012. Oxidative Stress: A Pathogenic Mechanism for Niemann-Pick Type C Disease. *Oxidative medicine and cellular longevity* 2012, pp. 205713-205711. doi: 10.1155/2012/205713

Waldron, K. J., Rutherford, J. C., Ford, D. and Robinson, N. J. 2009. Metalloproteins and metal sensing. *Nature (London)* 460(7257), pp. 823-830. doi: 10.1038/nature08300

Walker, C. F. and Black, R. E. 2004. Zinc and the risk for infectious disease. *Annual review of nutrition* 24(1), pp. 255-275. doi: 10.1146/annurev.nutr.23.011702.073054

Walkley, S. U. and Suzuki, K. 2004. Consequences of NPC1 and NPC2 loss of function in mammalian neurons. *Biochimica et biophysica acta. Molecular and cell biology of lipids* 1685(1), pp. 48-62. doi: 10.1016/j.bbalip.2004.08.011

Walter, M., Chen, F. W., Tamari, F., Wang, R. and Ioannou, Y. A. 2009. Endosomal lipid accumulation in NPC1 leads to inhibition of PKC, hypophosphorylation of vimentin and Rab9 entrapment. *Biology of the cell* 101(3), pp. 141-153. doi: 10.1042/BC20070171

Wang, J. et al. 2023. Revealing Mitochondrion–Lysosome Dynamic Interactions and pH Variations in Live Cells with a pH-Sensitive Fluorescent Probe. *Analytical chemistry (Washington)* 95(45), pp. 16609-16617. doi: 10.1021/acs.analchem.3c02878

Wang, M. L., Motamed, M., Infante, R. E., Abi-Mosleh, L., Kwon, H. J., Brown, M. S. and Goldstein, J. L. 2010. Identification of Surface Residues on Niemann-Pick C2 Essential for Hydrophobic Handoff of Cholesterol to NPC1 in Lysosomes. *Cell metabolism* 12(2), pp. 166-173. doi: 10.1016/j.cmet.2010.05.016

Wang, S. W., Hojabrpour, P., Zhang, P., Kolesnick, R. N., Steinbrecher, U. P., Gómez-Muñoz, A. and Duronio, V. 2015. Regulation of ceramide generation during macrophage apoptosis by ASMase and

de novo synthesis. *Biochimica et biophysica acta. Molecular and cell biology of lipids* 1851(11), pp. 1482-1489. doi: 10.1016/j.bbaliip.2015.08.002

Wang, Y., Yutuc, E. and Griffiths, W. J. 2021. Cholesterol metabolism pathways – are the intermediates more important than the products? *The FEBS journal* 288(12), pp. 3727-3745. doi: 10.1111/febs.15727

Wang, Y.-I. and Goren, M. B. 1987. Differential and Sequential Delivery of Fluorescent Lysosomal Probes into Phagosomes in Mouse Peritoneal Macrophages. *The Journal of cell biology* 104(6), pp. 1749-1754. doi: 10.1083/jcb.104.6.1749

Wanikawa, M., Nakamura, H., Emori, S., Hashimoto, N. and Murayama, T. 2020. Accumulation of sphingomyelin in Niemann-Pick disease type C cells disrupts Rab9-dependent vesicular trafficking of cholesterol. *Journal of cellular physiology* 235(3), pp. 2300-2309. doi: 10.1002/jcp.29137

Wasserstein, M., Godbold, J. and McGovern, M. M. 2012. Skeletal manifestations in pediatric and adult patients with Niemann Pick disease type B. *Journal of inherited metabolic disease* 36(1), pp. 123-127. doi: 10.1007/s10545-012-9503-0

Wasserstein, M. P., Aron, A., Brodie, S. E., Simonaro, C., Desnick, R. J. and McGovern, M. M. 2006. Acid sphingomyelinase deficiency: Prevalence and characterization of an intermediate phenotype of Niemann-Pick disease. *The Journal of pediatrics* 149(4), pp. 554-559. doi: 10.1016/j.jpeds.2006.06.034

Wasserstein, M. P. et al. 2015. Successful within-patient dose escalation of olipudase alfa in acid sphingomyelinase deficiency. *Molecular genetics and metabolism* 116(1-2), pp. 88-97. doi: 10.1016/j.ymgme.2015.05.013

Watari, H. et al. 1999. Niemann-Pick C1 Protein: Obligatory Roles for N-Terminal Domains and Lysosomal Targeting in Cholesterol Mobilization. *Proceedings of the National Academy of Sciences - PNAS* 96(3), pp. 805-810. doi: 10.1073/pnas.96.3.805

Wehrmann, Z. T., Hulett, T. W., Huegel, K. L., Vaughan, K. T., Wiest, O., Helquist, P. and Goodson, H. 2012. Quantitative comparison of the efficacy of various compounds in lowering intracellular cholesterol levels in Niemann-Pick type C fibroblasts. *PloS one* 7(10), pp. e48561-e48561. doi: 10.1371/journal.pone.0048561

Wenzlau, J. M. et al. 2007. The Cation Efflux Transporter ZnT8 (Slc30A8) Is a Major Autoantigen in Human Type 1 Diabetes. *Proceedings of the National Academy of Sciences - PNAS* 104(43), pp. 17040-17045. doi: 10.1073/pnas.0705894104

Westerheide, S. D. et al. 2004. Celastrols as Inducers of the Heat Shock Response and Cytoprotection[boxes]. *The Journal of biological chemistry* 279(53), pp. 56053-56060. doi: 10.1074/jbc.M409267200

White, B. H. and Kaczmarek, L. K. 1997. Identification of a Vesicular Pool of Calcium Channels in the Bag Cell Neurons of *Aplysia californica*. *The Journal of neuroscience* 17(5), pp. 1582-1595. doi: 10.1523/jneurosci.17-05-01582.1997

White, K. K. 2011. Orthopaedic aspects of mucopolysaccharidoses. *Rheumatology (Oxford, England)* 50(suppl\_5), pp. v26-v33. doi: 10.1093/rheumatology/ker393

Wilke, S., Krausze, J. and Büsow, K. 2012. Crystal structure of the conserved domain of the DC lysosomal associated membrane protein: implications for the lysosomal glycoalyx. *BMC biology* 10(1), pp. 62-62. doi: 10.1186/1741-7007-10-62

Williams, I. M., Wallom, K.-L., Smith, D. A., Al Eisa, N., Smith, C. and Platt, F. M. 2014. Improved neuroprotection using miglustat, curcumin and ibuprofen as a triple combination therapy in Niemann–Pick disease type C1 mice. *Neurobiology of disease* 67, pp. 9-17. doi: 10.1016/j.nbd.2014.03.001

Winchester, B. G. 2001. Lysosomal membrane proteins. *European journal of paediatric neurology* 5, pp. 11-19. doi: 10.1053/ejpn.2000.0428

Winkler, M. B. L. et al. 2019. Structural Insight into Eukaryotic Sterol Transport through Niemann-Pick Type C Proteins. *Cell (Cambridge)* 179(2), pp. 485-497.e418. doi: 10.1016/j.cell.2019.08.038

Wisniewski, K. E., Kida, E., Connell, F., Elleder, M., Eviatar, L. and Konkol, R. J. 1993. New subform of the late infantile form of neuronal ceroid lipofuscinosis. *Neuropediatrics* 24(3), pp. 155-163.

Wraith, J. E. and Imrie, J. 2009. New therapies in the management of Niemann-Pick type C disease: clinical utility of miglustat. *Therapeutics and clinical risk management* 5, pp. 877-887. doi: 10.2147/TCRM.S5777

Wu, L. et al. 2023. TMEM175: A lysosomal ion channel associated with neurological diseases. *Neurobiology of disease* 185, pp. 106244-106244. doi: 10.1016/j.nbd.2023.106244

Xu, H. and Ren, D. 2015. Lysosomal Physiology. *Annual review of physiology* 77(1), pp. 57-80. doi: 10.1146/annurev-physiol-021014-071649

Yamasaki, S. et al. 2007. Zinc is a novel intracellular second messenger. *The Journal of cell biology* 177(4), pp. 637-645. doi: 10.1083/jcb.200702081

Yanagisawa, H. et al. 2017. L-leucine and SPNS1 coordinately ameliorate dysfunction of autophagy in mouse and human Niemann-Pick type C disease. *Scientific reports* 7(1), pp. 15944-15949. doi: 10.1038/s41598-017-15305-9

Yang, C. and Wang, X. 2021. Lysosome biogenesis: Regulation and functions. *The Journal of cell biology* 220(6), p. 1. doi: 10.1083/jcb.202102001

Yao, X., Su, T. and Verkman, A. S. 2016. Clobetasol promotes remyelination in a mouse model of neuromyelitis optica. *Acta neuropathologica communications* 4(1), pp. 42-42. doi: 10.1186/s40478-016-0309-4

Yeagle, P. L. 1991. Modulation of membrane function by cholesterol. *Biochimie* 73(10), pp. 1303-1310. doi: 10.1016/0300-9084(91)90093-G

Yim, W. W.-Y. and Mizushima, N. 2020. Lysosome biology in autophagy. *Cell discovery* 6(1), pp. 6-6. doi: 10.1038/s41421-020-0141-7

Yonezawa, S., Takahashi, T., Wang, X. J., Wong, R. N., Hartsuck, J. A. and Tang, J. 1988. Structures at the proteolytic processing region of cathepsin D. *The Journal of biological chemistry* 263(31), pp. 16504-16511. doi: 10.1016/S0021-9258(18)37621-X

Yu, L. C., Faleck, H., Johnson, K., Payne, D. and Hariri, R. 2009. Human Placenta-Derived Stem Cell S (HPDSC) Augment Transplantation with Umbilical Cord Blood. *Biology of blood and marrow transplantation* 15(2), pp. 51-51. doi: 10.1016/j.bbmt.2008.12.156

Yu, S., Shen, G., Khor, T. O., Kim, J.-H. and Kong, A.-N. T. 2008. Curcumin inhibits Akt/mammalian target of rapamycin signaling through protein phosphatase-dependent mechanism. *Molecular cancer therapeutics* 7(9), pp. 2609-2620. doi: 10.1158/1535-7163.MCT-07-2400

Yu, Z., Persson, H. L., Eaton, J. W. and Brunk, U. T. 2003. Intralysosomal iron: a major determinant of oxidant-induced cell death. *Free radical biology & medicine* 34(10), pp. 1243-1252. doi: 10.1016/S0891-5849(03)00109-6

Yun, U.-J. et al. 2019. Anti-cancer effect of doxorubicin is mediated by downregulation of HMG-Co A reductase via inhibition of EGFR/Src pathway. *Laboratory investigation* 99(8), pp. 1157-1172. doi: 10.1038/s41374-019-0193-1

Zahran, A. M., Elsayh, K. I., El-Deek, S. E. M. and El-Baz, M. A. H. 2015. Oxidative Stress, Trace Elements, and Circulating Microparticles in Patients With Gaucher Disease Before and After Enzyme Replacement Therapy. *Clinical and applied thrombosis/hemostasis* 21(1), pp. 58-65. doi: 10.1177/1076029613489595

Zampieri, S. et al. 2016. SMPD1 Mutation Update: Database and Comprehensive Analysis of Published and Novel Variants. *Human mutation* 37(2), pp. 139-147. doi: 10.1002/humu.22923

Zeidan, Y. H. and Hannun, Y. A. 2007a. Activation of acid sphingomyelinase by protein kinase Cdelta-mediated phosphorylation. *The Journal of biological chemistry* 282(15), p. 11549.

Zeidan, Y. H. and Hannun, Y. A. 2007b. Translational aspects of sphingolipid metabolism. *Trends in molecular medicine* 13(8), pp. 327-336. doi: 10.1016/j.molmed.2007.06.002

Zhang, B.-y., Wang, P., Shi, L., Ma, X.-y., Xi, J.-k. and Zhang, X.-f. 2023. A pH-sensitive fluorescent probe based on hemicyanine dyes for responding microenvironment changes of cardiomyocytes induced by Zn<sup>2+</sup>. *Microchemical journal* 193, p. 109085. doi: 10.1016/j.microc.2023.109085

Zhang, J.-H. et al. 2011. The N-terminal Domain of NPC1L1 Protein Binds Cholesterol and Plays Essential Roles in Cholesterol Uptake. *The Journal of biological chemistry* 286(28), pp. 25088-25097. doi: 10.1074/jbc.M111.244475

Zhang, P., Sun, Y. and Ma, L. 2015. ZEB1: At the crossroads of epithelial-mesenchymal transition, metastasis and therapy resistance. *Cell cycle (Georgetown, Tex.)* 14(4), pp. 481-487. doi: 10.1080/15384101.2015.1006048

Zhao, N., Gao, J., Enns, C. A. and Knutson, M. D. 2010. ZRT/IRT-like Protein 14 (ZIP14) Promotes the Cellular Assimilation of Iron from Transferrin. *The Journal of biological chemistry* 285(42), pp. 32141-32150. doi: 10.1074/jbc.M110.143248

Zhou, H. et al. 2020. Cannabinoid receptor 2 promotes the intracellular degradation of HMGB1 via the autophagy-lysosome pathway in macrophage. *International immunopharmacology* 78, pp. 106007-106007. doi: 10.1016/j.intimp.2019.106007

Zhou, L., Xue, X., Yang, K., Feng, Z., Liu, M. and Pastor-Pareja, J. C. 2023. Convergence of secretory, endosomal, and autophagic routes in trans-Golgi-associated lysosomes. *The Journal of cell biology* 222(1), doi: 10.1083/jcb.202203045

Zhu, H., Yoshimoto, T. and Yamashima, T. 2014. Heat Shock Protein 70.1 (Hsp70.1) Affects Neuronal Cell Fate by Regulating Lysosomal Acid Sphingomyelinase. *The Journal of biological chemistry* 289(40), pp. 27432-27443. doi: 10.1074/jbc.M114.560334

Ziarani, G. M., Moradi, R., Lashgari, N. and Kruger, H. G. 2018. Metal-free synthetic organic dyes. *Metal-free synthetic organic dyes*. Elsevier, pp. 9-17.

Zimmerman, C. and Shenoy, S. 2020. Chimerism in the Realm of Hematopoietic Stem Cell Transplantation for Non-malignant Disorders-A Perspective. *Frontiers in immunology* 11, pp. 1791-1791. doi: 10.3389/fimmu.2020.01791

Zou, J., Guo, Y., Guettouche, T., Smith, D. F. and Voellmy, R. 1998. Repression of Heat Shock Transcription Factor HSF1 Activation by HSP90 (HSP90 Complex) that Forms a Stress-Sensitive Complex with HSF1. *Cell* 94(4), pp. 471-480. doi: 10.1016/S0092-8674(00)81588-3

## 9 Appendix

### 9.1 Appendix i

#### 9.1.1 Table of therapeutic treatments in Niemann-Pick

Data correct as of May 2024

Target disease	Manufacturer	Name of therapeutic	Type of therapeutic	Target protein	Mechanism of action	Phase of clinical trial	Date of most recent trial
NPA	University of California San Francisco.	ASMase gene replacement therapy (rhSMPD1).	Gene replacement therapy.	aSMase.	AAV9 viral vector based rhaSMase gene replacement therapy (Samaranch et al. 2019).	Preclinical <i>In-vivo</i> .	(2019)
NPA & NPB	Sanofi/Genzyme.	Xenozyme /Olipudase alfa / GZ402665 (rhaSMase).	Enzyme replacement therapy.	aSMase.	Recombinant human aSMase enzyme replacement therapy (Wasserstein et al. 2015; Diaz et al. 2021).	Phase 2/3* *Approved in Japan for use in non-CNS forms of aSMase deficiency.	2021
NPA & NPB	Duke University / Aldagen / Cytomedix.	ALD-101 (Umbilical cord blood (UCB) derived ALDHbr cells.	Adjuvant therapy of cells isolated from umbilical cord blood (UCB) for haematopoietic stem cell (HSC) transplant (HCT).	ASMase or NPC1/2.	ALD-101 contains a population of highly expressing Aldehyde Dehydrogenase (ALDHbr) hematopoietic, endothelial, and multipotent mesenchymal progenitors. These ALDHbr cells obtained from a healthy donor contain functional ASMase. It has been shown that using ALD-101 as an adjuvant to HCT leads to faster repopulation of the bone marrow, and a subsequent reduction in time for a full repopulation of the blood with donor HSC derived blood cells (Deibert et al. 2007; Gentry et al. 2007; Balber 2011; Kim et al. 2011).	Phase 3* *Not known if any Niemann-Pick patients are currently enrolled on the clinical trial as trial was for all lysosomal storage disorders.	2014

Target disease	Manufacturer	Name of therapeutic	Type of therapeutic	Target protein	Mechanism of action	Phase of clinical trial	Date of most recent trial
NPA, NPB & NPC	Duke University / Talaris Therapeutics Inc.	Mixed chimerism transplant (Haematopoietic stem cell (HSC) transplant (HCT)).	Haematopoietic stem cell (HSC) transplant (HCT), without removal of patient HSCs.	ASMase or NPC1/2.	Unlike traditional HCT, mixed chimerism targets to knock down, but not completely remove the patients HSC population. After transplantation with donor HSC, a mixed population of donor and patient HSCs will within the bone marrow niche. It is believed that the presence of the donor HSCs and subsequent derived cells that possess the fully functioning ASMase or NPC1/2 will overcome the disease symptoms, in addition to avoiding graft-versus-host-disease (GVHD) that can occur in non-chimeric HCT (Park et al. 2011; Tan et al. 2019; Zimmerman and Shenoy 2020; Tucci et al. 2021).	Phase 1/2*  *Not known if any Niemann-Pick patients are currently enrolled on the clinical trial as trial was for all lysosomal storage disorders.	2021
NPA, NPB & NPC	Duke University / The Marcus Foundation.	DUOC-01 (Umbilical cord blood (UCB) derived oligodendrocyte-like cells).	Adjuvant therapy of cells isolated from umbilical cord blood (UCB) for haematopoietic stem cell (HSC) transplant (HCT).	ASMase or NPC1/2.	DUOC-01 contains UCB derived oligodendrocyte-like cells, which produce functional versions of the mutant protein found in the patient, such as ASMase or NPC1/2 to cross-correct the functional protein deficiency. This therapy is an adjunctive designed to function as a bridging therapy to provide functional proteins for 1-6 months post UCB transplant, whilst allowing the UCB transplant to undergo engraftment and reach a therapeutic threshold which usually occurs within 3-6 months (Kurtzberg et al. 2015; Saha et al. 2016; Sun et al. 2016).	Phase 1*  *Not known if any Niemann-Pick patients are currently enrolled on the clinical trial as trial was for all lysosomal storage disorders.	2021
NPA, NPB & NPC	New York Medical College.	Human placental derived stem cells ((HPDSC) CD34+ progenitor cells).	Adjuvant therapy of HPDSC for haematopoietic stem cell (HSC) transplant (HCT).	ASMase or NPC1/2.	HPDSC is enriched in progenitor cell types. Non-clinical studies have shown that augmenting a UCB transplant with HPDSC results in a higher likelihood of successful engraftment of donor HSCs and an earlier engraftment as compared to UCB alone. It is hypothesized that the infusion of HPDSC following UCB transplantation improves transplant outcome, shorten for donor cells to replenish the population of cells in the blood (Yu et al. 2009; Elmacken et al. 2015).	Phase 1*  * Not known if any Niemann-Pick patients are currently enrolled on the clinical trial as trial was for all lysosomal storage disorders.	2019

Target disease	Manufacturer	Name of therapeutic	Type of therapeutic	Target protein	Mechanism of action	Phase of clinical trial	Date of most recent trial
NPA, NPB & NPC	Masonic Cancer Center / University of Minnesota.	Haematopoietic stem cell (HSC) transplant (HCT).	Bone marrow or umbilical cord cell transplant.	ASMase or NPC1/2.	HSC transplant is used to replace the patients' blood cells with those from a healthy donor. Prior to transplantation the patient undergoes chemotherapy or radiotherapy to destroy their own HSCs (also preventing an immune response), which is then followed by HSC transplant from a healthy donor. After 3-6 months the patient's blood will have repopulated with cells from the donor HSC. The donor HSC derived blood cells will contain normal functioning copies of the gene mutated in the patient: either ASMase or NPC1/2 (Schneiderman et al. 2005; Shah et al. 2005; Iravani et al. 2006; Bonney et al. 2010).	Phase 2*  * Not known if any Niemann-Pick patients are currently enrolled on the clinical trial as trial was for all lysosomal storage disorders.	2017
NPB & NPC	UZ Leuven / Pfizer.	Anti-oxLDL IgM antibodies.	Immunisation.	oxLDL.	IgM antibodies against oxLDL reduce presence of oxLDL in the blood, reducing cellular cholesterol uptake and reducing lysosomal cholesterol accumulation (Binder et al. 2003; Jeurissen et al. 2016; Grievink et al. 2020).	Phase 1.	2016
NPC	Oxford GlycoSciences / Actelion.	Miglustat (NB-DNJ) / OGT 918 / Zavesca / Brazaves.	Iminosugar / Substrate reduction therapy.	GlcCer synthase.	Miglustat inhibits GlcCer synthase, which catalyses the first step in glycosphingolipid synthesis, thus reducing cellular glycosphingolipid levels reducing the potential for downstream lipid storage (Platt et al. 1994; Cox et al. 2000; Heitner et al. 2002; Lachmann et al. 2004).	Approved by both EMA and FDA*  *Miglustat is approved for Gaucher disease only in US, being used off label for NPC.	Approved in 2002/2003
NPC	Mandos / Mallinckrodt Pharmaceuticals (Vtesse) / Cyclo therapeutics / Washington University Medical School.	Adrabetadex /VTS270 / Hydroxypropyl Betacyclo-dextrin (HP-β-CD) / Trappsol Cyclo.	Cellular constitutive secretion promoter.	MCOLN1 / unknown.	Mechanism of action is not fully understood. It is hypothesised that HP-β-CD binds to cellular cholesterol, functioning partially as an NPC1 mimetic, allowing NPC2 mediated cholesterol trafficking, in addition to promotes the secretion of the endosome/lysosomal content via MCOLN1 mediated exocytosis, thus reducing lysosomal cholesterol accumulation and subsequent trafficking defects (Peake and Vance 2012; Matsuo et al. 2014; Farmer et al. 2019; Hastings et al. 2019; Vacca et al. 2019).	Phase 3*  *Did not get regulatory approval and no plans for future clinical trials from Mallinckrodt, with IP being sold to Mandos. Cyclo Therapeutics are sponsoring an ongoing separate Phase 3 trial.	2021/2023

Target disease	Manufacturer	Name of therapeutic	Type of therapeutic	Target protein	Mechanism of action	Phase of clinical trial	Date of most recent trial
NPC	Biorex / CytRx / Orphazyme.	Arimoclomol.	Small molecule proteostasis regulators.	Heat shock Protein 70 (HSP70).	Arimoclomol upregulates HSP70, which chaperones and promotes correct folding of lysosomal lipid degrading enzymes (including ASMase) as well as NPC1 partially restoring their activity (Kirkegaard et al. 2010; Nakasone et al. 2014; Zhu et al. 2014; Kirkegaard et al. 2016; Fog et al. 2018).	Phase 3 completed; FDA rejected approval (CRL).	2021
NPC	Oxford University / IntraBio.	N-Acetyl-L-Leucine (NALL).	Small molecule prodrug.	Leucine / unknown.	Mechanism of action is unclear, possibly a prodrug for Leucine with a unique receptor (MCT1) mediated uptake. L-Leucine has been shown to ameliorate the enlargement of lysosomes in murine NPC1 -/- cells (Yanagisawa et al. 2017; Bremova-Ertl et al. 2021; Fields et al. 2021; Grant et al. 2021).	Phase 3*  Awaiting FDA decision.	2023
NPC	Leiden University / University of Amsterdam / Azafaros.	Nizubaglustat (AZ-3102).	Azasugar.	GlcCer synthase and GBA2 inhibitor.	Similar to Miglustat, the iminosugar component acts as a GlcCer synthase inhibitor, whilst the addition of a second moiety leads to GBA2 inhibition (Ghisaidoobe et al. 2014).	Phase 2.	2024
NPC	Niemann-Pick Spain Foundation / Merck patented Efavirenz for HIV.	Efavirenz (Sustiva).	Antiretroviral/ Small molecule enzyme activator.	CYP46A1.	Efavirenz activates the cholesterol-degrading enzyme CYP46A1, prevents brain cholesterol accumulation and pathology in a mouse model for NPC (Mitroi et al. 2019; Nunes et al. 2024).	Phase 2.	2022
NPC	Eunice Kennedy Shriver National Institute of Child Health and Human Development (NICHD).	Vorinostat.	Histone deacetylase (HDAC) inhibitor (HDACi).	HDAC1.	It is believed that Vorinostat functions as a HDACi, in turn leading to epigenetic changes and increased expression of the mutant NPC1, which with enough lysosomal localisation retains sufficient partial activity to correct the cholesterol accumulation and restore trafficking out of lysosomes (Wehrmann et al. 2012; Pipalia et al. 2017; Pugach et al. 2018).	Phase 1/2.	2016

Target disease	Manufacturer	Name of therapeutic	Type of therapeutic	Target protein	Mechanism of action	Phase of clinical trial	Date of most recent trial
NPC	Oxford University / Washington University / NHGRI / NICHD.	N-Acetyl-Cysteine (NAC).	Small molecule prodrug.	Glutathione / unknown.	Within cells NAC is deacetylated to cysteine, which undergoes further conversion to glutathione in turn undergoing reduction to form reduced glutathione (GSH). Reduced glutathione is used to neutralise reactive oxygen species (ROS). Oxidative stress is higher in NPC patients, so it was hypothesised that increasing glutathione levels could decrease the damage caused by oxidative stress (Dringen 2000; Vázquez et al. 2012; Fu et al. 2013; Torres et al. 2017).	Phase 1/2.	2013
NPC	Shanghai Jiao Tong University.	Lithium Carbonate.	Cholesterol synthesis pathway genes promoter.	NPC1 / unknown.	Therapies to treat bipolar disorder have been shown to upregulate genes involved in cholesterol synthesis, including both NPC1 and NPC2. Additionally, in-vivo work has shown that treatment with lithium reduced the levels of KC-7, a marker of NPC disease severity. However, how or on what specifically lithium acts to bring about these effects is not currently known (Tängemo et al. 2011; Dell'Osso et al. 2016; Kidnapillai et al. 2019; Han et al. 2021).	Phase 1.	2021
NPC	No Patent Holder.  Research and clinical trial by NIH.	Cholestyramine, DMSO, lovastatin, and nicotinic acid.	Cholesterol lowering agents.	Unknown.	In patients treated with all 4 drugs, reduced hepatic and plasma cholesterol levels were observed, however no direct mechanism of action was demonstrated (Patterson et al. 1993).	Phase 1.	1993
NPC	University of Pennsylvania / Galyatech/Bloomsbury Genetic Therapies.	GALYA-1 / Gene replacement therapy (rhNPC1)/ Bloomsbury Genetic Technologies (BGT-NPC).	Gene replacement therapy.	NPC1.	GALYA-1 is a AAV9 derived viral vector, allowing delivery of rhNPC1 gene replacement therapy (Chandler et al. 2017; Hughes et al. 2018).	Preclinical <i>in vivo</i> * *Currently seeking approval for Phase 1.	2023

Target disease	Manufacturer	Name of therapeutic	Type of therapeutic	Target protein	Mechanism of action	Phase of clinical trial	Date of most recent trial
NPC	No Patent holder or clinical trial registrar.  Research done by NIH.	Riluzole.	Glutamate receptor antagonist.	Several excitatory amino acid transporters, including EAAT1, EAAT2 and EAAT3.	Riluzole is a glutamate receptor antagonist which inhibits the release of pre-synaptic glutamate and facilitates glutamate uptake by excitatory amino acid transporters, in turn reducing glutamate mediated neurotoxicity (Doble 1996; Azbill et al. 2000) Riluzole has been demonstrated to protect Purkinje neurons in rodent cerebellar ataxia models (Janahmadi et al. 2009). In an NPC1 <sup>-/-</sup> mouse model, riluzole decreased astrogliosis, delayed Purkinje neuron loss improved the neurological phenotype and increased survival (Cognoux et al. 2021).	Pre-clinical <i>in vivo</i> *  <i>Riluzole is already EMA/FDA approved for the treatment of ALS.</i>	2021
NPC	No Patent holder or clinical trial registrar.  Research done by Pontificia Universidad Católica de Chile.	Neurotinib.	Tyrosine kinase inhibitor.	c-Abl inhibitor.	c-Abl inhibition induces autophagy through the overexpression of genes involved in this process, through upregulation of TFEB (Marín et al. 2022).	Pre-clinical <i>in vivo</i> .	2022
NPC	No Patent holder or clinical trial registrar.  Research done by University of Barcelona and University of Seoul.	UB-EV-52.	Enzyme inhibition (Soluble epoxide hydrolase (sEH) inhibitor (sEHi)).	Soluble epoxide hydrolase (sEH).	sEH regulate the degradation of epoxy fatty acids (EpFAs) EpFAs are involved in the regulation of several cellular processes including: autophagy, mitochondrial function, and inflammation. Inhibition of sEH has demonstrated to reduce cholesterol accumulation in human fibroblasts from NPC patients by reducing cholesterol synthesis and improving autophagic flux (Kang et al. 2018; Griñán-Ferré et al. 2021).	Pre-clinical <i>in vivo</i> .	2021
NPC	No Patent holder or clinical trial registrar.  Research done by Kumamoto University and Meharry Medical College.	Hydroxypropyl gammacycloc-dextrin (HP- $\gamma$ -CD).	Cellular constitutive secretion promoter.	MCOLN1 / unknown.	HP- $\gamma$ -CD shares a putative mechanism of action with HP- $\beta$ -CD, however HP- $\gamma$ -CD has been shown to be more efficacious and therefore can be used at lower concentrations providing a greater therapeutic range (Soga et al. 2015; Davidson et al. 2016; Singhal et al. 2018; Singhal et al. 2020).	Pre-clinical <i>in vivo</i> .	2020

Target disease	Manufacturer	Name of therapeutic	Type of therapeutic	Target protein	Mechanism of action	Phase of clinical trial	Date of most recent trial
NPC	No Patent holder or clinical trial registrar.  Research done by University of Helsinki and Virginia Commonwealth University.	FTY720/ fingolimod.	Histone Deacetylase (HDAC) Inhibitor (HDACi).	HDAC 1.	Upon entry in the cell FTY720 is phosphorylated by nuclear sphingosine kinase 2, and its active phosphorylated form (FTY720-P) is an inhibitor of class I histone deacetylases. The inhibition of HDAC class 1 leads to epigenetic changes in the genome leading to increased expression of the mutant NPC1, which with enough lysosomal localisation retains sufficient partial activity to correct the cholesterol accumulation and restore trafficking out of lysosomes (Blom et al. 2010; Brunkhorst et al. 2014; Newton et al. 2017).	Preclinical <i>in vivo</i> .	2017
NPC I1061T only	No Patent holder or clinical trial registrar.  Research done by Notre Dame / Scripps Research Institute / Seoul National University.	Valproic acid (VPA) and Chloroquine.	VPA – histone deacetylase (HDAC) inhibitor (HDACi).  Chloroquine – stabilises NPC1.	HDAC 7.	VPA decreases HDAC 7 activity, preventing acetylation of lysine residues, blocking post-translational ubiquitination of these residues, thus preventing ubiquitin mediated NPC1 degradation, so more NPC1 protein is able to be trafficked to lysosomes increasing lysosomal cholesterol trafficking. The combination of VPA with chloroquine, a known lysosomotropism compound led to improved stability of the I1061T mutant NPC1, particularly in late endosomes/lysosomes, in addition to neutralising the lysosomal acidification caused by VPA (Kim et al. 2007; Wehrmann et al. 2012; Subramanian et al. 2020).	Preclinical <i>in vivo</i> .	2020
NPC	Patent held by Fran Platt and Emyr Lloyd-Evans.  Research done by Cardiff University / Louisiana State University / Oxford University / Rutgers / University of Arizona / University of Birmingham / University of Lund / University of	Curcumin.	Sarcoplasmic / endoplasmic reticulum (ER) Ca <sup>2+</sup> ATPase / mTOR / NFKappa / NPC1L1 antagonist.	SERCA / Tau / mTOR / NFKappa / unknown.	Many cell pathways relevant to NPC1 neuropathology are affected by curcumin. Curcumin has been identified as a weak inhibitor of (SERCA), leading to significant ER Ca <sup>2+</sup> release raising cytosolic Ca <sup>2+</sup> levels, partially correcting endocytic trafficking defects and reducing lysosomal lipid storage. Another effect of curcumin is the ability to reduce tau hyperphosphorylation and prevent tau aggregation, of note in NPC. Curcumin inhibits signalling by the mammalian target of rapamycin (mTOR) as well as functioning as an antagonist of the NFKappa pathway, exerting pro-	<i>Preclinical in vivo</i> *  *Potentially dropped as Curcumin was found produce biphasic effects as well as limited <i>in vivo</i> efficacy.	2014

Target disease	Manufacturer	Name of therapeutic	Type of therapeutic	Target protein	Mechanism of action	Phase of clinical trial	Date of most recent trial
	Southampton / University of Washington.				apoptotic effects and modulation of the redox status of the cell. Additionally, curcumin inhibits the expression of NPC1L1, the plasma membrane localised cholesterol uptake protein (Bilmen et al. 2001; Logan-Smith et al. 2001; Hallows et al. 2006; Lloyd-Evans et al. 2008; Yu et al. 2008; Beevers et al. 2009; Feng et al. 2010a; Kumar et al. 2011; Borbon et al. 2012; Williams et al. 2014).		
NPC	No Patent holder or clinical trial registrar. Research done by University of Arizona / University of California San Francisco / Western University of Health Sciences.	Allopregnanolone (Allo).	Hormone replacement therapy.	NA / downstream targets of Allo.	Treatment is used to replace Allo lost through disrupted neurosteroidogenesis in NPC. Depletion of Allo is caused by both lysosomal cholesterol accumulation and decreased activity of neurosteroid synthesising enzymes, such as: 5 $\alpha$ -reductase, 3 $\alpha$ -hydroxy steroid dehydrogenase (3 $\alpha$ HSD), and 20 $\alpha$ -hydroxy steroid dehydrogenase (Griffin et al. 2004; Ahmad et al. 2005; Liao et al. 2009).	Preclinical <i>in vivo</i> *  *Potentially dropped as no new results or clinical trial in the last decade.	2009
NPA, NPB & NPC	No Patent Holder Research done by University of Massachusetts Medical School.	Cannabidiol.	Small molecule.	TFE3 promoter.	Cannabidiol has been shown to increase aSMase activity (Burstein et al. 1984). Work carried out included in this thesis shows that cannabidiol leads to promotion of expression of aSMase.	Preclinical <i>in vitro</i> .	1984
NPC	No Patent Holder Research done by National Center for Drug Research and Evaluation, Istituto Superiore di Sanità.	Dipyridamole.	Small molecule.	ENT1 Inhibitor.	Dipyridamole activates the adenosine A2AR receptor subtype subsequent due to the increased levels of extracellular adenosine due to the inhibition of ENT1 (Pepponi et al. 2022).	Preclinical <i>in vitro</i> .	2022
NPC	No Patent holder or clinical trial registrar.  Research done by Virginia Commonwealth University.	SK1-A.	Substrate reduction therapy.	Sphingosine kinase 1 (SphK1) activator.	In NPC, SphK1 has been identified as having decreased activity. SphK1 is regulatory enzyme controlling sphingolipid catabolism by phosphorylating sphingosine, in turn controlling sphingosine (and subsequently sphingolipid) degradation or recycled into ceramide. Therefore, activating SphK1 will increase sphingosine turnover, preventing lysosomal sphingosine and	Preclinical <i>in vitro</i> .	2020

Target disease	Manufacturer	Name of therapeutic	Type of therapeutic	Target protein	Mechanism of action	Phase of clinical trial	Date of most recent trial
					sphingolipid accumulation (Milstien and Spiegel 2003; Lee et al. 2014; Newton et al. 2020).		
NPC	No Patent holder or clinical trial registrar.  Research done by NIH and Universidad Católica de Chile.	δ-Tocopherol (Vitamin E).	Small molecule.	c-Abl/p73 inhibitor.	c-Abl inhibition induces autophagy through the overexpression of genes involved in this process, through upregulation of TFEB (63 (Greer et al. 1998; Marín et al. 2014).	Preclinical <i>in vitro</i> .	2014
NPC I1061T only	No Patent holder or clinical trial registrar.  Research done by Cornell University / Notre Dame / Sanford Burnham Prebys / Scripps Research Institute.	Panobinostat (LBH589).	Histone Deacetylase (HDAC) Inhibitor (HDACi).	HDAC 1, 2, & 4	It is believed that panobinostat functions as a HDACi, in turn leading to epigenetic changes and increased expression of the mutant NPC1, which with enough lysosomal localisation retains sufficient partial activity to correct the cholesterol accumulation and restore trafficking out of lysosomes (Wehrmann et al. 2012; Pipalia et al. 2017; Pugach et al. 2018).	Preclinical <i>in vitro</i> .	2018
NPC I1061T only	No Patent holder or clinical trial registrar.  Research done by University of Michigan.	DHBP (1,1'-diheptyl4,4'-bipyridium).	Ryanodine receptor (RyR) antagonists.	RyR.	DHBP is a known RyR antagonist, which leads to increased ER calcium storage levels, increasing correct NPC1 folding and subsequent overall increase in I1061T NPC1 protein levels. DHBP was also found to promote trafficking of mutant NPC1 to late endosomes and lysosomes and rescued the aberrant lysosomal lipid storage (Ting et al. 2012).	Preclinical <i>in vitro</i> .	2012

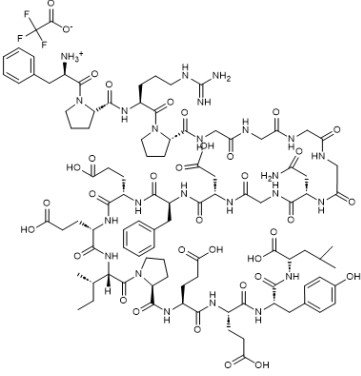
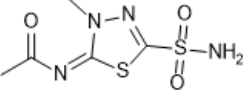
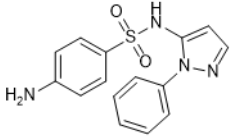
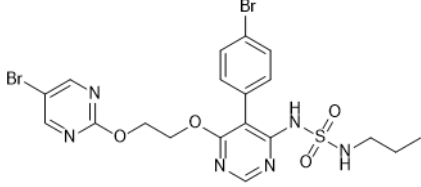
## 9.2 Appendix ii

### 9.2.1 Hits from zinc phenotypic screening

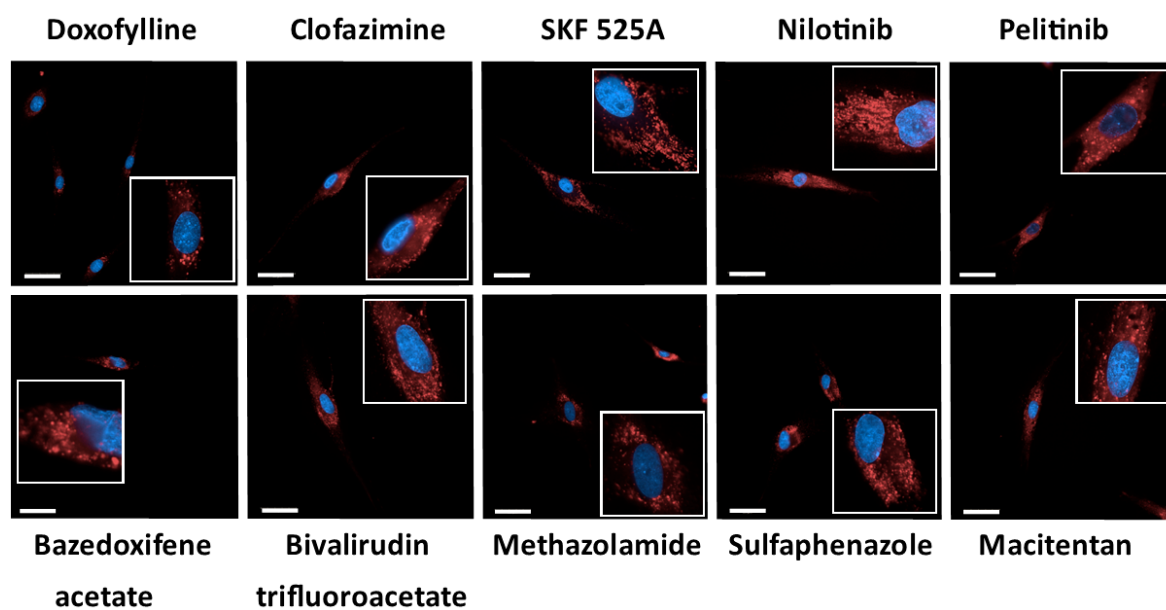
#### 9.2.1.1 Compounds that reduced zinc storage

##### 9.2.1.1.1 Table of zinc lowering compounds hits

Name	Structure	Effect on total zinc area	Effect on total lysosome area	Therapeutic use
Doxofylline		78% reduction	45% reduction	PDE inhibitor
Clofazimine		85% reduction	42% reduction	Tuberculosis drug
SKF 525A (hydrochloride)		29% reduction	41% reduction	Cytochrome P (CYP)450 inhibitor
Nilotinib		20% increase  *Reduced number of puncta by 90%	28% reduction	Bcr-Abl kinase inhibitor
Pelitinib (EKB-569)		32% reduction	19% reduction	EGFR inhibitor
Bazedoxifene acetate		2% reduction  *Reduced number of puncta by 95%	19% reduction	Estrogen receptor modulator

Bivalirudin Trifluoroacetate		65% reduction	19% reduction	Thrombin inhibitor
Methazolamide		37% reduction	17% reduction	Carbonic anhydrase inhibitor
Sulfaphenazole		56% reduction	13% reduction	CYP2C9 inhibitor
Macitentan		59% reduction	13% reduction	Endothelin receptor antagonist

9.2.1.1.2 LysoTracker Deep Red reference images for each drug treatment in NPC1 P237S/1061T cell lines

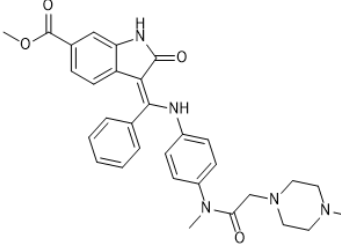
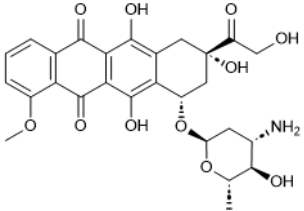
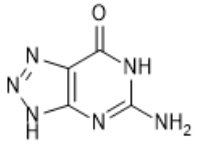
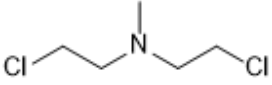
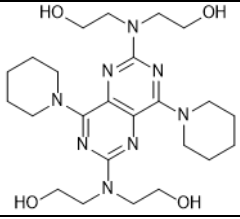
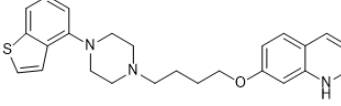
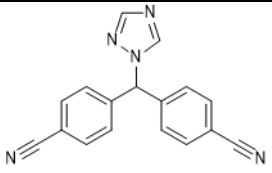
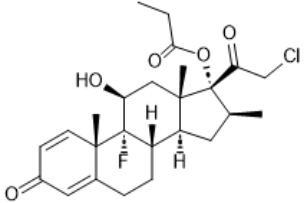


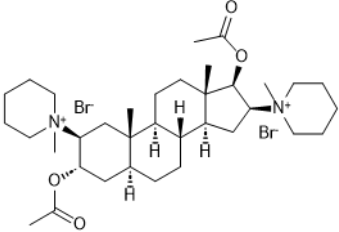
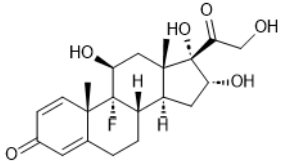
**Figure i. Representative LysoTracker Deep Red images for hit compounds**

Shown are reference images for compounds that reduced zinc storage and showed the most significant decrease in LysoTracker Deep Red staining. Scale bar represents 50 $\mu$ m.

### 9.2.1.2 Zinc raising compounds hits

#### 9.2.1.2.1 Table of compounds that increases zinc but reduced lysosomal volume

Name	Structure	Effect on total zinc area	Effect on total lysosome area	Therapeutic use
Nintedanib		95% increase	39% reduction	VEGFR/PDGFR/FGFR inhibitor
Doxorubicin		30% increase	27% reduction	Topo II inhibitor (Antibiotic)
Azaguanine-8		79% increase	24% reduction	Purine analog (Antineoplastic)
Meschlorethamine		16% increase *Increased puncta number by 74%	22% reduction	DNA synthesis inhibitor (Antineoplastic)
Dipyridamole		340% increase	22% reduction	PDE inhibitor
Brexpiprazole		97% increase	21% reduction	5-HT <sub>2A</sub> , $\alpha$ 1B/ $\alpha$ 2C receptor antagonist
Letrozole		20% reduction *15% increase in fluorescence intensity	20% reduction	Non-steroidal aromatase inhibitor
Clobetasol propionate		63% increase	19% reduction	Glucocorticoid receptor agonist

Pancuronium dibromide		40% reduction *77% increase in number of puncta	17% reduction	AChR antagonist
Triamcinolone		43% increase	17% reduction	Anti-inflammatory steroid

9.2.1.2.2 LysoTracker Deep Red reference images for hit molecules that increased zinc but reduced lysosomal volume in NPC1 P237S/1061T cell lines

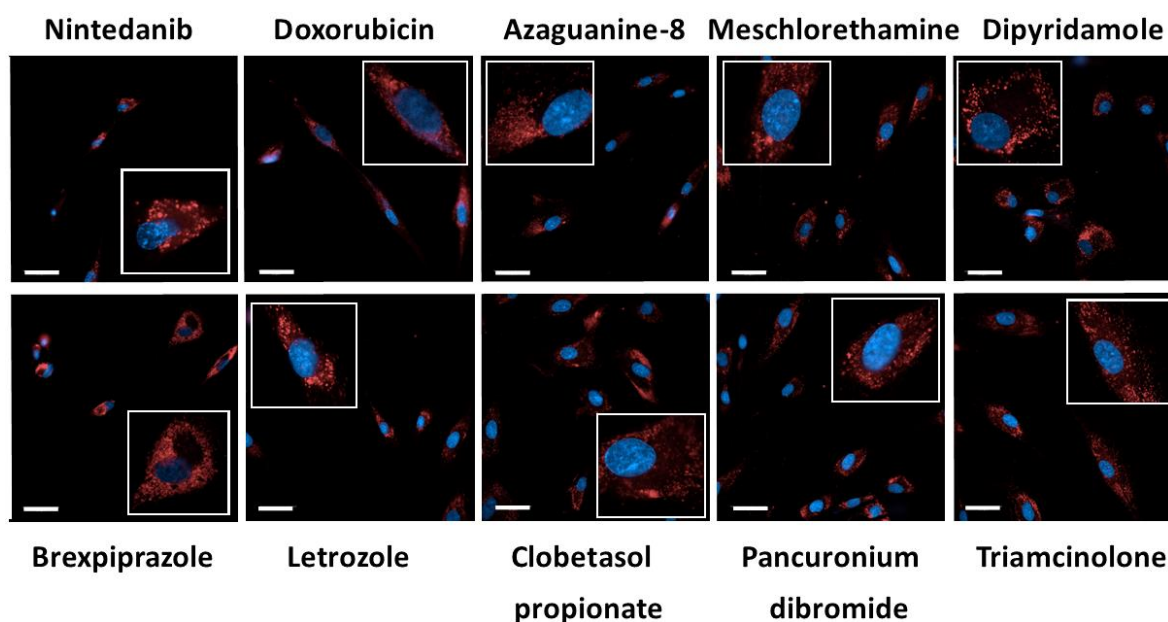


***Figure ii. Representative LysoTracker Deep Red images for identified hit compounds***  
*Images showing decreased LysoTracker Deep Red staining in cells treated with compounds that increased free zinc but decreased lysosomal volume. Scale bar represents 50µm.*

### 9.2.1.3 Zinc lowering compounds screening plate

	1	2	3	4	5	6	7	8	9	10	11	12
A		CP-945598 HCl	Enzastaurin	Aprepitant	LY2835219	Mianserin HCl	Pelitinib (EKB-569)	Cediranib (AZD217)	Macitentan	Ellagic acid	Tak-438	
B		Epirubicin HCl	Idarubicin HCl	Vortioxetine (Lu AA21004)	Aprotinin	Loratadine	ABT-888 (Veliparib)	Vemurafenib (PLX4032, RG7204)	CAL-101 (Idelalisib, GS-1101)	ABT-263 (Navitoclax)	Sorafenib	
C		(R)-Crizotinib	GDC-0449 (Vismodegib)	Bardoxolone methyl	Bazedoxifene acetate	Bivalirudin Trifluoroacetate	Dabigatran etexilate mesylate	Elacridar	Nilotinib	Disulfiram	PCI-24781 (CRA-024781)	
D		VX-680 (MK-0457, Tozasertib)	TG101348 (SAR302503)	Baricitinib (LY3009104, INCB028050)	Resveratrol	FG-4592 (ASP1517)	Lenalidomide	Birinapant (TL32711)	Cobicistat (GS-9350)	Sildenafil Citrate	Clarithromycin	
E		Pioglitazone HCl	TAK-700	Rivaroxaban	Apixaban	Pralatrexate	Anagrelide HCl	Pyrimethamine	Methazolamide	Lovastatin	Safinamide Mesylate	
F		Entinostat (MS-275, SNDX-275)	Guaifenesin	Indomethacin	Bromocriptine mesylate	Citric acid	Monobenzone	Oxeladin Citrate	Progesterone	Terfenadine	Azelidipine	
G		Bupivacaine HCl	Rupatadine Fumarate	Neostigmine Bromide	Broxyquinoline	Chlorquinaldol	Clofazimine	Closantel	Closantel Sodium	Cyclandelate	Dirithromycin	
H		Domiphen Bromide	Doxofylline	Peramivir Trihydrate	Imatinib	Napabucasin	SKF 525A (hydrochloride)	Imipramine (hydrochloride)	Sulfaphenazole	Doxepin	Ozagrel	

9.2.1.4 Zinc raising compounds screening plate

	1	2	3	4	5	6	7	8	9	10	11	12
A		Imatinib Mesylate	Doxorubicin	Carfilzomib	Elacridar	MK-4827	Trichostatin A	Rosiglitazone	Melphalan	Ispinesib	Ponatinib	
B		Tazarotene	Perindopril erbumine	Romidepsin	BT-787	Afatanib	Nintedanib	Estrone	Nicotine Difartrate	Nifenazone	Oxethazaine	
C		Fingolimod (FTY720)	Valaciclovir	Mesoridazine besylate	Brexipiprazole	Anidulafungin	Etomidate	Reserpine	L-Adrenaline	Phenoxybenzamine	Spirolactone	
D		Aminoglutethimide	Chloroquine diphosphate	Flunarizine	Azelnidipine	Clevidipine Butyrate	VULM 1457	Pancuronium dibromide	Aminothiazole	Amoxapine	Amprolium	
E		Antazoline	Letrozole	Acyclovir	Benzylamine HCl	Broxyquinoline	Esmolol HCL	Flubendazole	Fudosteine	Ibandronate	Meschlorethamine	
F		Penciclovir	Azaguanine-8	Phenazopyridine HCL	Ribostamycin Sulfate	Triamcinolone	Butoconazole	Carbimazole	Clobetasol propionate	Cyclosporin A	Dexamethasone acetate	
G		Dipyridamole	Pentoxifyverine citrate	Dyclonine	Hydrocortisone	Methacycline	Norethindrone	Nystatin	Prednisolone	Sulbactam	Sulphanilamide	
H		Toltrazuril	Dronedarone	Gliclazide	Enalapril Maleate	Naratriptan	Afusertib	Hydroxychloroquine	Lomitapide	Cetorelix	Chlorotrianisene	

### 9.3 Appendix iii

#### 9.3.1 AQ7

##### 9.3.1.1 AQ6 solubility issues

When cells were treated with concentrations of AQ6 above 50 $\mu$ M, non-soluble aggregates of AQ6 were observed. This debris is likely to be AQ6 that has come out of solution during the pulse phase of cell treatment and has remained in the well despite washing the cells before the chase phase. Of note, no detectable fluorescence was observed from the insoluble AQ6 particulate.

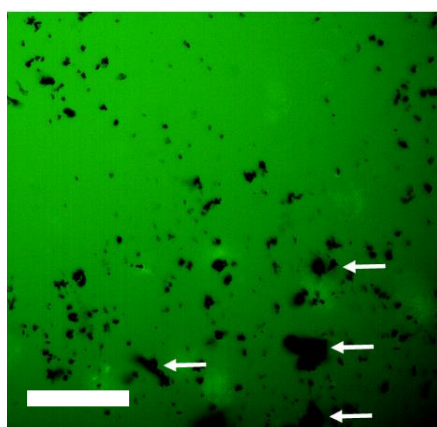


**Figure iii. AQ6 shows poor solubility in cell culture medium**

AQ6 shows poor solubility of AQ6 when used as a probe. Large clumps of particulate marked by white arrows can be seen in the image, which are aggregates of AQ6 stuck to the bottom of the Operetta plate, that have remained after the plate was washed. Image gathered using a x40 water objective on an Operetta CLS. Scale bars represent 50 $\mu$ m.

### 9.3.1.2 CellLight™ Nucleus-RFP, BacMam 2.0 optimisation

Optimisation of both concentration of CellLight™ Nucleus-RFP, BacMam 2.0, and the volume of media per well was optimised to ensure maximum number of cells showed nuclei staining before the nuclei probe is used in an assay.

Initial calibration assays with 150µl of media per well, showed a very limited uptake of the nuclei marker. To increase the transfection rate, initially the volume of media was reduced to 100µl, which showed a trend of increasing percentage of cells with nuclei fluorescence up to 6µl of probe; as shown in *Figure iii(c)*. The volume of media per well was further reduced to 75µl, which led to a noticeable increase in the percentage of cells that were expressing the nuclei localised RFP. Further decreasing the volume of media to 50µl did not appear to increase the percentage of transfected cells, as this remained at approximately 20%.

*Figure iii(b), (d)* and *(f)* show that nuclei fluorescence is independent of the volume of media, and volume of nuclei probe, as despite changing both. the nuclei fluorescence remains constant at 4000 RFU in transfected cells. This suggests that adding more nuclei probe would not increase the nuclei fluorescence intensity; instead, only affecting the number of cells transfected.

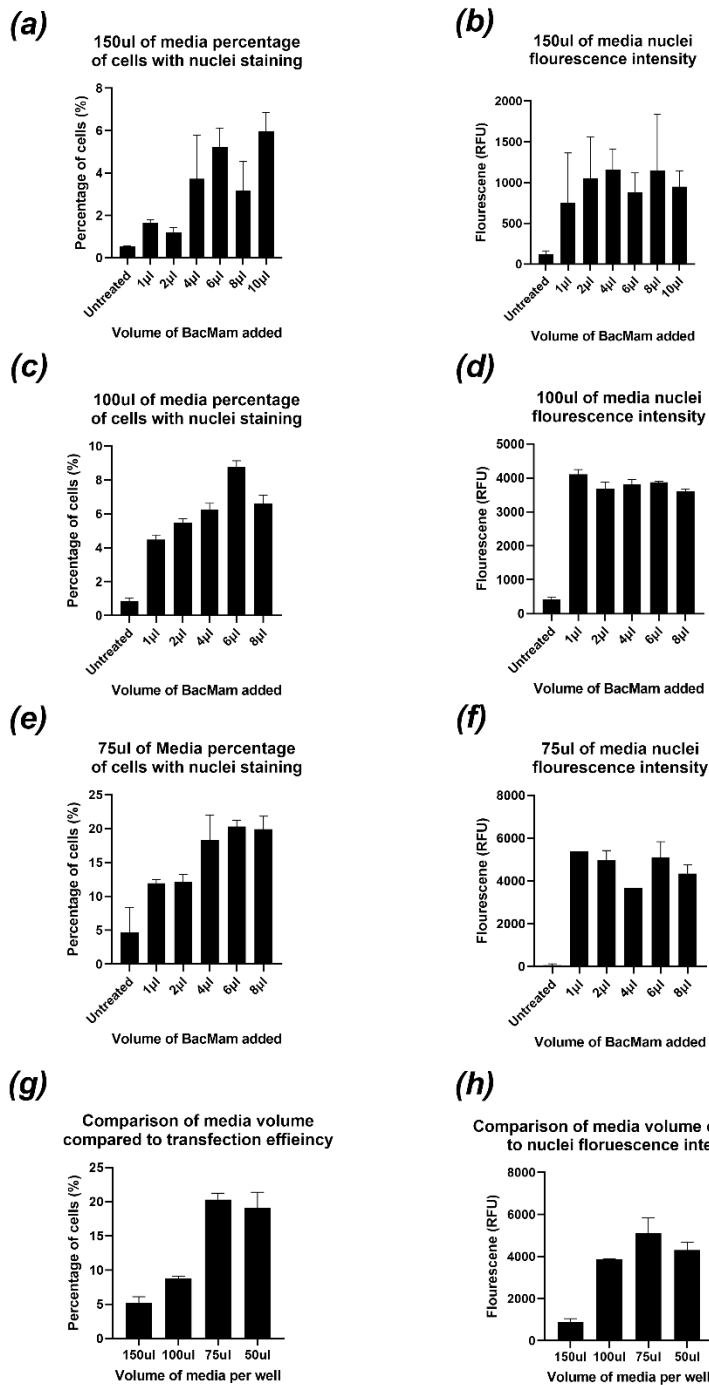


**Figure iii. Comparison of nuclei fluorescence in cells treated with CellLight RFP Nucleus probe**  
 In (a), (c) and (e), the percentage of cells expressing nuclei RFP signal is shown, when changing the volume of the CellLight nuclei probe. The graphs in (b), (d) and (f) show a comparison of the nuclei RFP fluorescence in cells that were successfully transfected, when changing the volume of CellLight reagent. Figure (g) shows a comparison of percentage transfected cells when changing the volume of media in a well, when cells were treated with 6μl of CellLight reagent. Figure (h) shows a comparison of nuclei RFP fluorescence intensity, when cells were incubated with different volumes of media, with the volume of CellLight kept at 6μl per well. Data is n=1 for all experiments, error bars are shown as Standard deviation of the mean.

### 9.3.1.3 pH sensitivity of AQ3 and AQ7

To utilise either AQ3 or AQ7 as a lysosomal probe it was required to demonstrate how the fluorescence of the probe related to changing pH. The data in *Figure v(b)* shows an increase in fluorescence for AQ7 with increasingly acidic pH, with an associated peak fluorescence at pH 4.5, corresponding to intracellular lysosomal pH. Comparison of fluorescence of AQ3 and AQ7 in *Figure v(c)*, shows that peak fluorescence intensity is approximately 4 times higher for AQ7 than AQ3 at pH 4.5. Therefore, based on these data it was determined that AQ7 does show pH sensitivity, with peak fluorescence emission at low pH.

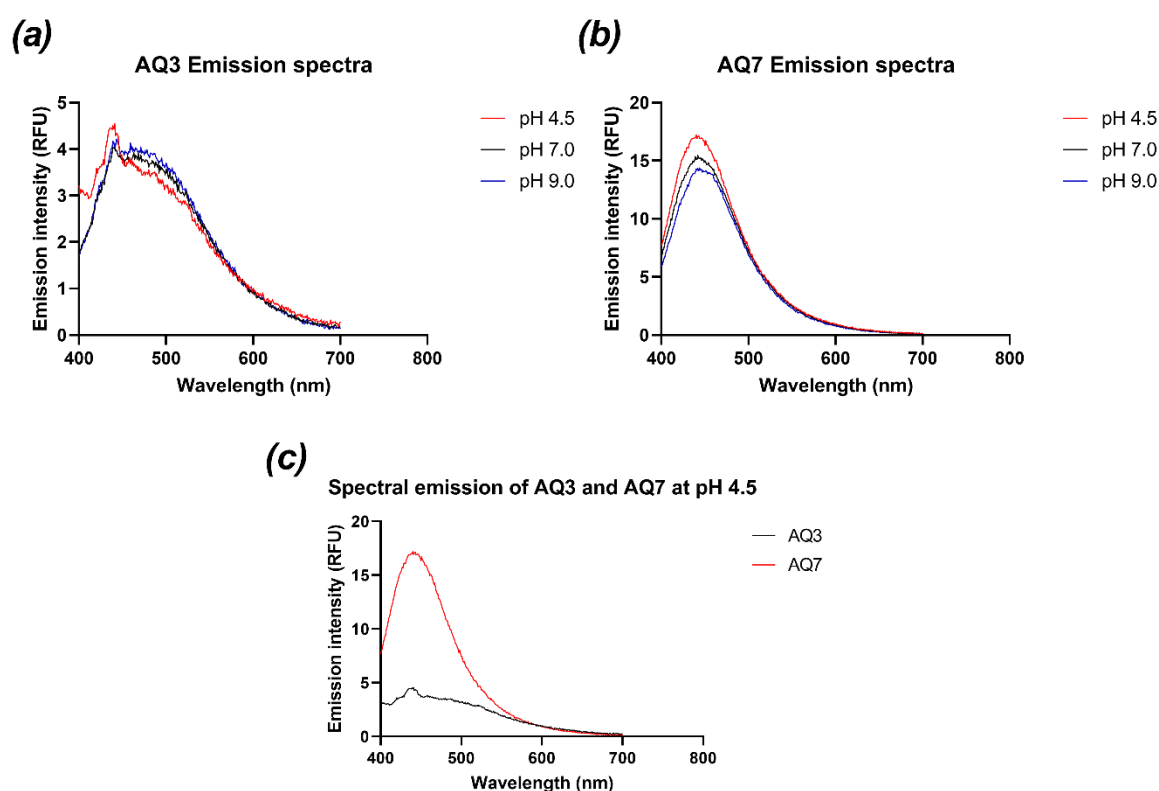


#### **Figure v. pH sensitivity of AQ3 and AQ7 fluorescence**

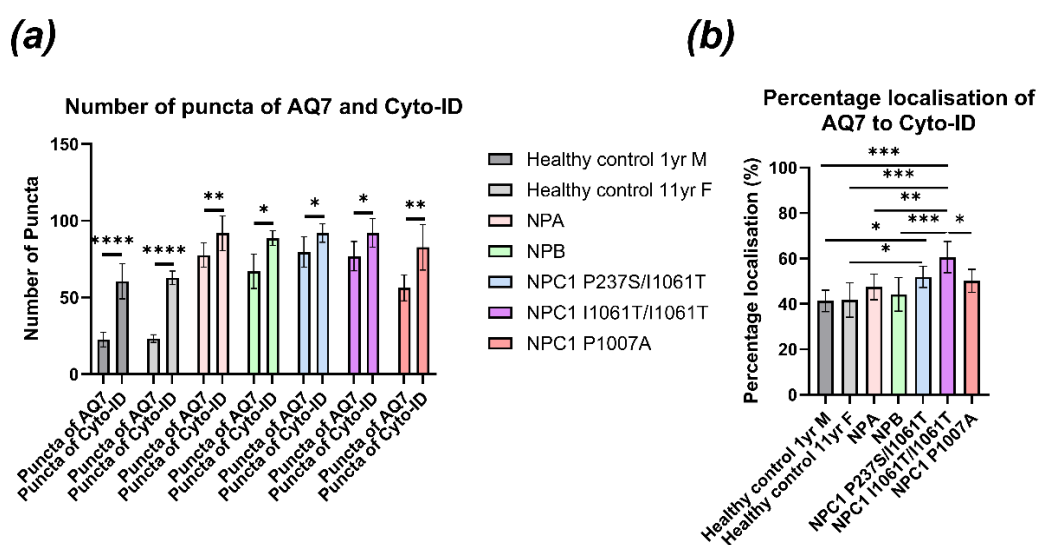
*Comparison of AQ3 and AQ7 fluorescence at varying pH. In (a) AQ3 and in (b) AQ7, comparison of fluorescence emission across three differing pH are shown. In (c) comparison of AQ3 and AQ7 fluorescence is shown when both molecules were in a pH 4.5 buffer. The emission wavelength for AQ7 is shifted, due to the use of 400nm excitation, away from the molecules preferred excitation wavelength in the 500nm range Data kindly provided by Dr. Deemah Alenazy, and Professor Simon Pope, Cardiff University.*

### 9.3.1.4 AQ7 only partially co-localises with Cyto-ID in Niemann-Pick cells

As shown in 3.2.6.2 and 3.2.6.11, AQ7 localises consistently to late endosomes and lysosomes, it was decided to determine if AQ7 also co-localises to autophagolysosomes. To do this, cells were co stained with AQ7 and Cyto-ID to visualise both the number of puncta of each probe, but also to determine the percentage of co-localisation occurring between AQ7 and Cyto-ID.

As shown in *Figure vi(a)* significant difference in the number of puncta of AQ7 and Cyto-ID were observed in all cell lines. In all cell lines the number of puncta of Cyto-ID were significantly higher than that of AQ7, with the number of puncta of Cyto-ID remaining consistent across Niemann-Pick disease cell lines, unlike the puncta of AQ7, which varied across Niemann-Pick disease cell lines.

Comparison of the co-localisation between AQ7 and Cyto-ID showed significant variation between cell lines. Both healthy control cell lines tested showed approximately 40% co-localisation of AQ7 and Cyto-ID, this number was higher in all the Niemann-Pick disease cell lines. Highest co-localisation of AQ7 to Cyto-ID was observed in both classical NPC cell lines, however it is not clear if this is due to there being a higher number of puncta of AQ7 in the classical NPC cell lines, or due to known autophagy defects in classical phenotype NPC cells. From the data in *Figure vi* AQ7 does not reliably co-localise with Cyto-ID, as the percentage localisation between AQ7 and Cyto-ID varies by cell line, therefore AQ7 is not a reliable marker for use as an autophagolysosome probe.



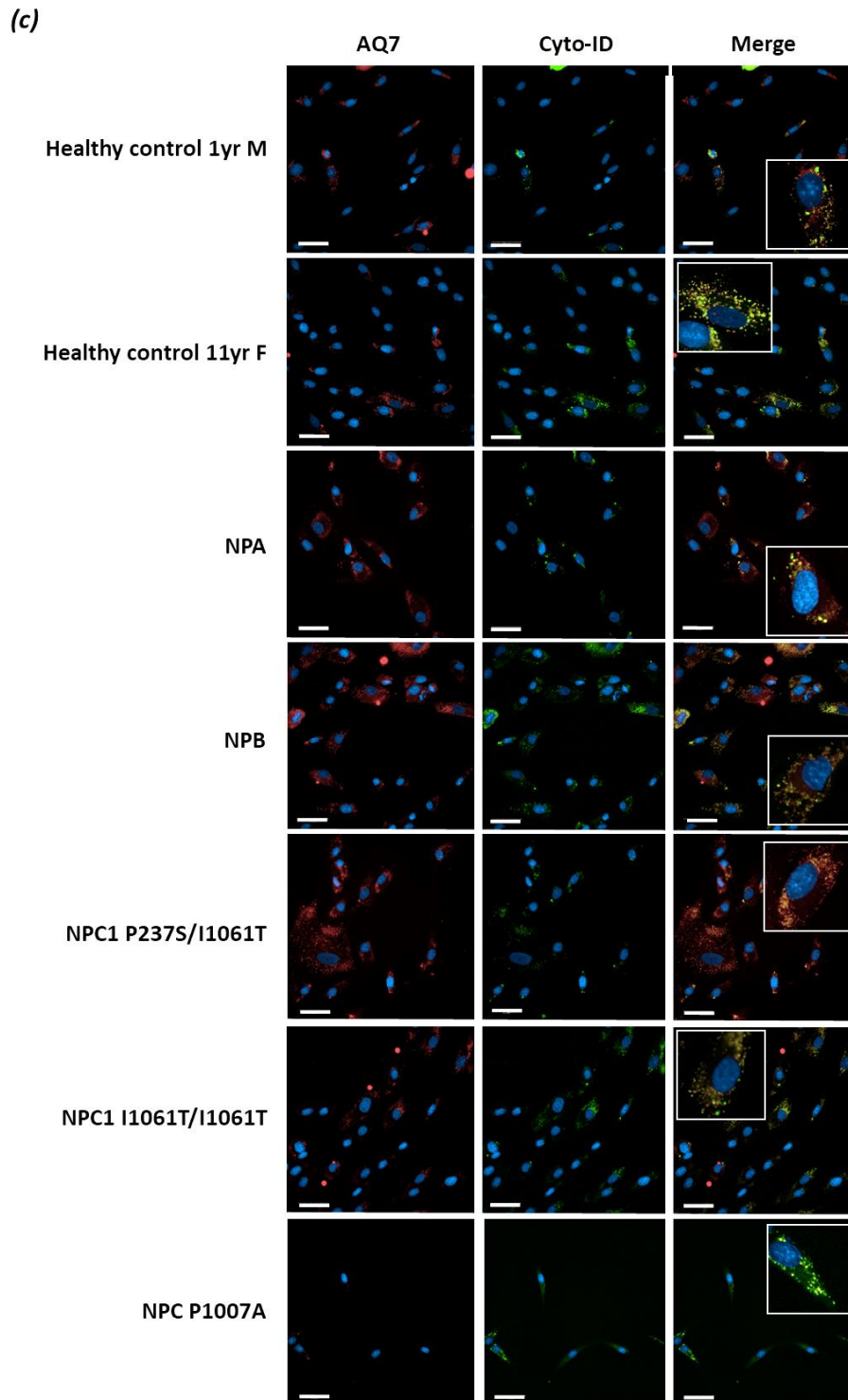
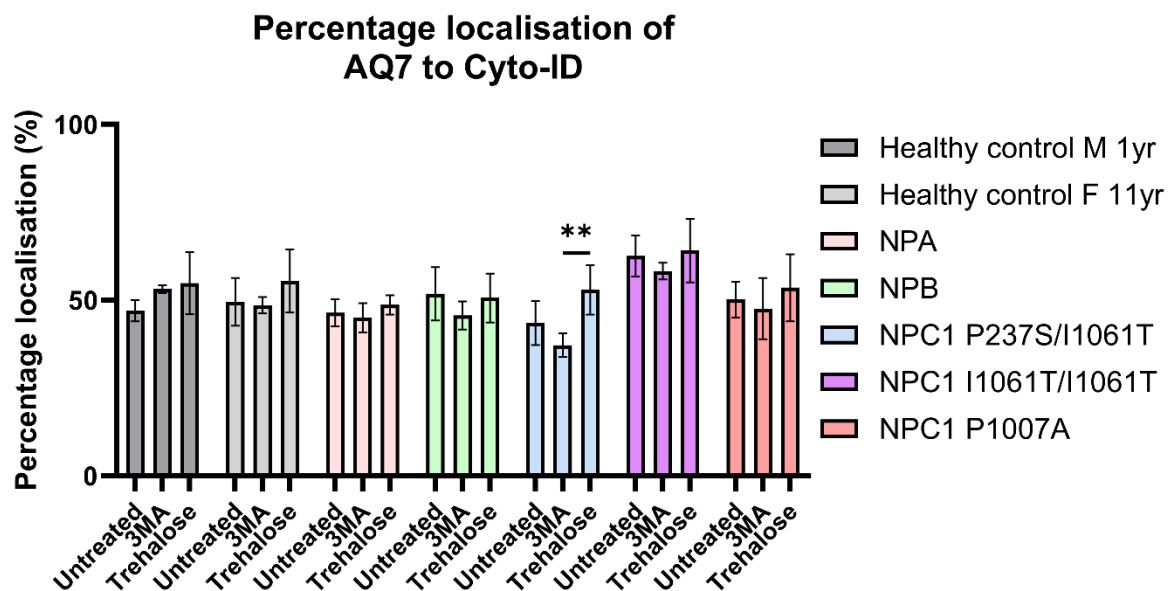


***Figure vi. AQ7 co localisation to autophagosomes is increased in Niemann-Pick disease cell lines***  
*Co-staining of patient derived fibroblasts with AQ7 and Cyto-ID. In (a), the mean number of puncta of each AQ7 and Cyto-ID for each cell line is shown. In (b), the percentage of puncta of AQ7 that is co-localised with Cyto-ID is shown. For co-localisation, cells were first pulsed with AQ7 for 4 hours before the addition of Cyto-ID for 30 minutes. In (c) reference images for all cell lines with AQ7, Cyto-ID and a merged image are shown. All data is n=3, with mean and standard deviation shown, in (a) statistical significance was determined through a two-way ANOVA with post-hoc Tukey tests. In (b) a one-way ANOVA, with post-hoc Tukey tests was used. Scale bars represent 50µm.*

### 9.3.1.5 AQ7 localisation to autophagosomes is unaffected by autophagy modulators

We determined whether the percentage of puncta of AQ7 and Cyto-ID that was co-localising changed when cells were treated with known autophagy modulators. The only cell line showing a significant change in localisation are the NPC1 P237S/I1061T cell, between the 3MA and Trehalose treated groups. However, neither 3MA or trehalose showed a significant effect on percentage localisation when compared to the untreated control.

Based on the data, the addition of 3MA or trehalose does not affect the localisation of AQ7 autophagolysosomes. The minor trend of increased localisation when trehalose is added is possibly due to the increase in the number of autophagolysosomes. However, from this data is clear that AQ7 is not a suitable probe for analysing autophagolysosomes, showing significantly more affinity for lysosomes over autophagosomes.



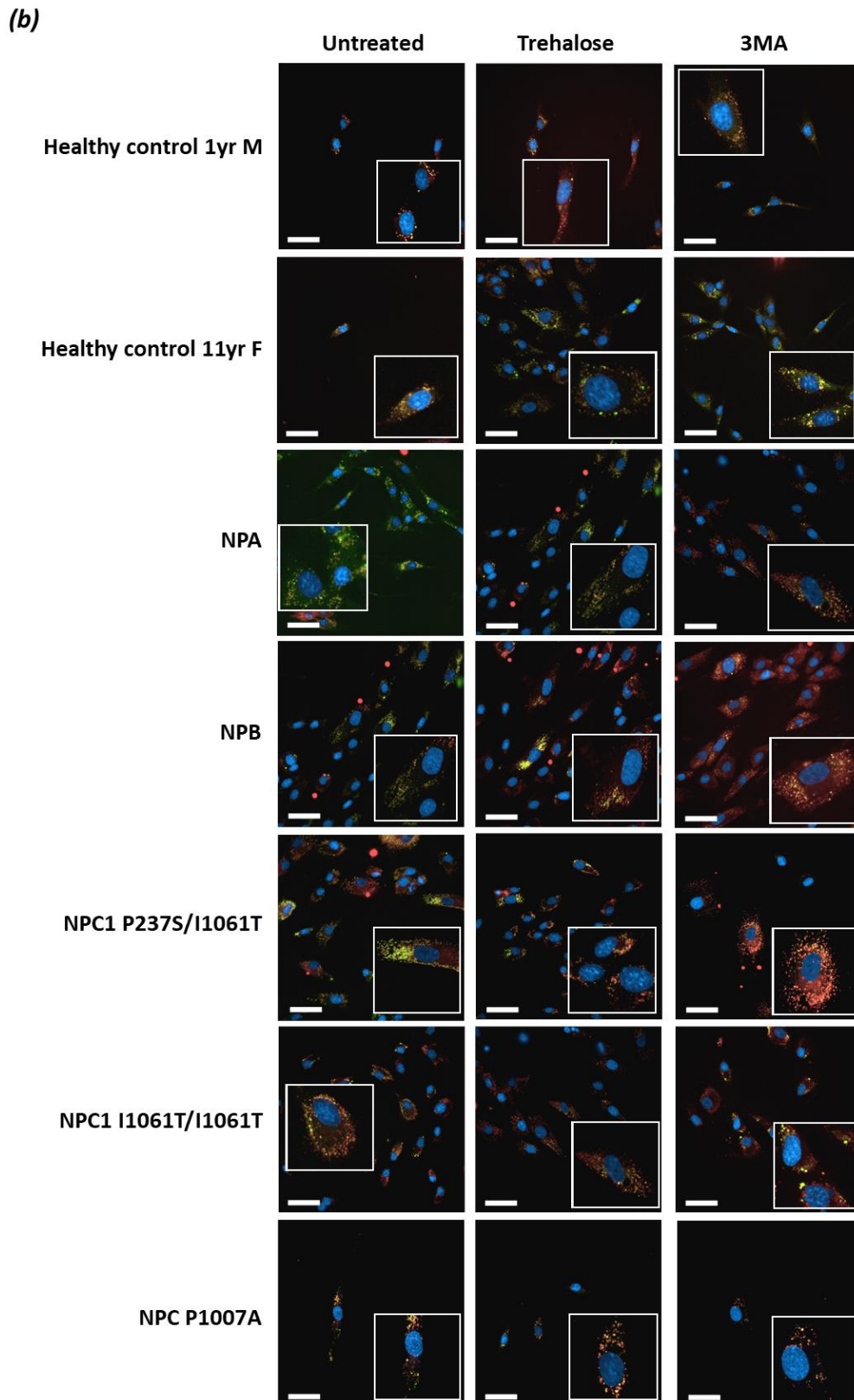


**Figure vii. AQ7 localisation to autophagolysosomes is not affected by 3MA or trehalose treatment**

The percentage of puncta of AQ7 that was co-localised to a puncta of Cyto-ID is shown in (a) for a range of Niemann-Pick disease and healthy control cells treated with 3MA and trehalose.

Representative images for each cell line, with each treatment are shown in (b), including an increased zoom image to show co-localisation. All data is  $n=3$ , statistical significance was determined through a two-way ANOVA, with post-hoc Tukey tests. Scale bars represent  $50\mu\text{m}$ .

## 9.3.2 Cannabidiol and copaiba

### 9.3.2.1 Cell seeding calibration assay for cellular toxicity assay using patient derived fibroblasts and RealTime-Glo™ MT.

To determine the optimal plating density for cell viability assays, seeding density optimisation for RealTime-Glo fluorescence was carried out for the different fibroblast cell lines. This was undertaken to ensure that the cells did not enter exponential or nonlinear growth, nor deplete nutrient or substrate, during the 72-hour period.

For the healthy controls, cells seeded at 1,000 and 5,000 cells per well experienced linear growth, while those seeded at 10,000, 25,000 and 50,000 experienced initial exponential increases in fluorescence, peaking before 24 hours, followed by a decrease in luminescence. For NPA and NPC fibroblasts (*Figure viii(d-f)*), linear growth was apparent at up to 10,000 cells per well, with higher densities leading to a decrease in luminescence after 24 hours. Based on this data, the seeding density for Real Time Glo cellular toxicity assays was decided as 5,000 (healthy control) or 10,000 (NPA and NPC) cells per well as this was the highest cell density where the luminescence remained linear for the whole 72-hour period.

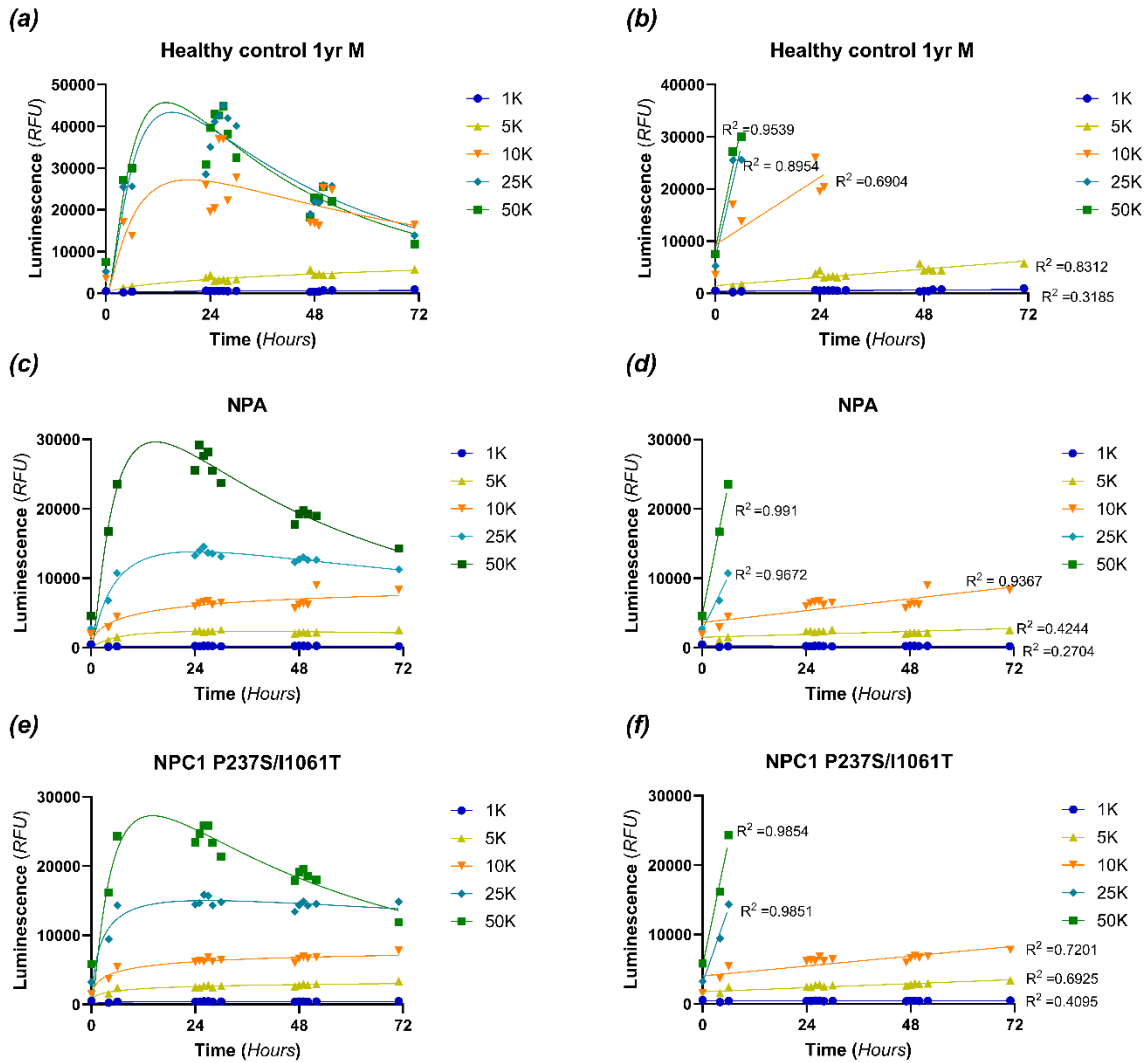


**Figure viii. Comparison of cell seeding densities detected using RealTime-Glo™ MT cell viability assay**

In (a), (c) and (e) the data is fitted with a nonlinear trendline for each graph with healthy control, NPA and NPC cell lines. In (b), (d) and (f) the data is fitted with a linear trendline, with the data points for each seeding density cropped to only include time points that fit on, or closely to, each respective trendline.  $N=1$  for all data.

### 9.3.2.2 Cannabidiol batch comparison

Initial toxicity testing with cannabidiol produced significant variability. Therefore, it was decided to quantify cannabidiol levels by UPLC-MS, and cell toxicity, in three separate batches from the same supplier to determine if the effects were driven by batch differences.

Liquid chromatography–mass spectrometry (LCMS) data were recorded on a Waters Acquity H class plus UPLC coupled to a Waters Acquity UPLC PDA detector and a Waters Acquity QDa API-ES mass detector. Samples were eluted through a BEH C18 2.1 mm × 50 mm, 1.7 µm column or a Cortecs C18 2.1 mm × 50 mm, 1.6 µm column using water and acetonitrile acidified by 0.1% formic acid and detected at 254 nm. The area under the corresponding cannabidiol peak being recorded for each batch, which had been standardised to 0.4%W/V based off stated mass and concentration of cannabidiol and compared to a range of known cannabidiol standard concentrations made from a mass-spec grade stock of cannabidiol.

Concentration of cannabidiol varied from that advertised by up to 22%. However, variability in batch toxicity was large, with LD50 values of 50nM, 100uM and 230uM at 24h (*Figure ix(b)*). Toxicity was unrelated to cannabidiol levels; batch 2, the most toxic, has the lowest cannabidiol level. For all future experiments, batch 3, intermediate in both toxicity and cannabidiol levels, was used.

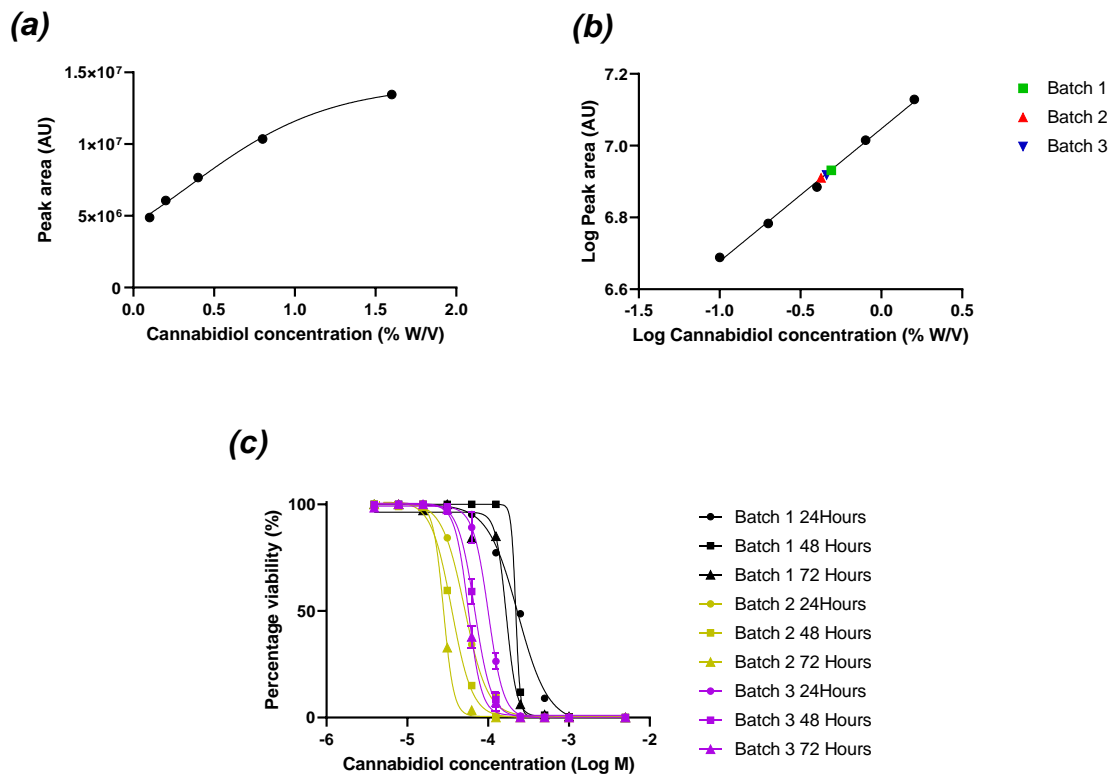


**Figure ix. Differing cannabidiol batches from the same supplier contain varying concentrations of cannabidiol**

In (a) the peak area of a reference standard of cannabidiol is compared at a range of concentration, when plotted a non-linear relationship between peak area and cannabidiol concentration is observed. (b) Log transforming both peak area and cannabidiol concentration, produces a linear relationship, which is fitted with a linear trendline. The log of the peak area of each batch of cannabidiol is also plotted on the graph, allowing a direct comparison between batches. (c) A toxicity assay was carried out in healthy control fibroblasts for all three batches of cannabidiol, with viability being recorded at 24, 48 and 72 hours across a range of cannabidiol concentrations. All LC50 estimates were determined using Boltzmann-Sigmoid curve fitting estimates. N=1 for all data, with data being plotted as mean  $\pm$  SD. Samples were run on UPLC-MS by Dr. Jason Gillespie.

### 9.3.2.3 Validation of specificity of recombinant European Lysenin

To detect sphingomyelin *in vitro*, recombinant Lysenin was used. Lysenin was produced, using an *E.coli* expression system. To confirm that the recombinant Lysenin was specific to sphingomyelin, lipid dot blot with sphingomyelin and other closely related lipids was carried out.

The data below clearly shows that the recombinant Lysenin shows specificity for sphingomyelin and does not bind to any other closely related lipids including lyso-sphingomyelin or cholesterol.

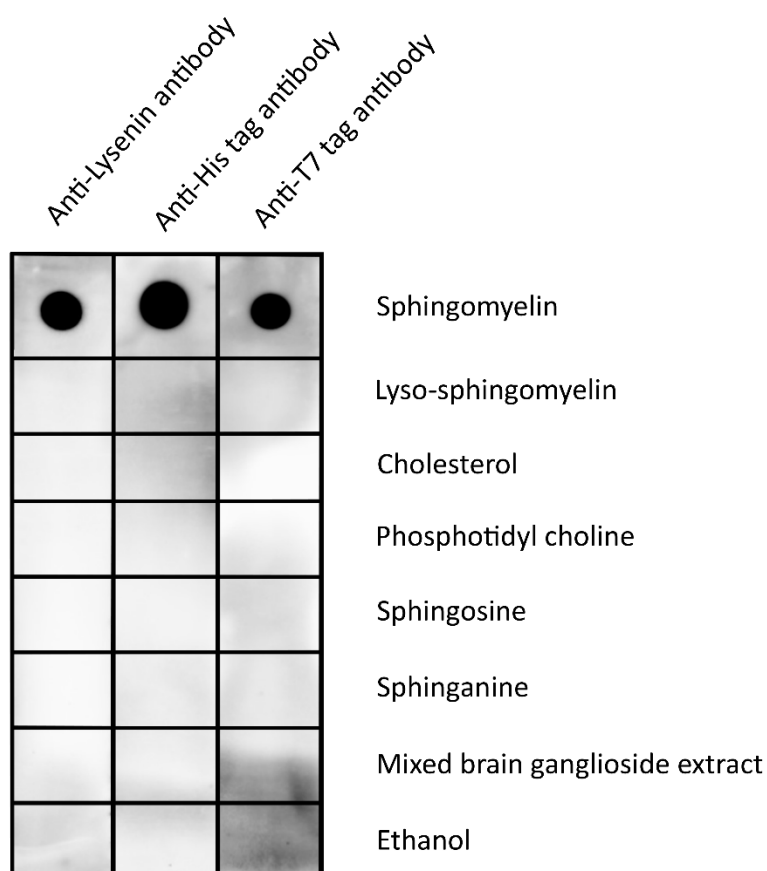


**Figure x. Recombinant Lysenin shows specificity for sphingomyelin**

Lipid dot blots with European Lysenin and three different primary antibodies, showing European Lysenin sole specificity for sphingomyelin and no difference in antibody binding between lysenin, His and T7 tag antibodies.

### 9.3.2.4 Treating cell homogenate with cannabidiol or copaiba, does not increase aSMase activity

From treating cell homogenate with cannabidiol and copaiba, it was clear that this did not increase aSMase activity. Therefore, cannabidiol and copaiba do not directly activate aSMase. If cannabidiol and copaiba are not activating aSMase directly, then we hypothesised that they must be either increasing protein synthesis or improving folding of aSMase or improving trafficking of aSMase resulting in more aSMase reaching lysosomes.

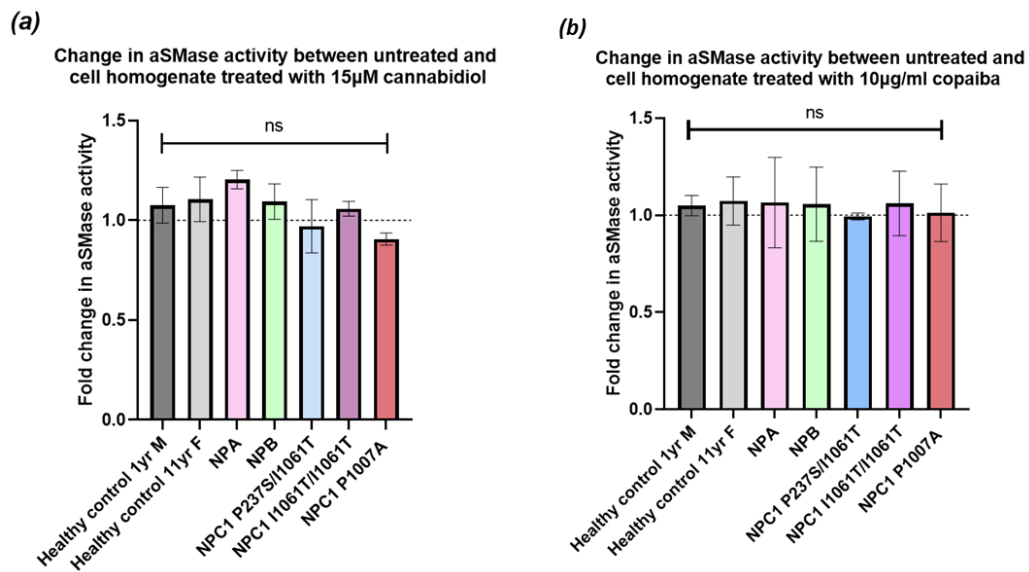


**Figure xi. Treatment of cell homogenate with cannabidiol does not lead to fold changes in acid sphingomyelinase activity compared to untreated control**

In (a) the aSMase activity ratio between untreated and homogenate treated with cannabidiol is shown. Cell homogenate was treated with cannabidiol for 1 hour, followed by aSMase activity assay as outlined in 2.4.1.2. In (b) the aSMase activity ratio between untreated and homogenate treated with copaiba is shown. Cell homogenate was treated with copaiba for 1 hour, followed by aSMase activity assay as outlined in 2.2.2.1. Statistical significance was calculated with a one-way ANOVA and a post-hoc Tukey's multiple comparison test. \*= $p < 0.05$ , \*\*= $p < 0.01$ , \*\*\*= $p < 0.001$ , \*\*\*\*= $p < 0.0001$ .  $N=3$  for all experiments, data shown is mean  $\pm$  SD.

### 9.3.2.5 Western blots

#### 9.3.2.5.1 Cannabidiol receptor 2

As cannabidiol and copaiba (BCP) are known modulators of Cannabidiol receptor 2 (CB<sub>2</sub>), we decided to see if treatment with either cannabidiol or copaiba would affect receptor expression, which may explain the effects observed in increasing aSMase activity.

A similar pattern of change in CB<sub>2</sub> expression was observed in both healthy control cell lines and the NPA/NPB cell line. In these cell lines cannabidiol and copaiba induced similar effects, however treatment only led to a significant increase in CB<sub>2</sub> expression in NPA cells.

In both NPC1 I1061T mutant cell lines, baseline CB<sub>2</sub> expression was higher than all other cell lines. However, treating with cannabidiol showed a non-significant trend of reduced receptor expression, but no change was observed with copaiba treatment. With the NPC1 P1007A cell line, cannabidiol led to a small increase in CB<sub>2</sub> expression, whereas copaiba, produced a marginally small decrease in CB<sub>2</sub> expression with neither change being significant.

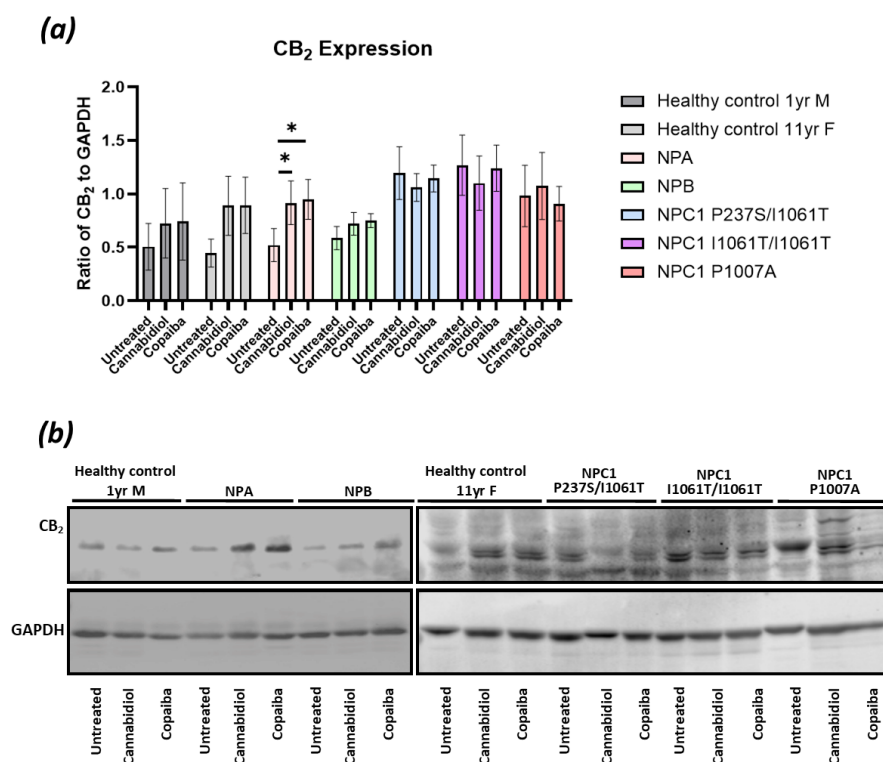


**Figure xii. Cannabidiol Receptor 2 expression is modulated by cannabidiol or copaiba treatment** Cannabidiol receptor 2 expression and changes upon cannabidiol or copaiba treatment was probed through western blotting. Antibodies specific to cannabidiol and GAPDH were used, with GAPDH being used a loading control. Species specific fluorophore secondary antibodies were used, and membranes imaged using a LI-COR Odyssey CLx. Statistical significance was calculated with a one-way ANOVA and a post-hoc Tukey's multiple comparison test.  $*=p<0.05$ ,  $**=p<0.01$ ,  $***=p<0.001$ ,  $****=p<0.0001$ .  $N=3$  for all experiments, data shown is mean  $\pm$  SD.

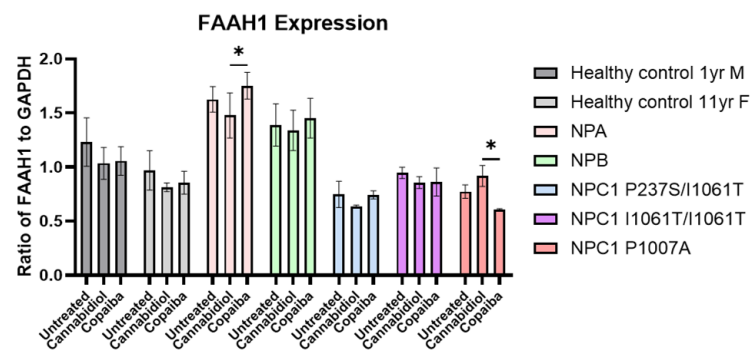
### 9.3.2.5.2 Fatty acid amide hydrolase 1

Fatty acid amide hydrolase 1 (FAAH1) is responsible for CB<sub>1</sub> and CB<sub>2</sub> receptor ligand degradation, and thus inhibition of FAAH offers a potential therapeutic pathway. BCP, the major constituent of copaiba oil, is a known FAAH inhibitor; and thus, some of the effects observed were possibly due to modulating FAAH expression.

Cannabidiol treatment did not lead to any significant changes in FAAH1 expression in any of the cell lines treated when compared to untreated. However, a general trend was for decreased FAAH1 expression when cannabidiol treated when compared to control. No significant changes were observed when comparing copaiba treated cells to untreated cells.

The only significant differences observed were between cannabidiol and copaiba treated NPA and NPC P1007A cell lines, whereby opposing effects were observed upon cannabidiol or copaiba treatment.

(a)



(b)

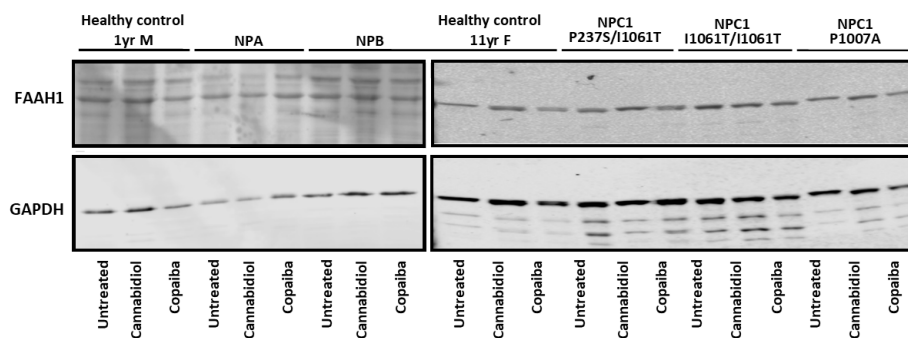


**Figure xiii. Minimal changes are observed in FAAH1 expression upon cannabidiol or copaiba treatment**

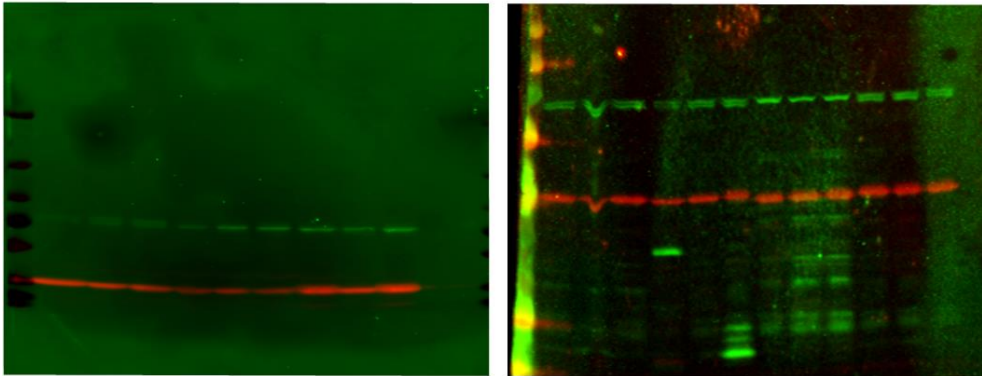
Expression of FAAH1 in patient fibroblasts was probed through western blotting, with specific FAAH1 antibody, and GAPDH, used as a standardisation loading control. Species specific fluorophore conjugated species-specific secondary antibodies were used. Membranes were imaged using a Licor ODYSSEY CLx. Statistical significance was calculated with a one-way ANOVA and a post-hoc Tukey's multiple comparison test. \*= $p < 0.05$ , \*\*= $p < 0.01$ , \*\*\*= $p < 0.001$ , \*\*\*\*= $p < 0.0001$ .  $N = 3$  for all experiments, data shown is mean  $\pm$  SD.

### 9.3.3 Western blot raw images

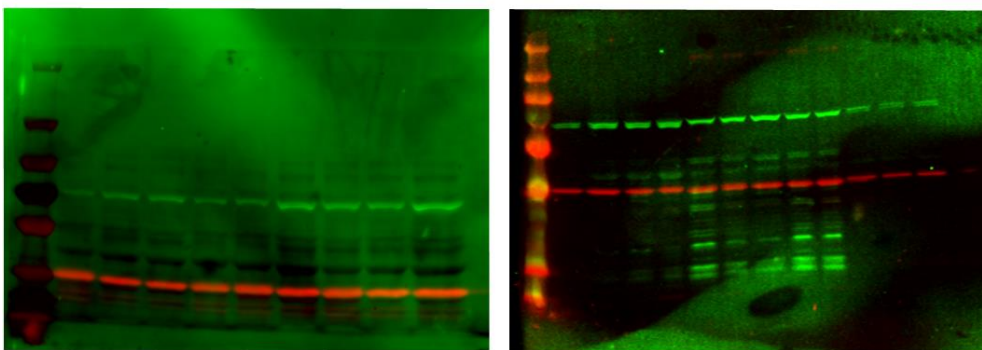
#### 9.3.3.1 Western blots in chapter 5

Included below are raw uncropped images of membranes for each set of proteins analysed in chapter 5.

Acid sphingomyelinase



HSP 70



Acid Ceramidase

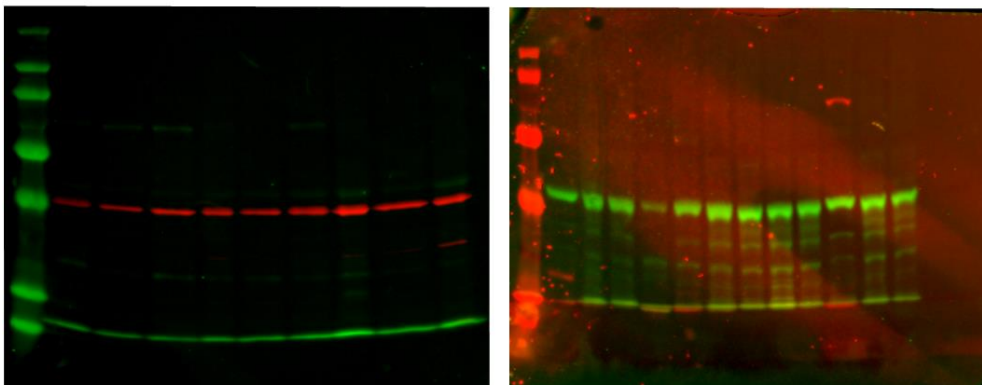


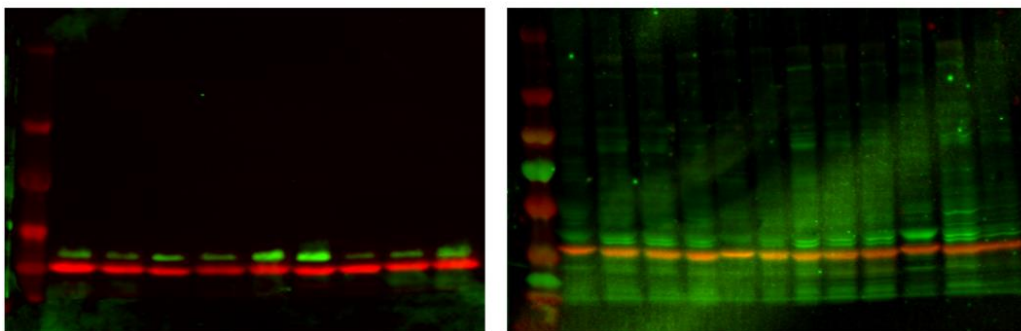
***Figure xiv. Raw images of western blots shown in main body of thesis***

*Raw images are shown for all western blots included in main body of thesis in chapter 5. Membranes were probed for proteins of interest using mouse and rabbit primary antibodies that allowed for both antibodies to be detected on the same membrane with species specific and different fluorophore conjugated secondary antibodies. Membranes were imaged with a LI-COR Odyssey CLx. For quantification of bands, single channel images were obtained with images converted to black and white.*

### 9.3.3.2 Western blots in appendix

Included below are raw uncropped western blots that have been included in figures in appendix.

#### Cannabinoid Receptor 2



#### FAAH 1

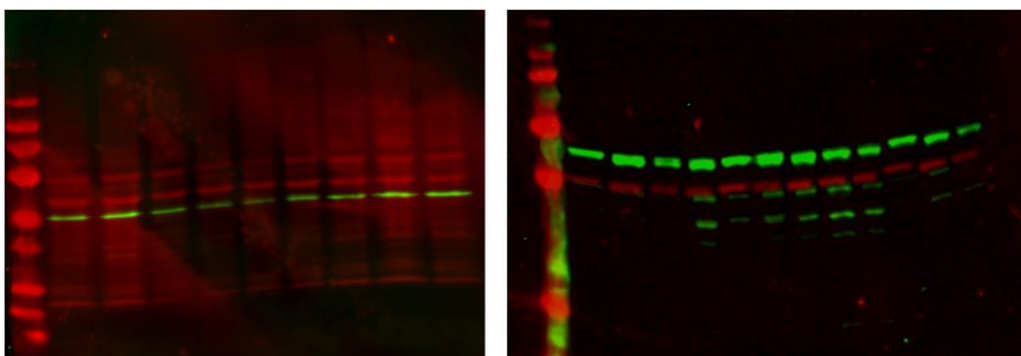


***Figure xv. Raw images of western blots shown in appendix***

*Raw images are shown for all western blots included in appendix thesis in chapter 9. Membranes were probed for proteins of interest using mouse and rabbit primary antibodies that allowed for both antibodies to be detected on the same membrane with species specific and different fluorophore conjugated secondary antibodies. Membranes were imaged with a LI-COR Odyssey CLx. For quantification of bands, single channel images were obtained with images converted to black and white.*

### *9.3.4 TSQ and zinc assay*

#### *9.3.4.1 Time and concentration effects upon TSQ staining.*

When live cells were being used, to improve the percentage of cells stained with TSQ, varying TSQ concentrations and incubations times were tested. Concentrations above and below the 100 $\mu$ M were tested to determine if uptake of TSQ was concentration and time dependant.

The data shows that in the 30 $\mu$ M samples, incubation time does not affect the number of cells with TSQ staining, whereas with the 150 $\mu$ M increasing time beyond two hours does increase the percentage of cells with TSQ staining. However, increasing TSQ concentration, does not increase the number of TSQ puncta, surprisingly higher TSQ concentrations led to lower corresponding puncta fluorescence.

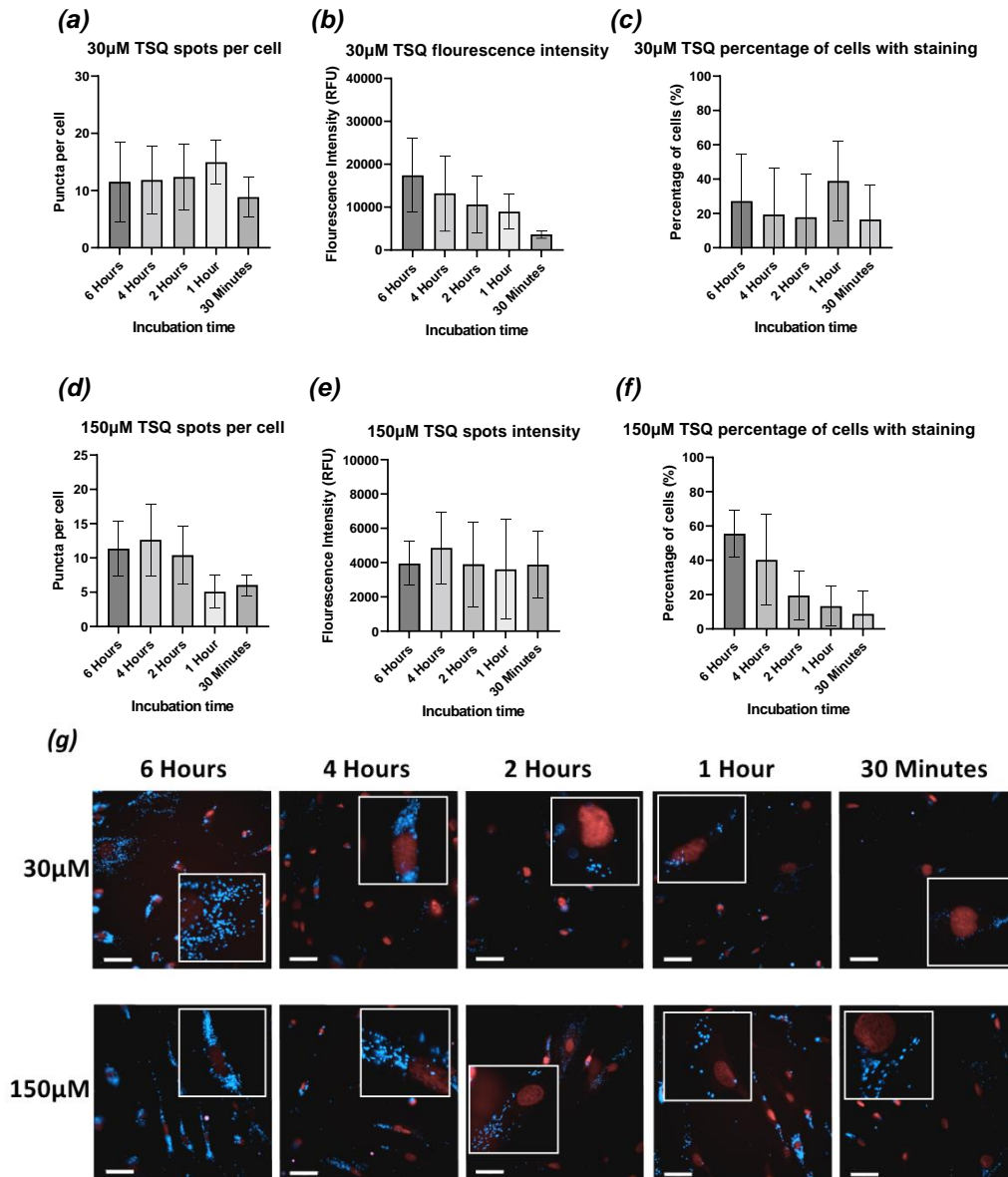


**Figure xvi. Effects of varying TSQ concentration and incubation time on puncta number and fluorescence intensity**

Healthy control fibroblasts were incubated with either 30µM or 150µM TSQ supplemented media for varying times. Prior to imaging, cells were incubated with Draq5. Comparison of the mean number of zinc puncta per cell, and the corresponding fluorescence intensity are shown in (a-b & d-e). Also shown in (c & f) are the percentage of cells that have puncta of TSQ staining. Representative images are shown in (g). All data is n=1, with mean, and standard deviation of three technical replicates shown. Scale bars represent 50µm.

#### *9.3.4.2 Cannabidiol and copaiba increase free zinc puncta in disease relevant cell lines.*

We had identified that cannabidiol and copaiba lead to intracellular changes in lysosomal activity, particularly within Niemann-Pick disease cells. In these cells, increases in lysosomal enzyme activity, and reduced lysosomal storage was observed.

Therefore, we wanted to determine the effects of cannabidiol and copaiba on intracellular zinc in Niemann-Pick, as well as another disease with known metal dyshomeostasis, Mucopolipidosis IV.

In all disease fibroblast lines, cannabidiol significantly increased the number of free zinc puncta. A corresponding increase in total puncta area was also observed in all disease cell lines when treated with cannabidiol, when compared to untreated control. Additionally, a significant increase in the total zinc staining area was observed in the healthy control cells when treated with cannabidiol.

Copaiba treatment did not significantly increase the number of zinc puncta in any of the cell lines treated, however a general trend of increased number of puncta was observed. When analysing total zinc puncta area, significant increases when compared to untreated were observed in all disease cell lines, but not healthy control. However, the effects of copaiba treatment upon total zinc puncta area were smaller than that observed upon cannabidiol treatment. Furthermore, no significant differences were identified between cannabidiol and copaiba treatment in either number of zinc puncta or total puncta area in any of the cell lines tested.

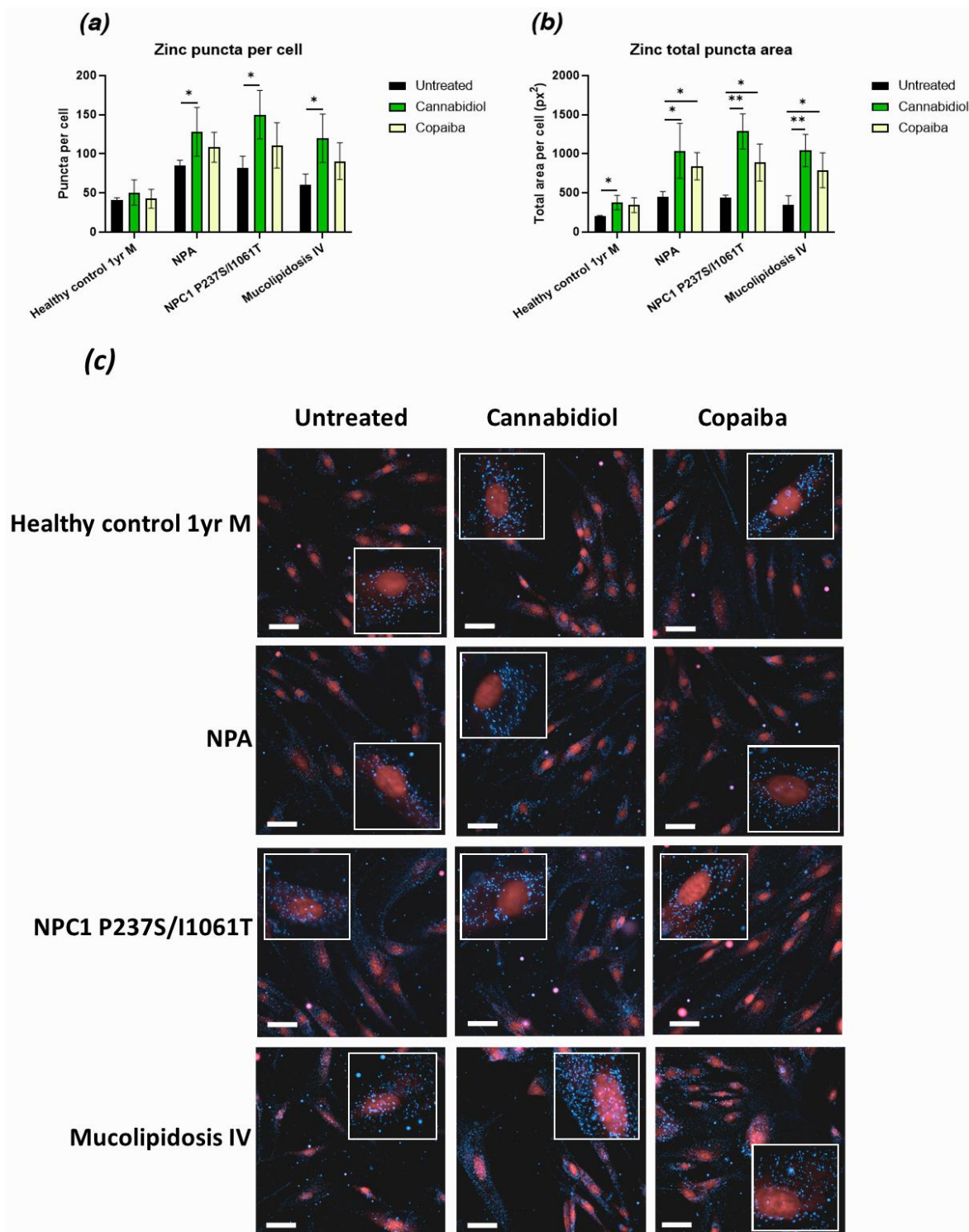


**Figure xvii. Effects of cannabidiol and copaiba upon zinc puncta in disease relevant fibroblasts**  
 Patient derived fibroblasts were treated with cannabidiol (15 $\mu$ M) or copaiba (10 $\mu$ g/ml) for 48 hours, after which cells were fixed. Free zinc was probed with TSQ, and nuclei stained with TO-PRO-3. In (a) the mean number of puncta per cell is shown, with the corresponding total TSQ staining are shown in (b). In (c) representative images for each cell line, with each treatment are shown. Statistical significance was calculated with a one-way ANOVA and a post-hoc Tukey's multiple comparison test. \*= $p < 0.05$ , \*\*= $p < 0.01$ , \*\*\*= $p < 0.001$ , \*\*\*\*= $p < 0.0001$ .  $N=3$  for all experiments, data shown is mean  $\pm$  SD. Scale bars represent 50 $\mu$ m.